SYNTHESIS AND PROTEIN ADSORPTION STUDIES OF PEGYLATED-POLYESTER NANOPARTICLES WITH DIFFERENT PEG ARCHITECTURES

A Dissertation

Presented to

The Graduate Faculty of The University of Akron

In Partial Fullfilment

of the Requirements for the Degree

Doctor of Philosophy

G. Rocío Montenegro-Galindo

December, 2013

SYNTHESIS AND PROTEIN ADSORPTION STUDIES OF PEGYLATED-POLYESTER NANOPARTICLES WITH DIFFERENT PEG ARCHITECTURES

G. Rocío Montenegro-Galindo

Dissertation

Approved:	Accepted:
_____	_____
Advisor Dr. Coleen Pugh	Department Chair Dr. Coleen Pugh
_____	_____
Committee Chair Dr. Matthew Becker	Dean of the College Dr. Stephen Cheng
_____	_____
Committee Member Dr. George Newkome	Dean of the Graduate School Dr. George Newkome
_____	_____
Committee Member Dr. William Landis	Date
_____	
Committee Member Dr. Chrys Wesdemiotis	

ABSTRACT

The development of polymeric drug delivery devices began five decades ago, starting with hydrogels in 1960. After that, nano-sized drug carriers were developed to increase the efficiency of the drug uptake. This has been accomplished by encapsulating the drug in polymer carriers that increase the circulation time of the drug in the blood, preventing early adsorption, elimination and targeting the drug where it needs to be delivered. One of the most important strategies to increase the circulation time of nanocarriers is PEGylation, in which poly(ethylene glycol) coats the device to prevent premature elimination from the bloodstream due to protein attachment.

The goal of this project is to compare the protein adsorption onto polymeric micelles that have either a cyclic or a linear architecture on the hydrophilic coating. We synthesized PEG-*b*-PCL amphiphilic diblock copolymers in which the PEG block is hydrophilic and the PCL block is hydrophobic. First, PEG macroinitiators were synthesized with either cyclic or linear architectures. The macroinitiators were then used for ring-opening polymerization of ε-caprolactone. These diblock copolymers were self-assembled into micelles suspended in water by a co-solvent evaporation method. These two types of polymers (no end groups and end groups) allowed us to study the role of polymer architecture on protein adsorption and circulation time.

DEDICATION

To God and my mom, who have kept me company and loved me during this journey.

ACKNOWLEDGEMENTS

There are numerous individuals who have contributed to my success during graduate school at the University of Akron. I would like to personally thank all those people here to show my appreciation for their energy, efforts, patience and time.

I am very thankful to God for all His gifts in particular happiness, enlightment, but specially for keeping me company and showing me His love in so many ways. I thank my mom for embracing so many hardships in order to provide anything and everything that I need to be successful and happy. Without her love and encouragement I would have not being able to have come so far. I thank my father for his advice and wishing me the best in life.

I am grateful to Professor Coleen Pugh in so many ways. At the beginning of my PhD she gave me the opportunity and welcomed me to her research group even though I had a chemical engineering rather than an organic chemistry background. She trusted me to become an independent and responsible researcher. I much appreciate her patience during my slow learning process on how to become a researcher. She has been always available when I needed to talk to her, supported my research, provided me with suggestions when I had difficulties, and has been critically fair in her decisions. Besides this, she has treated me with great generosity and kindness: she had made me feel more

like a friend than like a student. I cannot thank her enough and I wish her the best in her current and future projects.

I acknowledge my coworkers---Chau Tang, Anirudha Singh, Lisa Collette, James Baker, Abhishek Banerjee, William Storms, Guillermina Garcia, Colin Wright, Xiang Yang, César López, Stephanie Vivod, Ajay Amrutkar, Brian Gudhe, Paula Watt, Xia Lei, Peiyao Wang, Yangtian Lu, Jialu Yan, Nicole Swanson, Brinda Mehta, Bonan Yu, Weiran Wang, Xiang-Lin Yin, Zewei Wang and Carolyn Moore in the Pugh research group for their help, support, and time. Chau and Anirudha gave me encouragement as I started my graduate school and they were about to graduate. I thank Lisa, James, and Abhishek for answering my questions as I started working in the laboratory. I thank James and Abhishek for letting me learn from them how to take care of the Gel Permeation Chromatography (GPC) system. I also acknowledge the students that I worked with during their undergraduate program: Colin Wright, Carolyn Moore, and Yang Zhou. I enjoyed working with you and learning from the projects where you worked. I am very glad to see you being successful in graduate school. Each of you have being an inspiration for me, I admire your intelligence and hard work. Thank you for being available to discuss problems, solving them together and making a pleasant lab-environment. Carolyn, thank you for being available when I needed someone to talk to and for your advice: they mean a lot to me. Colin, thank you for letting me a part of your life: I cannot thank you enough for your generosity, I am very lucky to be able to share so many happy moments with you.

I thank Dr. Madalis Casiano, Nadrah Alawani, and Kai Guo for running my mass spectrometry samples. Madalis Casiano is one of the dearest friends I have. I thank Chih-Hao for taking the TEM pictures of the micelles and using the coated TEM grid that he prepared. I thank Dr. Adam Smith and Megan Kaliszewski in the chemistry department. I appreciate the time and energy that you spent working with me in developing methods to characterize the micelles and study protein binding using fluorescence correlation spectroscopy (FCS) and fluorescence cross-correlation spectroscopy (FCCS).

I thank all my committee members-- Dr. Matthew Becker, Dr. George Newkome, Dr. William Landis, and Dr. Chrys Wesdemiotis for listening to my presentations and giving me constructive feedback. I am grateful to have Dr. Becker serve as the chair of my dissertation defense and giving me valuable guidance in the use of Dynamic Light Scattering (DLS) for micelle characterization.

TABLE OF CONTENTS

LIST OF TABLES

LIST OF FIGURES

Figure Page

LIST OF SCHEMES

CHAPTER I

INTRODUCTION

We decided to conduct research on studying the role of PEG architecture in nanoparticle coatings on protein adsorption because we wanted to improve the current drug delivery devices particularly in regard to increasing the circulation time of these devices in the blood. Polycaprolactone (PCL) is used in drug delivery devices due to its biocompatibility and biodegradability.[1-4] Since it degrades more slowly than poly(lactic acid) (PLA) (i.e. due to the higher hidrophilicity of PLA), the biodegradability can be tuned by adjusting the amounts of PCL/PLA in a device.[2] Besides polymeric micelles, other materials have been used in controlled drug delivery: antibodies and their conjugates, liposomes, nanoparticles, unimolecular polymeric drugs and conjugates.[5] Controlled drug delivery prevents side effects that arise from toxic drug levels and provides a more consistent drug dose over time.[6,7]

Controlled release also helps patient compliance due to the fact that the drug does not need to be administered as frequently as in the case of the injection of a drug solution. Besides its advantages, controlled release systems also have to address certain challenges, such as drug elimination before achieving a therapeutic effect.

To reduce premature elimination, devices must be small in size (e.g <150 nm) and must be coated with a hydrophilic layer, usually PEG.[8-16]

Juliano and Stamp were one of the first researchers to study the effect of particle size on circulation time. [17] They found that smaller (i.e. unilamellar) liposomes circulated about ten times longer or more than larger (i.e. multilamellar) liposomes. Devine et al confirmed these results.[18] They found that larger liposomes (i.e. 400 nm) activated the complement system more effectively than smaller (i.e. 50 nm) ones. These researchers proposed that the difference in complement activation was due to different requirements for the assembly and activation of complement proteins. On the more curved surfaces of smaller liposomes, the proper geometric configuration for efficient complement activation is apparently less readily achieved than on larger liposomes. Moghimi and coworkers observed that a higher fraction of larger particles (i.e. 250 nm) were eliminated from the bloodstream to the liver and spleen than smaller (i.e. 60 nm) ones.[19] In 2011, Kataoka and coworkers showed that sub-100 nm micelles are more effective for efficient delivery of drugs in tumors with poor permeability.[20]

Kataoka and coworkers synthesized a PEGylated form of the anticancer drug adriamicin.[8] The result was an amphiphilic diblock copolymer, which self-assembled into micelles in water. The authors injected tumor-bearing mice with either the micelle suspension or a free-drug solution. They found that the concentration of the free drug solution decayed completely in 10 h while the micelle suspension decayed more slowly for a sustained delivery over 50 h.[8] In this example, PEGylation increased the drug

circulation time 5 times. Polymer architecture also affects circulation time. Frechet and coworkers plotted the half-life of polymer in the blood as a function of molecular weight for polymers with different architectures. They defined three regions. While the chemical structures of the polymers were not directly comparable, dendritic polymers had the longest half-lives at a particular molecular weight, globular and cyclic polymers had intermediate half-lives, and linear polymers had the shortest half-lives. Linear polymers can travel through a pore more easily. Cyclic, globular or dendritic polymers need to deform in order to go through a pore, which presumably increases their circulation time.[21] The significance of the polymer permeability in circulation time can be explained through the two-compartment model.

The two-compartment model describes a controlled drug delivery device distribution after injection. After the bolus injection, the drug goes to the blood compartment where it can either stay or go through pores in the tissues to the tissue compartment. The drug can travel back and forth between these two compartments or be excreted through the pores in the kidney. According to this model, the permeability of a polymer through a pore is one important factor related to the ability of a polymer device to remain circulating in the blood. The permeability of a polymer through a pore depends on: molecular weight, branching, molecular conformation, and flexibility.

The increased circulation times by changing the polymer architecture was the inspiration to prepare micelles using diblock copolymer with different architectures in the polymer that form the micelle corona (i.e. PEG).

Our hypothesis is that micelles prepared with diblock copolymers having a cyclic PEG block will circulate longer in the bloodstream due to lower protein adsorption. Lower protein adsorption onto micelles would also correlate with differences in *in vivo* micellar blood circulation times.

In this dissertation, I report the synthesis and characterization of PEG-*b*-PCL diblock copolymers using two different architectures for the PEG block: cyclic *vs*. linear. I also self-assembled these polymers into micelles. The micelles were characterized and protein adsorption studies showed that the use of a cyclic PEG architecture in the corona reduces or eliminates protein adsorption onto the micelle surface.

These preliminary *in vitro* studies are the precedence for future biodistribution studies that could lead to nanoparticles that circulate in the blood longer and thereby increase therapeutic efficiency.

CHAPTER II

LITERATURE REVIEW

2.1 Controlled Drug Delivery Devices

Throughout the years, different strategies have been used to improve the biodistribution and efficiency of drugs. Some of these strategies have focused on improving the solubility of drugs. One of the early strategies was based on the covalent attachment of different molecules, macromolecules or antibodies. Later on, other colloidal carriers were used and consisted of entrapping drugs in a lipid, sugar, or protein colloid. Finally, drugs have been entrapped in polymeric particles, achieving better biodistribution, efficiency, reduced toxicity, and targeting.[22]

2.1.1 Need for Controlled Drug Delivery Devices

Classical drug delivery devices have problems associated with reduced efficacy due to partial degradation of drugs, increased costs associated with excess dosing, compliance issues due to the pain and frequency of administration, and toxic levels of administration as shown in Figure 2.1. According to the Biopharmaceutical Classification System of Drugs, the bioavailability of class II and class III drugs is also challenged by their poor water solubility and poor membrane permeability,

respectively.[23,24] Controlled drug delivery devices had the goals to deploy the drug to a target site, reducing side effects, preventing drugs from degrading, maintaining therapeutic drug level for prolonged periods of time, having predictable and controllable release rates, reducing dosing frequency, increasing patient compliance, reducing the drug costs by improving the cost-effectiveness of the drug device, and improving bioavailability by increasing solubility and membrane permeability. [6,22,25]

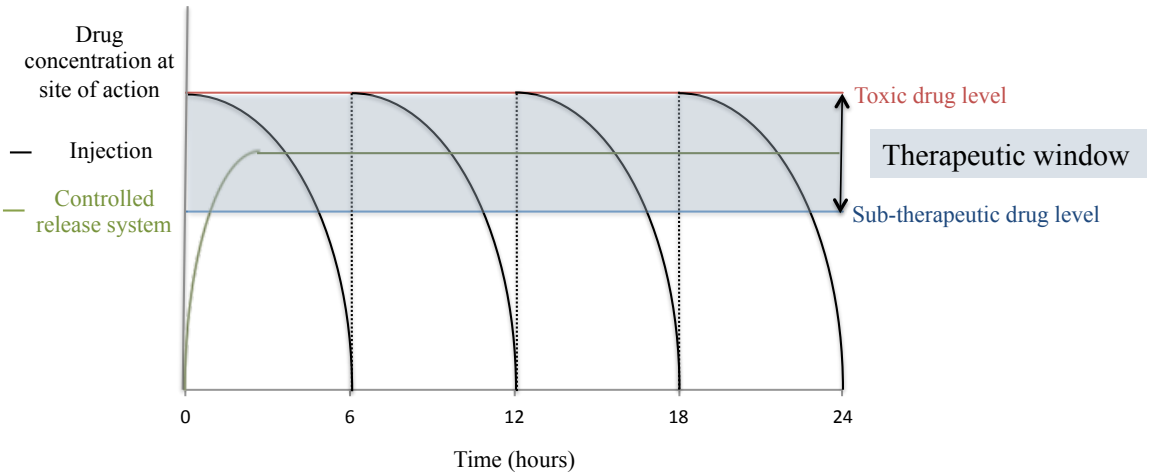

Figure 2.1: Drug concentration vs. time for injection and controlled release

2.1.2 Advantages of Controlled Drug Delivery Devices

The use of controlled drug delivery devices protects the bioactive compound from *in vivo* degradation and promotes storage stability.[6,22] They can also induce highly localized drug concentrations over extended periods of time (i.e. enhanced permeability and retention effect (i.e. EPR) in the case of cancer[7]), which in some cases enables the development of single-dose treatments.[6] Microparticles can be easily administered by a variety of routes, including oral, pulmonary, and parenteral. Microcarriers also reduce

drug elimination from the bloodstream by the complement system. Finally, FDA approval has been obtained for some biodegradable polymers, including poly(lactic acid) (PLA), poly(glycolic acid) (PGA), polyanhydrides, and poly(lactic-co-glycolic acid) (PGLA) for specific applications.

The main requirement of a drug delivery device is biocompatibility, which includes non-toxicity, non-immunogenicity and the possibility to degrade or excrete the non-bioactive part of the microcarrier.[22] Other desired characteristics of a drug microcarrier are described in the following phrases.[26] The agent to be encapsulated comprises a reasonable weight fraction of the total carrier system (e.g. more than 30%). High entrapment efficiency is also desirable, which means that the amount of bioactive compound used in the encapsulation process is incorporated into the final carrier at a reasonably high level. Bioactive compounds can be natural or synthetic, and catalyze or elicit a specific response within a given biological system. Some bioactive compounds include enzymes, peptides, polysaccharides, phospholipid analogs, antibodies, polyethylene glycol (PEG), antimicrobial agents and oligonucleotides. The particles should also be able to be freeze-dried and reconstituted in solution without aggregation. Saez and coworkers have studied the conditions to stabilize PLGA and polycaprolactone (PCL) by freeze drying with several bioprotective agents.[27] Another requirement for these particles is to have small size, generally smaller than 5 μm, and characteristics that prevent rapid clearance of the particles from the bloodstream, as will be explained further in Section 2.3. Control of the drug-release kinetics may be achieved by optimizing the

chemical composition of the diblock copolymers, drug loading, and the size of these microspheres.

2.1.3 Types of Controlled Drug Delivery Devices

Controlled drug delivery devices can be prepared by three main routes: chemical modification, drug entrapment in colloidal carriers, and drug entrapment in polymeric microcarriers. The term microcarrier refers to both microcarriers and nanocarriers unless indicated otherwise.

One of the main differences between these architectures is the size of the microcarrier, (i.e. usually the equivalent radius) as indicated in Figure 2.2.

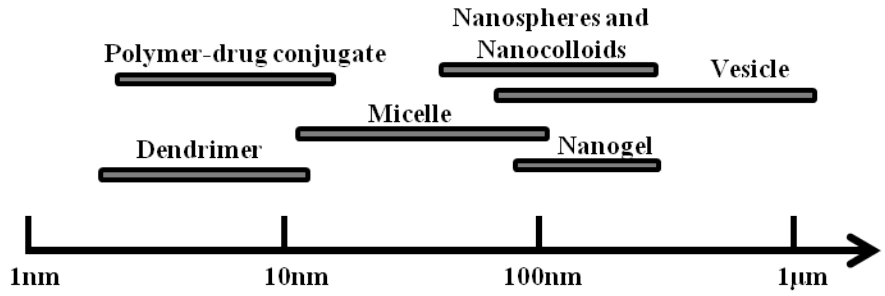

Figure 2.2: Most common sizes for different microcarrier architectures.[28]

In chemical modification, the bioactive compound is covalently attached to a molecule, a macromolecule, or a targeting ligand. This modification may make the drug more lipophobic or lipophilic, provide the drug with a specific transport mechanism,

and/or reduce toxicity.[25] Macromolecules, and in particular polymer-drug conjugates may also change the internalization pathway of small molecules by bypassing P-glycoprotein associated multi-drug resistance.[29] N-(2-hydroxypropyl)methacrylamide (HPMA) copolymer,[30] PEG,[31-34] poly(glutamic acid) (pGlu),[35] dextran,[36] and cyclodextrin-based[37] polymer are some of the polymers that have had preclinical success for small molecule conjugation. Conjugates of various anticancer drugs with these polymers are currently in clinical trials.[38-40]

Lipids, proteins, sugars, and surfactants are used for colloidal entrapment of drugs. When a vesicle is formed by a bilayer of phospholipids, the colloidal carrier is referred to as a liposome. Vesicles formed by bilayers of surfactants are called niosomes and the monolayers are micelles.

Polymeric microcarriers have been prepared with different architectures, including micelles, microspheres, microcapsules, microgels, vesicles, and dendrimers.[28] These types of micromedicines are usually prepared by drug entrapment.[41]

Amphiphilic block copolymers self-assemble in aqueous solution to form core-shell micellar microstructures when the concentration of the amphiphilic copolymer exceeds the critical micellar concentration. Kataoka and coworkers,[42,43], Lavasanifar[44], Torchilin,[45] Wooley and coworkers,[46] among others, have worked with different micellar block copolymer devices for drug delivery. Compared to polymer-drug conjugates with sizes generally around 10 nm or less, nano-aggregates formed through phase-separation

are larger, usually in a range of 20-100 nm for micelles,[43] and 100 nm to a few micrometers for polymer vesicles.[47-49]

Besides forming micelles, amphiphilic block copolymers form vesicles when the fraction (*f*) of the hydrophobic domain relative to the hydrophilic domain is controlled within a certain range (*f*=0.2-0.42).[50,51] Since polymer vesicles resemble liposome structures, they are also known as polymersomes.[47-55] Figure 2.3 illustrates the formation of self-assembled micelles or vesicles depending on the weight percent of the hydrophilic block.

Compared to liposomes, polymeric vesicles are more stable because their membrane-making polymers form much stronger hydrophobic interactions than the short hydrocarbon segments of liposomes. The degradation of PLA and PCL polymersomes upon hydrolysis has been studied by Discher and coworkers.[53]

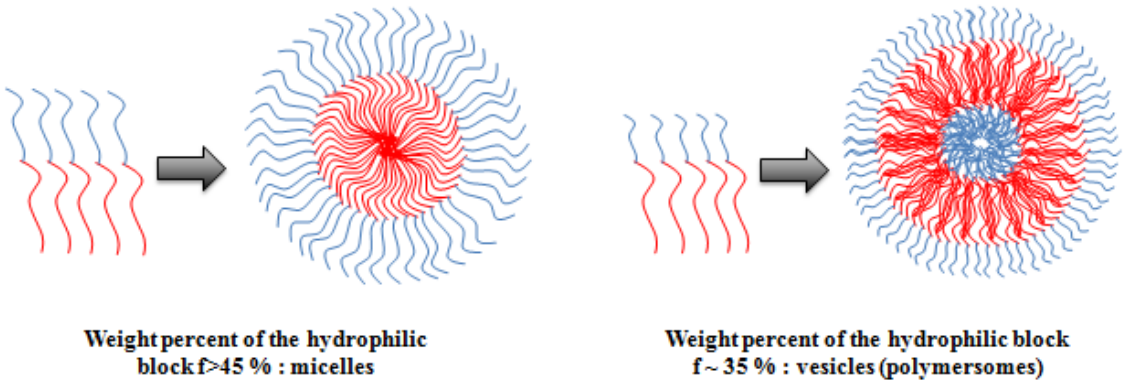

Figure 2.3: Morphology of self-assembled structure as a function of the weight percent of the hydrophilic block

Dendrimer syntheses were first reported in the late 1970s and early 1980s.[56-58] They have a unique architectural design: high degree of branching, symmetry, multivalency, globular architecture and monodispersity. Dendrimers contain layered structures also known as generations, which extend outwards from a multifunctional core on which dendritic units are attached. The sizes of dendrimers are in a range of 1-15 nm. These characteristics are taken advantage of for encapsulating bioactive agents (i.e. host-guest relation) into the interior or for covalent attachment of drugs (i.e. dendrimer-drug conjugates). In the past decade, different authors have explored potential applications of dendrimers in drug delivery.[59-66] Drug molecules can be either conjugated on the surface or encapsulated inside of the dendrimer. Despite numerous designs of dendrimer-based carriers, only a few of them have been evaluated for their *in vivo* antitumor activities.[67-69]

2.2 Biomaterials Used in Controlled Drug Delivery Devices

Polypeptides and biodegradable polyesters are commonly used as polymeric micellar core-forming blocks. Within polyester monomers, lactic acid and glycolic acid are commonly used as biomaterials for drug delivery. ε-caprolactone, more hydrophobic, favors encapsulation of more hydrophobic drugs while keeping the desired biodegradation properties of PLGA. Polycaprolactone is a Food and Drug Administration (FDA) approved material. A variety of drugs have been encapsulated within polycaprolactone beads for controlled drug release and targeted drug delivery.[5] Polycaprolactone also possesses good drug permeability,[70,71] which makes it more desirable for a controlled drug delivery or targeted drug delivery material.

Other advantages of using polycaprolactone include lower acidic environment generation during degradation compared to polylactides and polyglycolides, and the ability to form miscible blends with other polymers.[2]

PLA, PGA, PLGA and PCL have different degradation profiles, which can be used to tune drug release rates by blending or copolymerizing these polyesters. PEG-*b*-polyester polymers have been used to encapsulate different drugs, such as indomethacin,[72-74] dihydrotestosterone,[75] FK506,[76] nimodipine,[77] paclitaxel,[78] doxorubicin,[79] docetaxel.[80]

Apart from the synthetic methods to produce block copolymers, which will be summarized in the next section, some authors, like Lin and coworkers[81] used blends of polycaprolactone with PEG-containing polymers such as pluronics in order to take advantage of both polyesters and poly(ethylene glycol) in drug delivery applications.

2.3 Elimination Before Achieving Therapeutic Effect: One of the Main Problems of Drug Delivery Devices

Even though controlled drug delivery has brought many advantages compared to traditional drug delivery methods, there are some challenges that need to be addressed. The main two challenges are the non-selective drug adsorption and elimination before achieving a therapeutic effect. This elimination can occur either by a passive or an immune system-mediated mechanism.

2.3.1 Passive Elimination: Flow Through Pores

The biodistribution of polymer-bound or polymer-encapsulated drugs administered intravenously can be described by the two-compartment model.[82] After the bolus injection, the drug goes to the blood compartment and from there it can diffuse through pores into the tissue compartment. The drug can also pass through the pores into the kidney and be excreted. According to this model, polymer permeability through a pore is the most important property. Figure 2.4 shows a diagram of this model.

Some of the most important variables in polymer permeability are molecular weight (i.e M_n or M_w), molecular conformation, branching, and flexibility.[21] In order to prevent elimination from the body via urine, permeation through the kidney should be reduced. These pores have an average diameter of 5 nm. The general polymer molecular weight range required to reduce permeability is between 30 and 50 kDa. Other factors that influence the permeability include the molecular conformation. The polymer molecular conformation or shape of the polymer in solution depends on the molecular structure and the polymer's interaction with the solvent. Some polymer conformations are isotropic coil, ellipsoidal coil, and rod-like.[83] The more extended the polymer coil in three dimensions (for example in the isotropic coil), the lower the polymer permeability. By the same principle, an increased degree of branching and decreased polymer flexibility will decrease the polymer permeability because it will prevent the polymer from deforming to go through a pore compared to a linear structure.[21]

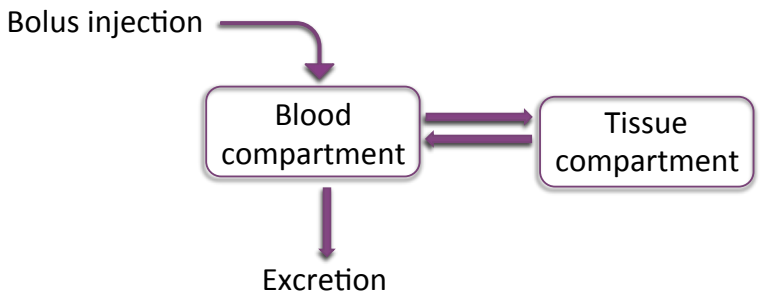

Figure 2.4: Two-compartment model

In order to analyze the effect of molecular weight, molecular conformation, and branching on circulation time, Frechet and coworkers[21] plotted the half life of polymers in the blood compartment as a function of molecular weight for polymers with different architectures. In Figure 2.5, the dendritic structures are shown in red and have the highest half lifes for similar molecular weights. In yellow, cyclic and globular polymers have intermediate half lifes, and finally linear polymers show the shortest half lifes. These authors suggest that dendrimers and dendritic structures adopt more rigid conformations which makes them less prone to deformation.

This limits their ability to pass through pores, leading to longer circulation times. Although this plot gives valuable insight on the effect of molecular conformation and branching, it uses polymers with different chemical structures. We believe a better comparison would be possible using a uniform chemical structure for the different architectures.

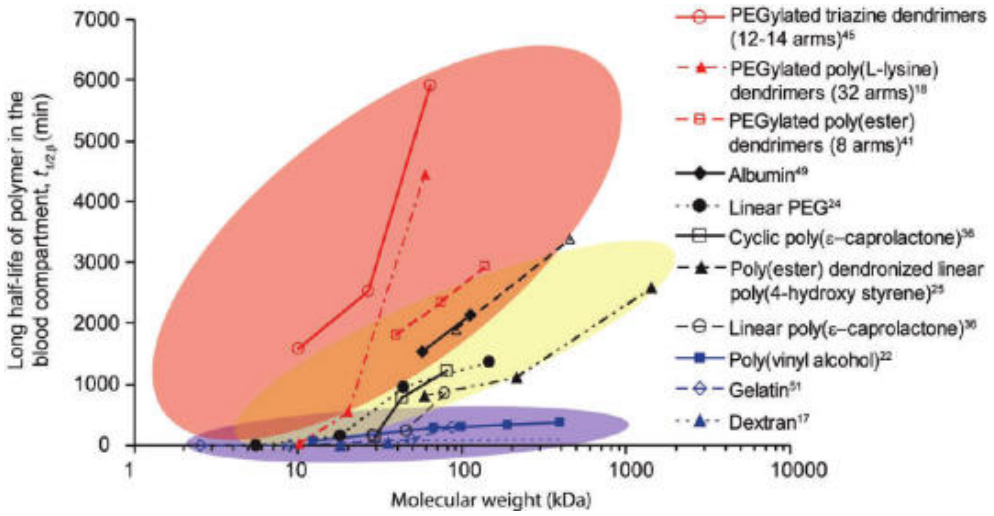

Figure 2.5: Half-life of polymers in the blood compartment as a function of time

2.3.2 Immune System and Elimination *via* Opsonization

The immune system is in charge of defending the body against foreign substances and microorganisms. It consists of mainly three parts: physical barriers, the innate immune system and the adaptive immune system. Skin and mucous membranes are a part of the physical barriers.

The innate immune system is a defense that all animals seem to have naturally since about 500 million years ago. Macrophages make up part of the innate immune system. They have receptors on their surfaces that recognize certain molecules present in common microbial invaders: fats and carbohydrates. When a macrophage finds a bacterium, it first engulfs it in a vesicle called a phagosome, which is taken inside the macrophage, where it fuses with another type of vesicle, a lysosome. Lysosomes contain certain molecules and enzymes that can destroy bacteria. This process is called

phagocytosis. Other parts of the innate immune system include the complement proteins, the professional phagocytes, and natural killer cells. Figure 2.6 illustrates how phagocytosis can convert a bacterium into soluble debris.

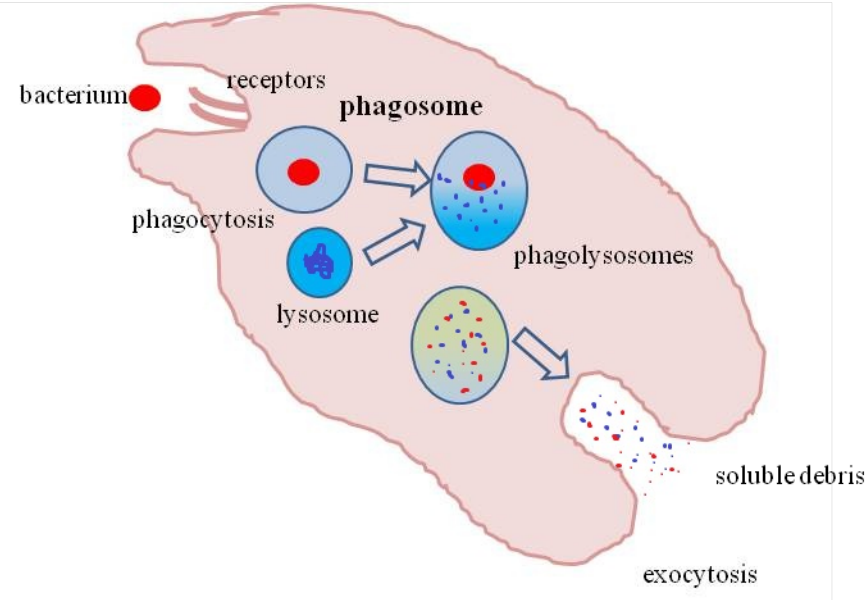

Figure 2.6: Phagocytosis

The complement system consists of 20 proteins and protein fragments that destroy invaders and send signals to other parts of the immune system regarding the presence of any foreign body. The proteins that make up the complement system are produced mainly in the liver, and are present at high concentrations in blood and tissues. Complement system can be activated through three pathways: alternative, lectin and classical. One major function of the complement system is to label pathogens and other foreign or toxic bodies for elimination from the host.[84]

In order to increase the circulation time of a particle in the bloodstream, it is necessary to prevent opsonization through the innate immune system. This can be achieved by avoiding certain functional groups on the particle surface:[85]

- Hydrophobic groups (classical pathway),
- -OH and -NH_2 (alternative pathway),
- Sugar residues (lectin pathway).

A discussion of how to avoid those groups on the surfaces of microparticles will follow in Section 2.3.3.

2.3.3 Protective Coatings Reduce Opsonization

By coating microcarriers with a hydrophilic substance, their circulation times are increased.[8-16,86] Apparently, this prevents activation via the classical pathway, but at the same time may also promote elimination via the alternative pathway. Research on coating with hydrophilic polymers to improve pharmacokinetics preventing opsonization of bioactive compounds started in the late 1960's and early 1970's with dextran as the modifying polymer.[87] In 1978, Frank Davis[87] started studies with PEG-enzyme adducts, his results motivated other authors to use PEGylation in order to improve the pharmacokinetics of other bioactive compounds.[10,13-15,26,28,75,88-100]PEG is highly flexible, highly water soluble, non-degradable and non-immunogenic. PEG is also biocompatible and FDA approved for certain drug delivery applications because of its very low toxicity.[101,102] PEG is eliminated by renal excretion (PEG<30kDa) or hepatic secretion

(PEG>20kDa).[103] When PEG is used to coat the microcarrier, the particle is referred to as PEGylated and the process by which it is incorporated, PEGylation.[88] The influence of the PEG corona thickness and density, as well as the influence of the nature of the core on the circulation time was studied by Gref and coworkers.[15] Other authors, such as Kingshott and coworkers,[104] Holmberg and coworkers[105] found a reduction in protein adhesion upon attachment of high density PEG onto surfaces.

The impact of PEGylation on circulation time can be observed in for different microcarriers. Some other benefits of PEGylation include solubilization of hydrophobic agents, stabilization of the conformation of proteins, and minimization of enzyme-catalyzed degradation in blood.

Table 2.1: Pharmacokinetic influence of PEGylated systems in terms of elimination half-life.[88]

Parent Drug and Peglated Form	Elimination Half-Life (h)
Interferon-α2a	3-8
Pegylated — Interferon-α2a	65
Interleukin-6	0.04
Pegylated — Interleukin-6	3.4
Tumor Necrosis Factor (TNF)	0.05
Pegylated — TNF	2.27
Doxorubicin	20-48
(PEG)-liposomal doxorubicin	45-55
Daunorubicin	0.75-3
(PEG)-liposomal daunorubicin	4

Jeon and Andrade designed mathematical models to explain the reduction in protein adsorption onto PE substrates when coated with PEG chains.[106,107] The model assumes PEG is a neutral homopolymer with linear and flexible chains terminally attached to a PE hydrophobic substrate in water which is a good solvent for PEG. According to these authors, the crucial parameters of the model are the distance between terminally attached PEG (i.e. a measure of surface density) and the degree of polymerization (i.e. a measure of chain length). The authors calculated the steric repulsion free energy per unit surface area using the method developed by Patel and coworkers[108] based on the treatment by de Gennes.[109] Patel's method considers steric repulsion to involve contributions of osmotic and elastic forces.

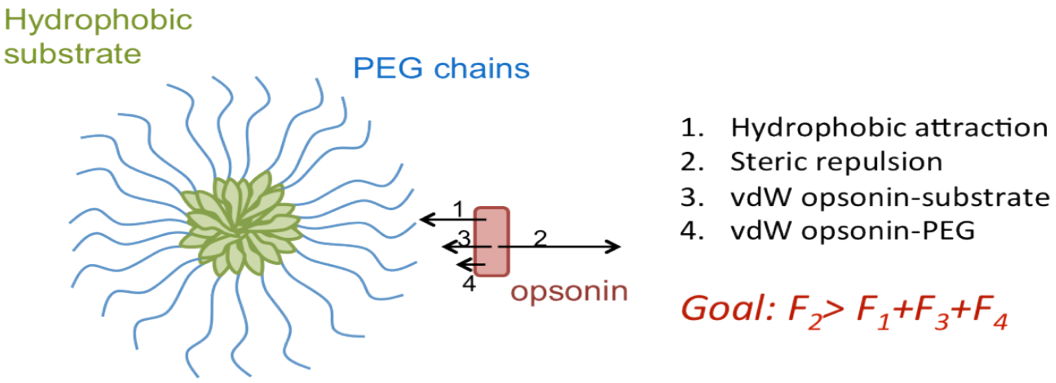

Figure 2.7: PEGylation forces model[78]

Figure 2.7 shows the forces included in the model. Jeon and Andrade suggested that a high PEG surface density and a long PEG chain length are necessary for low protein adsorption and that the effect of surface density predominates over the effect of chain

length.[107] Harris and Chess pointed out that the PEG polymer along with the associated water molecules behaves like a shield to protect the attached drug (i.e. bioactive compound) from enzyme degradation, rapid renal clearance, and interaction with cell surface proteins, limiting adverse immunological effects.[100]

2.4 Ways to Incorporate Protective Coatings

In 1995, Torchilin and coworkers presented PEG coating of liposomes by co-self assembly of PEG-*b*-PE diblock copolymers during liposome self-assembly.[86] They also coated particles by either physical adsorption of a polymer onto the particle's surface or by chemical grafting PEG chains onto the particle. Harris and Chess developed different chemistries for covalent pegylation of pharmaceuticals.[100] Other ways to incorporate protective coatings are by covalent modification of dendrimers or colloidal carriers, as well as the use of amphiphilic diblock copolymers (i.e. the corona block acts as the coating while the core block entraps or is covalently bound to the bioactive component). These methods will be discussed in the next three subsections.

2.4.1 Covalent Modification of Dendrimers

Fréchet and coworkers synthesized degradable polyester dendrimers with a bow-tie asymmetric architecture and PEG monomethyl ether segments.[62] They found that bow-tie dendrimers with M_n over 40 kDa exhibit plasma clearance half-lives greater than 24 h, which is significantly longer than linear polymer conjugates with similar M_n.[68] The

branched structure of the dendrimer may attribute to the reduced renal clearance and enhanced plasma half-lives since the dendrimers are more likely to hinder the glomerular filtration in the kidney than their linear analogues with similar M_n.[61] The conjugation of a large number of insoluble drugs to the surface of dendrimers may result in significantly increased peripheral hydrophobicity, which may subsequently lead to dendrimer aggregation and increased polydispersity. Increased hydrophobicity may also lead to enhanced elimination *via* the classical pathway. Another major risk in utilizing a highly branched or dendritic tether is overcrowding. After a certain point, continuing to increase the number of reactive functional groups in a given area may lead to overcrowding of the functional groups. In other words, if better PEG surface coverage is desired, more functional groups need to be in the last dendrimer generation in order to bind PEG chains, but if they exceed a certain number, steric hindrance will prevent PEG binding.

2.4.2 Covalent Modification of Colloidal Carriers

The use of liposome PEGylation has been studied as an approach for enhancing the delivery of parenteral chemotherapy agents.[110] Stealth liposomal doxorubicin (i.e. PEGylated liposomes) showed prolonged drug responses and favorable toxicity profile in refractory epithelial ovarian cancer in clinical trials.[111] Better therapeutic effects were also found when PEGylated liposomes were used in breast cancer treatment. [112,113] Despite these results, liposomes present some inconveniences such as limited physical stability and they are difficult to freeze-dry.

Liposomal physical stability also depends on physicochemical properties of the entrapped/covalently bound drug, especially if they it is hydrophobic.

2.4.3 Amphiphilic Block Copolymers

Amphiphilic block copolymers in which PEG is the hydrophilic block self-assemble in aqueous solutions to form micelles. When poly(ethylene glycol) is the hydrophilic block in the polymeric micelles described previously (i.e. Section 2.1.3), steric hindrance from the outer shell of PEG molecules increases the circulation time of the microparticles.[44,73,74,77,79,114-118] Polymeric micelles can accumulate in tumors after systemic administration due to the EPR effect (see Section 0). Their biodistribution is largely determined by their physical and biochemical properties, such as particle size, hydrophobicity, hydrophilicity of polymers and drugs, and surface biochemical properties.[119]

The use of amphiphilic diblock copolymers is the preferred method of particle coating due to the ease and wide variety of methods to synthesize and self-assemble diblock copolymers with tailored properties for drug delivery.[72,73,76,115,120-124]

The effect of size on polymer micelle biodistribution is organ specific and non-linear. Therefore, controlling the sizes of micelles in a predefined range can be critical for desired applications. Parameters controlling the size of micelles include relative length of polymer blocks, polymer composition, and the solvent and drug used for encapsulation.

Farokhzad and coworkers,[125] found that the volumetric size of PEG-*b*-PLGA micelles correlates linearly (linear correlation≈0.99) with polymer concentration during self-assembly. This correlation may be useful for preparing polymeric micelles with desirable sizes.

2.4.3.1.1 Configuration

The three main types of block copolymer configurations are diblock, triblock and graft. Diblock copolymers are the most commonly used configuration. However, triblock copolymers have been used as microcarriers as well.[126,127]

2.4.3.1.2 Architecture

Polymer chemistry allows the synthesis of a wide variety of molecular architectures depending on the functionality of precursors, polymerization mechanisms and other variables. The main types of polymer architectures are branched, crosslinked, linear, and cyclic. Within the branched category, there are dendrimers, hyperbranched polymers, stars, and comb polymers. Crosslinked polymers could be network or ladder. As mentioned in Section 2.3.1, architecture plays an important role in circulation time. Dendritic and globular polymers circulate longer than linear polymers of similar molecular weights. In the next subsections, other properties of polymers of different architectures will be described.

2.4.3.1.2.1 Linear *vs.* Cyclic and Hyperbranched Architecture

Molecular architecture affects the bulk and solution physical properties of polymers, even when they have the same chemical structure. In specific, cyclic polymers above the entanglement molecular mass and hyperbranched polymers have lower bulk viscosities than linear polymers.[128-131] Even small linear impurities change the properties of cyclic polymers to a high extent. Other properties of cyclic and hyperbranched *vs.* linear polymers are significantly different. In 1949, Zimm and Stockmayer defined the ratio of the mean square radius of a branched structure to that of a linear molecule (Eq. 2.1).[132]

$$g = \frac{\left\langle R_g^2 \right\rangle_{branched}}{\left\langle R_g^2 \right\rangle_{linear}} \qquad \text{(Eq. 2.1)}$$

Where $\langle R^2_g \rangle$ is the average squared distance of any point in a polymer coil from it's center of mass. Under theta conditions, "g" of ring *vs.* linear analogues have a value of 0.5.[132-135] The glass transition temperature decreases with increment of molecular weight for the case of cyclic polymers down to a plateau value, while T_g increases up to the same plateau value with increasing molecular weight for linear polymers.[136,137] Cyclic polymers diffuse faster compared to linear polymers with similar chemistry because of their smaller sizes and spherical shapes.[138-142]

Another difference between cyclic and linear polymers is end groups. Linear polymers always have end groups, whereas cyclic polymers do not have end groups, unless polymer chains are grafted onto the cyclic backbone. The lack of end groups with cyclic polymers might reduce chemical interactions with other molecules. For example, hydrophobic CH_3 end groups of monomethyl ether linear PEG activate the classical elimination pathway (i.e. C1q opsonins), while OH end groups of PEG activate the alternative elimination pathway (i.e. C3b opsonins).[85] Alternatively, cyclic PEG should not interact with C1q or C3b, leading to a better protection against opsonization. An introduction to these immune system pathways was presented in Section 2.3.2.

2.4.3.1.2.2 Hyperbranched Polymers

There are 6 main types of dendritic architectures: dendrimers, linear-dendritic hybrids, dendrigrafts or dendronized polymers, hyperbranched polymers, multi-arms star polymers and finally hypergrafted polymers. Only the first three structures have a degree of branching (DB) equal to 1.0.[143] Figure 2.8 shows the six different types of dendritic structures. The rest of this section will concentrate on hyperbranched polymers. The main differences in properties between hyperbranched polymers and linear polymers are due to the presence of branching and the large number of terminal functional groups. Two of the main properties that differentiate hyperbranched polymers from linear polymers are their high solubility in a variety of solvents and their low viscosity at similar molecular weights.[143]

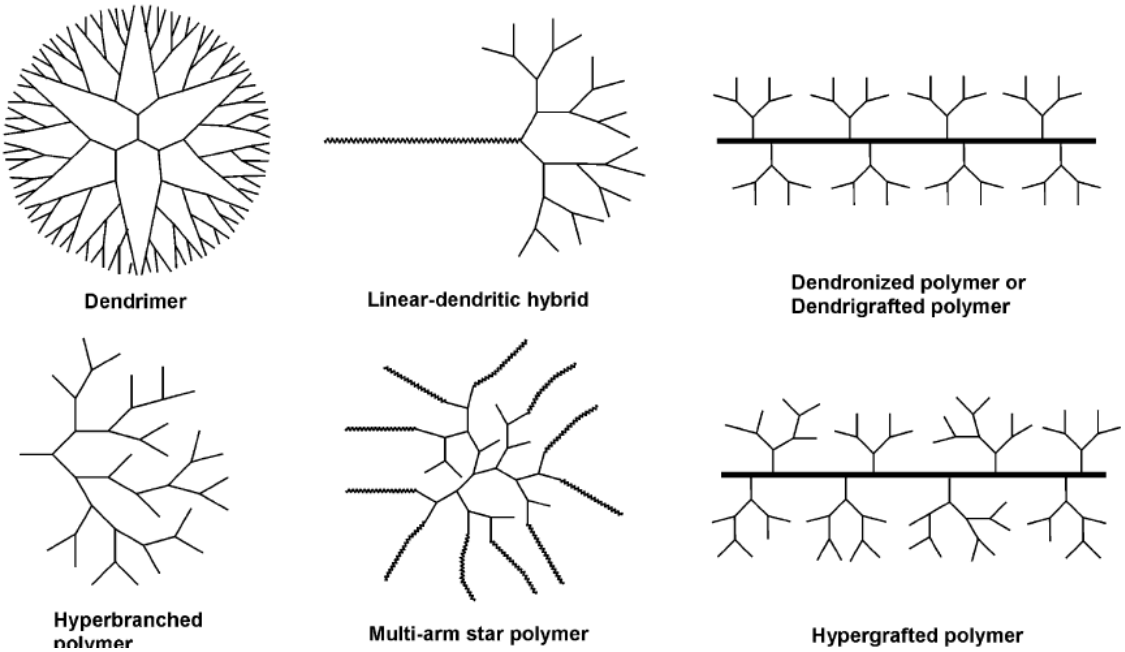

Figure 2.8: Types of dendritic structures

The term hyperbranched was coined in 1990 by Kim and Webster, who where studying ways to mimic micellar structure.[144] They prepared a hyperbranched structure by homocoupling of (3,5-dribromophenyl)boronic acid under modified Suzuki conditions.

2.5 Synthetic Methods to Produce Polyesters

Polyesters have been used since immemorial times. One example is shellac, a naturally occurring aliphatic polyester, whose usage was described in the Mahabharatha, written around 3000 B.C.[145] This biodegradable resin is a mixture of aliphatic

poly(hydroxy acid) lactones and polyesters. It was initially used in protective coatings. The success of shellac inspired Leo Bakeland in 1907 to synthesize Bakelite, one of the first polymers obtained from synthetic components. Bakelite and other phenol-formadelhyde resins have high strength and dimensional stability, combined with good resistance to impact, creep, solvents, and moisture.[146] In particular, aliphatic polyesters can be synthesized using two main synthetic approaches: polycondensation and ring-opening polymerization (ROP). This review gives a general introduction to different synthetic procedures to produce aliphatic polyesters, centered on the conditions for coordinative ROP of ε-caprolactone using tin(II) ethylhexanoate, also known as $Sn(Oct)_2$ as catalyst, including temperature, and the use of Lewis bases.

2.5.1 Polycondensation

Aliphatic polyesters can be synthesized by polycondensation of diacids and dialcohols or self-condensation of hydroxyacids. Some examples of commercially available polyesters produced by polycondensation of glycols with aliphatic dicarboxylic acids that are found under the trademark BIONOLLE are poly(butylene succinate), poly(butylenes succinate-adipate), and poly(ethylene succinate).[147] Some of the disadvantages of this procedure are the need for high temperatures (140-190 ºC), long reaction times, removal of reaction by-products, and a precise stoichiometric balance between reactive acid and hydroxy groups. Also, very high conversion is required to reach sufficiently high molecular weight for the polymer to have useful mechanical properties. Moreover, a high degree of polymerization is difficult to achieve by this

method because of side-reactions and the volatilization of monomers, which leads to a stoichiometric imbalance of reactants.

2.5.2 Ring-Opening Polymerization (ROP)

Ring-opening polymerization of lactones, cyclic diesters (lactides and glycolides) is an alternative method to polycondensation, and has been used to synthesize high molecular mass polymers under relatively mild conditions, in bulk and in solution (THF, dioxane, toluene). This polymerization method has limited side-reactions, which makes it possible to control properties like molecular weight and molecular weight distribution. These side reactions are intra- and intermolecular transesterifications. Intermolecular transesterification leads to cyclic oligomeric structures. Different methods can be used for ROP, including free radical, anionic, carbocationic, zwitterionic, enzymatic, the use of N-heterocyclic carbenes, and coordinative using metal catalysts.

The monomers that have been used for ROP include lactide, 1,4-dioxane-2,5-dione (i.e. glycolide), β-propiolactone, β-butyrolactone, γ-butyrolactone, δ-valerolactone, ε-caprolactone, 1,5-dioxepan-2-one, pivalolactone, 1,4-dioxane-2-one, 2-methylene-1,3-dioxolane, and 2-methylene-1,3-dioxepane, among others. Some of these monomeric structures are shown in Scheme 2.1.

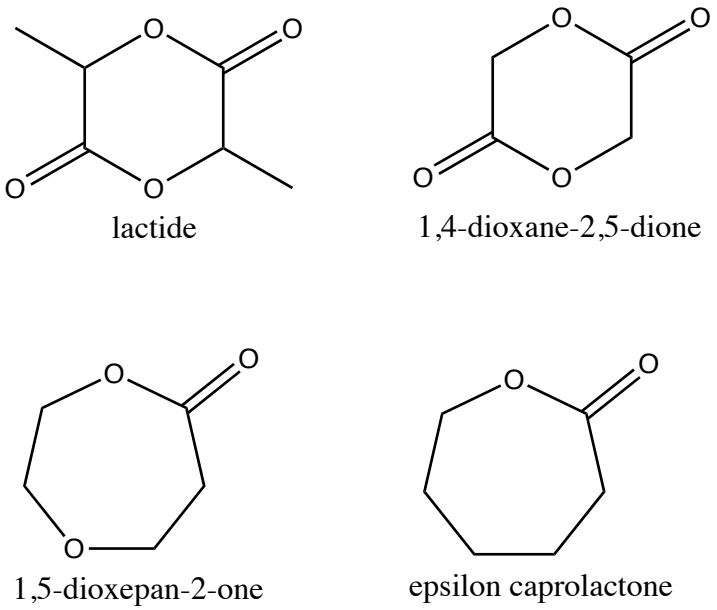

Scheme 2.1: Examples of cyclic monomers for ROP

Even though the entropy change during polymerization is negative, the polymerization is feasible due to the negative change in enthalpy. For highly strained (three and four membered) rings, the driving force is the release of angular strain (Bayer's strain). The presence of substituents at the ring carbons further increases the strain and thus increases the exothermicity of the reaction. In medium sized rings, such as ε-caprolactone, the relief of torsional strain (eclipsed interactions) and intramolecular crowding (transannular strain) is the driving force. ROP of lactones may proceed by either acyl-oxygen or alkyl-oxygen scission, as shown in Scheme 2.2.

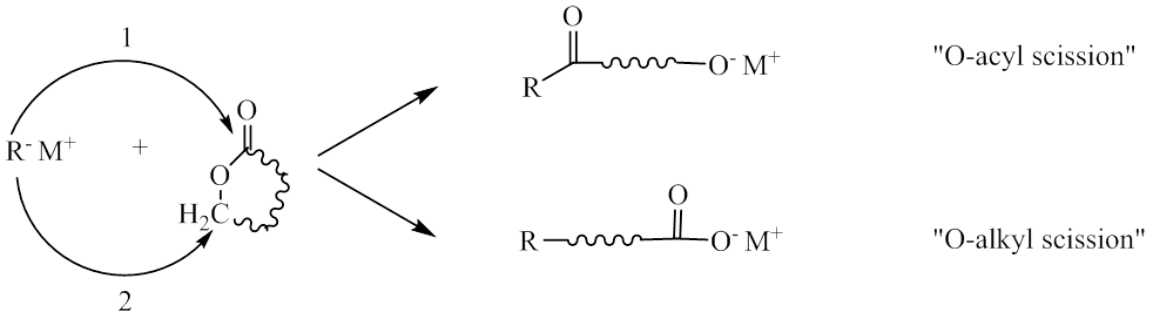

Scheme 2.2: Acyl-oxygen or Alkyl Oxygen Scission in ROP

2.5.2.1 ROP by Free Radical

ROP by the free radical method consists in the use of a free-radical initiator such as t-butyl hydroperoxide, t-butyl peroxide, and cumene hydroperoxide, with monomers that contain a vinyl group such as cyclic ketene acetals. This method has been used for the synthesis of poly(γ-butyrolactone), which cannot be prepared by the usual lactone route due to the stability of the five-membered ring towards ROP. In 1985, Bailey reviewed free radical ring closing and ring opening reactions.[148] He confirmed that the free radical ring opening polymerizations are rare. The reason for this being that unstrained five-and six-membered carbocyclic rings are usually involved in ring-closing reactions rather than ring opening.

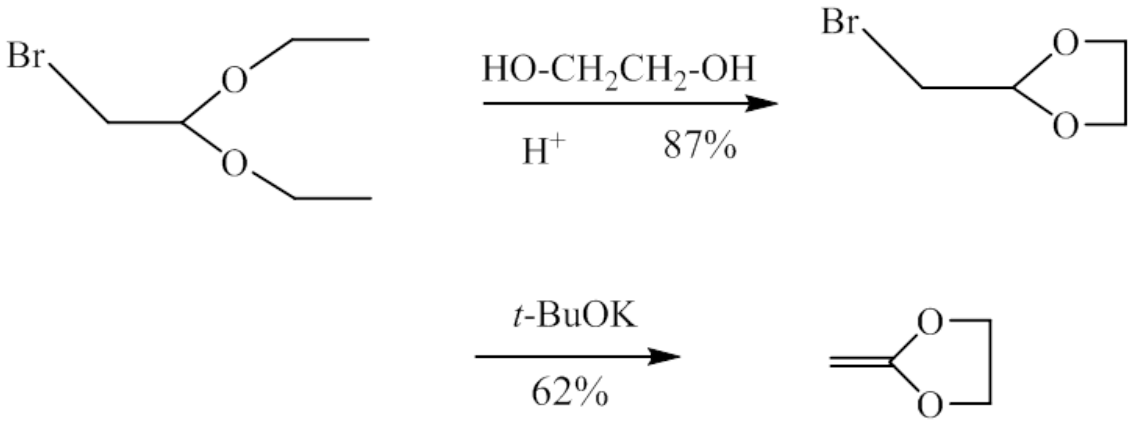

Scheme 2.3: Synthesis of 2-methylene-1,3-dioxolane

The few examples of free radical polymerization reported involve cyclopropane derivatives or highly strained bicyclic olefins. In 1948, McElvain and Curry synthesized 2-methylene-1,3-dioxolane and poly(γ-butyrolactone) using benzoyl peroxide at high temperatures as shown in Schemes 2.3 and 2.4, respectively.

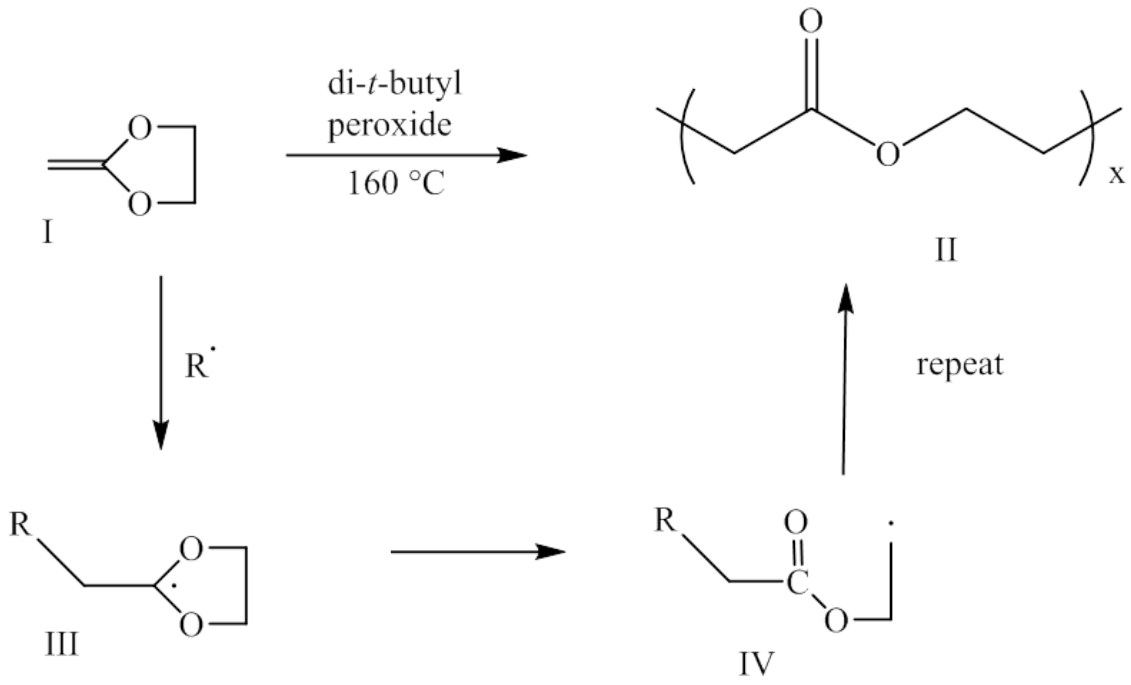

Scheme 2.4: Synthesis of Poly(gamma butyrolactone)

2.5.2.2 ROP by Anionic Mechanism

Anionic ROP uses initiators such as alkali metals, alkali metal alkoxides (lithium, sodium, or potassium), alkali metal naphthalenide complexes with crown ethers, and alkaline metals in graphite, as shown in Scheme 2.5. When the cycle contains greater than four atoms, chain growth takes place by acyl-oxygen bond scission leading to the formation of alkoxide end groups. Intra- and intermolecular transesterification reactions

in ring-opening anionic polymerization have been observed, as well as proton transfer.[149] The current interest in ionic ROP (i.e. anionic and cationic) has diminished compared to the use of coordination catalysts due to the low selectivity towards propagation.

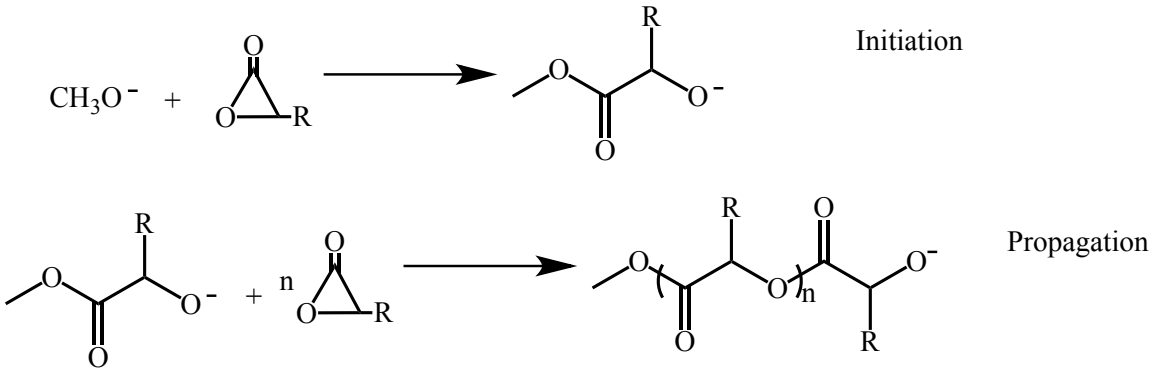

Scheme 2.5: Methoxide-initiated anionic ROP

2.5.2.1.1 ROP by Cationic Mechanism

Cationic ROP is not as efficient as anionic polymerization for obtaining high molecular weight polyesters. This is due to the higher occurrence of intramolecular transesterification (cyclization), proton and hydride transfer reactions. Initiation proceeds by the use of protonic acids (i.e. HCl, RCOOH, RSO_3), Lewis acids (i.e. $AlCl_3$, BF_3, $FeCl_3$, $ZnCl_2$) in the presence of a proton or carbenium ion source, stabilized oxocarbenium ions $[Et_3O^+BF_4^-]$, and oxocarbenium ion acylating agents $[CH_3CO]^+[OCl_4]^-$. Proton transfer to monomer, followed by ring opening and insertion into the chain, initiates the reaction when H^+ is the initiator, as shown in Scheme 2.6.[150]

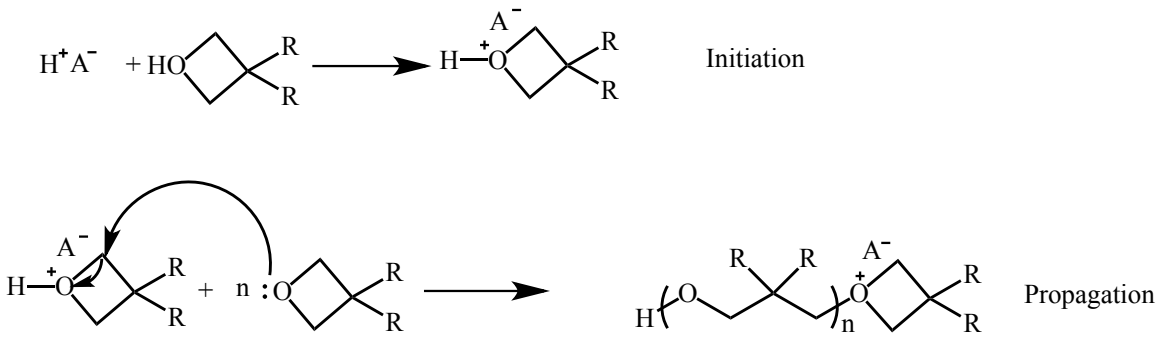

Scheme 2.6: Cationic ROP

2.5.2.1.2 *N*-Heterocyclic Carbenes

N-Heterocyclic carbenes are very efficient nucleophilic catalysts for ROP of lactones. They are attractive compared to coordinative catalysts because they do not leave metallic impurities behind, which would hinder polymer applications in medicine and microelectronics. Due to their high catalytic activity, polymerizations are carried out at lower temperatures compared to coordinative catalysts (i.e. 25-40 ºC vs. 50-130 ºC), which is also attractive commercially. The polymerization of different lactones is well controlled. For example, polymerization of 200 equivalents ε-caprolactone, using benzyl alcohol as the initiator and 1,3 dimethylimidazolium iodide as precatalyst, at 25 ºC in THF for 6 h achieved 98% conversion and gave PCL with DP_n=188 and PDI=1.16, as shown in Scheme 2.7.[151]

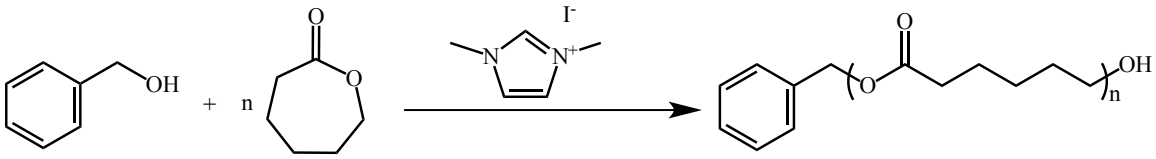

Scheme 2.7: ε-caprolactone polymerization in the presence of 1,3 dimethylimidazolium iodide

2.5.2.1.3 Coordinative Ring-Opening Polymerization

In coordinative ROP the propagating species is covalently bonded rather than ionic as in anionic and cationic ROP. As a result, the reactivity and the polymerization rate are reduced, which leads to fewer amounts of side reactions. Different organometallic initiators have been used. In coordinative ROP, metal alkoxides act as initiators. Kinetic first order in monomer and first order in initiator is observed for alkoxides generated in situ.[152]

2.5.2.1.3.1 Types of initiators

The most common initiators for coordinative ROP are dialkylaluminum alkoxides, aluminum trialkoxides, and metal carboxylates. Metal carboxylates are not accually initiators themselves but react with alcohols (and water) present in the polymerization system to give metal alkoxides that are the actual initiating species. As noted above, the most prevalent side reactions for this polymerization are inter- and intramolecular transesterification reactions. The intramolecular reactions result from

backbiting. Scheme 2.8 illustrates backbiting, which reduces the molecular weight, generates small cyclic oligomers, and broadens the polydispersity.

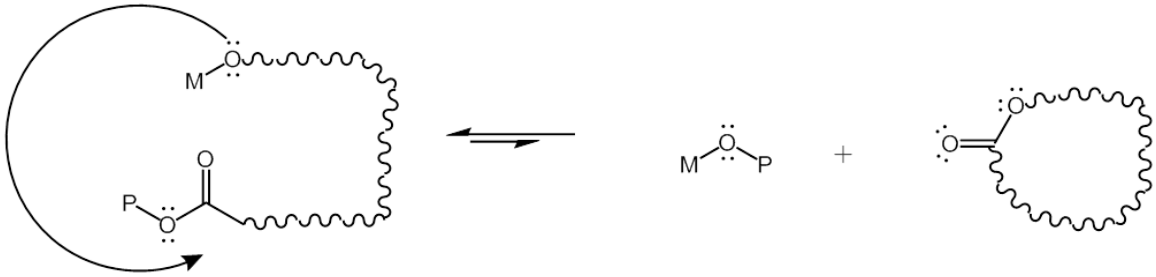

Scheme 2.8: Backbiting in Polyester Synthesis

Backbiting reactions depend both on the metal compound used as initiating species, and the ligands surrounding them. According to Agarwal and coworkers,[153] a good catalyst for coordinative ROP has bulky ligands shielding the active center from the growing polymer chain, thereby reducing transesterification reactions.

2.5.2.1.3.1.1 Dialkylaluminum alkoxides

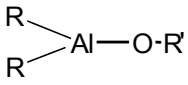

Scheme 2.9. Structure of a dialkylaluminum alkoxide

The typical structure of a dialkylaluminum alkoxide is shown in Scheme 2.9. Depending on the size of the substituents, dialkylaluminum alkoxides can be present as monomeric, dimeric, or trimeric species in solution; i.e. aggregates are in equilibrium with monomeric structures. The rate of interconversion depends on solvent, temperature, and the R and R' substituents. The aggregates are broken up in polar and nucleophilic solvents that are able to coordinate with Al atoms. If the solvent complexes stronger than the monomer itself, the "initiator" may be exclusively monomeric, but initiation may not take place at all or become very slow.

The degree of aggregation is a result of two opposing factors. Enthalpy dictates aggregation, because aggregation is exothermic. However, aggregation is endoentropic since at least translational entropy is lost when aggregates are formed. If the substituents R and/or R' are large, crowding causes repulsion and higher aggregates (e.g. trimers) cannot form. For example, diethylaluminum methoxide forms mostly a trimer, whereas diisobutylaluminum methoxide forms mostly a dimer.[149] The alkyl groups stay intact on Al and only the alkoxy group is involved in initiation. ε-Caprolactone polymerizations initiated by diethylaluminum methoxide, diethylaluminum allyloxide, and diisobutyl aluminum methoxide in THF at 20-25 ºC were well controlled with low PDI ($1.03<PDI<1.13$) and no backbiting.[154] Examples of these aluminum catalysts are shown in Scheme 2.10.

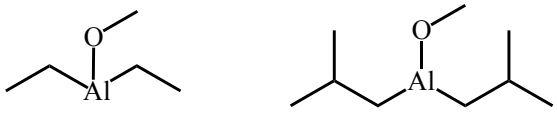

Scheme 2.10: Examples of dialkyl aluminum catalysts

These initiators would be ideal for a controlled polymerization of ε-caprolactone, except that when a particular end group is required in the polymer, that functionality need to be introduced first during the synthesis of the aluminum alkoxide initiator. For example, Hamaide and coworkers[155] synthesized an aluminum benzyl alkoxide supported on silica, and used benzyl alcohol in excess to synthesize benzyl ether-terminated PCL. Figure 1 shows how polymerization and transfer occurs. Scheme 2.11 is an interpretation of what the authors describe in their article. However, the reaction scheme presented by the authors is shown in Scheme 2.12 shows a divalent Al and appears to be a mistake. These authors do not report PDI although their GPC traces correspond to narrow MWD.

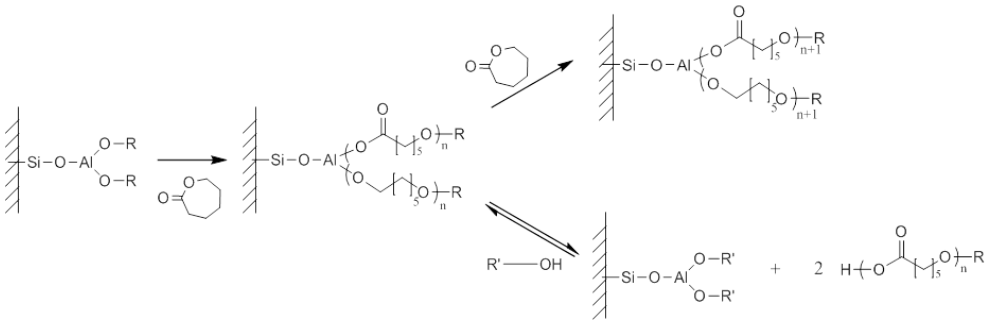

Scheme 2.11 ε-caprolactone polymerization initiated by benzyl alcohol using a heterogeneous catalyst. (Scheme drawn according to concept presented by Hamaide and coworkers.[155])

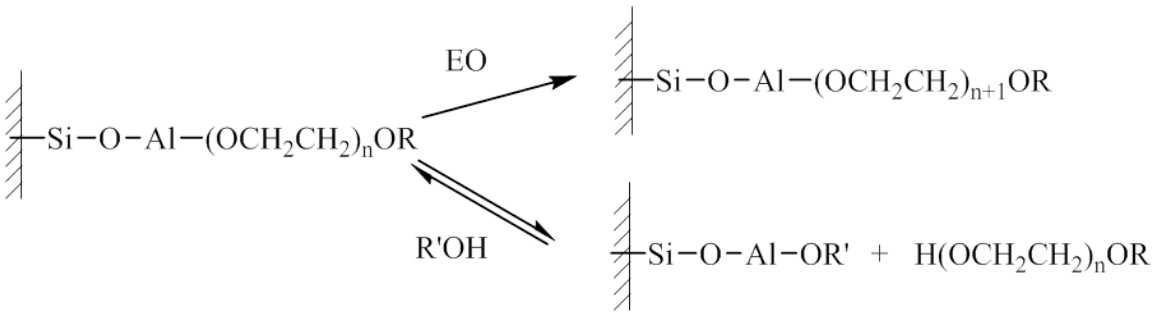

Scheme 2.12 Metal Alkoxides: Trialkoxyaluminums $Al(OR)_3$ and related compounds ($Sn(OR)_2$, $Fe(OR)_3$, $Ti(OR)_4$)

In the family of metal alkoxides, the most often used and the most thoroughly studied is aluminum tri-isopropoxide, although the highest reported molar mas obtained in fully controlled conditions, used $Sn(O^nBu)$.[156] When metal alkoxides are used as initators, all of the alkoxide groups initiate polymerization.[157] Aluminum isopropoxide exists as aggregates differing in reactivities. The rate of exchange between trimer (A_3) and tetramer (A_4) is slow enough to highly influence the kinetics of polymerization. In a mixture of A_3 and A_4, A_3 reacts with ε-caprolactone, initiating polymerization quantitatively, whereas A_4 remains almost unreacted, even after all of the ε-caprolactone has been consumed in propagation. [149,158]

Alkoxides of other metals (e.g. $Sn(O^nBu)_2$, $Fe(OEt)_3$, or $Ti(O^iPr)_4$ behave similarly to $Al(OR)_3$. Initiation of L,L-lactide with tin butoxide at 80 ºC in THF gave a

polymer with 1.12<PDI<1.84.[156] The 10^2 greater reactivity of tin(II) dialkoxides compared to Al trialkoxides can be explained by the larger ionic radius, Sn (140 picometers) compared to Al (125 picometers), 1 picometer= $1x10^{-12}$ m, resulting in a stronger polarization of the tin-oxygen bond. Sn(II) compounds are also more reactive than their Sn(IV) counterparts, which can be explained by the better steric accessibility of the tin atom in the divalent derivative and its greater ability to coordinate the approaching monomer molecule. The electron donation of four alkyl groups also decreases the reactivity of Sn(IV) towards nucleophilic agents.[156]

2.5.2.1.3.1.2 Metal Carboxylates

Carboxylates are less nucleophilic than alkoxides and apparently behave more like a catalyst than an initiator. In fact, metal carboxylates alone do not initiate polymerization.[159-162] Tin(II) 2-ethylhexanoate, $Sn(Oct)_2$, is a common example of this type of compound. However, carboxylates are not truly catalysts either. These metal compounds react with hydroxyl-containing molecules to form alkoxides, which are the actual active species. If no active hydrogen compound is added, the actual initiating species may be hydroxyl-containing impurities. Many authors have pointed how the relationship

$$DP_n = \frac{[M]_0 - [M]_{eq}}{[I]_0} \qquad \text{(Eq. 2.2)}$$

does not hold for $Sn(Oct)_2$ as a catalyst and an ROH as initiator of ROP but for alkoxides such as $Sn(O^nBu)_2$ and aluminum isopropoxide.[149,156,163] In essence, the only difference between the $Sn(OR)_2$ and the $Sn(Oct)_2$/ROH system is the presence of octanoic acid in the polymerization medium, and the fact that $Sn(OR)_2$ is preformed, whereas $Sn(Oct)_2$ and ROH react *in situ* to form the alkoxide in an equilibrium reaction. The role of octanoic acid has been studied:[159-161] it decreases the rate of polymerization, does not influence the molar mass, and can form octanoic ester end groups. The inhibiting effect is due to the reversible conversion of the active and inactive states of the growing species.[159-161] Dubois and coworkers compared the results obtained using preformed diethylaluminum alkoxides with those in which the alkoxides were synthesized *in situ.*[152] They found that the polymerization with preformed alkoxides is well controlled (i.e. 1.05<PDI<1.2) and less controlled for the *in situ* synthesized alkoxides (i.e. 1.4<PDI<1.8).[152] The authors explain the differences in results due to an exchange reaction between the aluminum alkoxide groups of the initiator and the unreacted alcohol, as shown in Scheme 2.13.

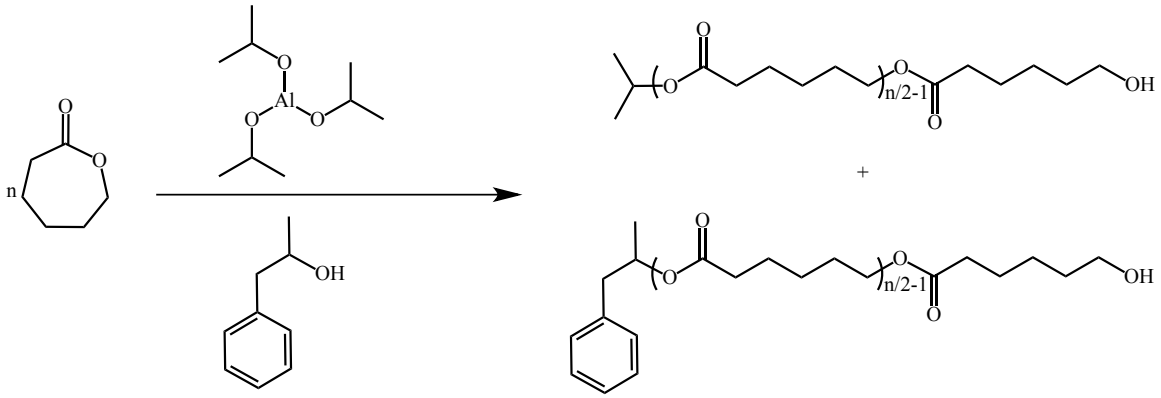

Scheme 2.13: Alcohol exchange in aluminum Alkoxide-Initiated ROP

This could explain why Eq. 2.2 usually holds when alkoxides are used as initiators, but not when metal alkoxides are used as catalysts.

The reactions proposed by Penczek and coworkers[161] to occur for the polymerization of lactones in the presence of carboxylates are show in Scheme 2.14 using CL as an example.

In Eq. 2.3, $Sn(Oct)_2$ reacts with a hydroxyl-containing compound to generate a tin alkoxide, which is the species that initates the polymerization. In Eq. 2.4, a tin dialkoxide is formed by reaction of the monoalkoxide with another ROH molecule. Eq. 2.5 is the initiation reaction with the tin alkoxide reacting with an ε-caprolactone molecule. In Eq. 2.6, the monomer reacts with the tin alkoxide chain end to propagate polymer chains. In Eq. 2.7, 2-ethylhexanoic acid (OctH) displaces the Sn alkoxide in the propagating chain to deactivate the PCL chain. This chain can be reinitiated by reaction with $Sn(Oct)_2$. In Eq. 2.8, dormant chains are reinitiated by reaction of the hydroxyl polymer end group with tin octoate. In Eq. 2.9, ROH reacts with a propagating chain, deactivating the chain and generating a tin alkoxide. ROH would serve as a chain transfer agent. This propagating chain can be reinitiated by reaction with $Sn(Oct)_2$, as in Eq. 2.3 and Eq 2.4. In Eq. 2.10, OctH reacts with the propagating chain, in an irreversible-termination, to generate a dead chain and tin hydroxide. In Eq. 2.11, the Sn hydroxide initiates a propagating chain leading to a "water-initated" polymer distribution after hydrolysis, which cleaves the bond with tin. In Eq. 2.13, ROH acts again as a chain transfer agent, but this time leads to a "water initiated" polymer distribution. Finally, in Eq. 2.14, OctH

reacts with a propagating chain leading to an irreversible-terminated polymer chain and a Sn alkoxide.

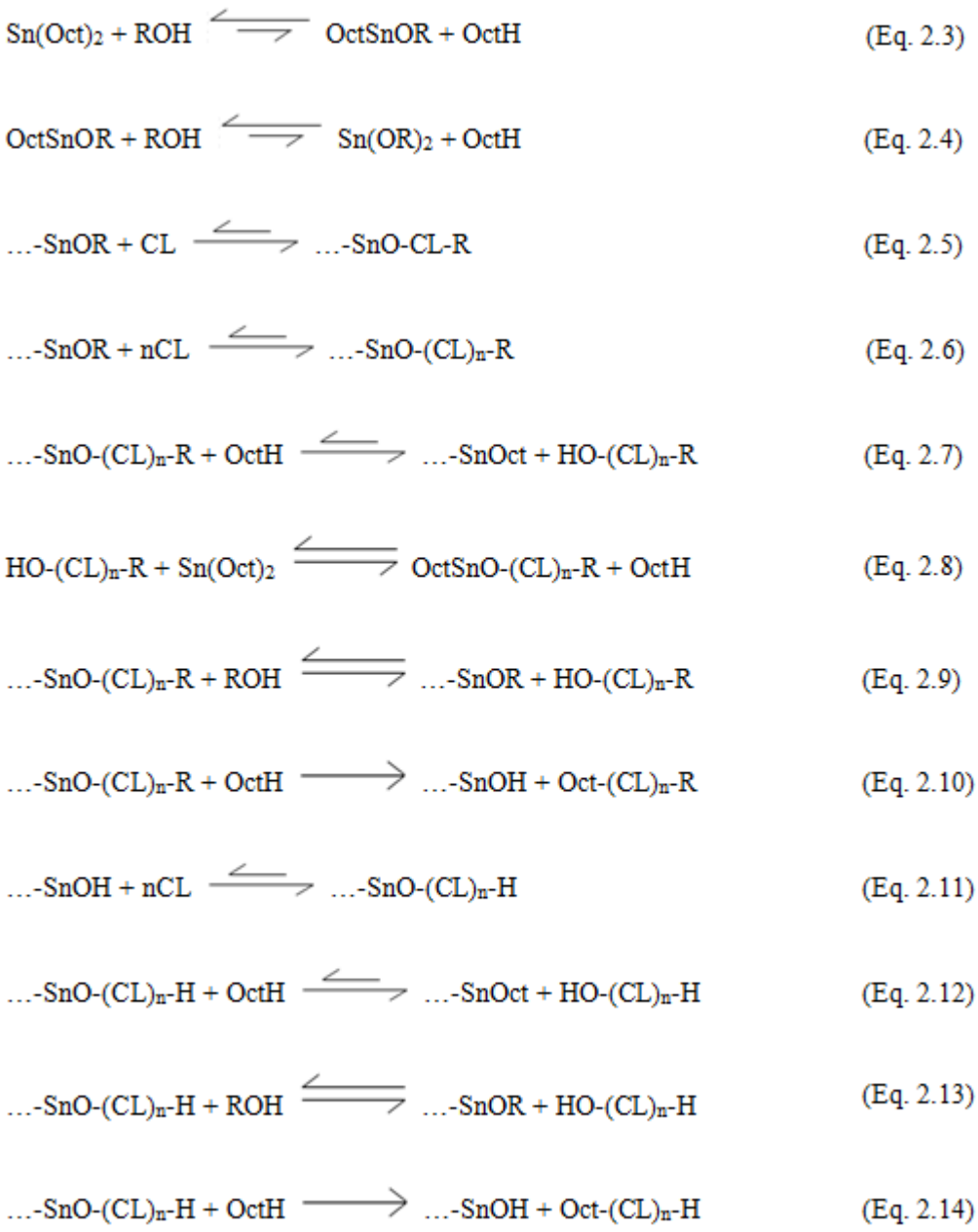

Scheme 2.14. ROP of Lactones in the Presence of Metal Carboxylates

In my experiments, the water-initiated distributions were small compared with the ROH-initiated ones, thus leaving Eqs. 2.3, 2.6, and 2.7 as the main occurring under my polymerization conditions, although Eq. 2.10 might be responsible for broadening the MWD; Eqs. 2.11 and 2.12 led to the small water-initiated distributions.

Hydroxyl chain-end esterification is observed only when the time of polymerization is much longer than the time needed to complete polymerization. Kricheldorf and coworkers[164] studied the esterification of ROH with OctH produced in the reaction of ROH with $Sn(Oct)_2$, or present as an impurity in $Sn(Oct)_2$. They first studied reaction of ROH and $Sn(Oct)_2$ at 20 ºC. They observed a rapid equilibration with liberation of OctH. At higher temperatures (i.e. up to 180 ºC, which is the temperature needed for the technical production of poly(*L*-lactide)), esterification of ROH + OctH was catalyzed by Sn^{2+} and not by the H^+ on OctH. This esterification liberated $Sn(Oct)_2$, which precipitated as SnO. SnO is a good initiator of lactide above 120 ºC. They studied different alcohols, including: benzyl alcohol, 1-decanol, triethylene glycol monomethyl ether, and neopentane diol. An interesting contribution to this area would be to study the

$$k_{eq} = \frac{[OctSnOR]\cdot[OctH]}{[ROH]\cdot[Sn(Oct)_2]} \qquad \text{(Eq. 2.15)}$$

equilibrium to be able to understand how this polymerization works and have a direct control of molecular weight by adjusting the ratio shown in Eq. 2.16.

$$\frac{CL_0 - CL_{eq}}{[ROH]_0 \cdot [Sn(Oct)_2]_0}$$ (Eq. 2.16)

Takasu and coworkers[165] polymerized ε-caprolactone using an immobilized scandium(III) trifluoromethanesulfonate [$Sc(OTf)_3$] catalyst under mild conditions. For polymerizations in toluene, with $[M]_0$ = 3 mol/L and [$Sc(OTf)_3$] = 1 mol%, the polymerization time was shortened and the polydispersity of the products was narrower when initiated by benzyl alcohol compared to those initiated by EtOH and 2-PrOH. This indicates that benzyl alcohol forms an alkoxide that provides better control over polymerization for ROP of ε-caprolactone.

2.5.2.1.3.1.3 Other Catalysts

Thomas and coworkers[166] synthesized yttrium initiators for the syndiospecific polymerization of racemic β-butyrolactone. They reported very fast polymerizations that reached 97% conversion in less than 1 minute at 20 ºC, with low PDI values lower than 1.18.

The selectivity towards propagation over transesterification (i.e. k_{pr}/k_{tr}) decreases in the following order for LA polymerization: $Sn(Oct)_2 \approx Sn(O^nBu)_2 > Al(O^iPr)_3 > Ti(O^iPr)_3 > Fe(OEt)_3 > La(O^iPr)_3 > Sm(O^iPr)_3 > MeO^-K^+$, according to Penczek and coworkers.[157]

2.5.2.1.3.2 Monomers

Lactones, lactides, and glycolides are common monomers used in ROP. Lactones are ambidentate, which means that they have two nucleophilic sites in the molecule. The carbonyl oxygen atom is the strongest nucleophile in ε-caprolactone molecule. Lactides have four nucleophilic sites per molecule, two of them are carbonyl oxygen atoms, as show in Scheme 2.15.

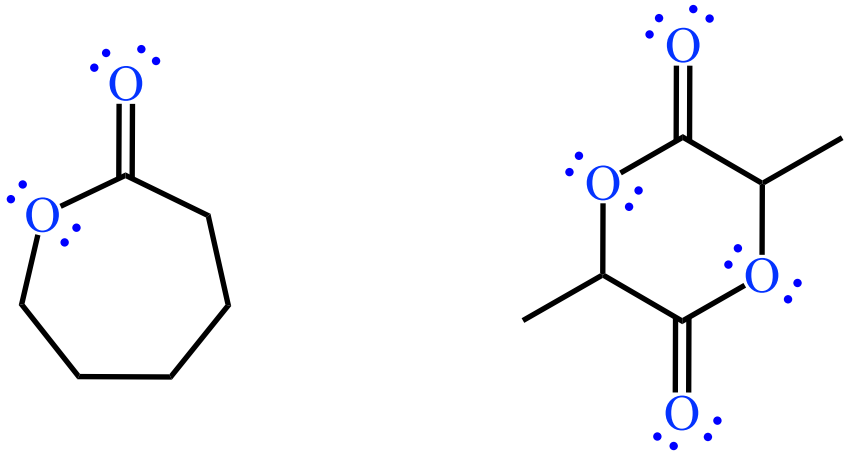

Scheme 2.15: Nucleophilic sites in e-caprolactone and lactide

2.5.2.1.3.3 Solvents and Bulk Systems

In general, polymerization is slower in bulk than in solution.[163] Also, it is more difficult to achieve complete conversions in bulk. Both phenomena are due to limited diffusion of the monomer in bulk polymer.[167] Common solvents for ROP of lactones are THF and toluene.

2.5.2.1.3.4 Temperature

Duda and coworkers synthesized PLA from L,L-lactide ROP initiated by aluminum isopropoxide in THF, with $[LA]_0 = 1\ mol \cdot L^{-1}$ and $[Al(O_iPr)_3]_0 = 0.01\ mol \cdot L^{-1}$ at different temperatures. PDI decreases with conversion up to 60% and then increases. This is consistent with the greater amount of intermolecular and intramolecular transesterification reactions competing with propagation at higher conversion due to the decreased amount of monomer. Also, the higher the temperature, the higher the PDI value for high conversions: PDI<1.2 for T < 50 ºC, PDI≈1.3 for T = 80 ºC, and PDI≈1.4. This confirms that the selectivity of the propagation reaction versus the transesterification reactions is reduced with increasing temperature.[158]

2.5.2.2 Enzymatic Polyesterification

As seen in sections 2.5.1 and 2.5.2, different basic, acidic, and organometallic initiators and catalysts are used in the synthesis of polyesters via polycondensation or ring-opening polymerization. Besides those catalytic options, enzymes have been successfully used in condensation and ring-opening polymerization. Lipases have been used for polyester syntheses from alcohols and carboxylic acids in organic solvents where the absence of water favors esterification. In this case, water must be removed efficiently to maximize conversions and molecular weights.[146] Lipases also catalyze the reaction of lactones by a similar mechanism compared to that for the enzymatic polymerization of hydroxyacids.[168-171]

2.6. Cyclization Reactions

DNA (i.e. in its cyclic form) is one of the most common cyclic polymers; it is synthesized using different enzymes such as topoisomerase I.[172] Cyclic peptides are synthesized by orthogonal coupling strategies using piperidine and benzotriazol-1-yloxytris(dimethylamino)phosphonium hexafluorophosphate (BOP). Cyclic oligosaccharides and polysaccharides are synthesized by the action of extracellular

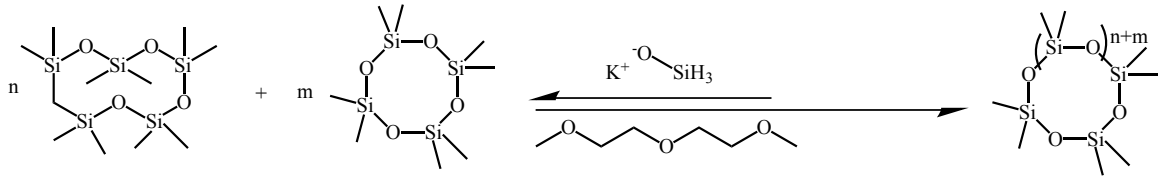

Scheme 2.16: Synthesis of cyclic PDMS

microbial enzyme cyclodextrin glucosyl transferase (CGTase) on starch.[173] In the case of synthetic polymers, cyclic polydimethylsiloxane (PDMS) is synthesized through ring-chain equilibration reactions carried under high dilution conditions, as shown in Scheme 2.16.[130]

Cyclic oligomers of polycarbonates and polyesters are synthesized under kinetically controlled conditions: phosgenation reactions; or purified from equilibrium concentrations from melt polymerization reactions.

Large crown ethers were synthesized by Williamson esterification from oligoethylene glycols by treating them with arenesulfonyl or alkanesulfonyl chlorides in

the presence of alkali metal hydroxide. Dimerization and trimerization prior to cyclization are side reactions.[174] Scheme 2.17 shows the chemical formulas.

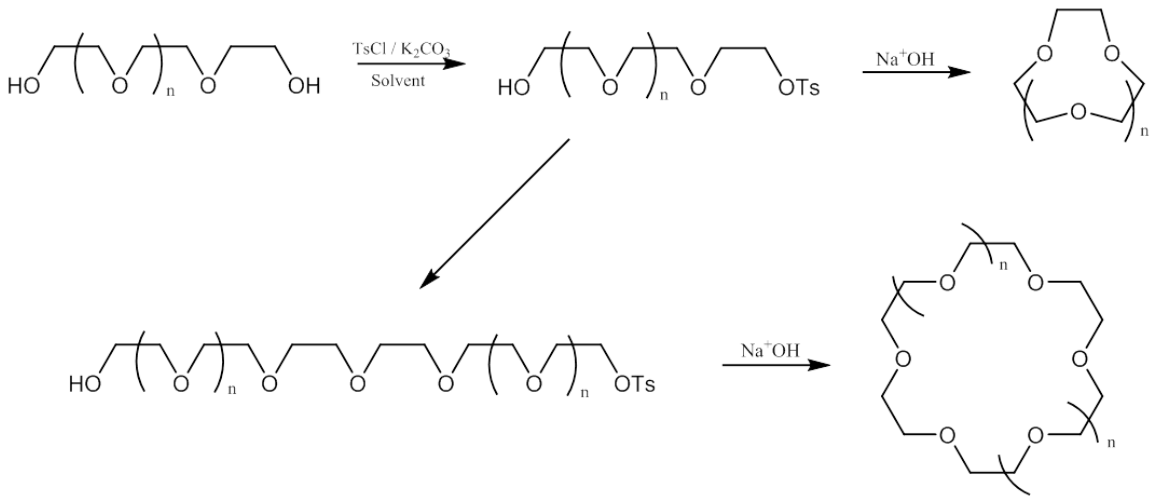

Scheme 2.17. Synthesis of crown ethers by Williamson esterification.[174]

In addition to thermodynamic stability, kinetic feasibility is important in determining the competitive position of cyclization relative to linear polymerization. The kinetic feasibility for the cyclization reaction depends on the probability of having the functional end groups of the reactant molecules approach each other. Jacobson and Stockmayer developed the random-flight model to predict the probability of cyclization as a function of chain length.[175] As the potential ring size increases, the monomers that would give rise to ring structures have many conformations, very few of which involve the two ends being adjacent. The probability of ring formation decreases as the probability of the two functional groups encountering each other decreases.[5]

2.7 Synthesis of hyperbranched polyesters with oligooxyethylene side chains

In general, hyperbranched polymers are attractive because they combine the stricture and properties of dendrimers (e.g. low viscosity, high functionality), with a much simpler synthesis.

2.7.1 Hyperbranched polymers by a chloroinimer approach

Pugh et al,[176] developed a method to synthesize hyperbranched polyacrylates that can have different free alkyl ester side chains, such as methyl, dodecyl, perfluoroalkyl, siloxane, oligooxyethylene, and mesogenic groups. The method requires the synthesis of an inimer, a molecule that contains both an initiating site and a polymerizable group. In particular, the synthesis uses D,L-serine as raw material and in 3 synthetic steps allows the synthesis of an inimer polymerizable by self-condensing vinyl polymerization (SCVP).

2.7.2 Inimers and Self Condensing Vinyl Polymerization

SCVP was first reported in 1995 by Frechet and coworkers.[177] At the time, the synthesis of hyperbranched polymers was limited to the polycondensation of AB_2 monomers. They introduced the concept of an AB vinyl monomer in which A is a vinyl group and B is a pendant group that can be activated by an external stimulus to a B* moiety that can initiate the polymerization of a vinyl monomer. Scheme 2.18 illustrates this concept.

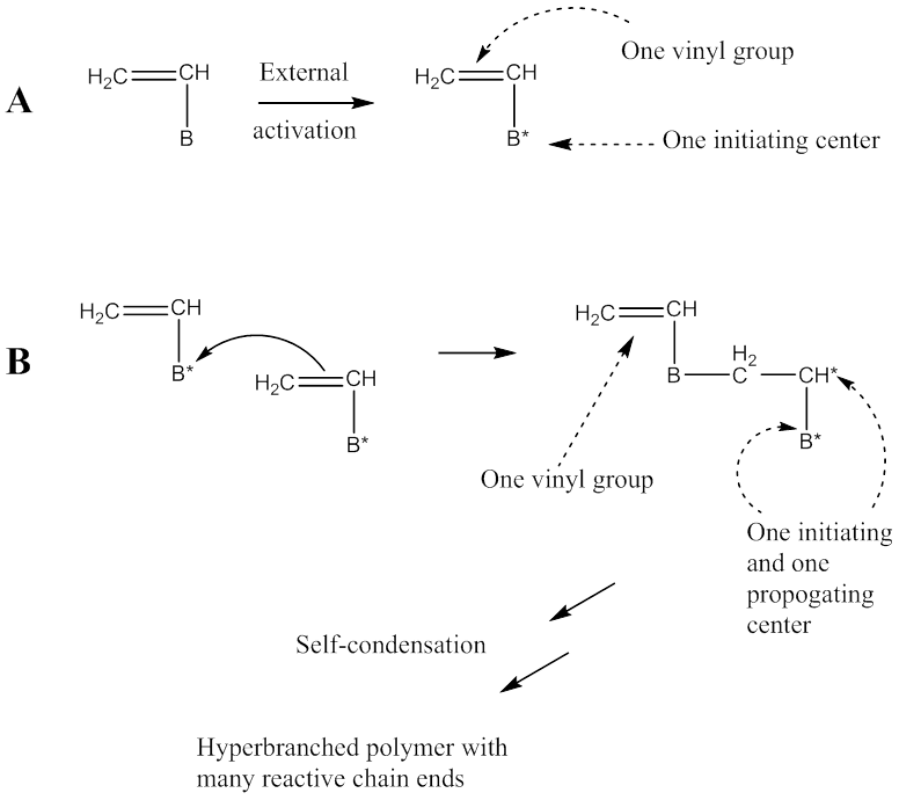

Scheme 2.18: Self-condensing vinyl polymerization[177]

The reaction of one initiating B* group with the double bond A of another AB* monomer produces a dimer with a vinyl group, an initiating center, and a propagating center. If the propagating and the initiating centers have the same reactivity, this system will behave as in a typical polycondensation with an AB_2 monomer. Therefore, the polyrmerization is called self-condensing vinyl polymerization since is a hybrid of classical polycondensations and vinyl polymerizations.

Müller and coworkers also studied the SCVP of inimers.[178,179] They focused their studies on the resulting molecular weight distribution and the degree of branching.

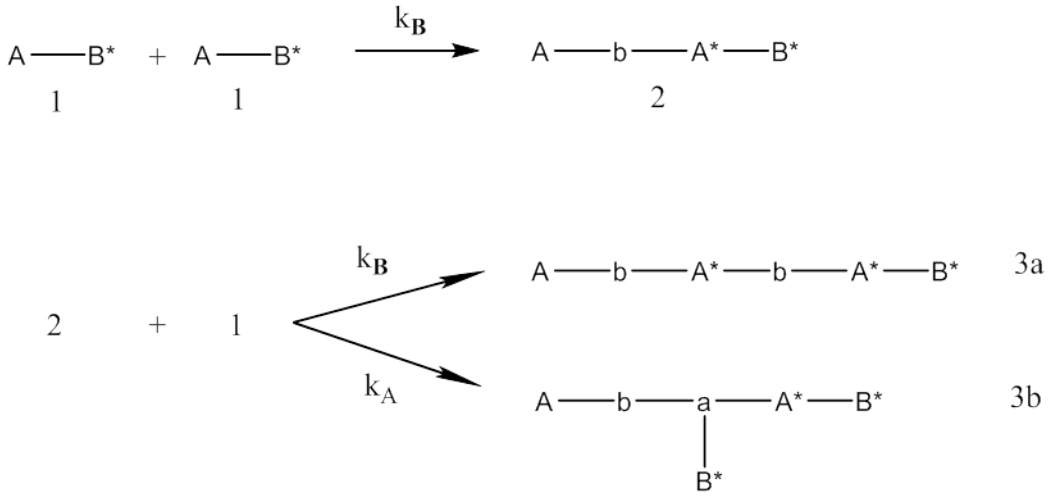

Scheme 2.19. Branching origin on SCVP

As seen in Scheme 2.19, the dimer produced by the reaction of an initiating B* group with the double bond of another AB* monomer has two active sites A* and B*. Either A* or B* can react with the vinyl group of another molecule with rate constants k_A and k_B, respectively. If the vinyl group adds to a terminal A* or B* center, a linear linkage is produced. In contrast, vinyl group addition to a side group B* or an A* center within the polymer backbone leads to a branching point. Ideally, all molecules possess exactly one double bond, and the number of active sites is equal to the number of monomer units.

Some important characteristics of this type of polymerization is that the polydispersity is broad (PDI>2) are usually obtained and increases as the polymerization proceeds.

2.7.3 Controlled/Living Polymerizations

In typical chain polymerizations, the lifetime of propagating radicals is limited by bimolecular termination and chain transfer. In 1956, Michael Szwarc discovered how to eliminate these two side reactions, which allowed the synthesis of well-defined polymers; these polymerizations are referred to as living polymerizations.[180] They allow the control of molecular weight and architecture, and the synthesis of block copolymers by the sequential addition of different monomers, among other advantages.[146] Szwarc's living anionic polymerization demanded fast initiation and relatively slow propagation in order to achieve low polydispersity (PDI). These requirements were achieved with the use of alkyl lithium initiators in non-polar solvents via dissociation of ion pairs or their aggregates. This technique also requires the use of special high vacuum techniques to minimize traces of moisture and air. In 1974, more than a decade later, Penczek and coworkers studied the living cationic ring-opening polymerization of THF and later extended it to other heterocyclic monomers.[181,182] While studying living anionic polymerization, Michael Szwarc also studied radical processes along with carbon-halogen bond dissociation energies.[183] At that time, free radical polymerization was also being studied, in particular how to control the overall radical polymerization rate through inhibition/retardation, for example using cupric chloride in DMF.[184] These attempts failed

to control molecular weights or molecular weight distributions and did not yield block copolymers due to the short lifetime of the growing chains (i.e. ~1 s). In typical radical polymerizations, inefficient initiation and bimolecular radical-radical coupling/disproportionation termination reactions are the main challenges that prevent control over molecular weight and PDI. Therefore, in order to better control the polymerization control, the termination rate must be much slower than propagation. Since termination is a second order reaction with respect to radical concentration while propagation is first order, the rate of termination becomes slower than that of propagation at very low radical concentrations.

Controlled radical polymerizations (CRP) focus on reducing the concentration of radicals by the establishment of a dynamic equilibrium between propagating radicals and various dormant species. Radicals may be either reversibly trapped in a deactivation/activation process or involved in a reversible, degenerative transfer process. The persistent radical effect (PRE) mediates radical trapping in deactivation/activation processes.[185] This is a self-regulating mechanism in which propagating radicals are rapidly trapped in a deactivation process by a stable radical or an organometallic species.[186] In systems that follow PRE, a steady state of growing radicals is established through the activation-deactivation process rather than initiation-termination as in conventional radical polymerization. These systems include nitroxide-mediated polymerization (NMP)[187] and cobalt mediated radical polymerization (CMRP)[188] in which the mediating species should be in stoichiometric amount since the trapping agent caps all dormant chains.

Systems that follow degenerative transfer follow typical radical polymerization kinetics with slow initiation and fast termination. The concentration of transfer agent is much larger than that of radical initiators. The transfer agent plays the role of the dormant species. The monomer is consumed by a very small concentration of radicals, which can terminate but also degeneratively exchange with the dormant species. Therefore, the transfer agent plays the role of the dormant species. In degenerative transfer, alkyl iodides are used as transfer agents; however, the most popular degenerative transfer is the specialized radical addition-fragmentation chain transfer (RAFT) in which a chain transfer agent such as cumyldithiobenzoate or a xanthate is used.[146]

2.7.4 Atom Transfer Radical Polymerization

Atom transfer radical polymerization (ATRP) is another example of a controlled radical polymerization that operates via the PRE. In contrast to NMP and CMRP, this is a catalytic process employing atom transfer between growing chains and a redox active catalyst. The amount of metal catalyst is usually substoichiometric. This catalyst consists of a transition metal species that can expand its coordination sphere and increase its oxidation number, and a ligand that complexes with the metal center.

Scheme 2.20 illustrates the definition of ATRP, using Cu as an example metal; however, a variety of other metals have also been used successfully for ATRP, including Ti, Mo, Re, Fe, Ru, Os, Rh, Co, Ni, and Pd.[186]

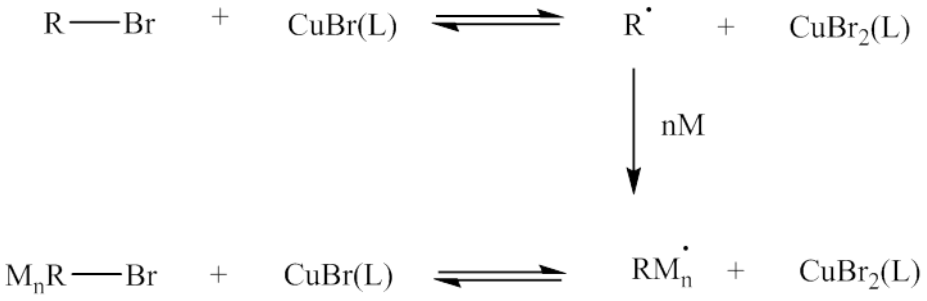

Scheme 2.20: ATRP definition

One of the advantages of ATRP over other controlled radical polymerizations include the commercial availability of all necessary ATRP reagents. The dynamic equilibrium between dormant species and propagating radicals can also be tuned by modifying the complexing ligand for the catalyst. The denticity of ATRP chelating ligands is in the range of 2-4 with rates constants of activation usually increasing with denticity. Other ligand characteristics such as the linking unit between the heteroatoms (always nitrogen), the topology of the ligand, and the bulkiness of the steric center also have an important effect on activation.[186]

2.7.4.1 Modified ARTP Initiating Systems

Despite the previously mentioned advantages of ATRP, its use for certain applications has been limited for different reasons. For example, special handling procedures are required to remove all oxygen and oxidants from systems that employ highly active catalysts. Many of the transition metal complexes are generally considered mildly toxic, requiring extensive post- polymerization purification of the product.

Table 2.2: Relative Reagent Concentrations in Different Types of ATRP

Method	M / *R*-*X* / $Cu^{I}X$ / $Cu^{II}X$	*L*	RA	AIBN
Normal ATRP	200/1/1/—	1	—	—
Reverse ATRP	200/—/—/1	1	—	0.5
SR&NI ATRP	200/1/—/0.2	0.2	—	0.1
AGET ATRP	200/1/—/0.2	0.2	0.18	—
ARGET ATRP	200/1/—/<0.01	0.1	<0.1	—
ICAR ATRP	200/1/—/<0.01	0.01	—	<0.1

Different initiating systems have been designed to circumvent these problems. The relative concentrations of monomer, initiator, metal salt, ligand, reducing agent, and free radical initiator in a polymerization are summarized in Table 2.2.[186]

2.7.4.1.1 Reverse ATRP

In reverse ATRP, the ATRP initiator and Cu(I) are generated in situ from conventional radical initiators (e.g. AIBN) and Cu(II), as shown in Scheme 2.21. Since the transferable halogen atom is added as a part of the copper catalyst in reverse ATRP, the catalyst concentration must be comparable to the concentration of initiator and cannot be independently lowered. Reverse ATRP limits the terminal functionality remaining on the initiator residue to that present on the standard free radical initiator.

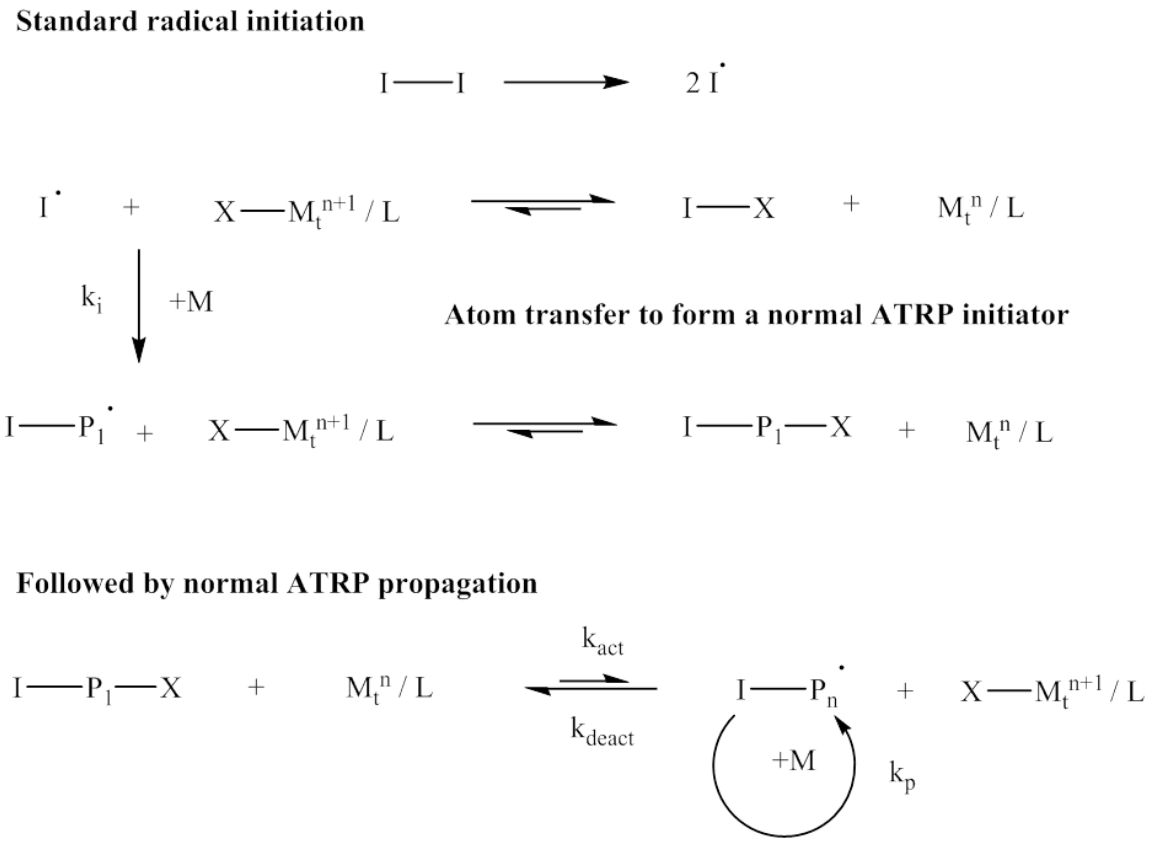

Scheme 2.21: Reverse ATRP Definition

2.7.4.1.2 Simultaneous Reverse and Normal Initiation (SR&NI)

SR&NI is a dual initiating system that has both a standard free radical initiator and a transferable atom or group. Radicals generated by AIBN (i.e. or another free radical initiator) are subsequently deactivated by and oxidatively stable CuX_2 catalyst forming CuX and some halogenated chains. CuX can then reactivate the alkyl halide initiator and concurrently mediate normal ATRP.

2.7.4.1.3 Activators Generated by Electron Transfer (AGET)

In this technique, reducing agents that are unable to initiate new chains (i.e. instead of organic radicals) are used to reduce the higher oxidation state transition metal complex, as shown on Scheme 2.22. No homopolymers are produced when this technique is used for the synthesis of block copolymers. Some of the reducing agents that have been used are tin (II) octoate, ascorbic acid, and triethylamine. This technique is particularly useful in aqueous and miniemulsion systems.

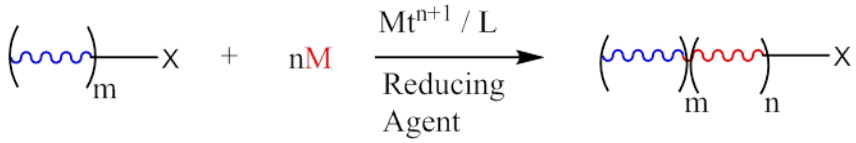

Scheme 2.22: ARGET ATRP

2.7.4.1.4 Activators Regenerated by Electron Transfer (ARGET)

In this technique, a reducing agent is used to regenerate CuX species from CuX_2 throughout the polymerization, instead of a quick CuX regeneration in the case of AGET, where nearly stoichiometric amounts of radicals and non-radical generating reducing radicals are used. Scheme 2.23 shows the ARGET definition. ARGET reduces the amount of necessary Cu catalyst from several thousand ppm under normal conditions to <50 ppm. The reduction of copper concentration not only simplifies the post polymerization purification process, but also makes the process more environmentally friendly since smaller quantities of catalyst need to be removed and disposed of.

Additionally, the catalyst and excess reducing agent can effectively scavenge and remove dissolved oxygen from the polymerization system.

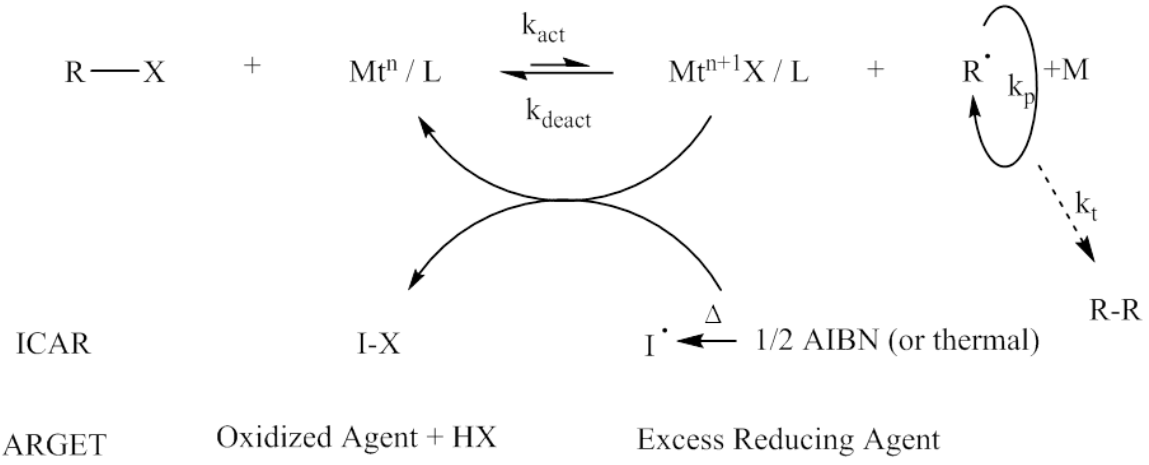

Scheme 2.23: ARGET and ICAR ATRP Definitions

2.7.4.1.5 Initiators for Continuous Activator Regeneration (ICAR)

In this technique, free radicals are slowly and continuously generated by conventional radical initiators to constantly reduce CuX_2, which accumulates as a persistent radical, and regenerates CuX. Scheme 2.23 shows the ICAR definition. One of the main differences between ICAR and SR&NI procedures is that a large excess of free radical is used in CuX_2 reduction, and the radicals are slowly generated over the course of the polymerization, in an analogous fashion as ARGET *vs.* AGET. Similarly, the amount of copper used in this technique is reduced with the advantages that were mentioned previously.

2.7.5 ATRP in Aqueous Systems

In addition to reducing the amount of catalyst used, polymerizations can be "greener" by the elimination of solvents or by the replacement of organic solvents with innocuous solvents such as water.[189] The use of water in ATRP systems has certain problems, including: (i) high equilibrium constant between active and dormant species, which produces high radical concentrations and many dead chains; (ii) partial dissociation of X-Cu^{2+}/L deactivator to free halide and Cu^{2+}/L complex; (iii) certain ligands dissociate from Cu complexes or cause Cu^{1+} species to disproportionate, and (iv) carbon-halogen bonds can hydrolyze.[186] Some ways to solve these problems are to: (i) add an excess of halide salt (e.g. tetraethylammonium bromide) to promote the reformation of deactivator complex; (ii) use certain ligands (e.g. TPMA) to prevent disproportionation; and (iii) mix water with organic solvents such as acetonitrile to reduce the equilibrium constant and reduce disproportionation. Figure 2.9 shows the predicted and experimental ATRP equilibrium constants in different solvents.

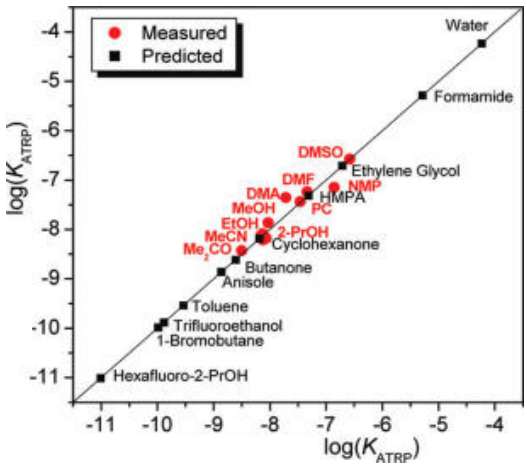

Figure 2.9: Predicted and experimental ATRP equilibrium constants in different solvents[187]

The ATRP equilibrium constant is four orders of magnitude larger in water than in acetonitrile.[190] Figure 2.10 shows the increase of the disproportionation constant in acetonitrile-water mixture with increasing water concentration. [191]

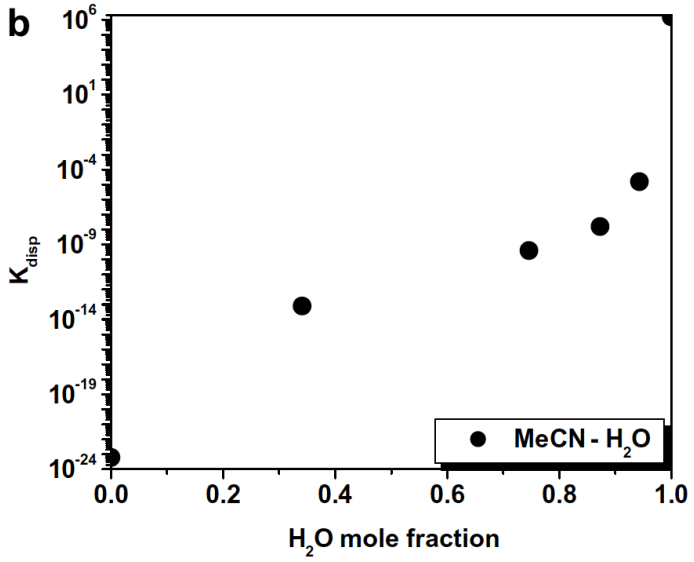

Figure 2.10: Disproportionation constant *vs.* water mole fraction in acetonitrile-water mixtures [188]

2.7.5.1 ARGET in Aqueous Systems

Matyjaszewski and coworkers polymerized oligo(ethylene oxide) methyl ether methacrylate (OEOMA) by ARGET ATRP in water using tris(2-pyridylmethyl)-amine (TPMA) as ligand.[192] Due to the high solubility of ascorbic acid in water, there is a loss of polymerization control when ascorbic acid is added all at once due to the high concentration of radicals produced. As a result, ascorbic acid is added continuously as a solution throughout the polymerization to provide an acceptable rate of polymerization

and good control of polymer properties (M_n and narrow PDI). These authors found polymerization conditions that provided first order kinetics in monomer, linear evolution of the molecular weight with conversion, and polymers with PDI<1.3.

2.7.5.2. ICAR in Aqueous Systems

Matyjaszewski and coworkers also developed conditions for polymerizing oligo(ethylene oxide) methyl ether acrylate by ICAR ATRP in water.[193] Since AIBN is not water soluble and has a high 10 h half-life decomposition temperature, 2,2'-azobis[2-(2-imidazolin-2-yl)propane]dihydrochloride (VA-044) was used as free radical initiator. They obtained polymers with low PDI (i.e. 1.15-1.28) using 20-100 ppm of an active CuBr/tris(pyridine-2-ylmethyl)amine-based catalyst in the presence of excess bromide anions at 44 °C.

2.8 Biodegradation

2.8.1 Significance

As with other polyesters, polycaprolactone is degraded by hydrolysis of its ester linkages. In particular, polycaprolactone is useful for preparing long-term implantable devices, due to its degradation, which is even slower than that of polylactide. By copolymerizing lactide and ε-caprolactone, the biodegradation rate can be tuned, as demonstrated by Wang and coworkers.[194] The biodegradation of polyesters is autocalalyzed. The liberated carboxylic acid end groups catalyze the hydrolysis, i.e. the

cleavage of additional ester groups.[195] The dynamics of polycaprolactone's degradation under different conditions was studied by Lam and coworkers.[196] Polycaprolactone biodegradation occurs in two phases. In the first phase, there is no mass loss but a reduction in the M_n in the range of 200,000 to 5000. The second phase is characterized by a decrease in the rate of chain scission and the onset of weight loss. This has been attributed to an increased probability that chain scission of a low molecular weight polymer will produce a fragment small enough to diffuse out of the polymer bulk and the breakup of the polymer mass to produce smaller particles with an increased probability of phagocytosis.[196] The decrease in the rate of chain scission is associated with an increase in crystallinity, since cleavage takes place in the amorphous region of the polymer.[5]

2.8.2 Studies

There are different experiments to determine the biodegradation profile (surface erodible or bulk), biodegradation time, and toxicity of degradation byproducts. The *in vivo* degradation process can be studied by implanting polycaprolactone-^{14}C in rats and measuring the radioactivity in urine, feces, expired air and the residual activity at the implant site. The only metabolites found upon degradation were ε-hydroxycaproic acid and tritiated water. The mechanism of bioabsorption was studied by Wang and coworkers[1] using electron microscopic examination of the tissue at the implant site. This study revealed the presence of intracellular polymer particles and demonstrated the role of phagocytosis in the final stage of polymer degradation.

Discher and coworkers studied the degradation of PLA and PCL polymersomes upon hydrolysis.[53] The particles were incubated in sodium hydroxide solutions for different incubation times until total destruction, and then neutralized by adding phosphate buffer. The optical densities of these solutions (OD1) were measured after addition of iodine complexation agent. Control experiments were performed with water instead of sodium hydroxide (OD2), and water instead of particle suspensions (OD3). OD1-OD3 is a measure of the amount of PEG detached during the degradation process. Encapsulated PEG chains that were not on the surface were not accessible to the iodine complexation agent.[197]

2.9 Block Copolymer Micelles

According to Eisenberg and coworkers,[121] the greatest contributions to the area of block copolymer micelles have been made by Kavanov and Kataoka. Kavanov studied micelles from Pluronic™ triblock copolymers as delivery vehicles for drug targeting across the blood brain barrier.[198] Kataoka's group, however, has mainly focused on micelles formed from copolymers containing a poly(amino acid) core-forming block.[79]

Amphiphilic diblock copolymers self assemble into micelles or vesicles depending on different characteristics of the system and process variables. In water the hydrophobic blocks form the core of the micelle, while the hydrophilic block forms the corona, when the concentration of block copolymer exceeds the critical micelle concentration (CMC).

3.9.1 Important Micelle Parameters

The stability of drug-entrapped self-assembled micelles depends primarily on the value of CMC, the glass transition temperature of the core block, the ratio between the hydrophobic and the hydrophilic blocks, and the conjugated drug content.[121]

Table 2.3 presents the relation between these factors and the micelle stability.[121] For example, the lower the CMC is, the higher the micelle stability. This relationship follows common sense, since the lower the CMC, the micelle will be able to stand higher dilution conditions and still be at a concentration higher than the CMC. The glass transition temperature is particularly important for the block that is in the micelle core.

If the core has a glass transition temperature above the use temperature, it will give structural stability to the micelle even below the CMC due to the formation of physical crosslinks.[199] In the case of water as the continuous phase, a higher hydrophobic to hydrophilic ratio for a constant hydrophobic block length will decrease the CMC, increasing stability. Higher hydrophobic to hydrophilic ratio also changes the micelle morphology from a hairy micelle to a crew-cut micelle. Figure 2.11 shows a schematic of these two morphologies. Finally, an increased conjugated drug content will favor formation of physical crosslinks in the core, increasing stability.

Table 2.3: Main factors that affect the thermodynamic or kinetic stability of block copolymer micelles

Parameter		Micelle stability
CMC	Low	↑
	High	↓
Tg	Low	↓
	High	↑
Hydrophobic-hydrophilic block ratio	Low	↓
	High	↑
Conjugated drug content	Low	↓
	High	↑

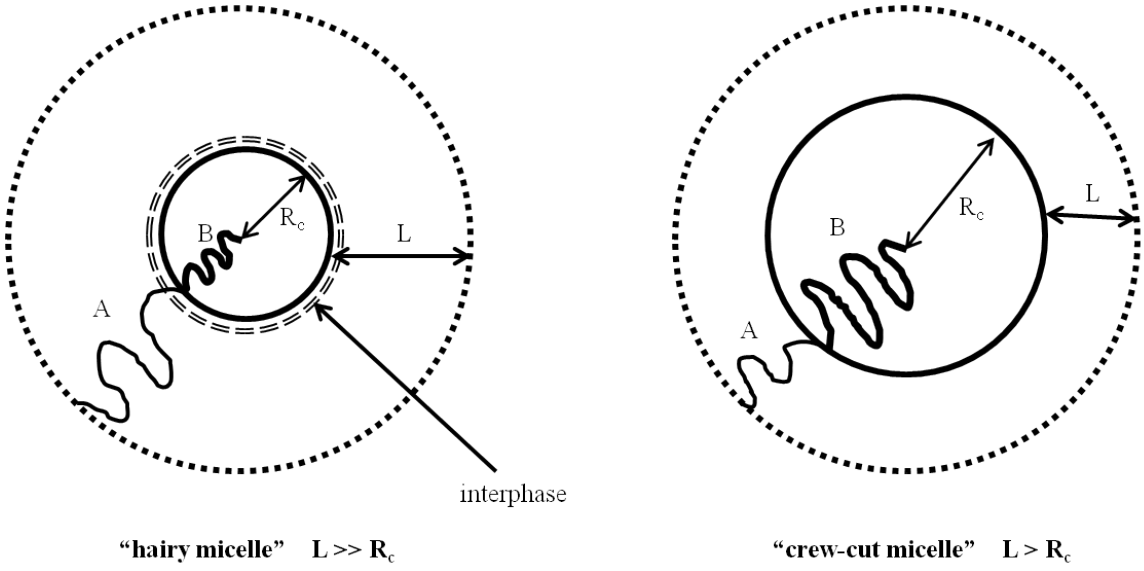

"hairy micelle" $L >> R_c$ **"crew-cut micelle" $L > R_c$**

Figure 2.11: Schematic representation of AB diblock copolymer micelles in a selective solvent for the A block. R_c: core radius, L: corona thickness[200]

3.9.2 Micelle Preparation Methods

Two types of techniques are most commonly used to prepare block copolymer micellar systems. In the first type, the block copolymer is first dissolved in a good solvent for both blocks and then the conditions of the system such as temperature or solvent composition are changed to promote the formation of micelles.[200,201] The second type of technique is the direct dissolution method.

2.9.2.1 Micelle Techniques with Former Dissolution in Organic Solvent

This section will describe dialysis and co-solvent evaporation method. As mentioned before, in these methods the amphiphilic diblock copolymer is first dissolved in a common solvent. After that, the selective solvent is added slowly to promote the self-assembly process. Finally, the common solvent is removed by dialysis or evaporation. Another possibility to promote self-assembly from the common solvent is to change the temperature. The latter method is feasible for those systems in which the solubility of only one of the copolymer blocks is significantly reduced by changes in temperature.

2.9.2.1.1 Dialysis

This method is commonly used for copolymers that are not very soluble in water. The polymer solution is placed in a dialysis bag and then immersed in an excess of precipitant (i.e. water in the case of micelles with hydrophobic core), allowing the common solvent to be gradually replaced by the selective solvent. This technique is

preferred when the common solvent has a high boiling point, such as DMF and DMSO, making challenging the elimination of this solvent by evaporation.[72,75,123,202-206] According to Jerome and coworkers,[205] the dialysis method is not reproducible and leads to very large and polydispersed particles (~1 μm).

2.9.2.1.2 Co-solvent Evaporation

Usually a bad solvent for one of the blocks is added slowly, following stripping the common solvent.[200] An alternative technique is to add the polymer solution to a large volume of the precipitant, followed by stripping the solvent. As an example, Lavasanifar and coworkers encapsulated cyclosporine in PEG-*b*-PCL diblock copolymers using acetone as good solvent for both blocks and water as a precipitant for the PCL block. They either added water to the polymer solution in acetone or the polymer solution to water and did not find major differences in the micelles prepared.[207] Table 2.4 shows the size and polydispersity of the micelles obtained.

Table 2.4: Characteristics of PEG-*b*-PCL block copolymer micelles prepared changing the order of addition of non-solvent. [203]

Order of addition	Ratio (organic: aqueous)	Average diameter of particles ± S.D. (nm)	PI
Acetone to water	1:2	87.8 ± 9.4	0.11
	1:6	63.0 ± 4.0$^{\alpha}$	0.142
Water to acetone	1:2	74.9 ± 1.9$^{\alpha}$	0.087
	1:6	57.2 ± 9.8$^{\alpha,\beta}$	0.117

$^{\alpha}$ Significantly different from 1:2 (p<0.05).
$^{\beta}$ Not significantly different from "acetone to water".

2.9.2.2 Direct Dissolution Method

In this technique, a solid sample of the copolymer is directly dissolved in the selective solvent. The micellar suspension is annealed by standing or by thermal treatment, usually through ultrasonic agitation. Sometimes the copolymer and water are mixed at high temperatures to favor micellization.[208]

3.9.3 PEG-*b*-PCL Micelles

Due to the biocompatibility properties of polycaprolactone for drug delivery applications and the stealth properties provided by PEG, PEG-*b*-PCL copolymers been widely studied. [72,73,75,76,115,120-124,202-206,209-214] A wide range of PEG molecular weights has been used. The lowest molecular weights were around 1.5-2.5 k Da,[75,76,121-124,206] intermediate molecular weights were around 3-5k Da,[72,73,115,120,122,202-206,209-211,213,215-217] and high molecular weights were around 10-13k Da.[120,206,216] Yang and coworkers present an exceptionally large PEG molecular weight of 31k Da.[212] In water, the PEG block forms the micelle corona, thereby affecting protein adsorption and thus biodistribution as mentioned in Section 2.3.3. As mentioned by Owens and Peppas,[11] the exact thickness of the hydrophilic PEG layer required to prevent protein adsorption depends on each particular system and on other factors such as surface chain density and conformation. At low surface coverage the PEG chains will have a larger range of motion taking a "mushroom" morphology where the PEG chains are mostly located closer to the surface of the particle. However, density that is too low will lead to gaps in the

hydrophilic layer where opsonins will freely bind to the nanoparticle surface. At very high PEG surface density, the PEG chains will adopt a "brush configuration" where the range of motion is restricted, decreasing the steric hindrance properties of the PEG layer. The two preferred methods of PEG-*b*-PCL micelle preparation are dialysis[72,73,75,76,120,123,202-206,215,218] and co-solvent evaporation.[115,122,124,210-212,216,217] Jérôme and coworkers studied the effect of the organic solvent used for micelle preparation using DMSO, THF, DMF, and dimethylacetamide (DMAc) on micelle size.[205] The smallest micelles were prepared in DMAc, followed by DMF, DMSO, and THF. They found that the closer the solvent solubility parameter resembled the PCL solubility parameter (~20.4), the larger the micelle. Table 2.5 shows the solvent viscosities, dielectric constants, solubility parameters for polymers and solvents used in PEG-*b*-PCL micelle preparation. These authors found that besides solubility parameters, other factors such as solvent viscosity and boiling point affected micelle size. For example, even though DMSO has the highest solubility parameter among the solvents studied, DMAc provided the smallest micelles. This is due to the high DMSO viscosity, which leads to a slower water-organic phase mixing and thus lower self-assembly rate.[219]

Table 2.5: Dielectric constant (ε), dynamic viscosity (η), and solubility parameters (δ) of solvents and polymers used for in PEG-*b*-PCL self-assembled micelles

	ε	η[a] (N s/m^2)	δ (J/cm^3)$^{1/2}$	δ_{Hoy}[b] (J/cm^3)$^{1/2}$	$\delta_{VanKrevelen}$[b] (J/cm^3)$^{1/2}$
DMSO	46.68	2.0	26.6-26.7		
DMAc	37.78	0.92	22.1-22.8		
THF	7.58	0.36	19.5		
DMF	36.71	0.80	24.9		
H2O	80.37	0.89	47.9-48.1		
PEO			20.2	21.46	21.58
PCL			/	20.38	20.97

(a) Measured at 25 °C
(b) Calculated according to [219]

3.9.4 Micelle Characterization

According to Eisenberg and coworkers, [121,205] the micelle properties that affect their efficiency as drug delivery carriers for hydrophobic drugs are size, size distribution, and CMC.

2.9.4.1 Size and Size Distribution

The most popular methods to measure size and size distribution are dynamic light scattering (DLS), static light scattering (MALLS), and scanning electron microscopy (SEM).

2.9.4.1.1 Dynamic Light Scattering (DLS)

Also known as quasi-elastic light scattering (QELS) or Photon Correlation Spectroscopy (PCS), this technique is used to determine the mean diameter of nanospheres and to follow their aggregation-deaggregation behavior. [9,220] The term dynamic indicates that the method gives information about the movement of the scattering particle. It is also referred to as quasielastic since the photons are scattered quasielastically by moving particles. Finally, most scattering techniques employ autocorrelation; hence the term correlation is employed.[221] This technique uses Brownian motion to measure the size of the particles. Oriented particles create interference patterns, each bright spot being a speckle. The speckle pattern moves as the particle moves, creating flickering. All the motions and measurements are described by correlation functions. $G_2(\tau)$ is the intensity correlation function that describes particle motion (i.e. experimental correlation function) and $g_1(\tau)$ is the electric field correlation function that describes measured fluctuations. Eq. 2.17 relates the two intensities. A is a background term related to the baseline value and B is an instrument-dependent factor. The electric field correlation function is an instrument-dependent factor.

$$G_2(\tau) = A + Bg_1^2(\tau) \qquad \text{Eq. 2.17}$$

The electric field correlation function of a monodisperse sample decays exponentially, decaying as shown in Eq. 2.18 where Γ is the decay constant.

$$g_1(\tau) = \exp(-\Gamma\tau) \qquad \text{Eq. 2.18}$$

The decay constant Γ is linearly related to the translational diffusion coefficient D_T of the particle according to Eq. 2.19,

$$\Gamma = D_T q^2 \qquad \text{Eq. 2.19}$$

where q is the modulus of the scattering vector and is given by Eq. 2.20,

$$q = \frac{4\pi n}{\lambda_0}\sin(\theta/2) \qquad \text{Eq. 2.20}$$

where n is the refractive index of the dispersion medium, θ the scattering angle (rad), and λ_0 the wavelength of the incident light in vacuum. Dynamic light scattering provides the particle diffusion coefficient, not the size. In the case of noninteracting, spherically-shaped, smooth, and rigid particles, the Stokes-Einstein equation (Eq. 2.21) correlates the diffusion coefficient with the size,

$$D = \frac{kT}{3\pi\eta d} \qquad \text{Eq. 2.21}$$

where k is the Boltzman's constant, T is the absolute temperature, η is the viscosity, and d is the apparent Stokes-Einstein particle diameter.

In the case of polydisperse samples, the electric field correlation function is an intensity-weighted sum of autocorrelation functions of the particles contributing to the scattering (Eq. 2.22),

$$g_1(\tau) = \int_0^\infty C(\Gamma)\exp(-\Gamma\tau)d\Gamma \qquad \text{Eq. 2.22}$$

where C(Γ) represents the distribution of decay rates. Eq. 2.22 is an ill-conditioned Laplace transform that has no definite solution. Several different size distributions will fit the measured autocorrelation. The measured data is usually contaminated by noise; therefore the baseline has to be evaluated and experimental uncertainties circumvented. Sophisticated methods have been developed for data analysis, including the cumulant method, a constrained regularization method (CONTIN), non-negative least squares (NNLS), the maximum entropy method (MEM), and the singular value analysis and reconstruction method (SVR).

CONTIN is a constrained regularization method developed by Provencher[222] and provide several numerical solutions to the particle size distribution. The best answer is selected using other evidence. The results are sensitive to the estimated baseline and may depend on the range of particle sizes measured.

2.9.4.1.2 Static Light Scattering (MALLS)

Static light scattering is also called elastic scattering, or multiangle laser light scattering.[223] In this technique, a dispersion is illuminated with a collimated beam, usually laser radiation, and the time-averaged intensity of scattered light as a function of the scattering angle is measured. The theories of light scattering are divided into three regimes depending on particle size: $D<\lambda/10$, $\lambda/20<D<\lambda$, and $D\geq\lambda$. For the smallest particles, the Rayleigh equation relates the particle polarizability to the intensity of the unpolarized incident light, its wavelength, the scattering angle, the scattered intensity, the distance from the sample, and the number of non absorbing particles in a unit volume. After the particle polarizability is obtained, the radius of the particle can be obtained taking into account the ratio of the refractive index of the particle to the surrounding medium. For the particles of intermediate size, the Rayleigh-Gans-Debye (RGD) equation applies and takes into account the fact that the scattering pattern is no longer symmetric about the line corresponding to the 90° scattering angle, but favors forward scattering over back scattering. Finally, the Mie theory applies for the largest particles. In this regime, the scattering behavior is more complex than in the RGD regime: the intensity exhibits maxima and minima at various scattering angles, as a function of the size parameter $\pi D/\lambda$ and the refractive index of the particle.[221] Using a MALLS set up, the intensity of scattered light as a function of incident angle can be measured for different micellar concentrations to determine the absolute molecular weight of a micelle and calculate its aggregation number (i.e. number of molecules per micelle) using a Berry or a Zimm Plot.

Eq. 2.23 shows the Zimm equation. By plotting Kc/R_θ as a function of $1/P(\theta)$ and making two extrapolations, Mw can be obtained.

$$\frac{Kc}{R_\theta} = \left(\frac{1}{\overline{M_w}} + 2A_2c\right)\frac{1}{P(\theta)} \qquad \text{Eq. 2.23}$$

2.9.4.1.3 Scanning Electron Microscopy (SEM)

Electron microscopy uses a beam of electrons to illuminate the sample.[224] Due to the very short wavelength of electrons, the resolving power of an electron microscope exceeds that of an optical microscope by about 200 times. The resolution is a function of the wavelength, which in turn depends on the accelerating voltage. The maximum magnification is above 200,000x but such high electron beam intensity may damage the sample. Usually the magnification is below 100,000x and the accelerating voltage is typically below 100-200 kV. Another advantage of electron microscopy is the increased depth of field, usually about 10 μm or about 10 times that of an optical microscope. Electron microscopy can be operated in transmission mode (TEM) or by scanning the surface of the specimen (SEM). SEM can show particle topography by scanning a very narrowly focused electron beam across the particle surface. The electron beam is directed normally or obliquely at the surface. The back-scattered or secondary electrons are detected in a raster pattern and displayed on a monitor screen. The secondary electrons are released by the sample upon impact of the electron beam. The image obtained from these secondary electrons exhibits good three-dimensional detail and is the main one used. However, the secondary electrons can reveal inside details of cavities in the surface

since the path of secondary electrons can be curved because of their low energy. To collect secondary electrons, the surface of the specimen is observed at an angle usually 30 to 45°.[221]

2.9.4.2 Critical Micelle Concentration (CMC)

As mentioned before, one of the preferred methods to prepare PEG-*b*-PCL self-assembled micelles is through co-solvent evaporation. A polymer solution is slowly added to a selective solvent, usually water. At the beginning of the addition, the water is transparent, because the water-soluble block and the organic solvent keep the block copolymer in solution. Upon further polymer addition, the liquid becomes cloudy, indicating the formation of micelles. The minimum block copolymer concentration required for the copolymer to form micelles in equilibrium with a small population of single chains is known as the critical micelle concentration (CMC). The organization of block copolymers into micelles changes the properties of the suspension drastically, which is reflected by a discontinuity in the suspension properties as a function of concentration at CMC. Different methods that measure suspension properties as a function of concentration can be used to determine CMC, including measuring the surface tension, electric conductivity, static or dynamic light scattering, refractive index, and the specific heat or heat of dilution.[225] In Figure 2.12 shows the CMC as the point in which the normalized intensity *vs.* concentration curve shows discontinuity.

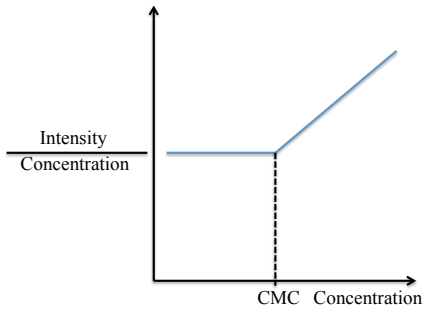

Figure 2.12: CMC Determination by Static Light Scattering

The CMC is a function of the nature and length of the hydrophobic block, the length of the hydrophilic block, and the total molecular weight of the copolymer. As mentioned in section 3.9.1, an increase in the hydrophobicity of the core-forming block or an increase on the molecular weight of this block reduces the CMC and thus increases the thermodynamic stability of the micelles.[121] Once formed, the micelles can remain kinetically stable for extended periods of time, even at concentrations below CMC, depending on their glass transition temperature and/or melting temperature if the core-forming block is semicrystalline.[226] In the case of PEG-*b*-PCL diblock copolymers, low CMC values were obtained (i.e. 10^{-8} to 10^{-7} M) over a wide range of molecular weights. These low CMC values impart micelle stability upon dilution.[115,120,121,206,215-217]

CHAPTER III

EXPERIMENTAL SECTION

3.1 Materials

Acetonitrile (Acros Organics, anhydrous), bovine serum albumin (BSA) (Sigma-Aldrich, lyophilized powder), D,L-serine (Alfa-Aesar, 99%), 3,4-dihydroxybenzaldehyde (Acros Organics, 97%), ethanol (Pharmco-Aaper, 200 proof absolute), fluorescein-labeled bovine serum albumin (Molecular Probes, 100%), 4-hydroxybenzyl alcohol (Sigma-Aldrich, 99%), hydrochloric acid (Fisher Scientific, 37.2%), potassium chloride monobasic (BHD, 99%), postassium phosphate (Fisher, 99.7%), KOH (Sigma-Aldrich, ≥ 85 %), methanesulfonyl chloride (Aldrich, 99.5%), sodium chloride (Sigma-Aldrich, 99%), sodium phosphate dibasic Na_2HPO_4 (Fisher, 99.9%), *N,N*-diisopropylethylamine-DIPEA (AK Scientific, 99%), potassium carbonate (Sigma-Aldrich, 99%), rhodamine lactone (Acros Organics, 99%), sodium nitrite (Alfa Aesar, 98%), and tin octoate (Aldrich. 94%) were used as received.

ε-Caprolactone (Acros Organics, 99%) was dried by distillation from CaH_2 prior to use. Dichloromethane (CH_2Cl_2) was dried by distillation from CaH_2. Diethylene glycol monoethyl ether (Aldrich, 99%) was dried by distillation from CaH_2 (Fluka, 95%) and

stored over 4 Å molecular sieves. PEG600 (Sigma–Aldrich) and PEG550 were azeotropically dried from toluene solutions prior to use. Sodium borohydride (Sigma-Aldrich, 98%) was stored in the drybox and used as received. Reagent grade tetrahydrofuran (THF) was dried by distillation from purple sodium benzophenone ketyl under N_2. *p*-Toluenesulfonic acid monohydrate (Mallinckrodt, organic reagent) was dried in a vacuum oven overnight at 30 ºC. Triethylamine (Sigma-Aldrich, 99%) was dried by distillation from KOH under nitrogen and was stored over KOH pellets. Ultrapure water (Synergy system) was deionized (the water resistivity was 18.2 M.cm @25 °C) and filtered through a 0.22 um PTFE filter. All other reagents and solvents were commercially available and used as received.

3.2 Techniques

All reactions were performed under a N_2 atmosphere using a Schlenk line or a Vacuum Atmospheres drybox unless noted otherwise. Silica gel (Sorbent Technologies, 63-200 mm mesh size, 60 Å pore size) was used for column chromatography. ^{1}H NMR and ^{13}C NMR spectra (δ, ppm) were recorded on either a Varian Mercury 300 (300 MHz and 75 MHz, respectively), or an INOVA 500 (500 MHz and 125 MHz, respectively) spectrometer. All spectra were recorded in $CDCl_3$ unless mentioned otherwise, and the resonances were measured relative to the residual solvent resonances and referenced to tetramethylsilane (0.00 ppm). Number- (M_n) and weight average (M_w) molecular weights relative to linear polystyrene (GPC_{Pst}) and polydispersities (PDI=M_w/M_n) were determined by gel permeation chromatography (GPC) from calibration curves of log M_n

vs. elution volume at 35 ºC using THF as solvent (1.0 mL/min), a set of 50 Å, 100 Å, 500 Å, 10^4Å, and linear (50-10^4 Å) Styragel 5 μm columns, a Waters 410 differential refractometer, and Millenium Empower 2 software. All samples (approximately 0.5 g/L) were dissolved overnight and filtered through a 0.45 μm PTFE filter.

For self-assembly experiments, acetone was filtered three times through a 0.45 μm Scientific Tisch PTFE membrane filter. The block copolymers used for self-assembly were diluted in acetone and the solutions were filtered three times through 0.45 μm PTFE filter, the acetone was then removed under vacuum before the polymers were used for self-assembly experiments. The vials, tubes and bottles used for self-assembly experiments were rinsed with filtered solvents. Phosphate buffer saline solution (PBS) was prepared by dissolving NaCl (2.0 g, 34 mmol), KCl (50 mg, 0.67 mmol), Na_2HPO_4*$7H_2O$ (0.68 g, 2.5 mmol), and KH_2PO_4 (60 mg, 0.44 mmol) into MilliQ Water or ultrapure water (200 mL and brought to 250 mL at the end), according to a standard recipe.[227] PBS and MilliQ Water used for self-assembly were filtered 3x through 0.45 μm ThermoScientific polyethersulfone membrane filters.

Micellar sizes and polydispersities were measured by dynamic light scattering (DLS) using a Brookhaven Instrument coupled with a BI-200SM goniometer, BI-9000AT correlator, and an EMI-9863 photomultiplier tube for photon counting. A Meller Griot 35 mW He-Ne laser (637 nm) was used as the light source. For each sample, measurements were taken in triplicate for 10 min each time at a 90° angle at 25 °C. BIC DLS software version 3.40 was used to obtain the hydrodynamic radius of PEG-*b*-PCL

micelles. The data was analyzed in terms of volume-weighted and number-weighted distributions. For samples that contained more than one size population, the average and standard deviation of each size population within a sample was calculated for the three acquisitions. Averages of the three acquisitions were reported as the final values for each size population. A cylindrical glass scattering cell with a diameter of 12 mm was placed at the center of the thermostated bath, and decahydronaphthalene was used for refractive index matching.

A Perkin-Elmer Pyris 1 differential scanning calorimeter was used to determine Tg values, which were read as the middle of the change in heat capacity. The reported Tg values of the polymers and copolymers are the mean values from the second and third heating scans. All heating and cooling rates were 10 °C/min. Transition temperatures were calibrated using indium and zinc standards.

Matrix-assisted laser desorption ionization time of flight mass spectrometry (MALDI ToF-MS) experiments were carried out on a Bruker Ultraflex III TOF/TOF mass spectrometer (Bruker Daltonics, Inc., Billarica, MA), equipped with a Nd:YAG laser (355 nm). All spectra were measured in positive reflector mode using 22% of the laser power and a pulsed ion extraction time of 10 ns. The instrument was calibrated prior to each measurement with an external PMMA standard. The preparation of the samples analyzed involved the following steps. THF solutions of the matrix, *trans*-2-[3-(4-*tert*-butylphenyl)-2-methyl-2-propenylidene]malononitrile (DCTB, 20 mg/mL) and the cationizing agent, potassium trifluoroacetic acid (KTFA, 10 mg/mL) in THF were mixed

in a 10:1 ratio, and 0.5 μL of the final mixture was deposited on microliter plate wells (MTP 384-well ground steel plate). After the spots were dried, 0.5 μL of a solution of the polymer in chloroform (10 mg/mL) was deposited on top of the matrix and salt layer.

Micelle pictures were taken using a transmission electron microscope (TEM Philips TECNAI) with an accelerating voltage of 120 kV. To observe micelle morphologies, a drop of the original micelle solution was placed on a Formvar/carbon-coated grid. The excess solution was blotted away with a Kimwipe. The grids were dried at room temperature and atmospheric pressure for several hours before examination in the TEM.

Fluorescence correlation spectroscopy (FCS) and fluorescence cross-correlation spectroscopy (FCCS) measurements of fluorescently labeled micelles, fluorescently labeled proteins and their mixtures were taken on a customized inverted microscope (Nikon Eclipse Ti, Toyko, Japan) in Professor Adam Smith's laboratory at The University of Akron. A SuperK continuum white light laser (NKT Photonics, Birkerod, Denmark) was the source for fluorescence excitation. The repetition rate of the laser was set to 10 MHz with an internal pulse picker. The output of the laser passed through a commercial wavelength splitter that isolated a 488 nm (±10nm) beam and a 450-800 nm beam, from the remainder of the infrared light. The 488 nm light passed through a cleanup filter (LL01-488-12.5, Semrock, Rochester, NY) and then was coupled to an 18 m single-mode optical fiber (QPMJ-3AF3U-488-3.5/125-3AS-18-1-SP, OZ Optics, Ottawa, Ontario). A 561 nm beam is isolated from the 450-800 nm beam (z405/561rpc,

Chroma Technology Corp, Bellows Falls, VT), passed through a cleanup filter (LL02-561-12.5, Semrock, Rochester, NY), and then coupled into a 3 m single-mode optical fiber (QPMJ-3AF3U-488-3.5/125-3AS-3-1-SP, OZ Optics, Ottawa, Ontario). As the beams exited the fibers, they were collimated with identical infinity corrected objective lenses (L-10x, Newport, Irvine, CA). The two beams were overlapped using a 503 nm cut-off dichroic beamsplitter (LM01-503-25, Semrock, Rochester, NY) before entering the optical path of the microscope via a laser TIRF filter cube (91032, Chroma Technology Corp. Bellows Falls, VT) with a two-color dichroic mirror and laser-blocking filter (zt488/561rpc and zet488/561m, Chroma Technology Corp. Bellows Falls, VT). A 100× TIRF objective, NA 1.49, (Nikon Corp., Tokyo, Japan) focused the excitation beam into the sample and the emitted fluorescence was directed into a custom-built detection module. The fluorescence signal passed through a 50 μm confocal pinhole (Thorlabs, Newton, NJ) placed at the image plane of the microscope. The light was collimated with a 100 mm focal length achromatic lens (AC254-100-A-ML, Thorlabs Inc., Newton, NJ) and then spectrally separated with a 560 nm long-pass beam splitter (FF560-FDi01-25x36, Semrock, Rochester, NY). Each signal beam was filtered (520/44nm[FF01-520/44-25]; 612/69nm[FF01-621/69-25], Semrock, Rochester, NY) and then focused onto the detector with an achromatic, 25 mm focal length lens (APAC18, Newport, Irvine, CA). The detectors were single photon avalanche diodes (SPAD) with a 50 mm active area, 30 ps timing resolution and 25 dark counts per second (Micro Photon Devices, Bolzano, Italy). A time-correlated single photon-counting (TCSPC) device recorded each photon arrival time (PicoQuant, TimeHarp 200, Berlin, Germany). The samples were kept at room temperature in a coverglass-bottom 96-well plate (Nunc

265300, Thermo Scientific, Waltham, MA) sample chamber during data acquisition. All images were taken with the Photometrics Evolve Electron Multiplying Charge Coupled Device (EMCCD) (Photometrics, Tucson, AZ) 5 μm above the surface. When taking FCCS measurements, the probe volume was at least 5μm above the surface and areas with obvious micelle agglomeration were avoided. Each sample was measured sequentially up to 10 times. The 8- and 16-hour incubated samples had an acquisition time of 30 s and the laser powers of each beam were kept at 5μW (measured before the light entered the microscope). The samples with untagged BSA were acquired for 45 s with laser powers of 5μW and 2μW for 561 nm and 488 nm respectively.

3.3 Synthesis of PEG Macroinitiators

Both cyclic and linear PEG macroinitiator were used in this project. The synthesis of the cyclic macroinitiator consisted of three synthetic steps and the synthesis of the linear macroinitator consisted of two steps.

3.3.1 Synthesis of Ms-PEG600-Ms

Ms-PEG600-Ms was synthesized in 65-91% as described previously,[228] as in the following example. Methanesulfonyl chloride (2.9 g, 25 mmol) was added dropwise over 30 min to an ice-cooled solution of PEG600 (5.0 g, 8.3 μmol) and triethylamine (4.2 g, 41 mmol) in dry dichloromethane (40 mL), and the solution was stirred at room temperature for 24 h. The solution was cooled with ice, then washed twice with ice-

cooled water (30 mL each), twice with 10% aqueous HCl (30 mL each), twice with saturated aqueous $NaHCO_3$ (30 mL each), and once with water (30 mL), and dried over $MgSO_4$. After filtration and removing the solvent by rotary evaporation, 4.7 g (78 %) of Ms-PEG600-Ms was obtained as a yellow oil. It was used in the following reaction without further purification. M_n=1.16*10^3 g/mole, PDI=1.06, ^{1}H NMR (500 MHz): 3.03 (s, -C*H*$_3$, 6 H), 3.62 (m, -OC*H*$_2$-, 44.8 H), 3.73 (m, -C*H*$_2$CH$_2$-OMs, 4 H), 4.35 (m, -C*H*$_2$OMs, 4 H). ^{13}C NMR (125 MHz): 37.4 (-*C*H$_3$), 68.8 (-*C*H$_2$OMs), 69.4 (-*C*H$_2$CH$_2$-OMs), 70.4 (-O*C*H$_2$-).

3.3.2 Synthesis of 3,4-(42-Crown-14)benzaldehyde (MC-CHO)

3,4-(42-Crown-14)benzaldehyde (MC-CHO) was synthesized in 39% yield as described previously,[228,229] except that we used acetonitrile and 87 ºC for the cyclization step, as well as a modified purification process. A solution of 3,4-dihydroxybenzaldehyde (0.50 g, 3.6 mmol), Ms-PEG600-Ms (2.7 g, 3.6 mmol), in acetonitrile (125 mL) was added dropwise over 13 h to a solution of K_2CO_3 (0.75 g, 5.4 mmol) in acetonitrile (25 mL) at 82 ºC. The temperature was then set to 87 ºC. After stirring for 72 h at 87 ºC, the reaction mixture was filtered through a fritted glass funnel to remove potassium salts. Acetonitrile was removed by rotary evaporation to obtain 2.7 g (102 %) of a brown oil. This brown oil contains dimeric and trimeric impurities and was purified by flash chromatography using 3:1 hexanes : acetone to obtain 1.0 g (39 %) of high purity MC-CHO as a yellow oil; M_n=0.815*10^3 g/mole, PDI=1.05. ^{1}H-NMR (500 MHz): 3.64-3.77 (m, -OC*H*$_2$-), 3.92 (dd, -C*H*$_2$CH$_2$OAr, ^2J = 8.5 Hz, ^3J = 3.9 Hz), 4.23 (dt, -C*H*$_2$OAr, ^2J =

14.4 Hz, ^{3}J = 4.8 Hz), 6.99 (dd, 1 aromatic H meta to –CH_2OAr, ^{2}J = 10.2 Hz, ^{3}J = 4.9 Hz), 7.43 (dd, 1 aromatic H ortho to –CHO, ortho and meta to –CH_2OAr and 1 aromatic H ortho to –CHO, meta and para to –CH_2OAr, ^{2}J = 13.7 Hz, ^{3}J = 6.5 Hz), 9.83 (s, -C*H*O). ^{13}C NMR (125 MHz): 70.93 (-O*C*H_2-), 112.25 (1 aromatic *C* metha to –CHO, ortho to –CH_2OAr), 112.84 (1 aromatic C ortho to –CHO, ortho to –CH_2OAr), 126.92 (1 aromatic *C* ortho to –CHO, metha to –CH_2OAr), 130.59 (1 aromatic C substituted with CHO), 191.13 (C=O). The purity of the MC-CHO unimer was confirmed using MALDI-ToF MS.

3.3.3 Synthesis of 3,4-(42-Crown-14)benzyl Alcohol (MC-BnOH)

3,4-(42-Crown-14)benzyl alcohol (MC-BnOH) was synthesized in 76 % yield as described previously.[228] A solution of $NaBH_4$ (0.79 g, 21 mmol) in absolute ethanol (70 mL) was added all at once to an ice-cooled solution of MC-CHO (13 g, 19 mmol) in ethanol (270 mL). The solution was stirred at room temperature for 24 h, and then poured into 350 mL of ice water, which was then acidified with 10% aqueous HCl. This mixture was extracted five times with dichloromethane (170 mL each) and the organic extracts were combined and dried over $MgSO_4$. The solution was filtered and the solvent was removed by rotary evaporation and then in vacuo at 75 ºC to yield 11 g (76 %) of MC-BnOH as a yellow oil; M_n=0.931*10^3 g/mole, PDI=1.08, ^{1}H-NMR (500 MHz): 2.81 (br s, -O*H*), 3.63 (-OCH_2-), 3.85 (dd, -CH_2CH$_2$OAr, ^{2}J = 10.1 Hz, ^{3}J = 4.8 Hz), 4.16 (dd, -CH_2OAr, ^{2}J = 10.7 Hz, ^{3}J = 5.9 Hz), 4.57 (s, ArCH_2OH), 6.88 (s, 2 aromatic H ortho to -OCH_2-), 6.99 (s, 1 aromatic H ortho to -CH_2OH), 9.83 (s, 1H). ^{13}C-NMR (125 MHz):

63.95 (Ar*C*H_2OH), 69.63 (-OC*H_2*-), 113.03 (1 aromatic C metha to –CHO, ortho to –CH_2OAr), 113.86 (1 aromatic C ortho to –CHO, ortho to –CH_2OAr), 117.31 (1 aromatic C ortho to –CHO, metha to –CH_2OAr), 119.17 (1 aromatic C substituted with CHO).

3.3.4 Synthesis of α-Methyl Ether, ω-Mesylated Polyethylene Glycol 550 (MeOPEG550Ms)

α-Methyl ether, ω-mesylated poly(ethylene glycol) 550 (MeOPEG550Ms) was synthesized in 73-78% yield by mesylating MeOPEG550OH similar to the mesylation of both ends of poly(ethylene glycol) 600,[228] as in the following example. Methanesulfonyl chloride (2.9 g, 25 mmol) was added dropwise over 30 min to an ice-cooled solution of MeOPEG550OH (5.0 g, 8.3 μmol) and triethylamine (4.2 g, 41 mmol) in dichloromethane (40 mL), and the solution was stirred at room temperature for 24 h. After cooling the solution in ice, it was washed twice with ice-cooled water (30 mL each), twice with 10% aqueous HCl (30 mL each), twice with saturated aqueous $NaHCO_3$ (30 mL each), and once with water (30 mL), and dried over $MgSO_4$. After filtration and removing the solvent by rotary evaporation, 4.7 g (78 %) of MeO-PEG550Ms was obtained as a yellow oil. M_n=1.01*10^3 g/mole, PDI=1.09. ^{1}H-NMR (300 MHz): 3.07 (s, -OS(=O)$_2$C*H_3*), 3.38 (s, C*H_3*O-), 3.54 (t, -CH_3OC*H_2*-, *J* = 4.4 Hz), 3.64 (s, -OC*H_2*-), 3.76 (t, -C*H_2*CH_2-OMs, *J* = 4.5 Hz), 4.38 (t, CH_2C*H_2*OMs, *J* = 4.5 Hz).

3.3.5 Synthesis of α-Methyl Ether, ω-Benzyl Alcohol Polyethylene Glycol 550 (MeOPEG550BnOH)

α-Methyl ether, ω-benzyl alcohol poly(ethylene glycol) 550 (MeOPEG550BnOH) was synthesized in 64-76% yield as in the following example. A solution of MeOPEG550Ms (9.0 g, 14 mmol), *p*-hydroxybenzyl alcohol (3.0 g, 24 mmol), potassium carbonate (2.9 g, 21 mmol), potassium iodide (93 mg, 0.56 mmol) in acetonitrile (90 mL) was stirred at 90 ºC for 48 h. The potassium salts were filtered off and the filtrate was passed through basic activated alumina to remove unreacted *p*-hydroxy benzyl alcohol. After removing the solvent by rotary evaporation, 6.0 g (64 %) of MeOPEG550BnOH was obtained as a clear oil; M_n=1.78*10^3 g/mole, PDI=1.13. ^{1}H-NMR (300 MHz): 3.38 (s, C*H*$_3$-), 3.65 (m, -OC*H*$_2$-), 3.86 (t, -C*H*$_2$CH$_2$-OAr-, J = 4.9 Hz), 4.13 (t, -CH$_2$C*H*$_2$-OAr-, J = 4.9 Hz), 4.62 (s, -C*H*$_2$OH), 6.91 (ArC(2,6)H), 7.30 (ArC(3,5)H).

3.4 Synthesis of Diblock Copolymers

As described in the following subsections, PEG-*b*-PCL diblock copolymers were synthesized by polymerizing ε-caprolactone from the cyclic and linear PEG macroinitiators described in the previous section.

3.4.1 Synthesis of MC-BnOPCL diblock copolymers

CyclicPEG-*b*-linearPCL (MC-BnOPCL) diblock copolymers were synthesized in 36-70% yield as in the following example. A mixture of MC-BnOH (71 mg, 0.10

mmol), ε-caprolactone (66 mg, 58 mmol), and a stock solution of tin octoate (50 mg, 0.12 mmol) in dry THF (1.9 mL) in a Schlenk tube was degassed by two freeze-pump-thaw (10-30-20 min) cycles, and then stirred at 80 °C for 19 h. The solution was condensed by rotary evaporation. The resulting viscous solution was precipitated in hexanes (60 mL) and reprecipitated twice from dichloromethane (0.5 mL) into hexanes (60 mL) to yield 97 mg (70%) of a white solid. M_n= 3.14*10^3g/mole, PDI=1.23. ^{1}H-NMR (500 MHz): 1.38 (C*H*$_2$(CH$_2$)$_2$C=O), 1.58 (C*H*$_2$CH$_2$C*H*$_2$CH$_2$OH), 1.65 (C*H*$_2$CH$_2$C*H*$_2$CH$_2$OC=O), 2.30 (-C*H*$_2$(C=O)O-), 2.35 (-ArCH$_2$O(C=O)C*H*$_2$-), 3.64 (-CH$_2$O-), 3.75 (-C*H*$_2$CH$_2$OAr), 3.87 (-C*H*$_2$OAr), 4.06 (-C*H*$_2$O(C=O)-), 4.16 (C*H*$_2$OH), 5.01 (s, ArC*H*$_2$OH), 6.89 (*Ar*). ^{13}C-NMR (125 MHz): 24.71 (C*H*$_2$CH$_2$C=O), 25.66 (-C*H*$_2$(CH$_2$)$_2$(C=O)-), 28.48 (C*H*$_2$CH$_2$O), 32.45 (-C*H*$_2$(C=O)-, last repeating unit), 34.25 (-C*H*$_2$(C=O)-), 62.75 (C*H*$_2$OH), 64.28 (-C*H*$_2$O(C=O)-), 66.24 (ArC*H*$_2$-), 69.84 ((-C*H*$_2$CH$_2$OAr), 70.72 (-C*H*$_2$O- in PEG), 70.96 (-C*H*$_2$OAr), 173.68 (C=O).

3.4.2 Synthesis of MeOPEG550BnO-PCL diblock copolymers

LinearPEG-*b*-linearPCL (MeOPEG550BnO-PCL) diblock copolymers were synthesized in 29-54% yield as in the following example. A mixture of MeOPEG550BnOH (45 mg, 82 μmol), ε-caprolactone (0.19 g, 1.7 mmol), and a stock solution of tin octoate (33 mg, 82 μmol) in dry THF (1.1 mL) in a Schlenk tube was degassed by two freeze-pump-thaw (10-30-20 min) cycles, and then stirred at 80 °C for 19 h. The solution was condensed by rotary evaporation. The resulting viscous solution was precipitated in hexanes (60 mL) and reprecipitated twice from dichloromethane (0.5

mL) into hexanes (60 mL) to yield 0.13 g (54%) of a white solid. M_n=2.54*10^3 g/mole, PDI=1.20. ^{1}H-NMR (500 MHz): 1.38 (C*H*$_2$(CH$_2$)$_2$C=O, 37H), 1.59 (t, C*H*$_2$CH$_2$C*H*$_2$CH$_2$OH, *J* = 7.5 Hz), 1.65 (-C*H*$_2$CH$_2$C*H*$_2$CH$_2$OC=O-), 2.31 (-C*H*$_2$(C=O)O-), 2.36 (t, -C*H*$_2$(C=O)OCH$_2$Ar, *J* = 7.3 Hz), 3.38 (s, C*H*$_3$O), 3.55 (CH$_3$OC*H*$_2$-, *J* = 4.7 Hz), 3.71 (-C*H*$_2$CH$_2$OAr), 3.85 (t, -C*H*$_2$OAr, *J* = 4.9 Hz), 4.06 (-C*H*$_2$O(C=O)), 4.12 (t, -C*H*$_2$OH, *J* = 4.9 Hz), 5.04 (-ArC*H*$_2$), 6.88 (2 aromatic H meta to C*H*$_2$), 6.90 (2 aromatic H ortho to C*H*$_2$).^{13}C NMR (125 MHz): 24.59 (-*C*H$_2$(CH$_2$)$_3$OH), 24.80 (-*C*H$_2$CH$_2$(C=O)-), 25.52 (-*C*H$_2$CH$_2$CH$_2$OH), 25.76 (-*C*H$_2$CH$_2$CH$_2$O(C=O)-), 28.57 (-*C*H$_2$CH$_2$O(C=O)-), 32.54 (-*C*H$_2$(CH$_2$)$_4$OH), 34.35 (-*C*H$_2$(C=O)-), 59.25 (*C*H$_3$O-), 62.85 (-*C*H$_2$OH), 64.38 (-*C*H$_2$O(C=O)-), 70.77 (-*C*H$_2$O- PEG backbone), 71.05 (CH$_3$OCH$_2$*C*H$_2$-), 72.15 (CH$_3$O*C*H$_2$-), 114.85 (2 aromatic C ortho to O), 130.20 (2 aromatic C meta to O), 173.77 (*C*=O).

3.5 Synthesis of Fluorescently-Labeled Polymers

Fluorescently labeled polymers were synthesized in order to study protein binding onto micelles of the amphiphilic PEG-*b*-PCL diblock copolymers described above. First a fluorescently labeled model PCL homopolymer and then a fluorescently labeled PEG-*b*-PCL diblock copolymer were synthesized.

3.5.1 Synthesis of MeOPCL

In a Schlenk flask a mixture of ε-caprolactone (3.0 g, 26 mmol) and tin octoate (57 mg, 0.14 mmol) was dried by azeotropic distillation using 25 mL of toluene twice. Methanol (63 mg, 2.0 mmol) was added in the drybox, the mixture was stirred 80 °C for 7.5 h and quenched by immersing it in liquid nitrogen. Conversion by ^{1}H NMR spectroscopy is 77% and M_n=1.4*10^3 g/mole. The polymer was precipitated from chloroform (0.7 mL) into hexanes (250 mL). The polymer was collected into a fritted glass funnel to obtain 1.7 g (56%) of polycaprolactone monomethyl ether (MeOPCL) as a white solid; M_n=2.66*10^3 g/mole, PDI=1.10. ^{1}H-NMR (500 MHz): 1.38 (-C*H*$_2$(CH$_2$)$_2$(C=O)-), 1.59 (t, -C*H*$_2$CH$_2$C*H*$_2$CH$_2$OH, J = 7.5 Hz), 1.65 (m, (-C*H*$_2$CH$_2$C*H*$_2$CH$_2$O(C=O)- 69H), 2.31 (m, -C*H*$_2$(C=O)O-, 38H), 3.65 (t, -C*H*$_2$OH, J = 6.5 Hz, 2H), 3.67 (s, C*H*$_3$O-), 4.06 (-C*H*$_2$O(C=O)). ^{13}C NMR (125 MHz): 24.52 (-*C*H$_2$(CH$_2$)$_3$OH), 24.55 (-(C=O)CH$_2$*C*H$_2$-), 24.65 (CH$_3$O(C=O)CH$_2$*C*H$_2$-), 25.27 (CH$_3$O(C=O)(CH$_2$)$_2$*C*H$_2$-), 25.50 (-*C*H$_2$CH$_2$CH$_2$O(C=O)-), 28.32 (-*C*H$_2$CH$_2$O(C=O)-), 33.86 (-*C*H$_2$(CH$_2$)$_4$OH), 34.09 (-O(C=O)*C*H$_2$-), 34.20 (CH$_3$O(C=O)*C*H$_2$-), 51.48 (*C*H$_3$O-), 62.60 (-*C*H$_2$OH), 64.12 (-*C*H$_2$ O(C=O)-), 173.51 (*C*=O).

3.5.2 Synthesis of MeOPCLMs

Methanesulfonyl chloride (0.2 mL, 2 mmol) was added all at once to an ice-cooled solution of polycaprolactone monomethyl ether (1.7 g, 1.5 mmol) and triethylamine (0.5 mL, 4 mmol) in THF (10 mL). The mixture was stirred at room

temperature for 18 h. ^{1}H NMR spectroscopy shows 100% functionalization based on the resonances at 1.78, 4.23, due to methylene groups alpha and beta to the mesyl group, and at 3.02 ppm due to the methyl group of the mesyl group. The solution was eluted through a plug of silica gel and condensed by rotary evaporation and dried in vacuo on a Schlenk line to obtain 1.8 g (99%) of α-methyl ether, ω-mesyl polycaprolactone (MeOPCLMs) as a white solid; M_n=2.87*10^3 g/mole, PDI=1.11. ^{1}H-NMR (500 MHz): 1.39 (-CH_2(CH$_2$)$_2$(C=O)-), 1.46 (-CH_2(CH$_2$)$_2$OH), 1.65 (-CH_2CH$_2$CH_2CH$_2$O(C=O)-), 1.78 (t, -CH_2CH$_2$CH_2CH$_2$OH, J =7.38 Hz), 2.31 (m, -CH_2(C=O)-), 3.02 (s, CH_3S(=O)$_2$O-), 3.67 (s, CH_3O(C=O)-), 4.06 (m, -CH_2O(C=O)-), 4.23 (t, -CH_2Ms, J =6.35 Hz). ^{13}C NMR (125 MHz): 24.29 (-*C*H$_2$CH$_2$CH$_2$CH$_2$Ms), 24.55 (-O(C=O)CH$_2$*C*H$_2$-), 24.98 (-*C*H$_2$CH$_2$CH$_2$Ms), 25.51 (-O(C=O)CH$_2$CH$_2$*C*H$_2$-), 28.32 (-CH_2CH$_2$O(C=O)-), 28.82 (-*C*H$_2$CH$_2$Ms), 33.90 (-*C*H$_2$(CH$_2$)$_3$CH$_2$Ms), 34.09 (CH$_3$O(C=O)*C*H$_2$-), 37.32 (*C*H$_3$S(=O)$_2$O-), 51.48 (*C*H$_3$O-), 64.11 (CH$_3$O(C=O)(CH$_2$)$_4$*C*H$_2$-), 69.75 (-*C*H$_2$Ms), 173.50 (*C*=O).

3.5.3 Synthesis of MeOPCL_Rhodamine

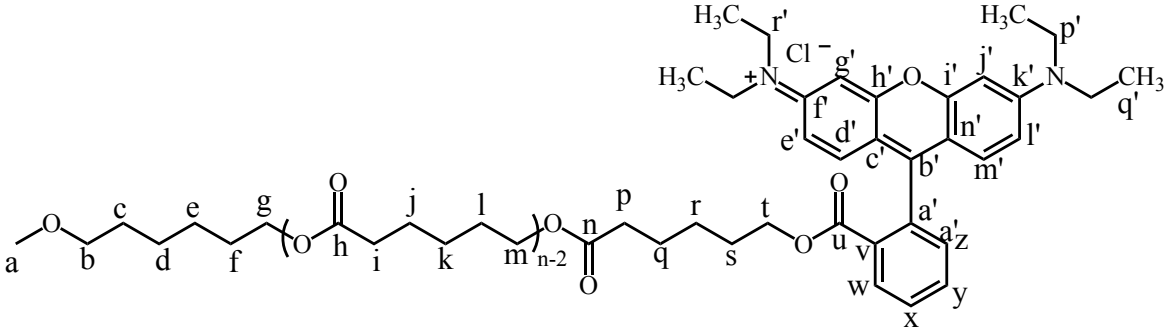

In a round bottom flask, a mixture of MeOPCLMs (0.2 g, 0.4 μmol), rhodamine lactone (0.11 g, 0.6 mmol), and N,N-Diisopropylethylamine (0.09 mL, 0.5 mmol) in dry acetonitrile (2 mL) was stirred at 82 °C for 98.5 h. The reaction reached 100% conversion by ^{1}H NMR spectroscopy according to the disappearance of resonances at 1.78, 3.02, and 4.23 ppm. The solution was condensed by rotary evaporation to obtain a purple solid (0.3 g, 95%). This solid was purified by column chromatography using 2:1 acetone : hexanes as a purple solid (76 mg, 22%). The polymer was precipitated from dichloromethane (2 mL) into hexanes (100 mL) to obtain to obtain MeOPCL_Rhod with traces of unreacted rhodamine of α-methyl ether, ω-rhodamine polycaprolactone (MeOPCL_Rhodamine) as a purple powder 50 mg (15%); M_n=2.99*10^3 g/mole, PDI=1.13. The sample does not contain unreacted rhodamine according to ^{1}H NMR spectroscopy.. ^{1}H-NMR (500 MHz): 1.34 (t, CH_3CH_2-, J = 7.2 Hz), 1.39 (-O(C=O)$(CH_2)_2CH_2$-), 1.48 (t, $CH_3O(C=O)(CH_2)_3CH_2$-, J = 7.6 Hz), 1.54 (t, $CH_3O(C=O)CH_2CH_2$-, J = 7.7 Hz), 1.65 (-$CH_2CH_2CH_2CH_2O(C=O)$-), 2.23 (t, $CH_3O(C=O)CH_2$-, J = 7.5 Hz), 2.31 (-O(C=O)CH_2-), 2.78 (-$CH_2(CH_2)_4O(C=O)$Ar-), 3.64 (t, -CH_2CH_3, J = 7.3 Hz), 3.67 (s, CH_3O-), 4.06 (-$CH_2O(C=O)$-), 6.84 (d, $H_{g'}$ and $H_{j'}$, J = 2.4 Hz), 6.90 (dd, $H_{d'}$ and $H_{m'}$, ^{1}J = 9.5, ^{2}J = 2.4 Hz), 7.08 (d, $H_{e'}$ and $H_{l'}$, J = 9.5 Hz), 7.33 (H_z,), 7.75 (t, H_x, J = 7.7 Hz), 7.82 (t, H_y, J = 7.5 Hz), 8.29 (d, H_w, J = 7.9 Hz). ^{13}C NMR (125 MHz): 12.65 (CH_3CH_2-), 24.46 (-$CH_2(CH_2)_2CH_2O(C=O)$Ar-), 24.57 (-O(C=O)CH_2CH_2-), 25.40 ((-$CH_2CH_2CH_2O(C=O)$Ar-), 25.53 (-O(C=O)$CH_2CH_2CH_2$-), 28.07 (-$CH_2CH_2O(C=O)$Ar-), 28.34 (-O(C=O)$(CH_2)_3CH_2$-), 33.89 (-$CH_2(CH_2)_4O(C=O)$Ar-), 34.12 (-$CH_2(CH_2)_4O(C=O)$-), 39.41 (-NCH_2CH_3), 46.14 (=N$^+CH_2CH_3$), 51.51 (CH_3O-), 64.14 (-$CH_2O(C=O)$-), 65.43 (-$CH_2O(C=O)$Ar-), 96.37 ($H_{g'}$ and $H_{j'}$), 113.54 ($H_{l'}$), 114.22

($H_{e'}$), 128.17 ($H_{m'}$), 128.55 ($H_{c'}$), 130.07 (H_x), 130.26 (H_z), 130.40 (H_v), 131.28 ($H_{d'}$), 131.31 (H_w), 133.07 (H_y), 133.48 ($H_{a'}$), 155.56 ($H_{k'}$), 157.75 ($H_{f'}$), 158.88 ($H_{b'}$), 165.08 (H_u), 173.38 ($CH_3O(C{=}O)$-), 173.55 (*C*=O), 173.95 (-O(*C*=O)Ar-).

3.5.4 Synthesis of MeOPEG550PCL

A mixture of tin octoate (0.55 g, 1.4 mmol), ε-caprolactone (3.0 g, 26 mmol), and previously dried MeOPEG550OH (3.0 g, 5.4 mmol) was azeotropically dried twice by trap-to-trap removal of dry toluene (30 mL). After stirring at 80 °C for 12 h, the polymerization reached 100% conversion according to ^{1}H NMR spectroscopy by the disappearance of the monomer resonances at 1.78, 1.87 ppm. The added polycaprolactone molecular weight was around 400 g/mole according to ^{1}H NMR spectroscopy. The polymer was precipitated twice from bulk into hexanes (350 and 400 mL, respectively) to obtain 6.0 g (100%) of monomethylether poly(ethylene glycol)-*b*-polycaprolactone (MeOPEG550PCL) as a viscous liquid; M_n=1.99*10^3 g/mole, PDI =1.17. ^{1}H-NMR (500 MHz): 1.39 (-O(C=O)$(CH_2)_2C\mathit{H}_2$-), 1.57 (-O$(CH_2)_2$O(C=O)$CH_2C\mathit{H}_2$-), 1.65 (-$CH_2C\mathit{H}_2CH_2C\mathit{H}_2CH_2O$(C=O)-), 2.31 (-O(C=O)$C\mathit{H}_2$-), 2.35 (- $C\mathit{H}_2(CH_2)_4OH$), 3.38 ($C\mathit{H}_3O$-), 3.55 ($CH_3OC\mathit{H}_2$-), 3.62-3.59 ($CH_3OCH_2C\mathit{H}_2$-), 3.65 (-O$C\mathit{H}_2C\mathit{H}_2$O-), 3.70 (-$OCH_2CH_2O$-$CH_2C\mathit{H}_2$O(C=O)-), 4.06 (-$C\mathit{H}_2$O(C=O)-), 4.22 (-$C\mathit{H}_2$OH). ^{13}C NMR (125 MHz): 24.43 (-*C*$H_2CH_2CH_2CH_2OH$), 24.52 (-O(C=O)$CH_2C\mathit{H}_2$-), 24.70 (-O$(CH_2)_2$O(C=O)$CH_2C\mathit{H}_2$-), 25.33 (-O$(CH_2)_2$O(C=O)$(CH_2)_2C\mathit{H}_2$-), 25.47 (-O(C=O)$(CH_2)_2C\mathit{H}_2$-), 28.28 (-O$(CH_2)_2$O(C=O)$(CH_2)_3C\mathit{H}_2$-), 30.87 (-O$(CH_2)_2$O(C=O)$C\mathit{H}_2$-), 32.25 (-*C*H_2CH_2OH), 34.06 (-O(C=O)$C\mathit{H}_2$-), 58.92 (*C*H_3O-),

62.17 (-*C*H_2OH), 63.39 (-O(CH_2)$_2$O(C=O)(CH_2)$_4$*C*H_2-), 64.08 (-O(CH_2)$_2$O(C=O)(CH_2)$_4$*C*H_2-), 69.08 (CH_3O(C=O)CH_2*C*H_2-), 70.47 (-OCH_2CH_2O-), 71.84 (CH_3O(C=O)*C*H_2-), 173.41 (-(*C*=O)(CH_2)$_5$OH), 173.50 (-O(*C*=O)CH_2-), 173.72 (-O(CH_2)$_2$O(*C*=O)CH_2-).

3.5.5 Synthesis of MeOPEG550PCLMs

Methanesulfonyl chloride (0.2 mL, 3 mmol) was added all at once to an ice-cooled solution of MeOPEG550PCL (2.0 g, 2.1 mmol) and triethylamine (0.7 mL, 5 mmol) in dry THF (10 mL) and stirred at room temperature for 18 h. The solution was eluted through a plug of silica gel to obtain 2.4 g (100%) of α-methyl ether, ω-mesyl poly(ethylene glycol)-*b*-polycaprolactone (MeOPEG550PCLMs) as a yellow oil; M_n=1.99*10^3 g/mole, PDI =1.17. ^{1}H-NMR (300 MHz): 1.38 (-O(C=O)(CH_2)$_2$C*H*$_2$-), 1.65 (-CH_2C*H*$_2$$CH_2$C*H*$_2$$CH_2$O(C=O)-), 2.31 (-O(C=O)C*H*$_2$), 3.00 (C*H*$_3$S(=O)$_2$O-), 3.38 (C*H*$_3$O-), 3.56 (CH_3OC*H*$_2$-), 3.64 (-OC*H*$_2$C*H*$_2$O-), 4.06 (-C*H*$_2$O(C=O)-), 4.23 (-C*H*$_2$Ms). ^{13}C NMR (125 MHz): 24.26 (-O(CH_2)$_2$O(C=O)CH_2*C*H_2-), 24.53 (-O(C=O)CH_2*C*H_2-), 24.94 (-O(CH_2)$_2$O(C=O)(CH_2)$_2$*C*H_2-), 25.46 (-O(C=O)(CH_2)$_2$*C*H_2-), 28.29 (-O(C=O)(CH_2)$_3$*C*H_2-), 28.78 (-*C*$H_2$$CH_2$Ms), 33.92 (-O($CH_2$)$_2$O(C=O)*C*$H_2$-), 34.05 (-O(C=O)*C*$H_2$-), 37.29 (*C*$H_3$S(=O)$_2$O-), 58.92 ($CH_3$O-), 63.40 (-O(C=O)($CH_2$)$_4$*C*$H_2$-), 64.07 (-O(C=O)($CH_2$)$_4$*C*$H_2$-), 69.10 ($CH_3$O*C*$H_2$-), 69.74 ($CH_3OCH_2$*C*$H_2$- and –*C*$H_2$Ms), 70.50 (-*C*$H_2$*C*$H_2$O-), 71.86 (-O$CH_2$*C*$H_2$O(C=O)-), 173.45 (C=O).

3.5.6 Synthesis of MeOPEG550PCL_Rhod

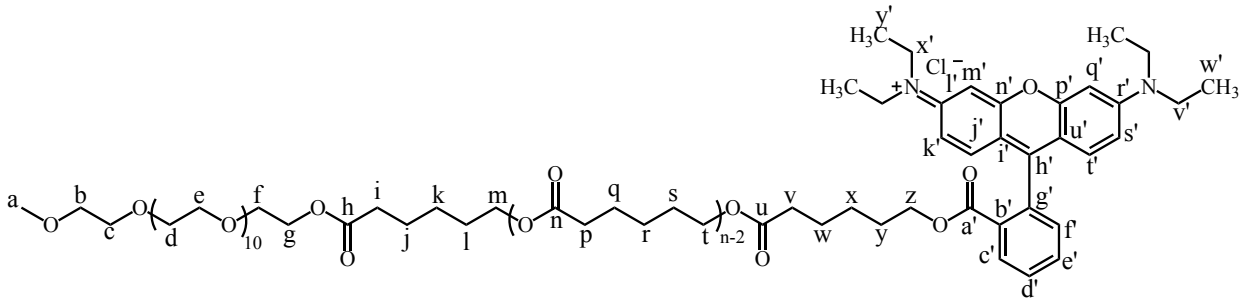

A solution of MeOPEG550PCLMs (0.25 g, 0.24 mmol), *N,N*-Diisopropylethylamine (0.2 mL, 1 mmol), and rhodamine lactone (0.16 g, 0.36 mmol) in dry acetonitrile (2 mL) was stirred at reflux temperature for 72 h. After cooling down to room temperature, the solution was precipitated into hexanes (150 mL), collected, and then reprecipitated from dichloromethane (2 mL) into hexanes (150 mL) to obtain 0.19 g (53%) of a purple solid. The functionalized polymer was purified by column chromatography using silica gel as the stationary phase and 3:1 acetone : hexanes as the eluent to obtain 90 mg (25%) of α-methyl ether, ω-rhodamine poly(ethylene glycol)-*b*-polycaprolactone (MeOPEG550PCLRhod) as a yellow oil; M_n=1.80*10^3 g/mole, PDI =1.17. ^{1}H-NMR (500 MHz): 1.24 ($H_{w'}$, J = 26.7 Hz), 1.34 ($H_{y'}$), 1.39 (-O(C=O)$(CH_2)_2$CH_2-), 1.66 (-CH_2C$H_2$$CH_2CH_2$$CH_2$O(C=O)-), 2.22 (-O$(CH_2)_2$O(C=O)$CH_2CH_2$-), 2.31 (-O(C=O)C$H_2$-), 2.77 (-C$H_2$$(CH_2)_4$O(C=O)Ar-), 3.37 (C$H_3$O-), 3.55 ($CH_3OCH_2$-), 3.65 (-OC$H_2$$CH_2$O-), 4.07 (-C$H_2$O(C=O)-), 4.23 (-C$H_2$Ar and -O$CH_2CH_2$O(C=O)$CH_2$-), 6.83 ($H_{m'}$ and $H_{q'}$), 6.90 ($H_{j'}$ and $H_{t'}$), 7.09 ($H_{k'}$ and $H_{s'}$), 7.76 ($H_{d'}$), 7.82 ($H_{e'}$), 8.28 ($H_{c'}$). ^{13}C NMR (125 MHz): 11.64 ($C_{w'}$ and $C_{y'}$), 23.48 (-

CH_2(CH_2)$_2$$CH_2$O(C=O)Ar-), 23.55 (-O(C=O)CH_2*C*H_2-), 24.38 (-*C*$H_2$$CH_2$$CH_2$O(C=O)Ar-), 24.51 (-O(C=O)CH_2*C*H_2-), 27.05 (-*C*$H_2$$CH_2$O(C=O)Ar-), 27.33 (-*C*$H_2$($CH_2$)$_3$O(C=O)Ar-), 32.96 (-*C*$H_2$($CH_2$)$_4$O(C=O)Ar-), 33.10 (-O(C=O)*C*H_2-), 45.12 (-*C*$H_2$$CH_3$), 57.98 (*C*$H_3$O-), 62.43 (-*C*$H_2$O(C=O)Ar-), 63.11 (-*C*$H_2$O(C=O)-), 64.40 (-O$CH_2$$CH_2$O(C=O)($CH_2$)$_4$*C*$H_2$-), 68.14 (-O$CH_2$*C*$H_2$O(C=O)-), 69.55 (-O*C*$H_2$*C*$H_2$O-), 70.92 ($CH_3$O*C*$H_2$-), 95.36 ($C_{q'}$ and $C_{m'}$), 112.53 ($C_{s'}$), 113.22 ($C_{k'}$), 127.26 ($C_{t'}$), 127.53 ($C_{i'}$), 129.11 ($C_{d'}$), 129.24 ($C_{f'}$), 129.40 ($C_{b'}$), 130.29 ($C_{j'}$), 132.05 ($C_{e'}$), 132.43 ($C_{m'}$ and $C_{q'}$), 154.57 ($C_{p'}$), 156.74 ($C_{l'}$), 157.86 ($C_{h'}$), 164.06 (-(*C*=O)Ar-), 172.31 (-(*C*=O)(CH_2)$_5$O(C=O)Ar-), 172.40 (-O(CH_2)$_2$O(*C*=O)-), 172.49 (*C*=O).

3.6 Preparation of Diblock Copolymer Micelles

Amphiphilic diblock copolymer micelles were prepared by a co-solvent evaporation method using acetone as common solvent[230] and fully characterized using dynamic light scattering (DLS) and Transmission Electron Microscopy (TEM) then the micelle preparation protocol was modified in order to use fluorescence correlation and cross-correlation spectroscopy (FCS) and FCCS to characterize them.

3.6.1 Micelles Characterized by DLS and SEM

Polymeric micelles were prepared from amphiphilic diblock copolymers either MeOPEG550BnOPCL or MCBnOPCL diblock copolymers as in the following example modifying a procedure found in the literature.[230] MilliQ water (15 mL) was added *via* a

syringe pump (0.1 mL/min) to a vigorously stirred solution of diblock copolymer (2.5 mg) in acetone (0.1 g) at room temperature. The micelles were stirred covered by a kimwipe inside a ventilation hood for 2.5 h at room temperature and normal pressure and then stirred overnight inside a bell jar while applying aspirator vacuum to remove acetone.

3.6.2 Preparation of Fluorescently Tagged Micelles for Protein Adsorption Experiments

Fluorescently tagged micelles were prepared from either MeOPEG550BnOPCL or MCBnOPCL diblock copolymers and MeOPEGPCLRhod as in the following example. Ultrapure water (15 mL) was added *via* syringe pump (0.1 mL/min) to a solution of MeOPEG550BnOPCL (0.2 mg) and MeOPEGPCL_Rhod (4.4 μg) in acetone (0.1 g). The micelles were stirred covered by a kimwipe inside a ventilation hood for 2.5 h at room temperature and normal pressure overnight to remove acetone. DLS on these micelles shows three size distributions: 100 nm, 700 nm, and 8400 nm. Filtered micelles through a 0.45 μm poly(ether sulfone) filter. The filtered micelles have only one size distribution that corresponds to 100 nm.

3.7 Protein Adsorption Studies

Dynamic light scattering and fluorescence spectroscopy were used to measure protein adsorption onto self-assembled micelles.

3.7.1 Protein Adsorption Experiments Using Dynamic Light Scattering

In a 15 mL falcon tube BSA protein solutions with different concentrations were prepared into PBS (11 mL). For example, in order to obtain the biological concentration of 45 mg/mL, BSA (0.50 g) were mixed with PBS (11 mL). The tubes were there inverted several times to favor mixing and vortexed when necessary. The solutions sat overnight before use. For the protein adsorption experiments, micelle suspension (750 μL) and protein solution (750 μL) were mixed into 1.5 mL eppendorf tubes. These suspensions were then incubated for 16 h in a shaker at 250 rpm and 37 °C. Dynamic light scattering measurements were performed on the suspensions at room temperature.

3.7.2 Protein Adsorption Studies Using Fluorescence Spectroscopy

Fluorescein tagged Bovine Serum Albumin (BSA) stock solutions were prepared by dissolving lyophilized protein (1.0 mg) into either PBS or ultrapure water (1.0 mL). One half of the stock solutions were kept in the refrigerator and the other half were kept frozen for future use. Protein solutions of different concentrations were prepared from the stock solution as in the following example. Mixed PBS (1.2 mL) and BSA stock solution in PBS (74.5 μL) into a 1.5 mL eppendorf tube. Protein adsorption experiments were set up using protein solutions with different concentrations as in the following example. Mixed a protein solution (150 μL) and a micelle suspension into a 1.5 mL eppendorf tube. The suspensions were mixed a couple of times by inversion and then incubated in a shaker at 250 rpm and 37 °C for either 8 or 16 h. Fluorescence correlation

and cross-correlation spectroscopy data was used to determine the diffusion coefficients for micelles and proteins in the sample.

3.8 Synthesis of an Oligooxyethylene Inimer

An oliogooxyethylene inimer was synthesized in three steps. The first step is the synthesis of 2-chloro-3-hydroxypropionic acid by diazotization of D,L serine. [2-(2'-Ethoxyethoxy)ethyl] 2-chloro-3-hydroxypropionate is then synthesized by esterification with 2-(2'-ethoxyethoxy)ethanol, and finally an esterification with acryloyl chloride yields the [2-chloro-2-(2'-ethoxyethoxy)ethan-1-oxycarbonyl]ethyl acrylate inimer.

3.8.1 Synthesis of 2-Chloro-3-hydroxypropionic Acid (chlorohydrin)

2-chloro-3-hydroxypropionic acid was synthesized in 37% yield as described previously.[4] Sodium nitrite (68 g, 0.99 mol) was added in portions over 3 h to a solution of D,L-serine (52 g, 0.50 mol), potassium chloride (130 g, 1.8 mol), and HCl (116 g, 38% w/w, 1.2 mol) in water (490 mL), while maintaining the temperature at approximately -10 ºC. After stirring at room temperature for 24 h, the reaction mixture was saturated with NaCl and extracted five times with ethyl acetate (100 mL each). The combined extracts were washed 5 times with saturated aqueous NaCl (50 mL each), and dried over $MgSO_4$. After filtration and removing the solvent by rotary evaporation, the residue was recrystallized from CH_2Cl_2 (200 mL) to obtain (23 g, 37%) of 2-chloro-3-hydroxypropionic acid as a white solid.

^{1}H NMR (300 MHz): 4.05 (d, C*H*$_2$OH, *J*= 5.30 Hz), 4.49 (t, C*H*Cl, *J*=5.31 Hz).

3.8.2 Synthesis of [2-(2'-Ethoxyethoxy)ethyl] 2-Chloro-3-hydroxypropionate

[2-(2'-Ethoxyethoxy)ethyl] 2-chloro-3-hydroxypropionate was synthesized in quantitative yield as described previously.[4] A solution of 2-chloro-3-hydroxypropionic acid (3.2 g, 26 mmol), *p*-toluenesulfonic acid (0.14 g, 0.71 mmol), and 2-(2'-ethoxyethoxy)ethanol (18 g, 0.13 mol) in toluene (10 mL) was stirred at 130 ºC for 2 h, using a Dean-Stark trap apparatus. The contents of the trap was replaced with fresh toluene (10 mL) and stirred at 130 ºC for 22 h. The reaction mixture was passed through a plug of neutral activated alumina and the unreacted alcohol and toluene were removed under vacuum using a short path (1 mmHg, 57 ºC) using an oil bath at 82 ºC to obtain 6.6 g (100%) of [2-(2'-ethoxyethoxy)ethyl] 2-chloro-3-hydroxypropionate as a clear oil. ^{1}H-NMR ($CDCl_3$): 1.22 (t, C*H*$_3$), 2.89 (t, O*H*), 3.51 (t, CH_3CH_2), 3.57 (t, $CH_2OCH_2CH_3$), 3.64 (t, $CH_2CH_2OCH_2CH_3$), 3.74 (t, $CO_2CH_2CH_2$), 3.96 (dd, C*H*HOH), 4.05 (dd, CH*H*OH), 4.37 (t, CO_2CH_2), 4.41(dd, C*H*Cl,). ^{13}C-NMR (125 MHz): 15.0 (CH_3), 57.1 (*C*HCl), 64.1 (CO_2CH_2), 65.0 ($HOCH_2$), 66.7 (CH_2CH_3), 68.6 ($CH_2OCH_2CH_3$), 69.7 ($CO_2CH_2CH_2OCH_2$), 70.5 ($CO_2CH_2CH_2O$), 168.4 (CO_2).

3.8.3 Synthesis of [2-Chloro-2-(2'-ethoxyethoxy)ethan-1-oxycarbonyl]ethyl acrylate

[2-Chloro-2-(2'-ethoxyethoxy)ethan-1-oxycarbonyl]ethyl acrylate was synthesized in 24% yield as described previously.[4] A solution of acryloyl chloride (7 mL, 0.09 mol) in THF (15 mL) was added dropwise over 10 min to an ice-cooled solution of

[2-(2'-ethoxyethoxy)ethyl] 2-chloro-3-hydroxypropionate (4.2 g, 17 mmol) and pyridine (7.0 mL g, 87 mmol) in THF (400 mL). After stirring at 25ºC for 24 h, pyridinium hydrochloride was filtered off using a fritted glass funnel and the solution was concentrated by rotary evaporation. The concentrated solution was then purified by column chromatography using 3:1 hexanes : acetone passed through a plug of basic activated alumina. The product (R_f=0.36) was purified by silica gel column chromatography using a mixture of ethyl acetate/hexanes (40/60, v/v) as the eluent to yield (1.24 g, 24 %) of a colorless liquid. ^{1}H-NMR 1.21 (t, C*H*$_3$, *J*=7.01 Hz), 3.52 (t, C*H*$_2$CH$_3$, *J*=7.01 Hz), 3.58 (t, C*H*$_2$OCH$_2$CH$_3$, *J*=4.60 Hz) 3.65 (t, CO$_2$CH$_2$CH$_2$OC*H*$_2$, *J*=4.82 Hz), 3.74 (t, CO$_2$CH$_2$C*H*$_2$, *J*=4.82 Hz), 4.37 (t, CO$_2$C*H*$_2$, *J*=4.84 Hz), 4.52 (t, C*H*HOH, *J*=3.19 Hz), 4.56 (t, C*H*Cl, *J*=2.47 Hz), 4.60 (t, CH*H*OH, *J*=3.36 Hz), 5.89 (dd, =C*H trans* to CO$_2$, J_1 = 10.4 Hz, J_2 = 1.40 Hz), 6.13 (dd, =C*H gem* to CO$_2$, J_1 = 17.3 Hz, J_2 = 10.4 Hz), 6.45 (dd, =C*H cis* to CO$_2$, J_1 = 17.29 Hz, J_2 = 1.390 Hz). ^{13}C-NMR (125 MHz): 15.0 (*C*H$_3$), 53.6 (*C*HCl), 64.4 (CO$_2$*C*H$_2$CH$_2$), 65.4 (CO$_2$*C*H$_2$CHCl), 66.6 (O*C*H$_2$CH$_3$), 68.5 (*C*H$_2$OCH$_2$CH$_3$), 69.6 (CO$_2$CH$_2$CH$_2$O*C*H$_2$CH$_2$), 70.6 (CO$_2$CH$_2$*C*H$_2$O), 127.3 (=*C*H$_2$), 132.0 (=*C*H), 165.1 (*C*O$_2$CH$_2$CH$_2$), 167.1 (*C*O$_2$CH$_2$CHCl).

CHAPTER IV

PREPARATION OF PEG MACROINITIATORS AND PEG-*b*-PCL DIBLOCK COPOLYMERS

4.1 Introduction

This chapter discusses the syntheses of cyclic (MC-BnOH) and linear (MeOPEG550BnOH) PEG macroinitiators as well as PEG-*b*-PCL diblock copolymers synthesized from these macroinitiators. MC-BnOH has been synthesized before in low yields and using time-consuming purification techniques.[228,229] Lower molecular weight analogs of MeOPEG550BnOH have been synthesized using different routes.[231-233] The linear macroinitiator syntheses presented here involve a mesylation followed by an etherification. The assignments of resonances for the compounds shown in this chapter were based on the methods described by Silverstein et al.,[234] prediction from ChemBioDraw 13.0, and/or the literature.

4.2 Synthesis of PEG Macroinitiators

In order to compare the protein adsorption onto micelles from PEG-*b*-PCL diblock copolymers with different polymer architectures in the corona, a cyclic (MC-BnOH) macroinitiator and a linear (MeOPEG550BnOH) PEG

macroinitiator were synthesized in three and two synthetic steps, respectively. MCBnOH lacks end groups while MeOPEG550BnOH has a methyl end group.

4.2.1.1 Synthesis of a Cyclic PEG Macroinitiator: MC-BnOH

MC-BnOH was synthesized in three steps from PEG 600. First, a mesylation of they hydroxyl groups on PEG600 leads to MsPEG600Ms, then, an intramolecular cyclization using 3,4-dihydroxybenzaldehyde yields MC-CHO, and finally a reduction of the benzaldehyde group produces MC-BnOH. Note that these molecules have a narrow distribution of PEG chain lengths, although the strucutres and names specify 13 ethylene oxide repeat units.

4.2.1.1.1 Synthesis of Bismesylated PEG 600 (MsPEG600Ms)

Pugh and coworkers[228,229] synthesized MsPEG600Ms in 81–93% yield in the presence of triethylamine in dichloromethane with methanesulfonyl chloride. Here, MsPEG600Ms was synthesized in 65-91% yield using the route in Scheme 4.1, similar to Pugh and coworkers.

Figure 4.1 and Figure 4.2 show the ^{1}H and ^{13}C NMR spectra, respectively of MsPEG600Ms at room temperature. The resonances in these spectra correspond to the literature values.[228]

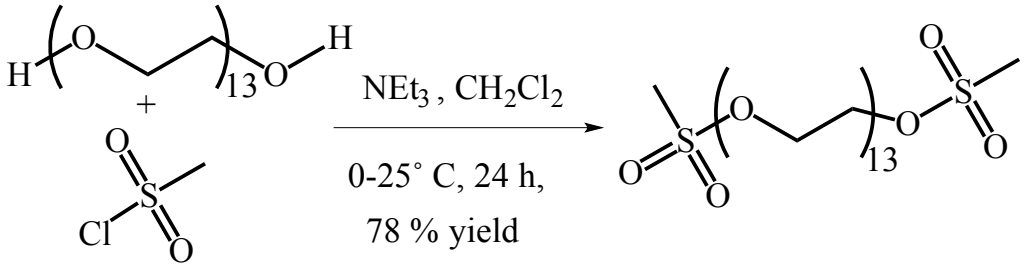

Scheme 4.1: Synthesis of MsPEG600Ms

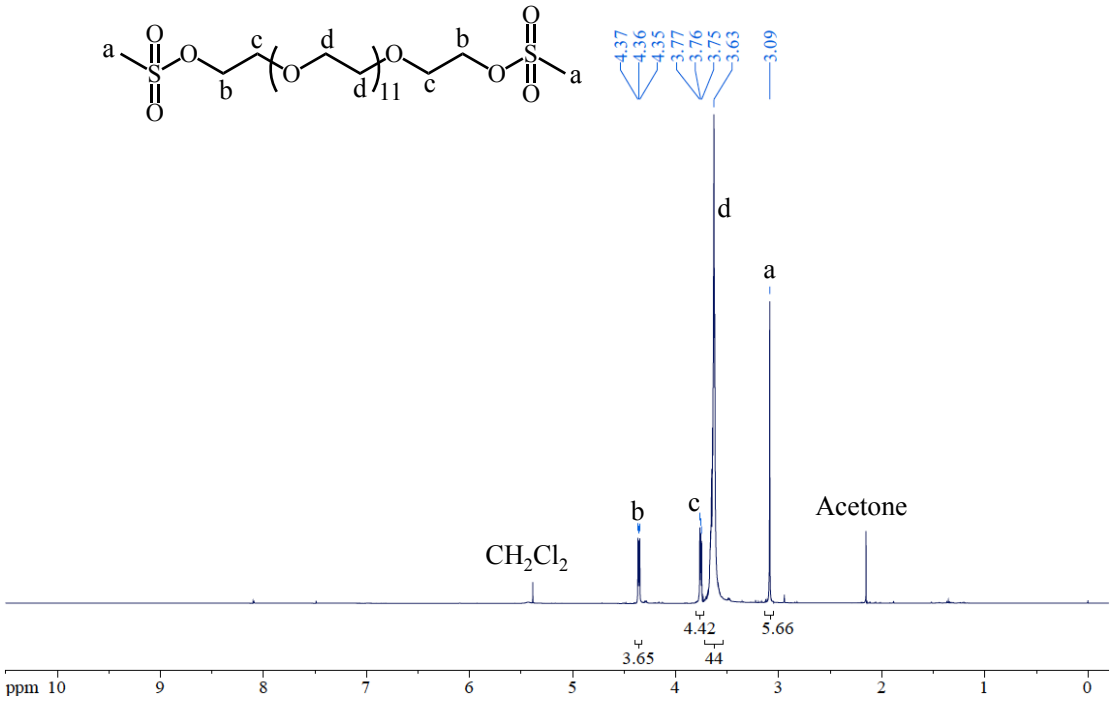

Figure 4.1: ^{1}H NMR Spectrum of MsPEG600Ms

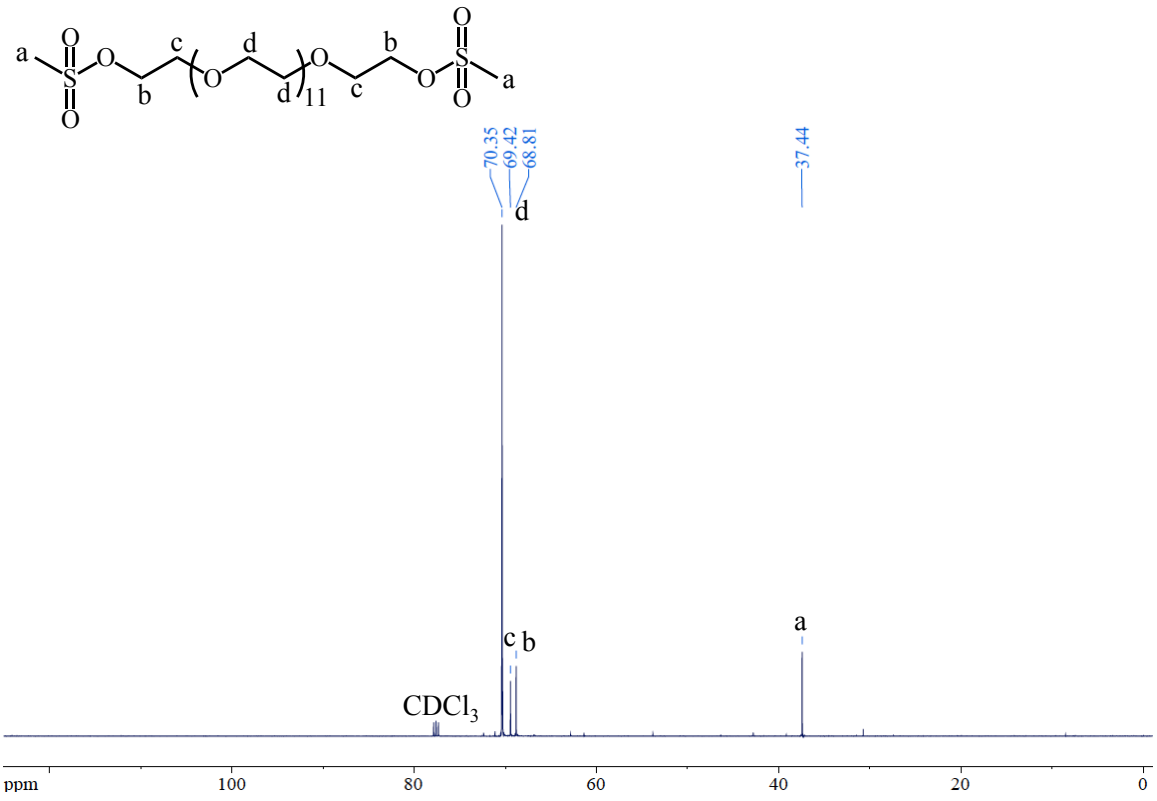

Figure 4.2: ^{13}C NMR Spectrum of MsPEG600Ms

In Figure 4.3, the MALDI-ToF MS of MsPEG600Ms shows both potassiated and sodiated distributions of MsPEG600Ms as well as a trace of a monomesylated polymer distribution (MsPEG600). The traces of monomesylated polymer distribution will lead to side polymer distribution in the next step of the synthesis.

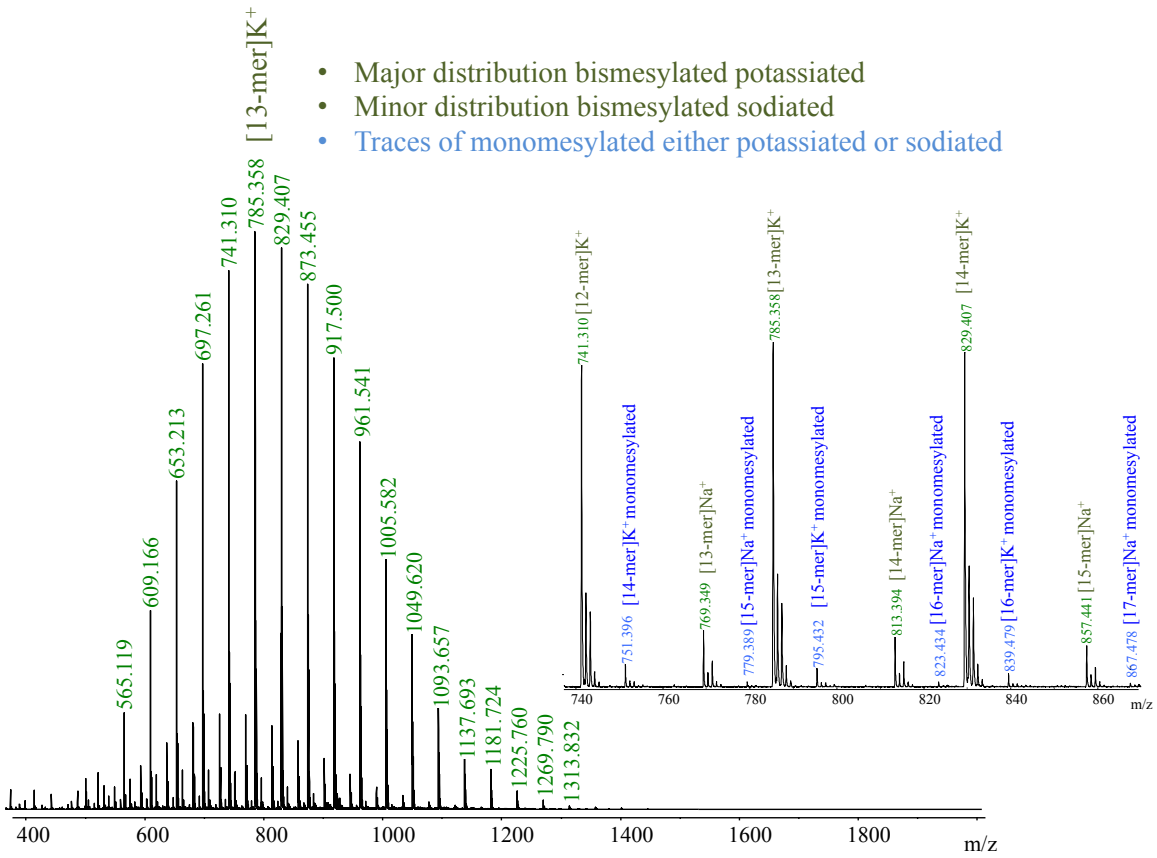

Figure 4.3: MALDI-ToF MS of MsPEG600Ms

4.2.1.1.2 Synthesis of 3,4-(42-Crown-14)benzaldehyde (MC-CHO)

Pugh and coworkers synthesized 3,4-(42-Crown-14)benzaldehyde using pseudo-high dilution conditions in *N*,*N*-Dimethylformamide (DMF) to favor PEG intramolecular cyclization *vs.* chain extension and intermolecular cyclization.[228,229] MC-CHO was

prepared by adding a solution of 3,4-dihydroxybenzaldehyde and MsPEG600Ms in DMF over 1 h[228] or 16 h[229] to a solution of potassium carbonate in DMF at 70 °C. The temperature was raised to 125 °C and the reaction was stirred for 72 h. After filtering the potassium salts off at room temperature, DMF was distilled off under reduced pressure and the residue was purified either by three reprecipitations into hexanes from THF[228] and/or by flash chromatography using silica gel as the stationary phase and chloroform and methanol as eluents to obtain an oil containing mostly cyclic oligomers, especially cyclic unimers, contaminated with a small amount of linear oligomers according to MALDI-ToF MS.[228,229] Pure cyclic oligomers were obtained in 19% yield after a second column chromatography using chloroform and methanol as eluents, as well as Soxhlet extraction of the material supported on silica using hexanes for 96 h.[229]

Here, MC-CHO was obtained in 27% yield using a procedure similar to Pugh and coworkers,[228,229] but adding a solution of 3,4-dihydroxybenzaldehyde and MsPEG600Ms in acetonitrile over 13 h to a solution of potassium carbonate in acetonitrile at 82 °C. The temperature was then raised to 87 °C and stirred for 72 h. The synthetic route is shown in Scheme 4.2.

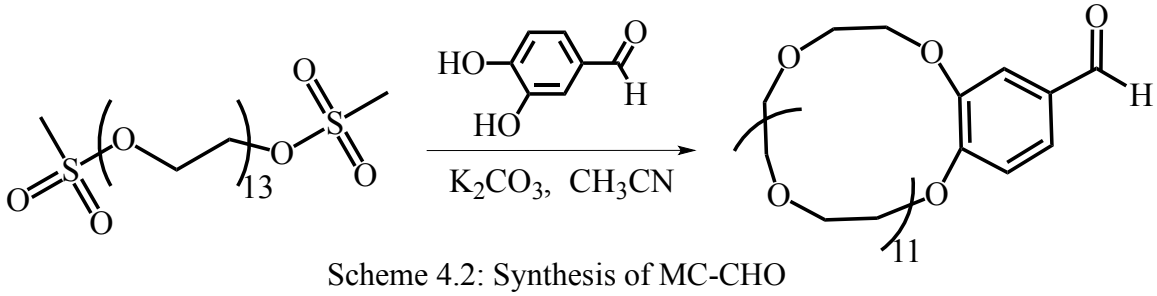

Scheme 4.2: Synthesis of MC-CHO

After filtering the potassium salts off at room temperature, acetonitrile was distilled off under reduced pressure to yield a brown oil (100%) that contained cyclic unimer (two structural units) as well as linear trimeric (three structural units) impurities, as shown in Figure 4.4. MS of aromatic aldehydes by electron ionization is characterized by an M-1 peak (-Ar-CO^+) that is always large and may be larger than the molecular ion peak.[234] In this case, MALDI-ToF gives rise to a potassiated distribution of the complete cyclic unimer MC-CHO. The structure of the linear trimeric species is shown in Figure 4.5. This oligomer distribution is the side product from the monomesylated PEG mentioned in section 4.2.1.1.1. This spectrum also shows the loss of CO from the aromatic aldehyde (i.e. M-28 Da). The structure of this oligomer distribution is shown in Figure 4.5. Note that unlike the synthesis in DMF[228,229] this crude material does not contain significant unimeric or dimeric impurities.

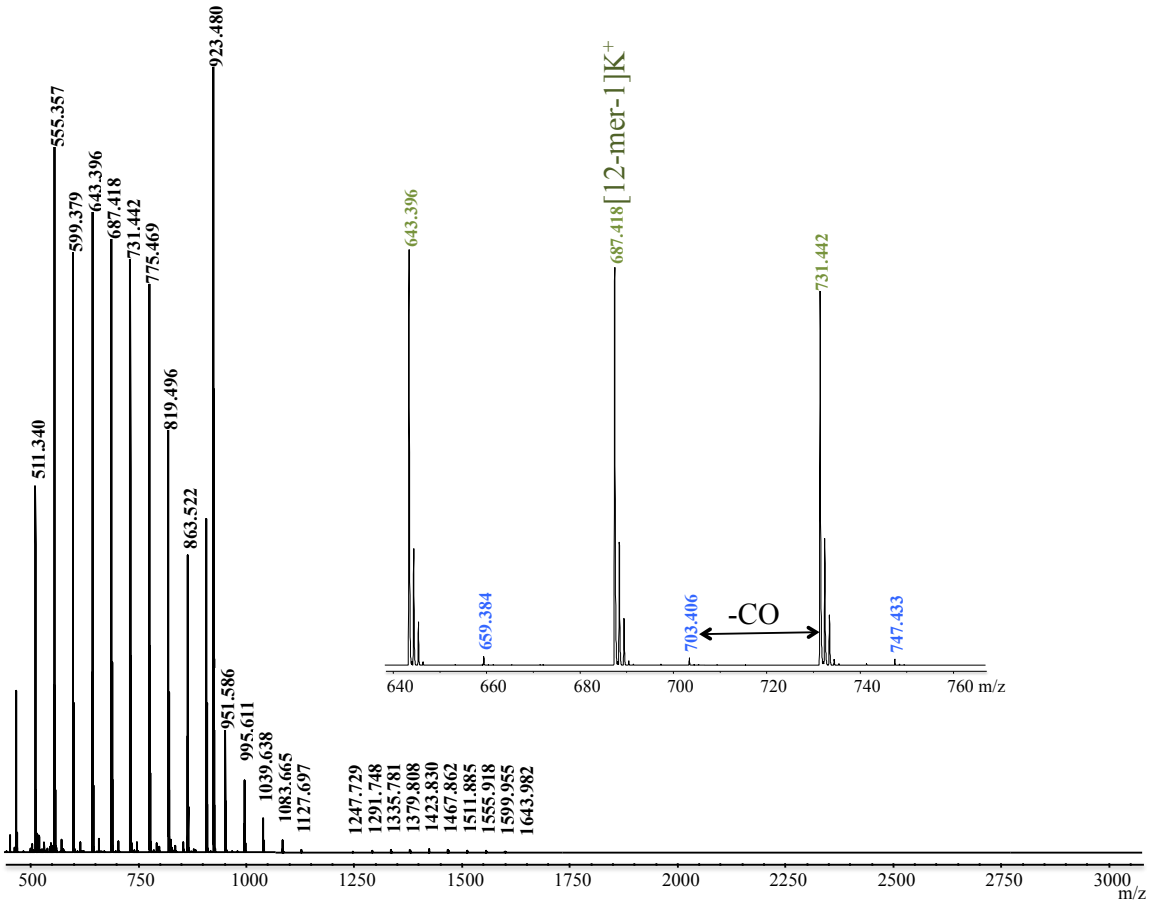

Figure 4.4: MALDI-ToF MS of Crude MC-CHO

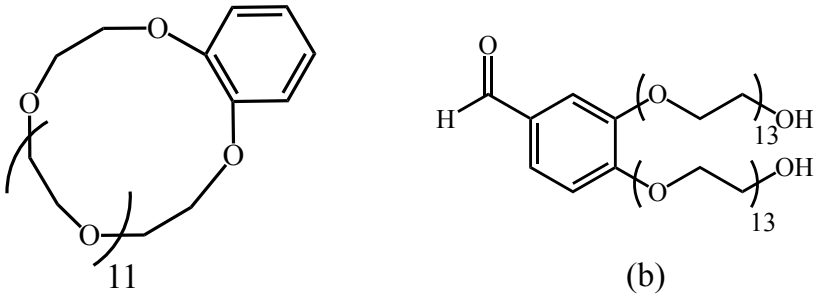

Figure 4.5: Polymer structures detected in the MALDI-ToF MS of MC-CHO: (a) Cyclic Unimer After Losing CO (b) Linear Trimeric Impurity

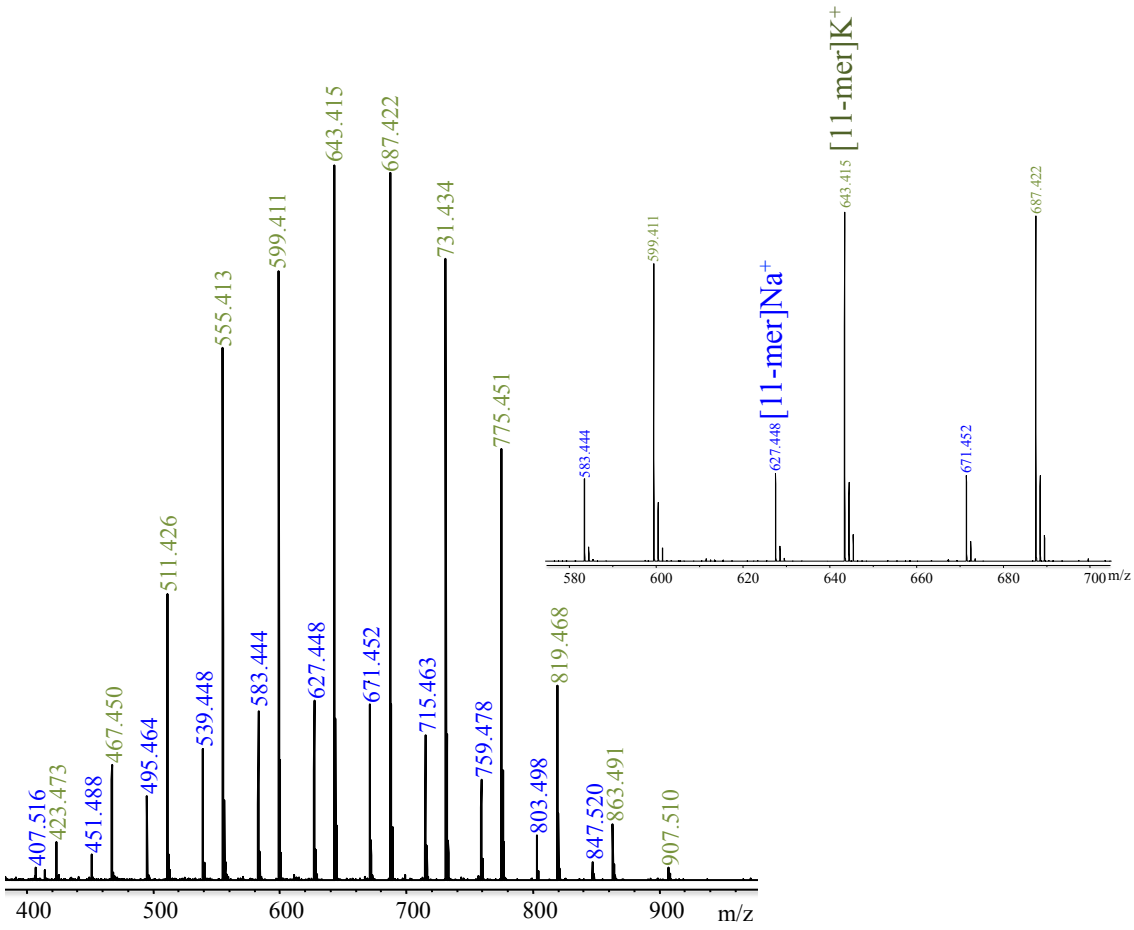

Figure 4.6: MALDI-ToF MS of First Fraction Purified MC-CHO

The crude oil from this MC-CHO synthesis was purified by flash chromatography using 3:1 hexanes : acetone to obtain cyclic unimer in 27% yield. Figure 4.6 shows the MALDI-ToF MS for the purified product. There are only two polymer distributions. One corresponds to the potassiated cyclic unimer and the other one corresponds to the sodiated cyclic unimer. The second fraction from the flash chromatography also looks like it only contains cyclic unimer and traces of non-functionalized PEG according to MALDI-ToF MS as shown in Figure 4.7.

The main polymer distribution corresponds to the potassiated cyclic unimer. The small polymer distribution corresponds to the loss of CO, as explained in the previous paragraph.

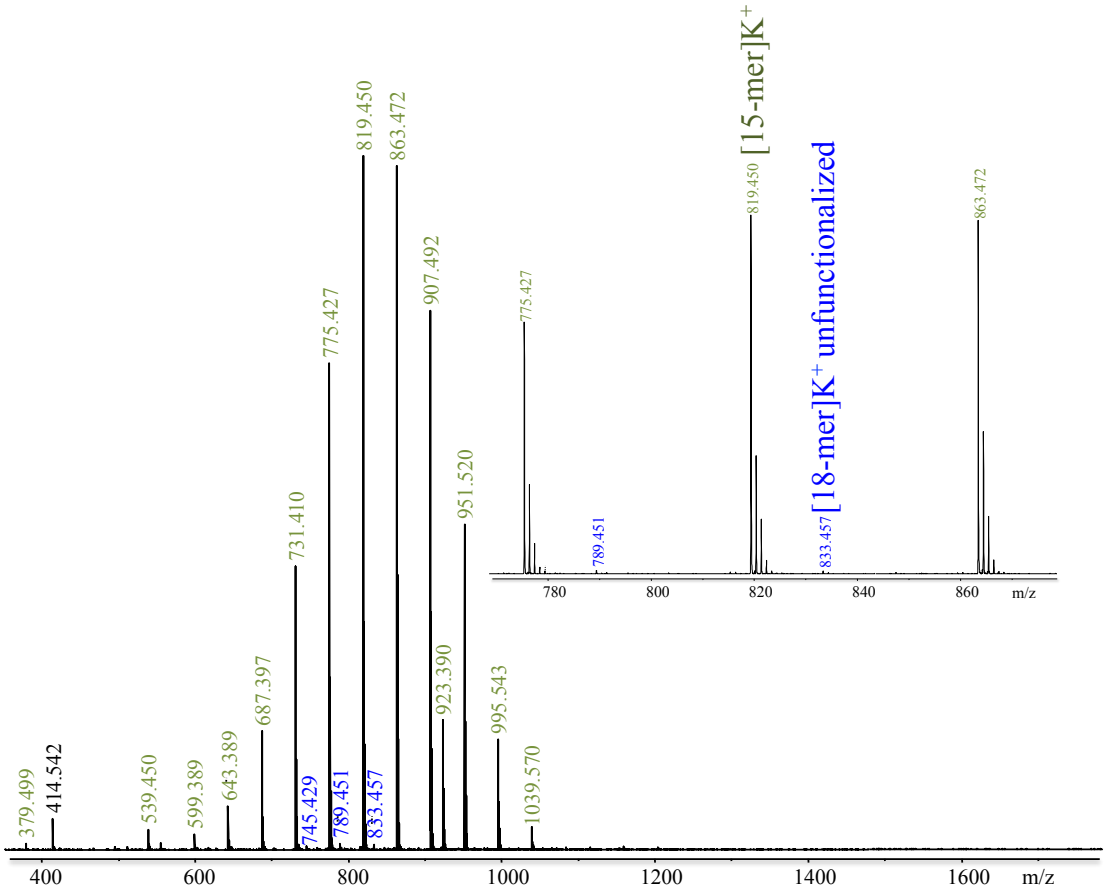

Figure 4.7: MALDI-ToF MS of Second Fraction Purified From Crude MC-CHO

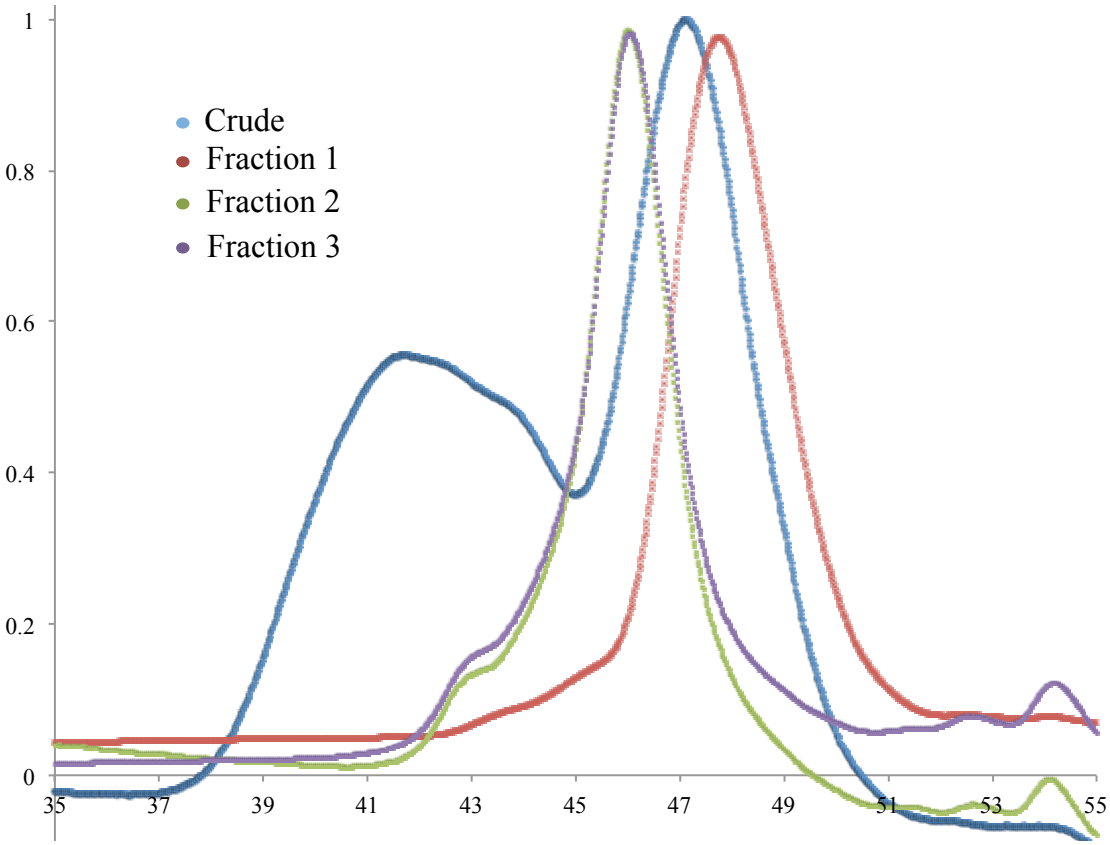

Figure 4.8: GPC Traces for MC-CHO Crude and Purified Fractions

Figure 4.8 shows GPC traces of the crude MC-CHO product as well as the purified and later fractions. While both Figure 4.6 and Figure 4.7 showed mainly cyclic unimer, fraction 1 has lower molecular weight fraction to fraction 2. Fraction 2 and fraction 3 have the same polymer molecular weights.

The method presented here for the synthesis and purification of MC-CHO increased the yield from 19% to 39% and reduced the work up time and expense by eliminating the need for a second column and 96 h of Soxhlet extraction.

4.2.1.1.3 Synthesis of 3,4-(42-Crown-14)benzyl Alcohol (MC-BnOH)

Pugh and coworkers synthesized 3,4-(42-Crown-14)benzyl Alcohol in 53-87% using sodium borohydride in absolute ethanol.[228] Here MC-BnOH was synthesized in 76% yield using a similar procedure shown in Scheme 4.3. Figure 4.9 and Figure 4.10 show the ^{1}H and ^{13}C NMR spectra of MC-BnOH. The resonances in these spectra correspond to the literature values.[228] Figure 4.9 shows the GPC traces of MCBnOH synthesized drom fractions 1-3 of MC-CHO, and its precursors. This figure shows the reduction in hydrodynamic radius upon cyclization of MsPEG600Ms and the similar hydrodynamic radius of MC-CHO and MC-BnOH.

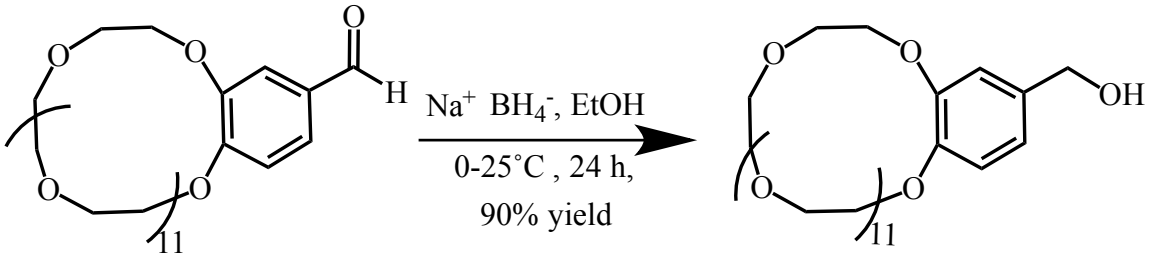

Scheme 4.3: Synthesis of MC-BnOH

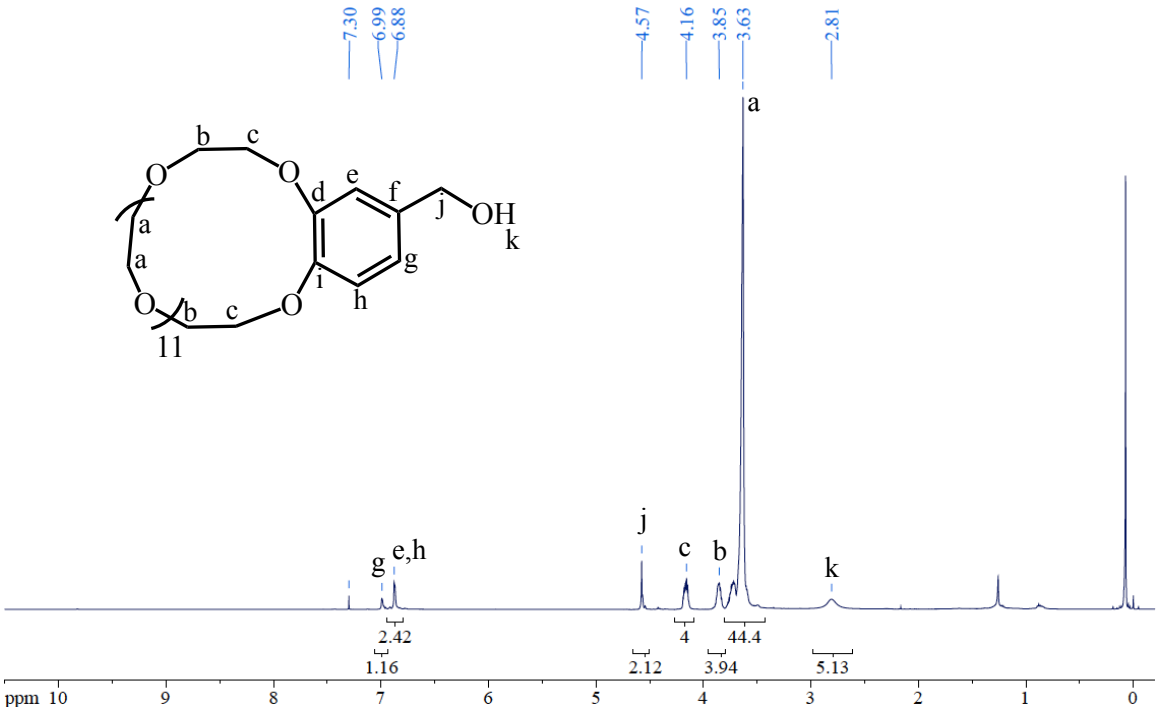

Figure 4.9: ^{1}H NMR Spectrum of MC-BnOH

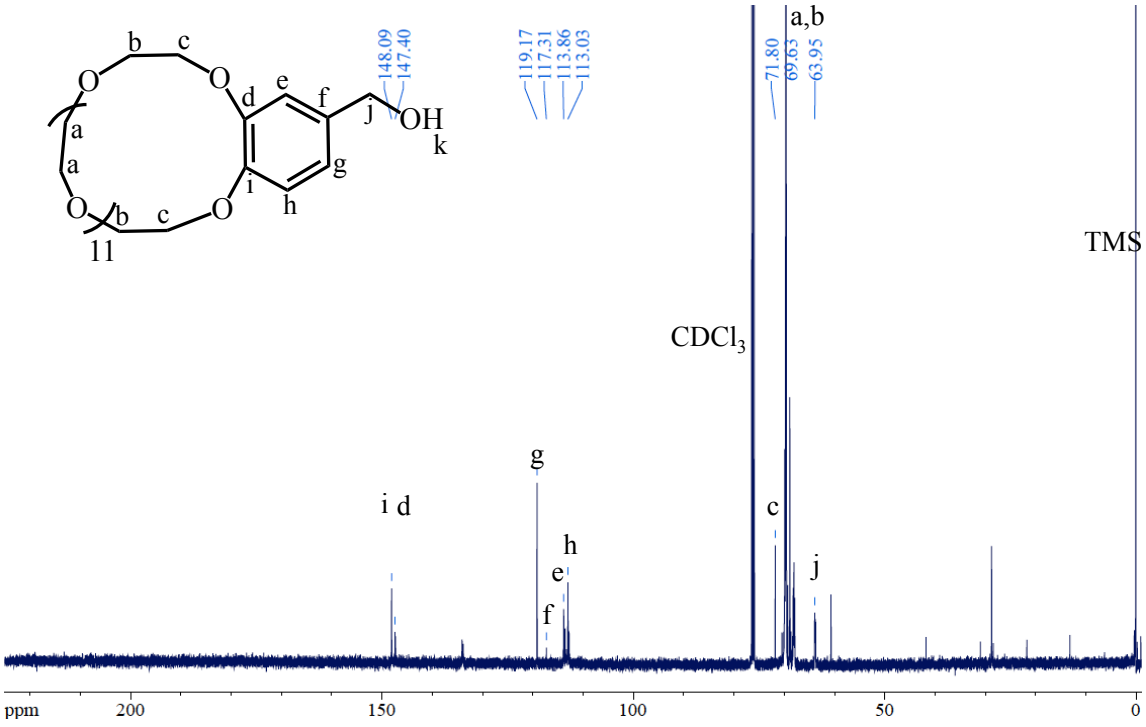

Figure 4.10: ^{13}C NMR Spectrum of MCBnOH

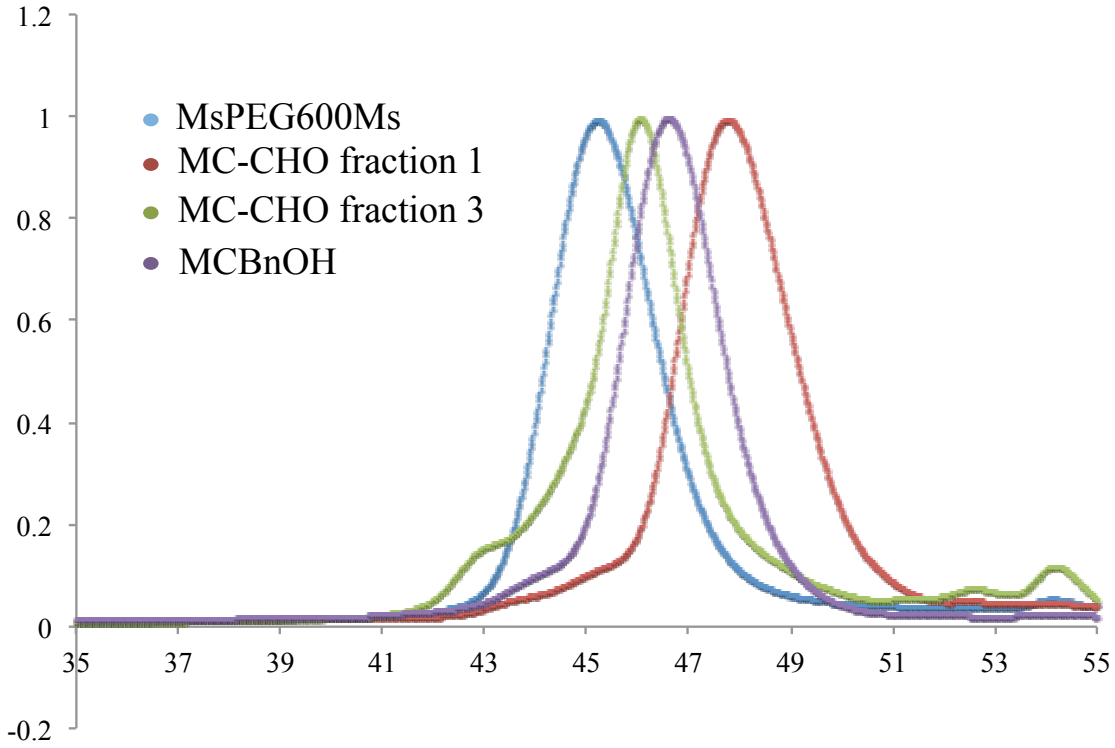

Figure 4.11: GPC Traces of MC-BnOH and its Precursors

4.2.1.2 Synthesis of Linear PEG Macroinitiator: MeOPEG550BnOH

MeOPEG550BnOH was synthesized in two steps from MeOPEG 550. First, a mesylation leads to MeOPEG550Ms, and then an etherification with *p*-hydroxybenzaldehyde yields MeOPEG550BnOH.

4.2.1.2.1 Synthesis of MeOPEG550Ms

As mentioned in section 4.2.1.1.1, Pugh and coworkers[228,229] synthesized MsPEG600Ms in 81–93% yield from PEG600 and methanesulfonyl chloride in the

presence of triethylamine in dichloromethane. Here, MePEG550Ms was synthesized in 73-78% yield using a similar procedure by mesylating MeOPEG550 similar to the mesylation of both ends of poly(ethylene glycol) 600. Scheme 4.4 shows the synthetic route. Figure 4.10 shows the ^{1}H NMR spectrum of MeOPEG550Ms. The resonances correspond to literature values.[228]

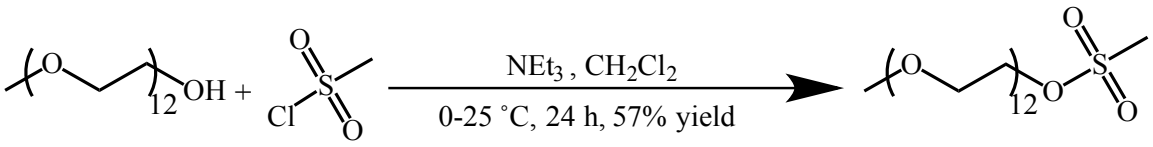

Scheme 4.4: Synthesis of MeOPEG550Ms

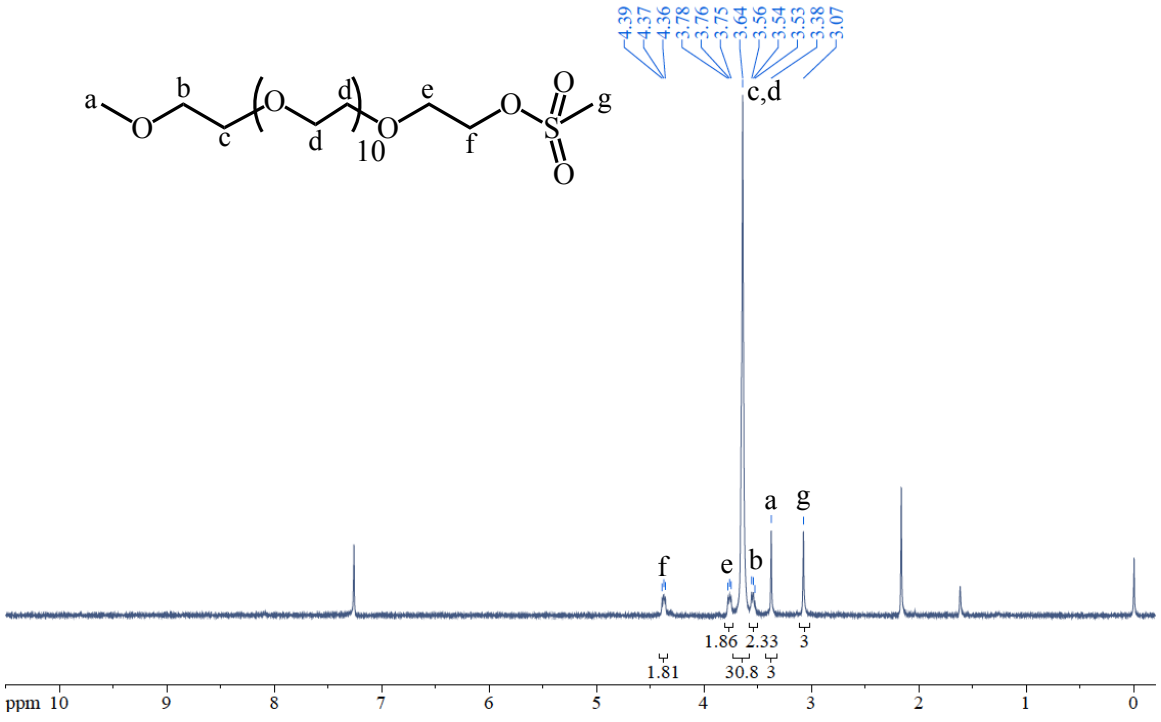

Figure 4.12: ^{1}H NMR Spectrum of MeOPEG550Ms

4.2.1.2.2 Synthesis of MeOPEG550BnOH

Different authors synthesized (4-(2-(2'-methoxyethoxy)ethoxy)phenyl)methanol, a low molecular weight analog of MeOPEG550BnOH by various synthetic routes. Heath and coworkers prepared (4-(2-(2'-methoxyethoxy)ethoxy)phenyl)methanol in 60% yield using methyl 4-hydroxybenzoate (i.e. instead of 4-hydroxybenzyl alcohol) and toluene-4-sulfonic acid 2-(2'-methoxyethoxy)ethyl ester for the etherification step, followed by cleavage of the ester to benzyl alcohol using $LiAlH_4$, as shown in Scheme 4.5 (a).[232] Boyer and coworkers used ethyl 4-hydroxybenzoate and 1-bromo-2-(2'-methoxyethoxy)ethane to obtain (4-(2-(2'-methoxyethoxy)ethoxy)phenyl)methanol in 56% yield, by the two steps shown in Scheme 4.5 (b).[233] Finally, Holzl and coworkers synthesized (4-(2-(2'-methoxyethoxy)ethoxy)phenyl)methanol using 4-hydroxybenzaldehyde and 1-bromo-2-(2'-methoxyethoxy)ethane instead of the mesylated one. This was followed by reduction of the benzaldehyde to benzyl alcohol, as shown in Scheme 4.5 (c). These authors did not report the yields for these reactions.[231]

Here, MeOPEG550Ms was etherified using an excess of 4-hydroxybenzyl alcohol and slightly substoichiometric amounts of K_2CO_3 relative to 4-hydroxybenzyl alcohol to prevent deprotonation of the benzyl alcohol that would lead to coupling between PEG chains. This synthetic route is shown in Scheme 4.7. Figure 4.11 shows the ^1H NMR spectrum of MeOPEG550BnOH. The resonances in these spectra correspond to the literature values.[232] Figure 4.125 shows the MALDI-ToF MS of MeOPEG550BnOH, which confirms the synthesis and purity of this macroinitiator.

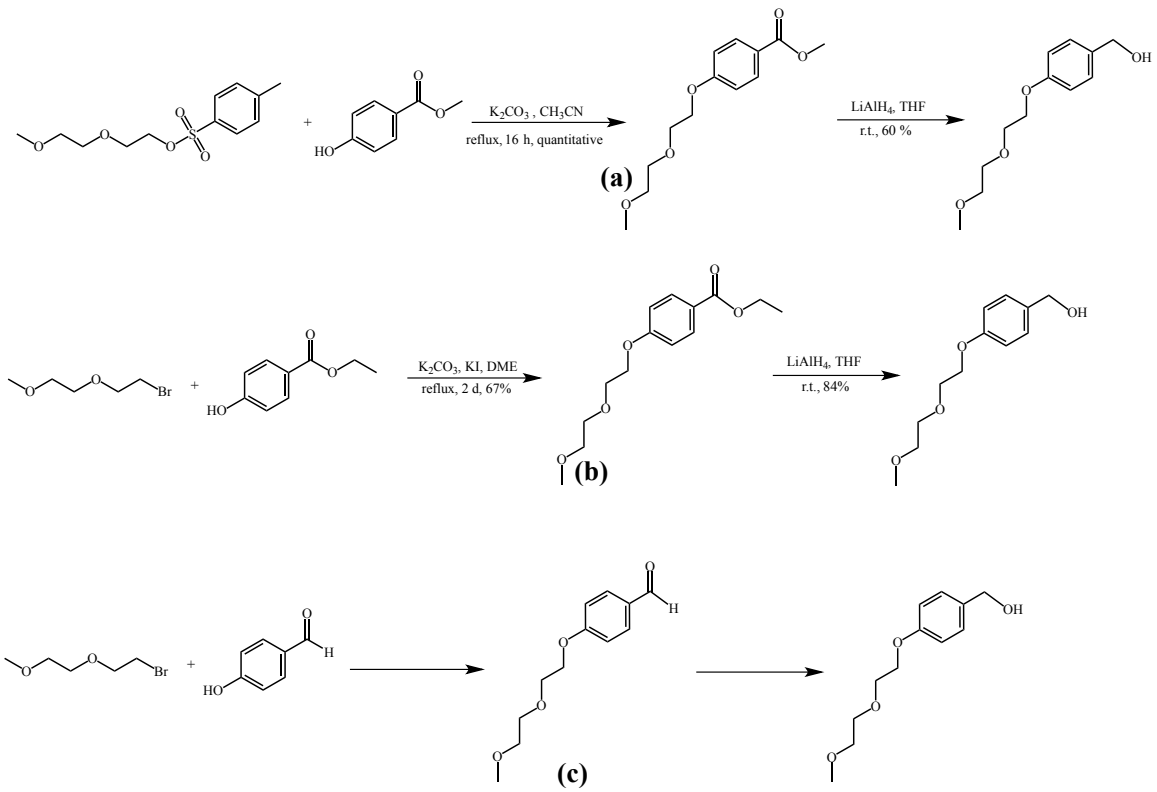

Scheme 4.5: Literature Precedence for the Synthesis of MeOPEGBnOH

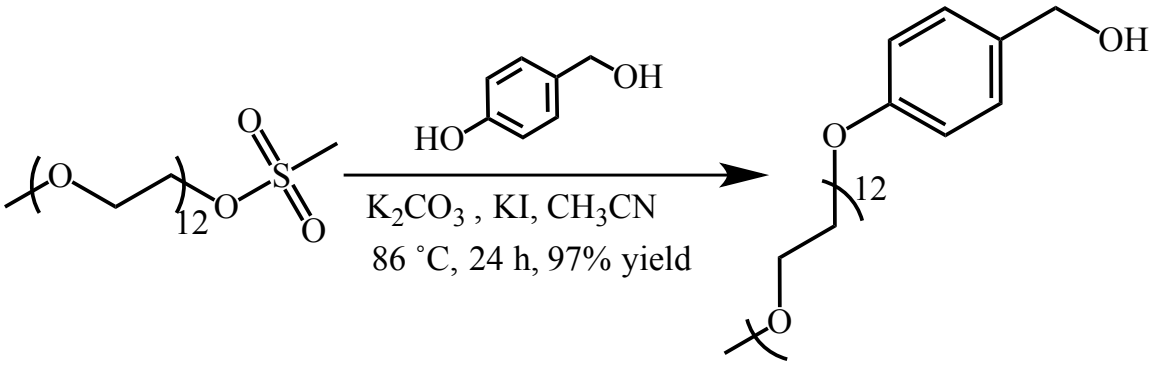

Scheme 4.6: Synthesis of MeOPEG550BnOH

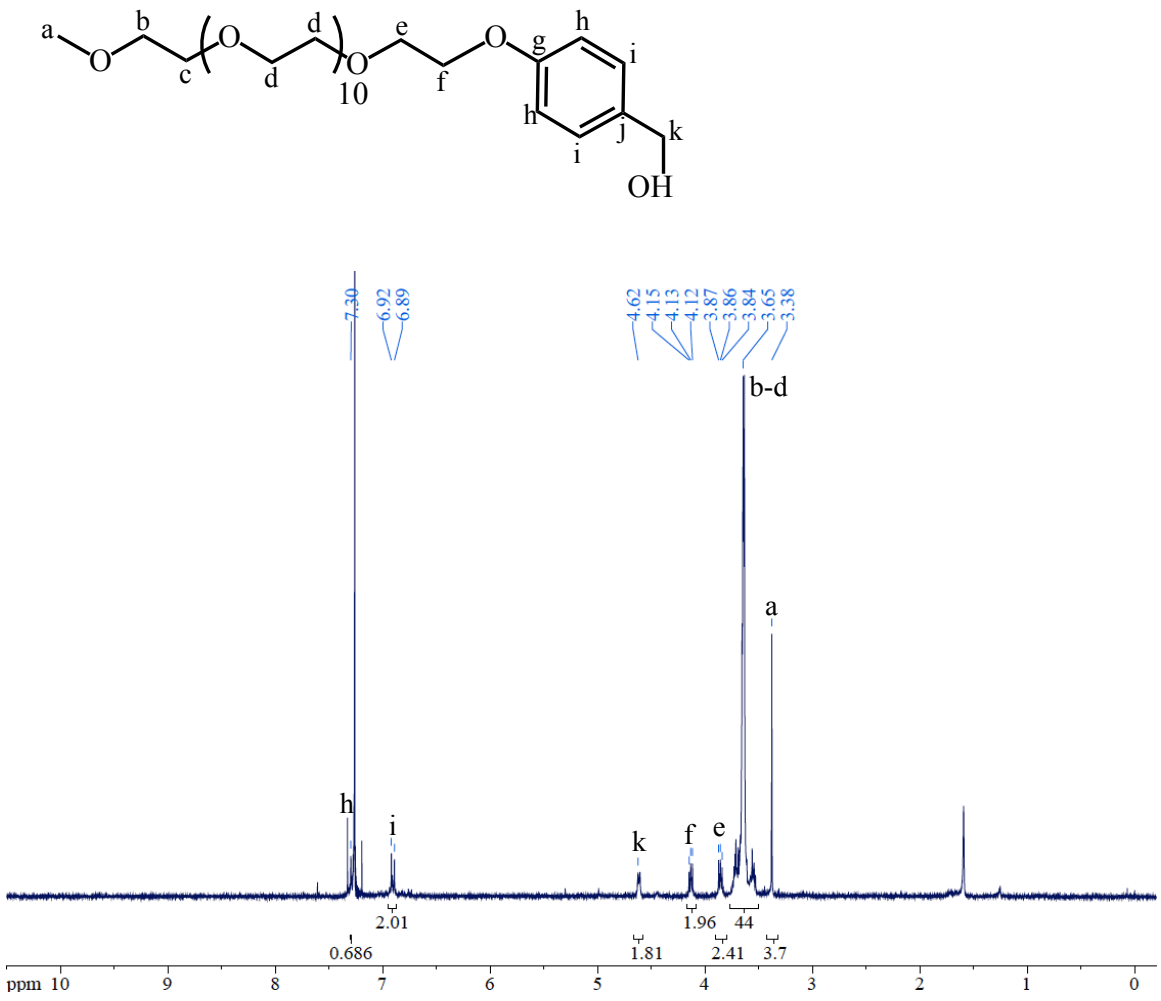

Figure 4.13: ^{1}H NMR Spectrum of MeOPEG550BnOH

Compared to the work of Heath and coworkers the method presented here for the synthesis and purification of MeOPEG550BnOH has reduced the number of synthetic steps from 3 to 2.[232]

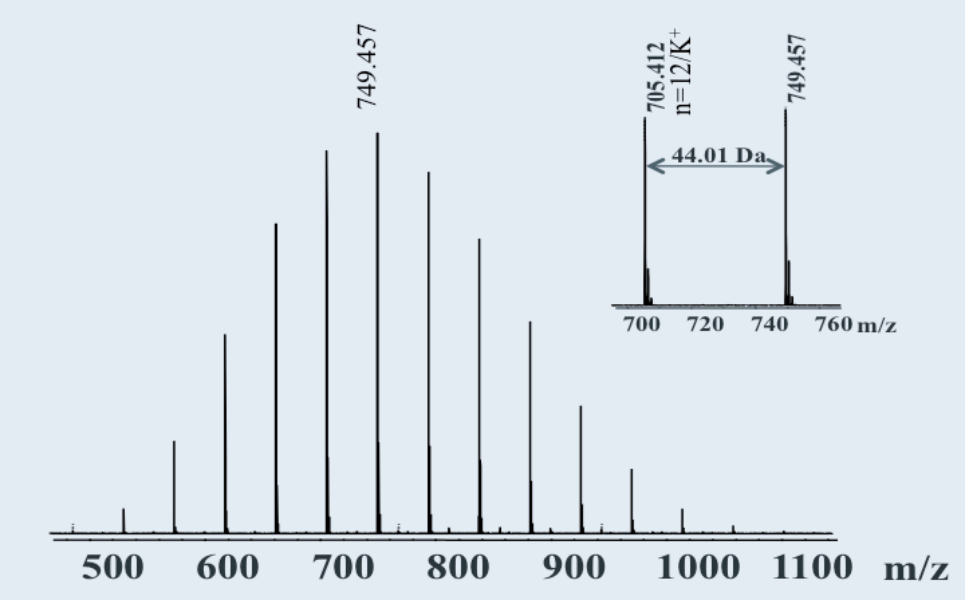

Figure 4.14: MALDI-ToF MS of MeOPEG550BnOH

This method is also cheaper than the ones proposed by Boyer and coworkers[233] and Holtz and coworkers[231] who used 1-bromo-2-(2'-methoxyethoxy)ethane instead of di(ethylene glycol) methyl ether as raw material. The first compound is 500 times more expensive than the second one.

4.2.2 Synthesis of PEG-*b*-PCL Diblock Copolymers

Amphiphilic PEG-*b*-PCL diblock copolymers were synthesized from the PEG macroinitiators described in section 4.2. These diblock copolymers have either a linear or a cyclic architecture in the PEG block.

4.2.2.1 Synthesis of Cyclic-*b*-linear MC-BnOPCL Diblock Copolymers

Although several authors have synthesized PEG-*b*-PCL diblock copolymers and a good number of them have prepared self-assembled micelles from them,[78,80,115,201,213,235-249] there is no report of PEG-*b*-PCL diblock copolymers having a cyclic architecture in the PEG block. Scheme 4. shows the synthesis of MCBnOPCL (i.e. cyclic-*b*-linear) diblock copolymer by ring-opening polymerization of ε-caprolactone using tin octoate as a catalyst and THF as solvent similar to literature polymerizations of ε-caprolactone.[80,235,236,238,240-242,244-246] MCBnOPCL copolymers with three different polycaprolactone molecular weights were synthesized corresponding to one, three, and five times the molecular weight of the PEG block by the synthetic route shown in Scheme 4.8.

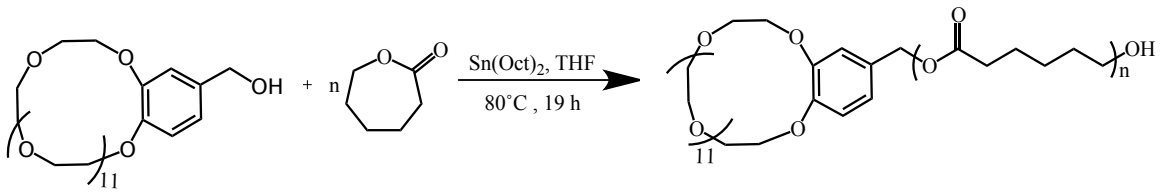

Scheme 4.7: Synthesis of MCBnOPCL Diblock Copolymers

Table 4.1 shows the polymerization conditions and molecular weight data of these copolymers. Figure 4.15 and Figure 4.16 show the ^{1}H NMR and ^{13}C NMR spectra, respectively of the MCBnOPCL copolymer with the highest PCL molecular weight (MCBnOPCL5x). The resonances in these spectra correspond to the literature values.[214,250,251] Figure 4.17 shows the MALDI-ToF MS of the same diblock copolymer,

along with an expanded region between 1350 and 1444 Da. The expanded region has the assignments for the number of ethylene glycol and caprolactone units in the potassiated diblock copolymers. For example, $MC_{10}BnOPCL_7K^+$ has a mass of 1399.8 Da. Figure shows the GPC traces of MCBnOH and the MCBnOPCL diblock copolymers. As expected, the retention times increase as the PCL molecular weight increases. Note that there is not a significant difference between the retention time for MCBnOH and MCBnOPCL(1x). Even though ^{1}H NMR spectroscopy confirms the presence of the PCL block in the diblock copolymer, there is not a significant increase in the hydrodynamic radius of the polymer (GPC) due to the presence of the lowest PCL molecular weight.

Table 4.1: Polymerization Conditions and Characterization of MCBnOPCL

$\frac{[M]}{[I]}$	$\frac{[I]}{[Sn(Oct)_2]}$	Conv (%)	MCBnOPCL M_n (kg/mol)				PDI
			Theo at 100 % conv.	Theo with conversion	^{1}H NMR	GPC	
6	0.8	93	0.646	0.600	0.679	1.76	1.12
15	0.8	100	1.77	1.70	1.69	2.31	1.17
24	0.8	92	2.70	2.48	2.51	3.14	1.23

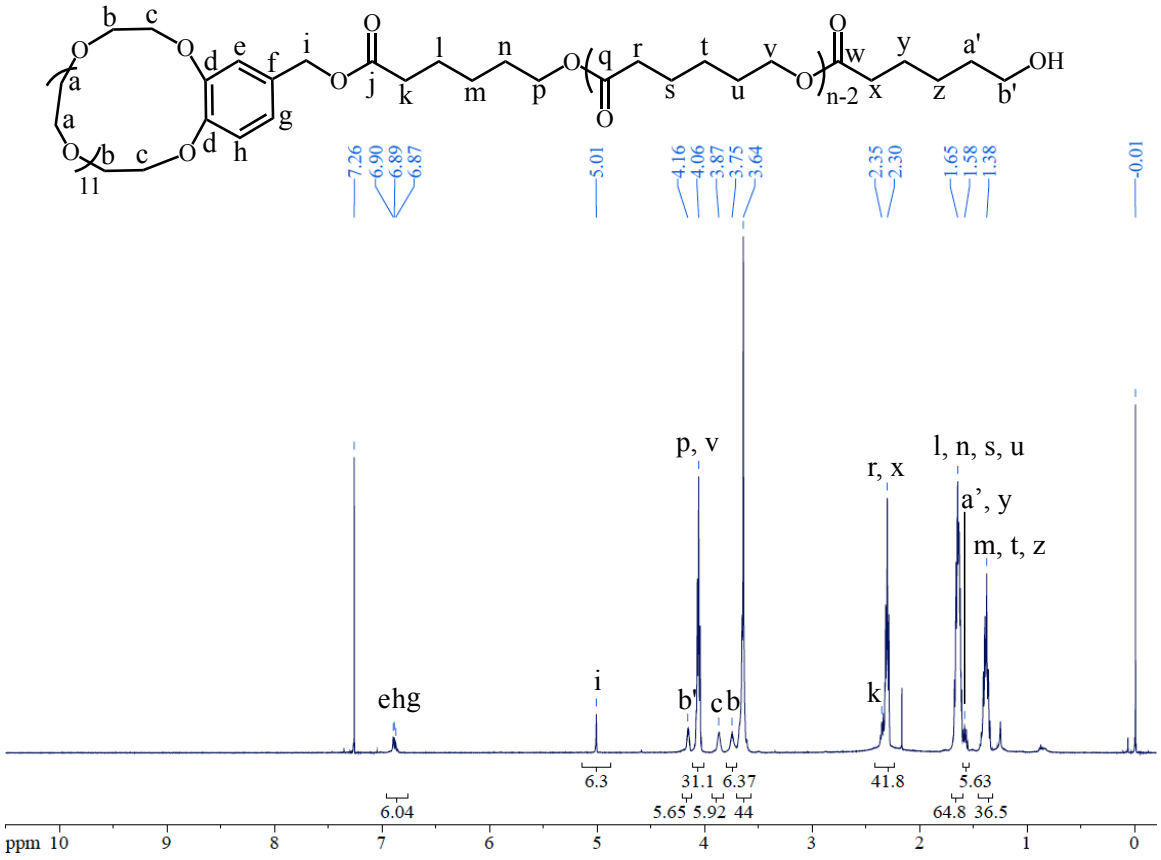

Figure 4.15: ^{1}H NMR Spectrum of MCBnOPCL5x

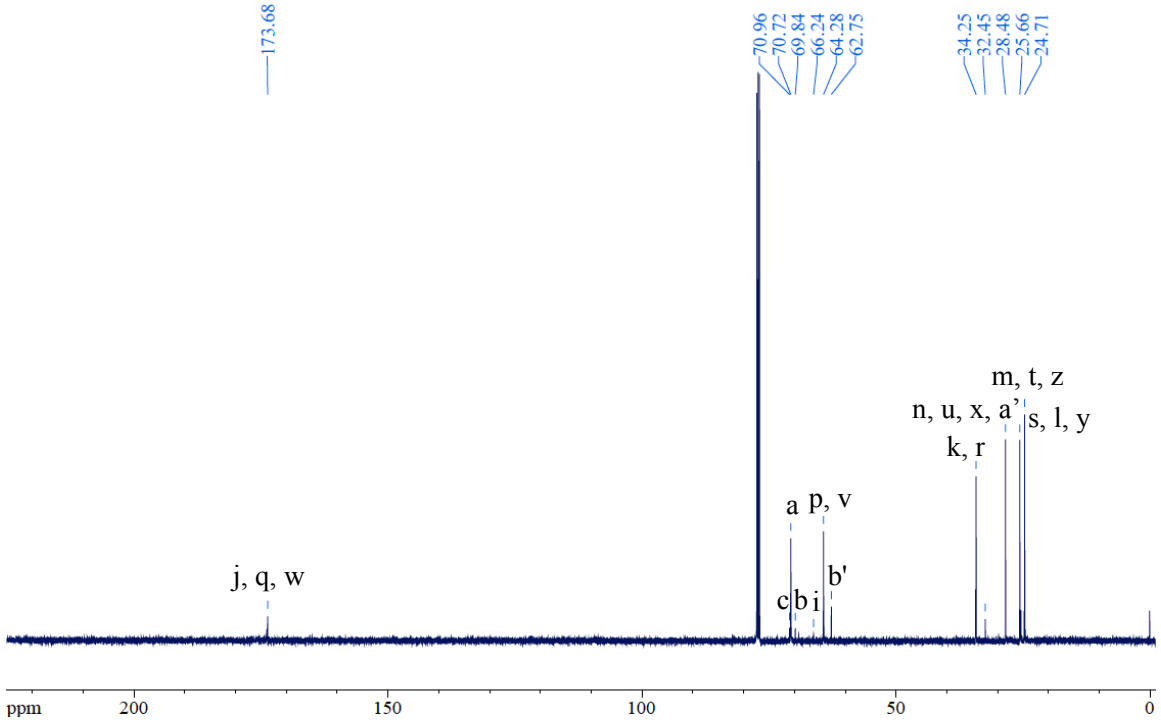

Figure 4.16: ^{13}C NMR Spectrum of MCBnOPCL5x

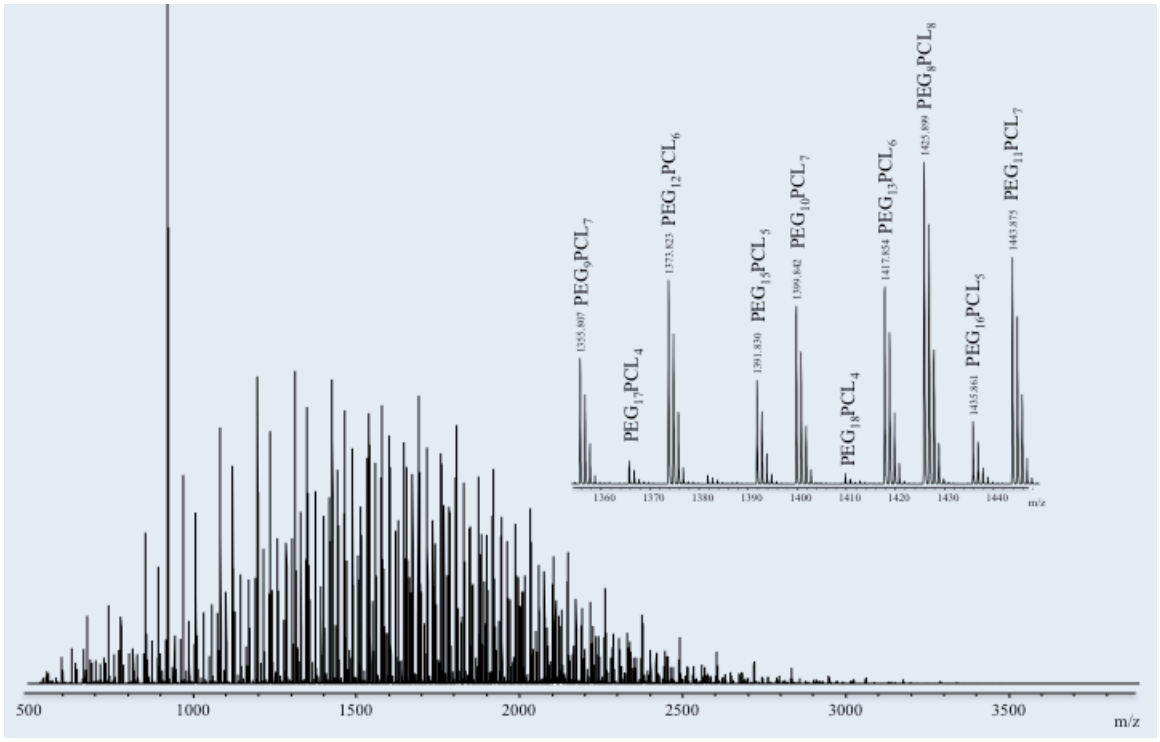

Figure 4.17: MALDI-ToF MS of MCBnOPCL

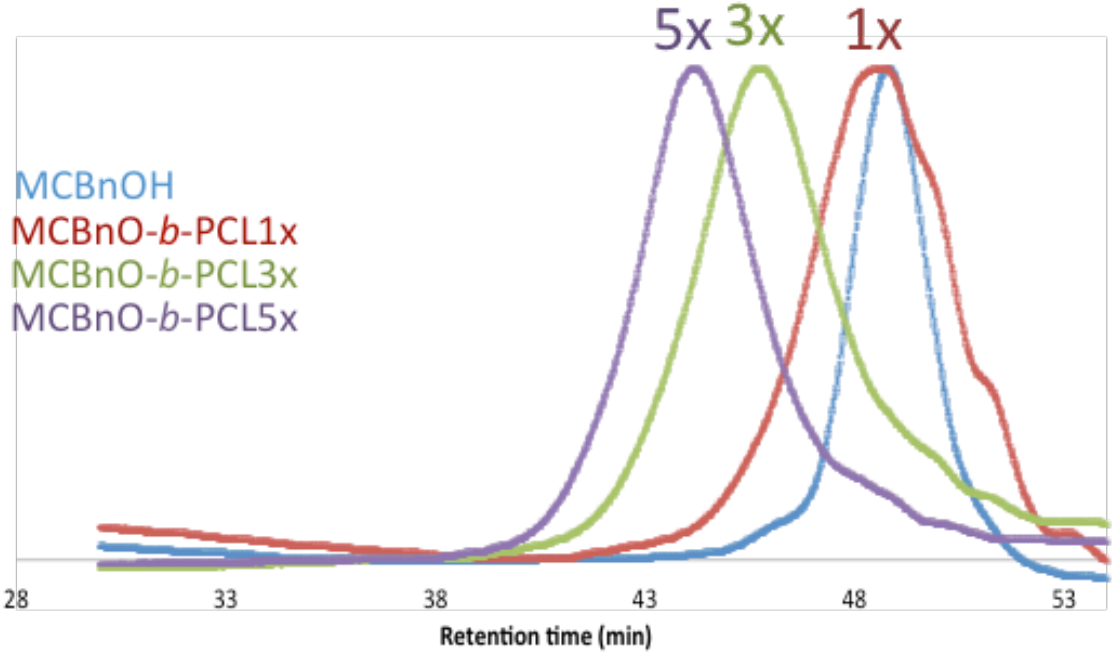

Figure 4.18: GPC Traces of MCBnOH and MCBnOPCL Diblock Copolymers

The published thermal transitions of polycaprolactone homopolymers with a molecular weight of 8000 g/mole are Tg at -60 °C, crystallization temperature at 33 °C, and melting temperature at 55 °C.[214,251,252] In the case of PEG homopolymer with a molecular weight of 4000 g/gmole, Tg is at -22 °C, crystallization temperature at 38 °C, and melting temperature at 52 °C.[214,251,252] Differential scanning calorimetry (DSC) of the cyclic-*b*-linear PEG-*b*-PCL diblock copolymers between -20 and 80 °C should show only melting and crystallization transitions because PEG with a molecular weight lower than 1000 Da does not crystallize. As seen in Figure , MCBnO-*b*-PCL2000 is polymorphic after heating through the melting point at 47 °C and then cooling at 10 °C min. The second and third heating scans show melting transitions at around 34 °C. In contrast, MCBnO-*b*-PCL2500 does not show polymorphic behavior, although the melting temperature decreases from 53 °C on the first heat scan to 41 °C on the second and third heating scans. The melting transitions increase with increasing the molecular weight of polycaprolactone, as expected.

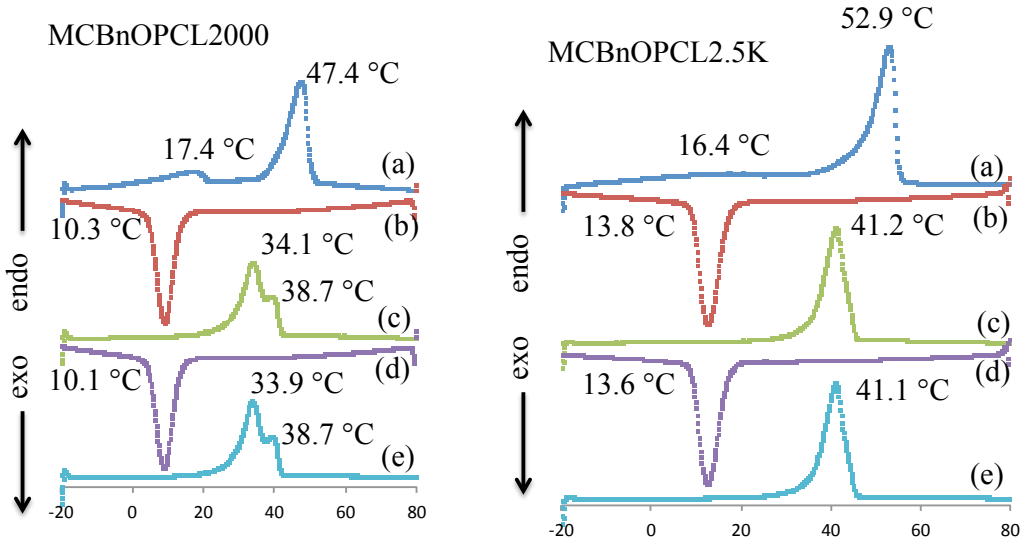

Figure 4.19: DSC Traces of MCBnOPCL Diblock Copolymers: (a) 1st heat, (b) 1st cool, (c) 2nd heat, (d) 2nd cool, and (e) 3rd heat

4.2.2.2 Synthesis of Linear-*b*-linear MeOPEG550PCL Diblock Copolymers

As mentioned in the previous section, several authors have synthesized PEG-*b*-PCL linear-*b*-linear diblock copolymers[80,235,236,238,240-242,244-246] and a good number of them have prepared self-assembled micelles from these diblock copolymers.[78,80,115,201,213,235,237-241,243,247-249] Here we also synthesized linear-*b*-linear diblock copolymers as a control to compare the effect of the PEG architecture on micelle self-assembly. These linear-*b*-linear diblock copolymers were synthesized in a analogous way to MCBnOPCL: by ring-opening polymerization of ε-caprolactone using MeOPEG550BnOH as macroinitiator, tin octoate as catalyst, and THF as solvent. Scheme 4.8 shows the synthetic route to the MeOPEG550BnOPCL diblock copolymers. shows the polymerization conditions and molecular weight data of these copolymers. Table 4.2 shows the polymerization conditions and molecular weight data of these copolymers.

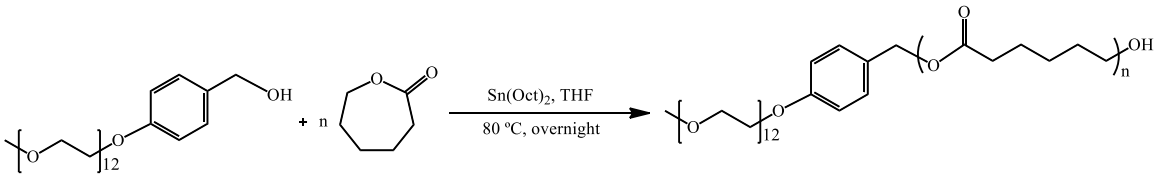

Scheme 4.8: Synthesis of MeOPEG550BnOPCL Diblock Copolymers

Table 4.2: Polymerization Conditions and Characterization of MeOPEG550BnOPCL

$\frac{[M]}{[I]}$	$\frac{[I]}{[Sn(Oct)_2]}$	Conv (%)	MeOPEGBnOPCL M_n (kg/mol)				PDI
			Theo at 100 % conv.	Theo with conversion	^{1}H NMR	GPC	
4	1.0	100	0.444	0.444	0.374	1.56	1.03
12	1.1	100	1.32	1.27	1.12	2.01	1.09
20	1.0	100	2.32	2.30	1.88	2.54	1.20

Figure 4.20 and Figure 4.21 show the ^{1}H and ^{13}C NMR spectra, respectively of the MeOPEG550BnOPCL polymer with the highest molecular weight. The resonances in these spectra correspond to the literature values. [214,250,251] In Figure 4.22, MALDI-ToF of the same diblock copolymer with a zoomed in region between 1363 and 1441 Da shows some of the repeating units for each block. For example, $MeOPEG_{10}PCL_7K^+$ has a mass of 1415.8 Da.

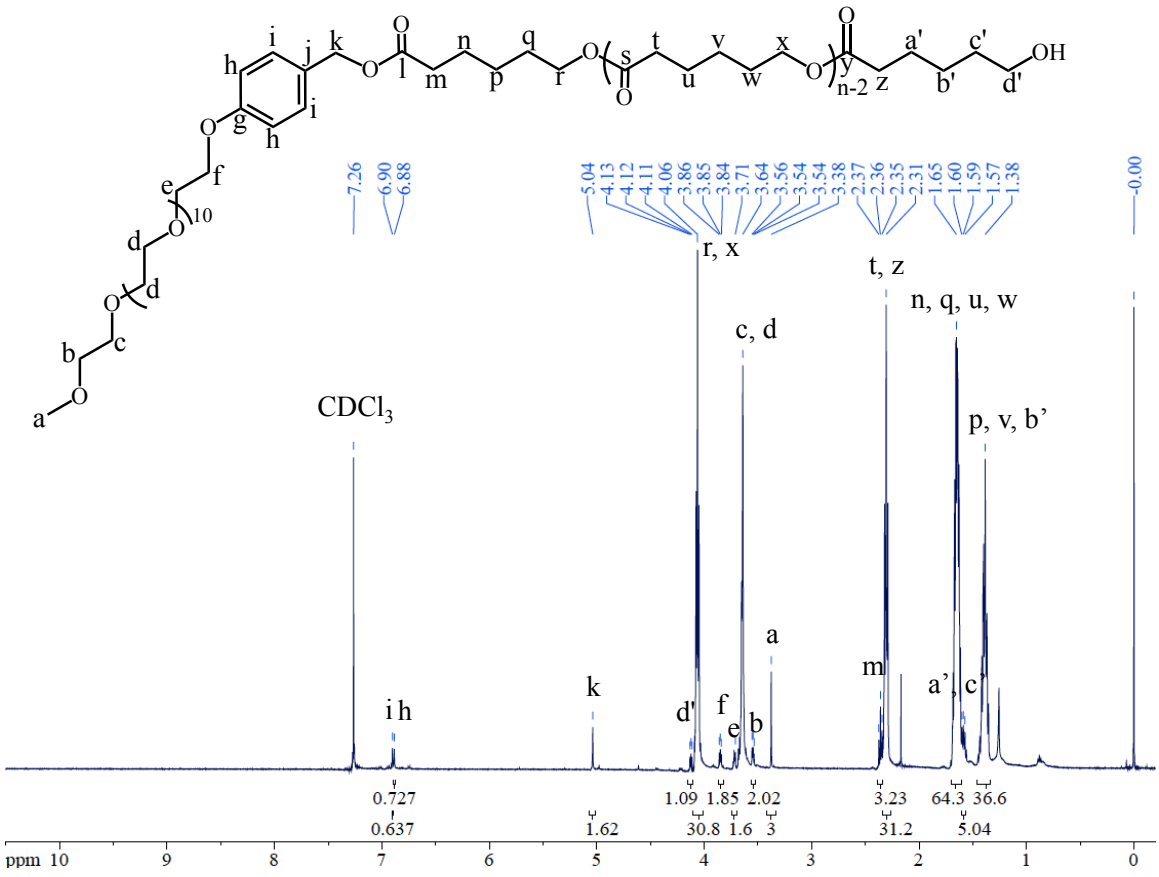

Figure 4.20: ^{1}H NMR Spectrum of MeOPEG550BnOPCL5x

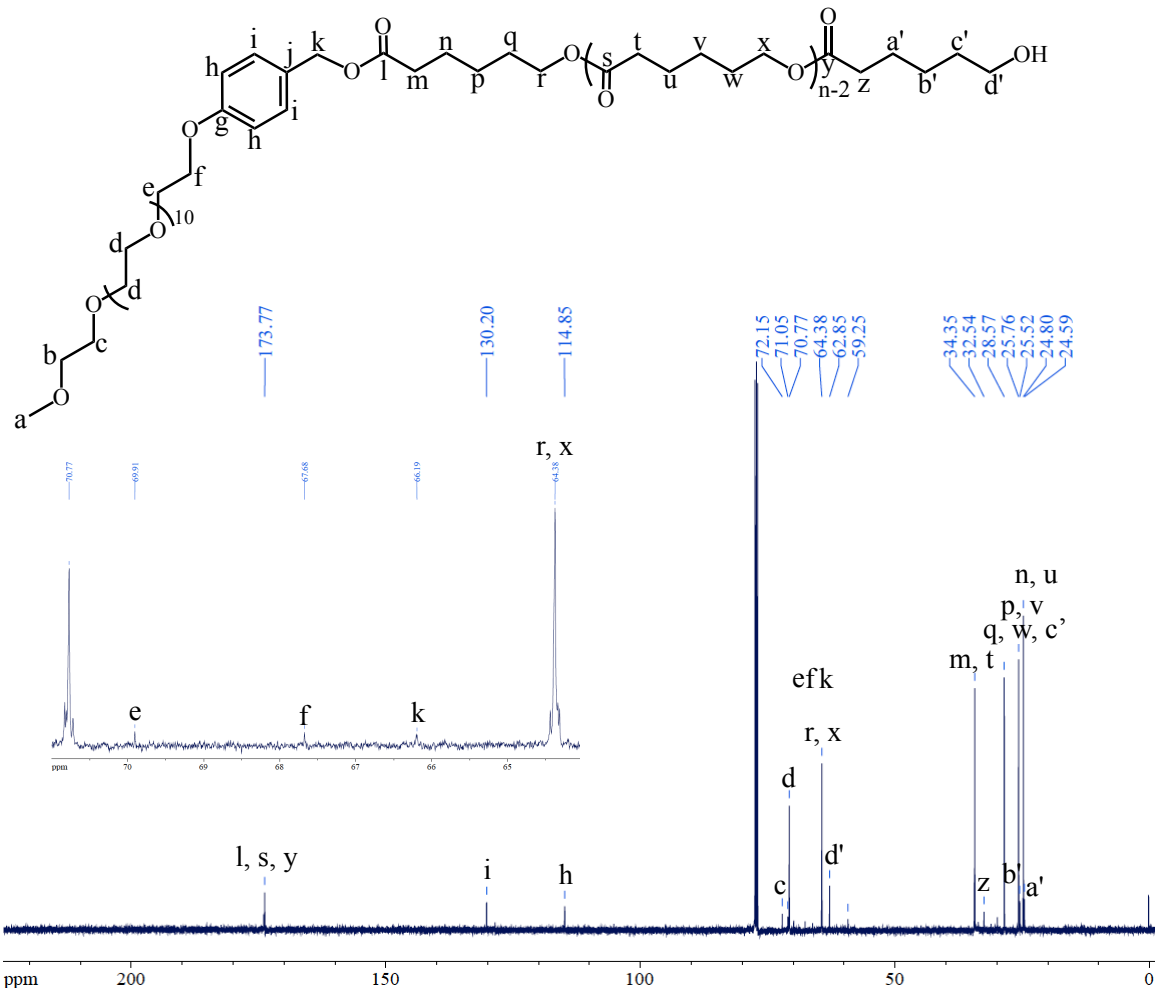

Figure 4.21: ^{13}C NMR Spectrum of MeOPEG550BnOPCL5x

In Figure 4.23, gel permeation chromatography traces show the gradual increment of molecular weight from MeOPEG550BnOH for diblock copolymers with PCL molecular weights that correspond to one time, three times, and five times the molecular weight of the PEG block. As in the case of MCBnOPCL copolymers, ^{1}H NMR spectroscopy confirms the presence of the PCL block in the diblock copolymer for MeOPEGPCL1x but there is not a significant increase in the hydrodynamic radius of the polymer due to the presence of PCL.

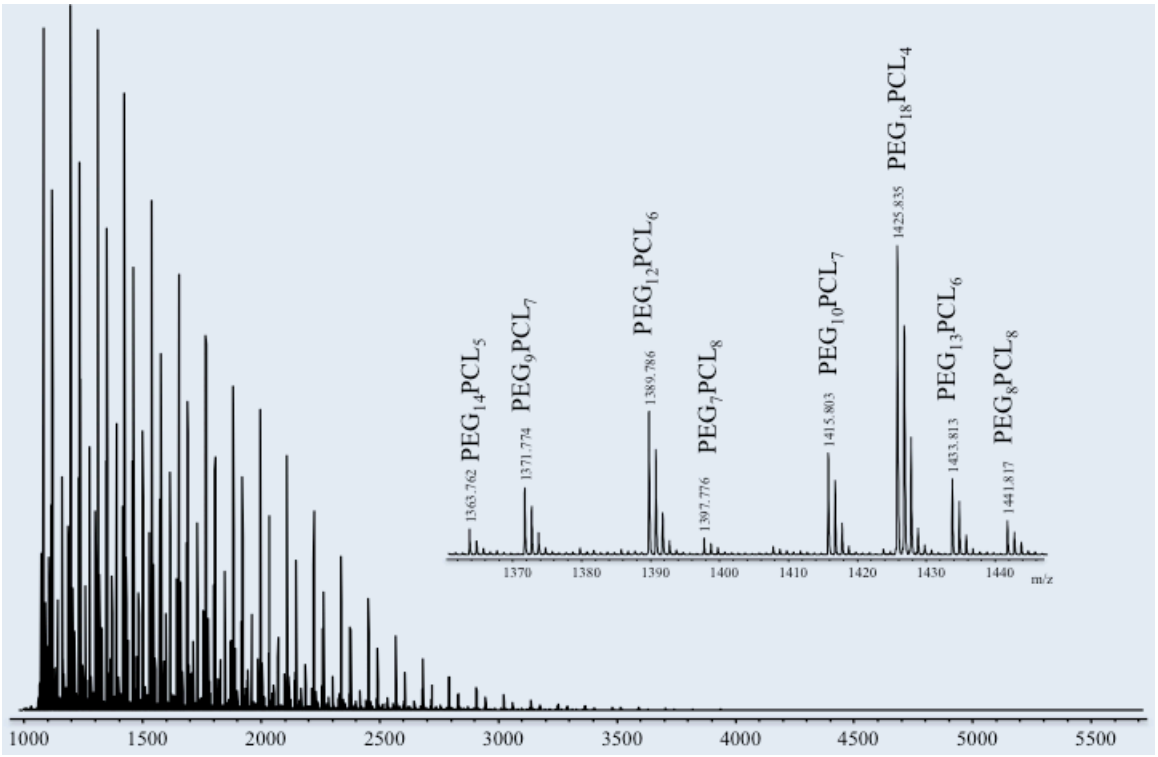

Figure 4.22: MALDI-ToF MS of MeOPEG550BnOPCL5x

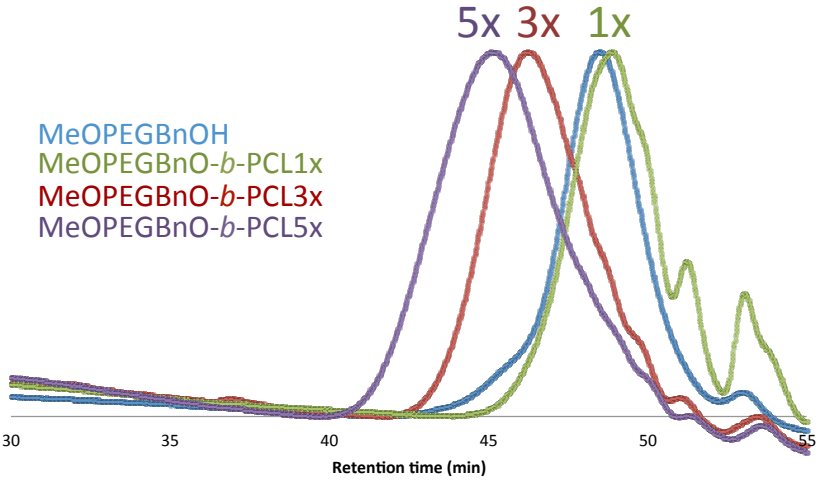

Figure 4.23: GPC Traces of MeOPEG550BnOH and MeOPEG550BnOPCL

The DSC traces in Figure 4.24, shows that MeOPEG550-*b*-PCL1000 is polymorphic in all three heating scans. However, the highest transition temperature decreases from 44 C on the fisrt heating scan to 32 C and 28 C on the second and third heating scans, respectively. with melting temperatures around 28 °C. In contrast, MeOPEG550-*b*-PCL2000 shows less of a polymorphic behavior and the melting transitions on the second and third heating scans are at 41 °C, similar to the thermal behavior of MCBnO-*b*-PCL2500. The melting transitions increase with increasing molecular weight of polycaprolactone. The PCL block of MeOPEG550-*b*-PCL polymers seem to crystallize better than that MCBnO-*b*-PCL.

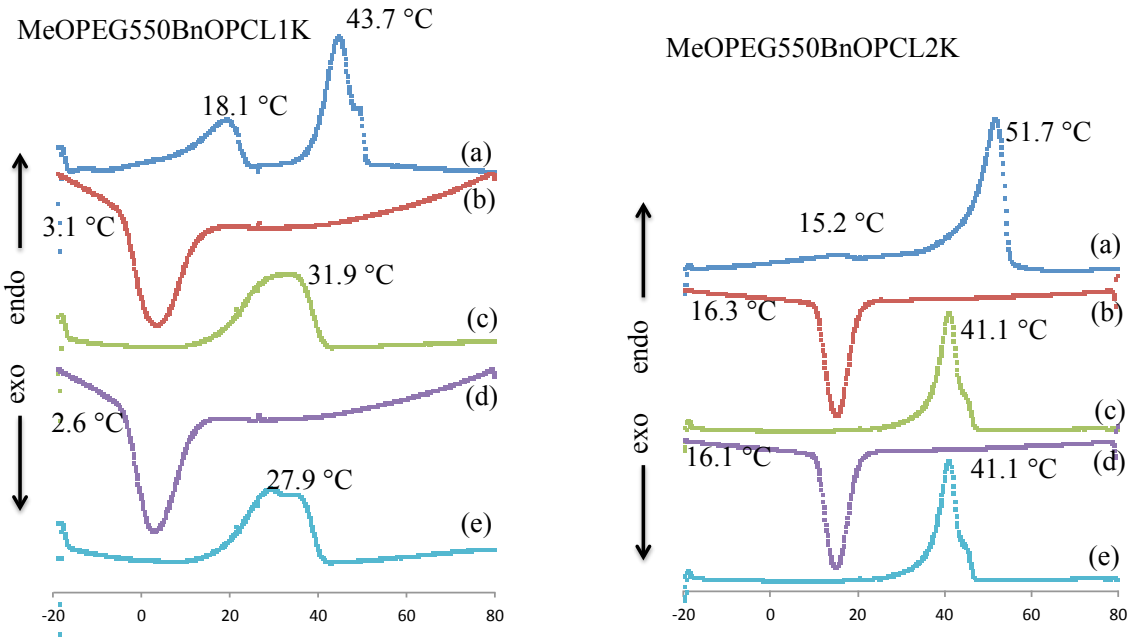

Figure 4.24: DSC Traces of MeOPEG550BnOPCL Diblock Copolymers

4.2.3 Conclusion

Mesylation and etherification reactions were used for the synthesis of PEG macroinitiators with cyclic and linear architectures. The improved cyclization step for the synthesis of a cyclic PEG macroinitiator (i.e. MC-CHO) increased the yield from 19% to 39% relative to literature reports and reduced the work up time by eliminating the need for a second column chromatography and 96 h of Soxhlet extraction. Compared to the work of Heath and coworkers,[232] the method presented here for the synthesis and purification of MeOPEG550BnOH reduced the number of synthetic steps from 3 to 2. This method is also cheaper than the ones reported by Boyer and coworkers[233] and Holtz and coworkers[231] who used 1-bromo-2-(2'-methoxyethoxy)ethane instead of di(ethylene glycol) methyl ether as the starting material. The first compound is 500 times more expensive compared to the second one. Finally, PEG-*b*-PCL diblock copolymers with different architectures in the PEG block were synthesized in high yields and low polydispersities by ring-opening polymerization of ε-caprolactone from PEG macroinitiators.

CHAPTER V

PREPARATION OF MICELLES AND PROTEIN ADSORPTION STUDIES

5.1 Introduction

This chapter discusses the motivation for this project, the relation between blood circulation time and protein adsorption, methods of micelle preparation, a description of fluorescence correlation spectroscopy (FCS), and fluorescence cross-correlation spectroscopy (FCCS). There is also a discussion of the synthesis of fluorescently labeled polymers, and preparation of micelles. Finally, protein adsorption experiments using either FCS and FCCS, DLS, or both are discussed.

This section presents the motivation for this research work in regards to increasing the circulation time of nano/microparticles in the bloodstream for drug delivery purposes. The relation between circulation time and protein adsorption is discussed, highlighting the use of human serum albumin (HSA) and bovine serum albumin as model proteins.

5.1.1 Relation Between Circulation Time and Protein Adsorption

As mentioned in chapter II, one of the main problems of drug delivery devices is their premature elimination from the bloodstream through mechanisms used by the immune system. Finding ways to keep drug delivery devices circulating for longer times in the bloodstream would be an important improvement in the medical field. Since biodistribution studies in animals are so expensive, preliminary *in vitro* studies are beneficial in the early stages of development of long-circulating drug delivery devices.

This section discusses the relation between the circulation time of a particle in the blood and the protein adsorption onto its surface. Different authors have reported the accumulation of colloidal carriers in the liver and spleen through the mononuclear phagocytic system (MPS), also called the reticuloendothelial system (RES).[253] This accumulation is beneficial if the targeted organs are part of the MPS. If this is not the case, increased blood circulation time is preferred. Vittaz, Alexis, and others observed nanoparticle elimination from the bloodstream via phagocytosis.[9,26,254-256] These authors showed the relation between opsonins (i.e. proteins present in the blood) and phagocytosis.[11,39,254-257] Ilum and coworkers confirm that there is a direct correlation between non-recognition by the reticuloendothelial system and a significantly prolonged circulation time.[253] Ilum and Davis also confirmed that particles coated with opsonins from the complement system are rapidly cleared from the blood and end up in the liver and spleen.[258] These authors also state that the hydrophilic coating (i.e. in their case by adsorption of Poloxamer) does not block the reticuloendothelial system but only prevents

particle opsonization and thus particle clearance by the RES. While there might be several mechanisms by which nanoparticles are eliminated from the bloodstream, complement activation seem to be one of the most important ones. Labarre et al.[254] recommend evaluating nanoparticle candidates for long blood circulation in terms of opsonization *in vitro*. The phagocytic process is mediated by opsonization and serum complement is a major component of the opsonin system. In their 1996 article, Labarre et al. state that since phagocytosis is mediated by opsonization, the complement system is likely to be involved in the fast clearance of surfactant-coated PLA particles.[254] Alexis et al. point out that the major limiting factor for long-circulating nanoparticle systems is protein adsorption.[255] Avgoustakis and coworkers studied both the blood clearance and the mononuclear phagocyte system uptake.[259] They found that a decrease of nanoparticle concentration in blood corresponded to an increase in the concentration in the MPS (i.e. particularly in the liver and spleen). In other words, the authors realized that the removal of the particles from the blood with time was due to their capture in the MPS. Panagi and coworkers,[259] also studied the effect of nanoparticle dose on blood circulation and MPS uptake for PEG-PLGA and PLGA particles. Different doses of PEG-PLGA gave the same biodistribution between MPS and blood. Eighty percent of the PEG-PLGA nanoparticles were eliminated from the blood in 6 h. On the other hand, PLGA particles had biodistribution profiles dependent on the dose. Increasing the PLGA dose in the blood increased the circulation time of the particles. For example an 80% reduction in percentage dose in the blood was achieved in 15 seconds for particle doses between 65-125 μg/mouse, whereas the same reduction of percentage of dose was achieved in 60 seconds for particles administered at a dose of 750 μg/mouse. It seemed like the

MPS organs (i.e. liver and spleen) were saturated with nanoparticles faster in the case of the higher PLGA dose, thus preventing their uptake. The other possibility is that there was a faster depletion in plasma opsonins at a higher dose.[259] A similar behavior could be expected in the case of liver and spleen saturation with PLGA particles on a first dose: reduced liver and spleen uptake could be expected in subsequent doses.

5.1.2 Plasma Proteins and *In Vivo* Protein Adsorption Experiments

As explained in section 5.1.1, the motivation for this work is to improve the efficiency of drug delivery devices by increasing their circulation time in the blood. Section 5.1.1 also showed the relation between circulation time and protein adsorption onto particles: the lower the protein adsorption onto the particles, the longer the blood circulation time.

The two main protein constituents of blood plasma are albumin and fibrinogen.[260] Albumin is the predominant plasma protein; it is about 60-70% of the total concentration of plasma proteins.[261] Different globulins have the second highest concentration, followed by fibrinogen. Fibrinogen takes part in blood coagulation and immediately adsorbs onto implanted biomaterials.[262] For this reason, fibrinogen is used in the biocompatibility study of implants, while albumin is used to estimate protein adsorption onto materials that circulate in the blood.

Different authors have compared human serum albumin (HSA) with bovine serum albumin (BSA).[263,264] Both proteins display approximately 67% sequence homology, as well as a comparable repeating pattern of disulfides.[261,263] The main difference between BSA and HSA is that BSA has two tryptophan residues (W^{135} and W^{214}), while HAS has only one (W^{214}). The additional tryptophan residue in BSA is buried in a hydrophobic pocket. Seetharamappa and coworkers studied BSA or HSA binding to gemcitabine hydrochloride,[264] while Tabak and Gelamo studied BSA or HSA binding to different surfactants.[263] Both research groups found that binding to BSA *vs*. HSA had in general the same orders or magnitude. Due to their similarities, BSA is used instead of HSA to predict plasma protein adsorption onto nanomaterials circulating in the blood.[216,265]

In order to determine how to compare the protein adsorption onto micelles from PEG-*b*-PCL diblock copolymers, the relevant literature was reviewed. Rezwan and coworkers studied BSA adsorption onto colloidal Al_2O_3 particles.[261] They prepared a 2 vol % stock solution of Al_2O_3 particles in water and solutions of BSA in water with different concentrations, including zero BSA concentration. A measured amount of Al_2O_3 stock solution was then mixed with a measured volume of BSA solution and the samples were stirred at room temperature for 1 or 16 h. The amount of protein adsorbed onto the particles was quantified by comparing the initial protein concentration with the protein left in supernatant solution after stirring with the particles and centrifuging them. Since micelles have high buoyancy, complete precipitation upon centrifugation cannot be guaranteed and therefore this method cannot be used here. Section 5.3.1 describes an alternative method to quantify protein adsorption onto micelles.

5.2 Micelle Preparation

This section gives an introduction to micelle preparation, including a description of different methods to obtain micelles. It also provides literature precedence on micelles prepared from PEG-*b*-PCL diblock copolymers with different architectures in the PEG block and different PCL molecular weights. After that, the set up and conditions used for micelle preparation from MeOPEG550BnOCPL and MCBnOPCL is described. Finally, it will present the characterization of these micelles by dynamic light scattering (DLS) and transmission electron microscopy (TEM).

5.2.1 Introduction

Polymeric micelles have shown different advantages over free bioactive molecules in drug delivery systems. Some of these advantages include the solubilization of poorly soluble molecules, sustained release, and protection of encapsulated substances from degradation and metabolism.[266] In order to prepare a micelle, a molecule should have at least two segments of different chemical nature, in which one of the segments is solvophobic and the other one is solvophilic. In aqueous solutions, the hydrophobic segment will be solvophobic and the hydrophilic segment will be solvophilic. This difference in solubility leads to the formation of supramolecular assemblies called micelles in solvents that selectively solvate one of the blocks. The micelle preparations shown here use a co-solvent evaporation method. Section 2.9 has a more extensive discussion on this topic.

According to my knowledge of the literature, cyclic-*b*-linear PEG-*b*-PCL diblock copolymers have not been prepared. Therefore, micelles with a cyclic PEG block in the corona are also novel.

5.2.1.1 Methods of Micelle Preparation

Two types of techniques are most commonly used to prepare block copolymer micellar systems. In the first type, the block copolymer is first dissolved in a good solvent for both blocks and then the conditions of the system such as temperature or solvent composition are changed to promote the formation of micelles.[200,201] The second type of technique is the direct dissolution method. These methods are described in detail in section 2.9. The micelle preparations shown here use a co-solvent evaporation method.

5.2.1.2 Other Micelles from PEG-*b*-PCL Diblock Copolymers

As discussed in section 2.9, different authors have prepared micelles from PEG-*b*-PCL diblock copolymers.[72,75,76,115,120-124,202-206,209-213,216,217] Table 5.1 shows the molecular weights of the PEG and PCL blocks, micelle size, critical micelle concentration (CMC), and the method of micelle preparation. The polymers in the table have a PEG M_n of 2-20*10^3 g/mole and a PCL M_n between 1.5 and 29*10^3 g/mole. The micelle sizes were between 25 to 200 nm, and the critical micelle concentrations were between 1.2*10^{-8} to 1.2*10^{-5} M. Lavasanifar and coworkers studied the effect of the solvent used in the preparation of PEG-*b*-PCL micelles by a co-solvent evaporation method.[207] They found that smaller micelles were prepared in acetone and acetonitrile compared to THF. The

polymers used for Lavasanifar's study had PCL molecular weights that were one, times, and five times the molecular weight of the PEG block. These same ratios between hydrophilic and hydrophobic block were used in the polymers and micelles studied here, as shown in Table 5.2. The same table introduces a nomenclature for the micelles; for example, L3x is the micelle prepared with a polymer with a linear PEG that has a PCL molecular weight that is three times the molecular weight of PEG.

Table 5.1: Micelles from PEG-*b*-PCL Diblock Copolymers

PEG M_n (g/mole)	PCL M_n (g/mole)	Size (nm)	CMC (M)	Method	Ref
4k, 10k	21k, 29k	150 to 200	10^{-7} to10^{-8}	Dialysis	22
5k	5k, 13k, 25k	64-200	10^{-7}	Co-solvent evaporation	23
5k	5k, 7k, 10k	77-130	10^{-7}	Dialysis	46
2k	2.5k	NA	$2.8*10^{-7}$	NA	25
2k	1.5k, 2.5k	50	NA	Dialysis, DMF	26
2k, 5k	2k, 2.5k, 5k, 8.5k, 25k	17-86	NA	Co-solvent evaporation, THF	27
2k	2.5k	25	NA	Dialysis	28
2.5k	1.5k-4.5k	20-25	NA	Co-solvent evaporation, THF	29
5k	3k, 5k	124-144	NA	Dialysis	30
5k	3k-13k	54-130	NA	Dialysis, DMF	31
5k	3k-13k	<200	NA	Dialysis, DMF	32
2k	2.5k	NA	NA	Dialysis, DMF	33
5k	1.8k	30-100	NA	Dialysis, THF, DMF, DMSO, DMAc	34
2k, 5k, 10k	11k-18k	25-81	10^{-7} to10^{-8}	Dialysis, THF	35
5k	10k	NA	NA	Solvent extraction, acetone	36
5k	10k	NA	NA	Co-solvent evaporation, acetone	37
3k	1k, 2k	51-81	NA	Co-solvent evaporation, THF	38
3k	1k	30	NA	Co-solvent evaporation, THF	39
5k	5k	60	NA	Near critical point/solvent evaporation, acetone	40
5k, 10k, 20k	5k	49-115	$1.2*10^{-5}$, $7.6*10^{-6}$	Co-solvent evaporation, DMF	17
3k	14k	154	10^{-7}	Co-solvent evaporation, THF	41

Table 5.2: PEG-*b*-PCL Diblock Copolymers Used for Micelle Preparation

	Micelle	Initiator	[M]/[I]	[I]/[Sn(Oct)$_2$]	Conv (%)	PEG-*b*-PCL M_n (kg/mol)				PDI	T_m (°C)	
						Theo at 100 % conv.	Theo with conversion	^{1}H NMR	GPC		PEG	PCL
Linear	L1x	MeOPEG550BnOH	4	1.0	0.44	100	0.444	0.374	1.56	1.03	NA	NA
	L3x	MeOPEG550BnOH	12	1.1	1.32	100	1.27	1.12	2.01	1.09	18.1	29.9
	L5x	MeOPEG550BnOH	20	1.0	2.32	100	2.30	1.88	2.54	1.20	15.2	41.1
Cyclic	C1x	MC-BnOH	6	0.8	0.65	93	0.60	0.679	1.76	1.12	NA	NA
	C3x	MC-BnOH	15	0.8	1.77	96	1.70	1.69	2.31	1.17	17.4	34
	C5x	MC-BnOH	24	0.8	2.70	92	2.48	2.51	3.14	1.23	16.4	41.1

5.2.2 Set Up and Conditions for Self-Assembly

As mentioned in section 5.1.1, the objective of this study is to compare protein adsorption onto micelles from PEG-*b*-PCL diblock copolymers that have cyclic *vs.* linear architecture. In order to use the results obtained in these *in vitro* studies as precedence for biodistribution studies, we have tried to reproduce biological conditions as much as possible. Micelles were prepared either in water alone or in phosphate buffer saline (PBS). PBS conditions reproduce biological pH and ionic strength conditions.[227] The method chosen for micelle self-assembly is co-solvent evaporation using acetone. As mentioned in the previous section, these conditions were successfully used by Lavasanifar and coworkers with PEG-*b*-PCL diblock copolymers.[207]

For the self-assembly, PEG-*b*-PCL were dissolved in acetone. Then water or PBS was slowly added at 0.1 mL/min using a syringe pump while rapidly stirring the solution. The set up used for this process is shown in Figure 5.1.

5.2.3 Micelles from MeOPEG550BnOPCL and MCBnOPCL Diblock Copolymers

Figure 5.1 and Table 5. show the micelle sizes prepared either in PBS or in MilliQ water measured by DLS. As mentioned in chapter II, one of the variables that affect

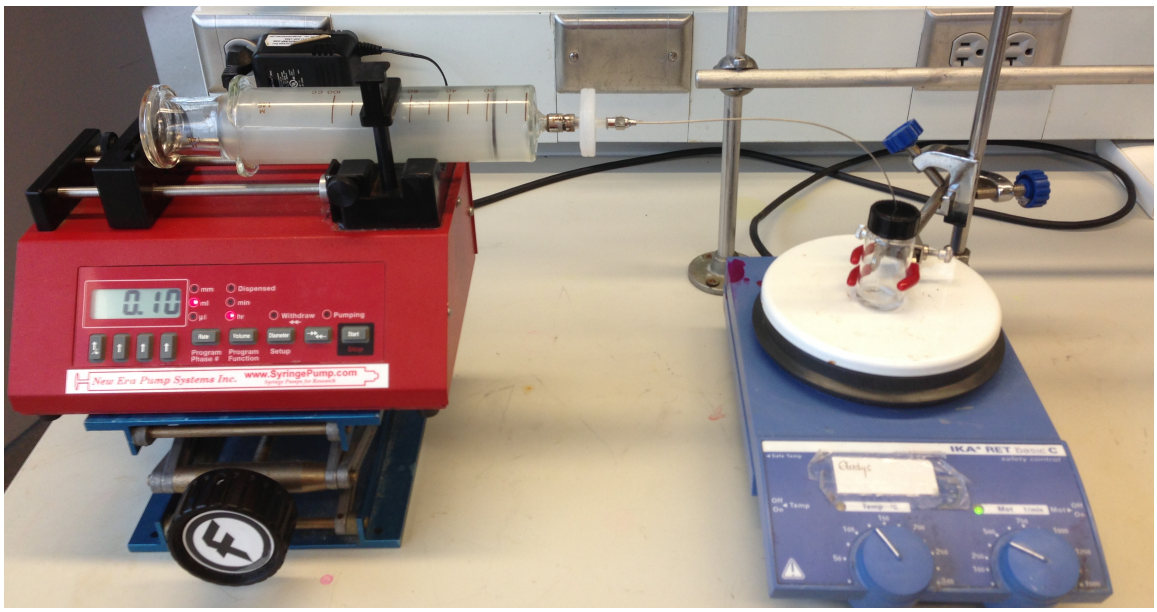

Figure 5.1: Self-assembly Set-Up

micelle size and stability is the molecular weight of the core. As the molecular weight of the PCL block in the core increases, the melting point increases leading to more thermodynamically stable micelles.

The micelles prepared with linear-*b*-linear PEG-*b*-PCL diblock copolymers (i.e. L1x, L3x, and L5x) have sizes that are inversely proportional to the PCL molecular weight. This effect is particularly clear for micelles prepared in PBS *vs.* MilliQ water. In this case, it is possible that the highest PCL molecular weight provides a more stable and therefore a more compact core, reducing the micelle size.[121] The previous statement

might indicate that the smaller micelles are L5x and C5x; however, this is not the case for L5x in MilliQ water nor C5x. Since L3x and C3x have higher molecular weights than L1x and C1x, but their PCL melting temperatures are similar to L1x and C1x, L3x and C3x are larger than L1x, L5x, C1x, and C5x. This is seen in MilliQ water for all polymers and in PBS for C1x-C5x.

Micelle sizes were larger in PBS than in water. Micelles made with cyclic-*b*-linear polymers formed large micelle aggregates in PBS. This might be due to the ability of MCBnOH to coordinate with the cations in solution, favoring micelle-micelle interactions.

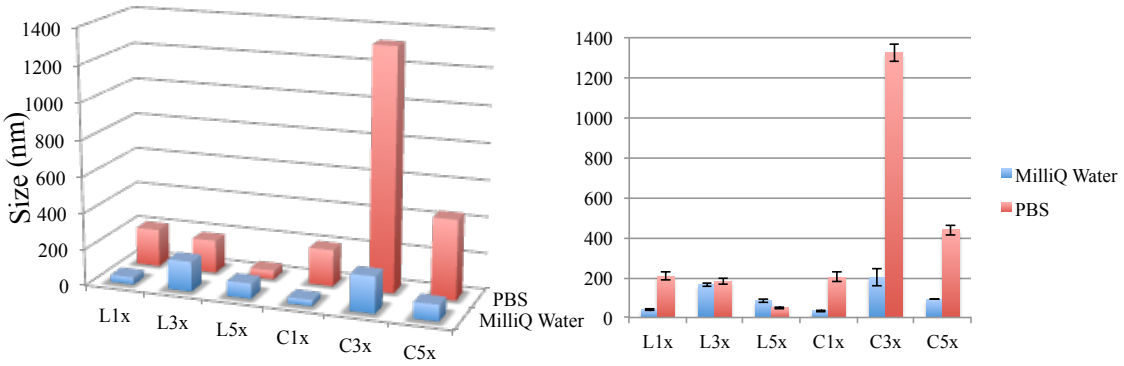

Figure 5.1: Micelle size of L1x-L5x and C1x-C5x PEG-*b*-PCL copolymers measured by DLS in PBS *vs.* water

Table 5.3: Micelle size of L1x-L5x and C1x-C5x PEG-b-PCL copolymers measured by DLS in PBS *vs.* water

	MilliQ Water		PBS	
Sample	**Size (nm)**	**Error (nm)**	**Size (nm)**	**Error (nm)**
L1x	39	5	207	22
L3x	164	9	181	14
L5x	83	9	48	6
C1x	33	4	201	24
C3x	200	41	1326	44
C5x	89	0	439	26

More defined micelles were prepared from cyclic-*b*-linear than from linear-*b*-linear diblock copolymers. Figure 5.2 presents TEM pictures (a)-(f) of micelles from linear-*b*-linear diblock copolymers. Micelles in pictures (a)-(c) were prepared in water and pictures (d)-(f) were prepared in PBS. Except for picture (d), it is difficult to see micelle cores or coronas in these pictures. In contrast, defined micelles are shown in pictures (g)-(l) corresponding to micelles from cyclic-*b*-linear diblock copolymers.

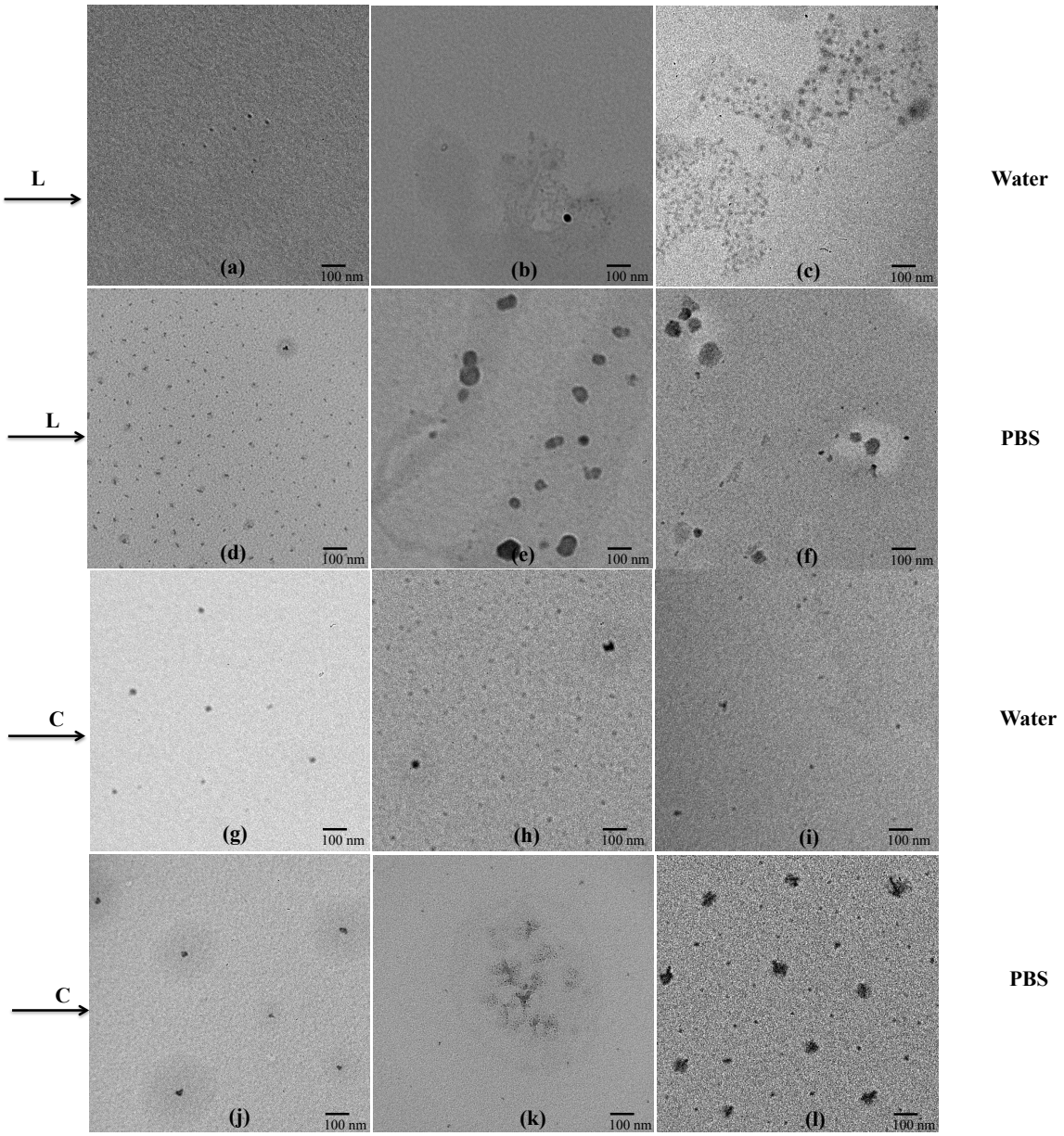

Figure 5.2: TEM Pictures of Micelles. MilliQ Water: (a) L1x, (b) L3x, (c) L5x, (g) C1x, (h) C3x, (i) C5x. PBS: (d) L1x, (e) L3x, (f) L5x, (j) C1x, (k) C3x, (l) C5x

Pictures (g)-(i) show micelles prepared in MilliQ water while pictures (j)-(l) show micelles prepared in PBS. The darkest spots are the cores of micelle agglomerates, the light dark shadows around them are micelle coronas. Figure 5.2 confirms micellar sizes measured by DLS and show that the micelles have spherical shapes.

5.2.3.1 Conclusion

Self-assembled micelles were prepared from PEG-*b*-PCL diblock copolymers with linear or cyclic architectures in the PEG block. The molecular weights of the PCL blocks were one, three, or five times the molecular weight of the PEG block. Two different self-assembly media were used: MilliQ water and PBS. The micelles from these low molecular weight polymers had larger sizes in PBS than in MilliQ water. More defined micelles were prepared from cyclic-*b*-linear diblock copolymers than from linear-*b*-linear diblock copolymers according to TEM.

5.3 Fluorescence Correlation Spectroscopy, Fluorescence Cross-correlation Spectroscopy, and Fluorescent Polymers

This section gives an introduction to fluorescence correlation spectroscopy (FCS) and fluorescence cross-correlation spectroscopy (FCCS). Attempts to encapsulate fluorescent dyes during the self-assembly process highlight the need to synthesize a fluorescently labeled diblock copolymer. The synthesis and characterization of fluorescently labeled polymers is discussed for a model polycaprolactone homopolymer

and PEG-*b*-PCL diblock copolymers with a rhodamine moiety covalently bound to the PCL hydroxyl end group.

5.3.1 Introduction

Fluorescence is the emission of light by a substance that has absorbed light or other electromagnetic radiation. In 1972, Madge, Elson, and Webb introduced fluorescence correlation spectroscopy (FCS) to measure diffusion and chemical dynamics of DNA-drug intercalation.[267] FCS is a correlation analysis of fluctuation of the fluorescence intensity. The parameter of primary interest is not the emission intensity itself, but the spontaneous intensity fluctuations caused by the Brownian motion of the particles. These fluctuations are quantified in their strength and duration by auto-correlating the recorded intensity signal. FCS can be used to obtain quantitative information such as diffusion coefficients and hydrodynamic radii. In 1997, Schwille and coworkers introduced the dual-color fluorescence cross-correlation spectroscopy (FCCS).[268] Using this technique the concentration and diffusion characteristics of two fluorescent species in solution, as well as their interaction, can be measured simultaneously. In FCCS, excitation is performed by two different lasers, and the fluorescence light is divided into two channels, simultaneously measuring red and green signals and cross-correlating them.

FCCS may quantify the interactions between fluorescently labeled micelles and fluorescently labeled BSA for the *in vitro* protein adsorption experiments described in section 5.1.2.

5.3.2 Entrapment of Fluorescent Dyes in Micelles

Different research groups have entrapped hydrophobic drugs into PEG-*b*-PCL self-assembled micelles.[73,75,76,115,122,209,249] We attempted to label micelles by entrapping fluorescent dyes into PEG-*b*-PCL self-assembled micelles by dissolving either a curcumin dye (i.e. macrolex fluorescent yellow 10GN) or rhodamine lactone in acetone along with the PEG-*b*-PCL diblock copolymer and using this solution in the self-assembly process described in section 5.2.2.

The entrapment of yellow 10GN was effective in terms of the absence of visible free dye in the micelle suspension. However, the quantum yield of the entrapped dye was low, leading to the noisy FCCS average curves shown for the correlation B (green) in Figure 5.3.

The entrapment of rhodamine lactone was even less effective than yellow 10 GN; there was free dye visible in the micelle suspension after entrapment due to the higher solubility of rhodamine lactone in water compared to yellow 10 GN. Attempts to remove the free dye by dialysis were also unsuccessful. An alternative to entrapping free fluorescent dyes during the self-assembly process is to synthesize a diblock copolymer

with a fluorescence moiety covalently bound to the hydrophobic block. The following sections describe the synthesis of a model PCL homopolymer and then PEG-*b*-PCL diblock copolymers that have a rhodamine moiety covalently attached.

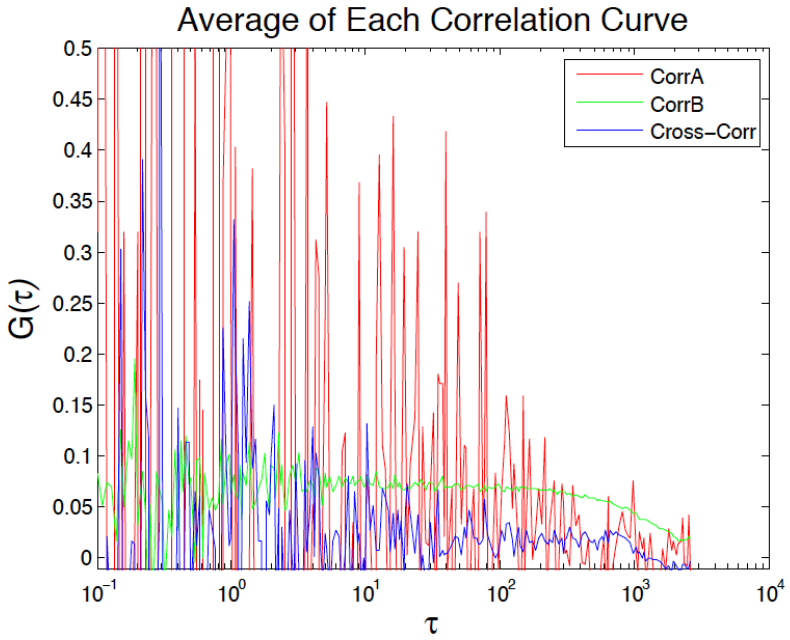

Figure 5.3: FCCS Average Curves for Micelles of PEG-*b*-PCL copolymer with Entrapped Yellow 10 GN

5.3.3 Synthesis of a Model Fluorescent PCL Homopolymer

Maysinger and coworkers synthesized the only example found in the literature of rhodamine-labeled PEG-*b*-PCL diblock copolymers.[123] They reacted tetramethylrhodamine-5-carbonyl azide with the hydroxyl PCL end-group in toluene at 80 °C for 5 h and dialyzed against DMF to remove the unreacted rhodamine to obtain rhodamine-conjugated polymer in 60% yield.

Here, a model rhodamine-labeled PCL diblock copolymer was synthesized in two steps from MeOPCL to yield MeOPCL-Rhod in 15% yield.

5.3.3.1 Synthesis of Model Polycaprolactone Homopolymer

The ring-opening polymerization of ε-caprolactone using tin octoate as a catalyst has been fully documented in the literature.[80,235,236,238,240-242,244-246] Here, α-methyl, Ω-hydroxy polycaprolactone was synthesized in 56% yield using methanol as initiator and tin octoate as catalyst at 80 °C, as shown in Scheme 5.1. Figure 5.5 and Figure 5.6 show the ^{1}H and ^{13}C NMR spectra, respectively of MeOPCL. The resonances correspond to the literature values.[250]

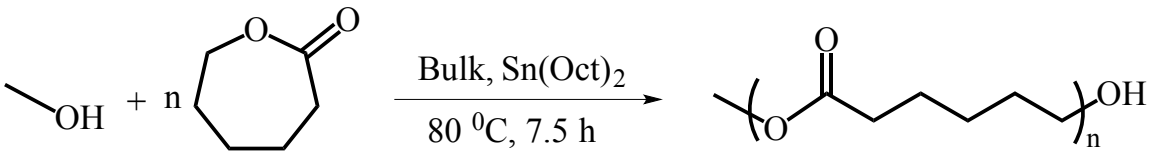

Scheme 5.1: Synthesis of MeOPCL

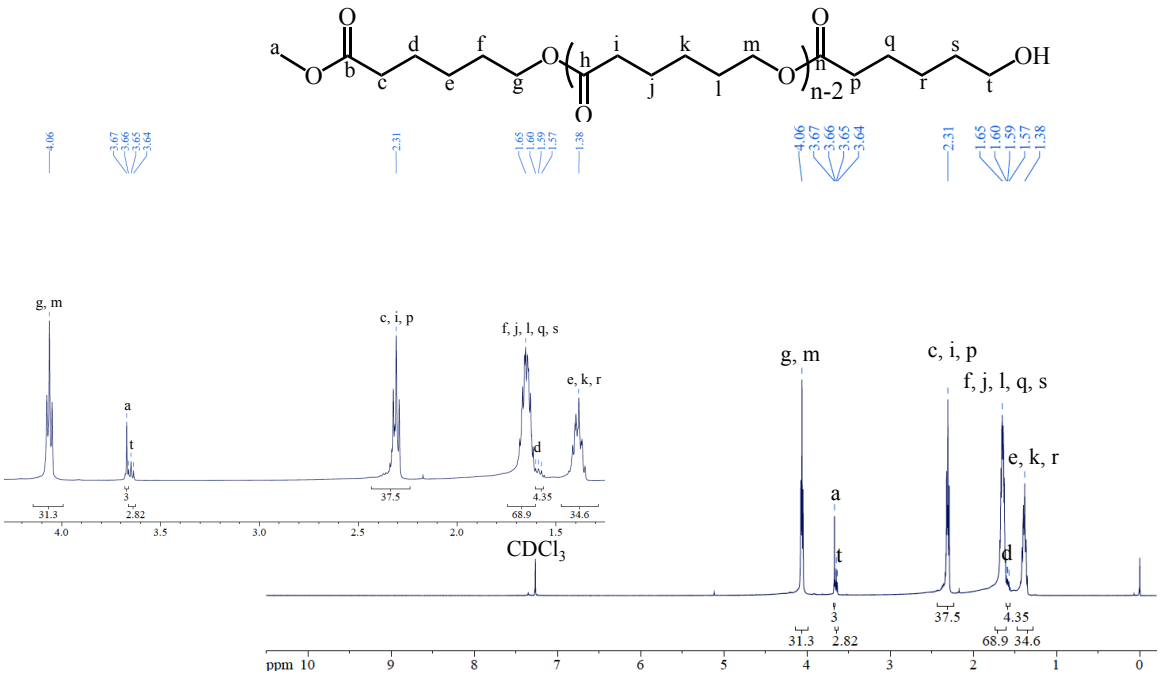

Figure 5.5: ^{1}H NMR Spectrum of MeOPCL. M_n=2.66*10^3 g/mole, PDI=1.10

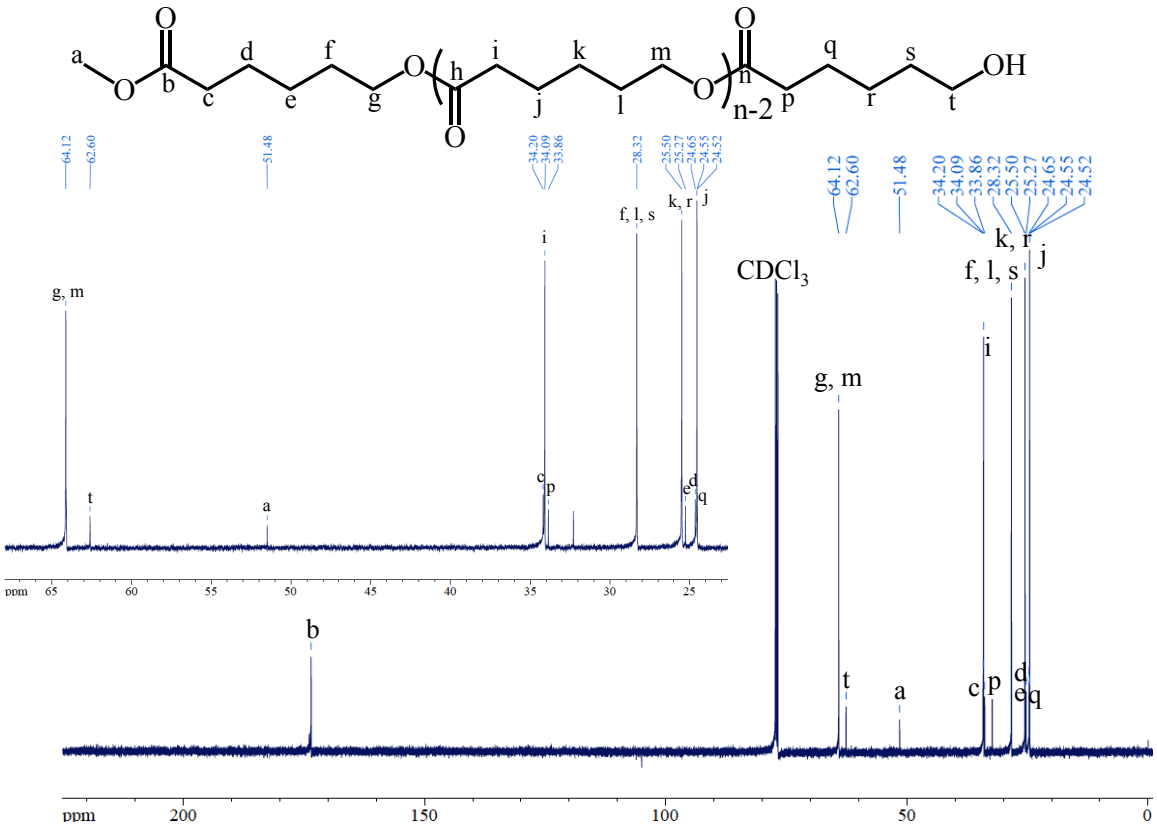

Figure 5.6: ^{13}C NMR Spectrum of MeOPCL M_n=2.66*10^3 g/mole, PDI=1.10

5.3.3.2 Synthesis of Mesylated Polycaprolactone (MeOPCLMs)

Pugh and coworkers[228,229] synthesized MsPEG600Ms in 81–93% yield in the presence of triethylamine in dichloromethane with methanesulfonyl chloride. Here, MeOPCLMs was synthesized in 99% yield using the route in Scheme 5.2, similar to Pugh and coworkers, using THF as solvent instead of dichloromethane. Figure 5.4 and Figure 5.8 show the ^{1}H and ^{13}C NMR spectra of MeOPCLMs at room temperature. The resonances in these spectra correspond to the literature values. [228,250]

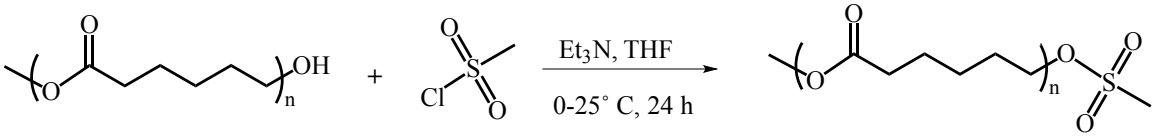

Scheme 5.2: Synthesis of MeOPCLMs

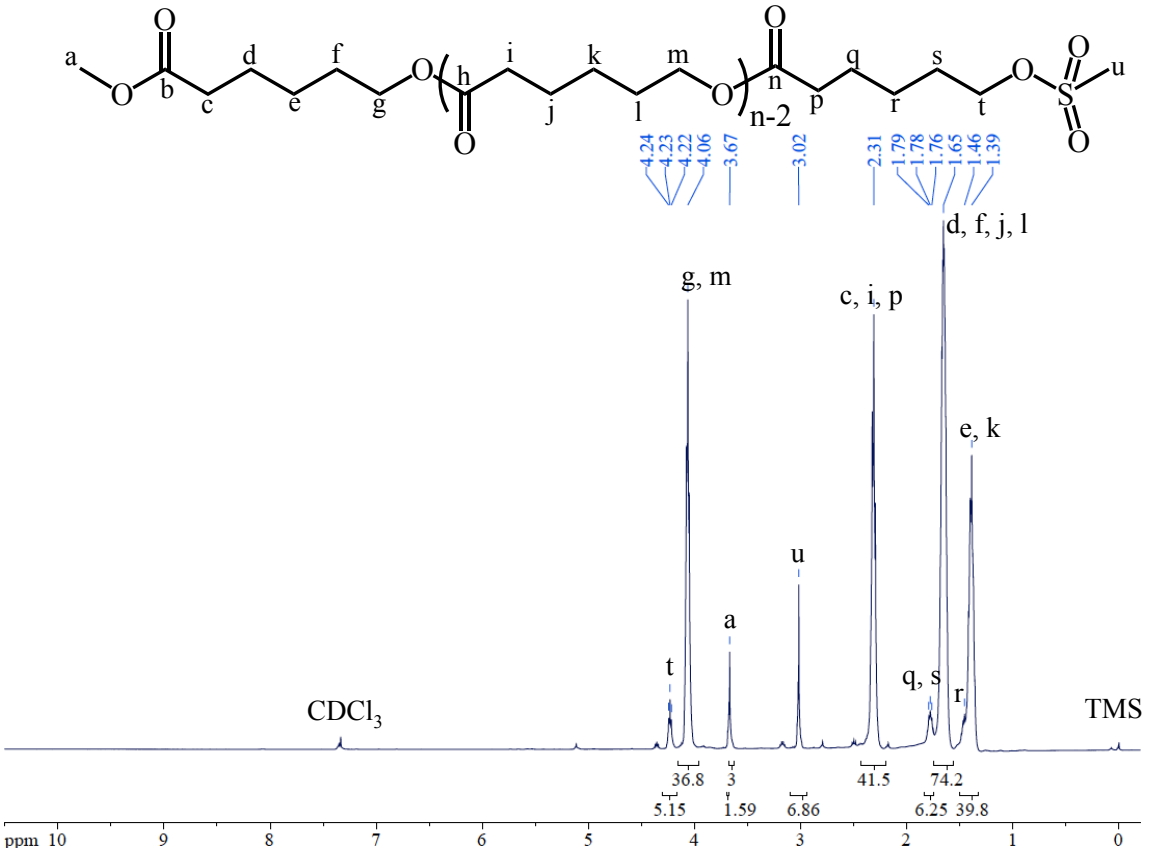

Figure 5.4: ^{1}H NMR Spectrum of MeOPCLMs. M_n=2.87*10^3 g/mole, PDI=1.11

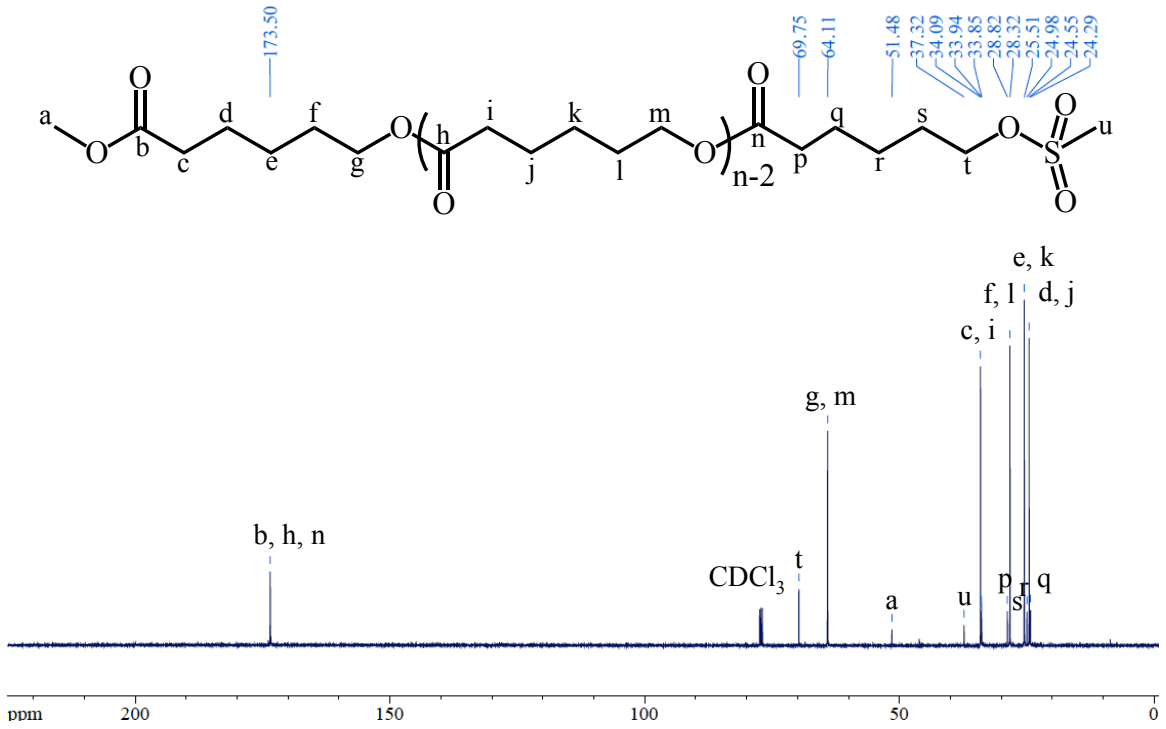

Figure 5.8: ^{13}C NMR Spectrum of MeOPCLMs. M_n=2.87*10^3 g/mole, PDI=1.11

5.3.3.3 Synthesis of Rhodamine-polycaprolactone (MeOPCLRhod)

Moscatelli and coworkers synthesized a fluorescently labeled PMMA by funtionalizing (hydroxyethyl)methacrylate with rhodamine using DCC coupling and then copolymerizing it with methyl methacrylate.[269] Maysinger and coworkers synthesized PEG-*b*-PCLRhod using tetramethylrhodamine-5-carbonyl azide.[123] Alternatively, Packard and coworkers synthesized ^{18}F-labeled rhodamine B esters in 74-83 % yield for positron emission tomography by reaction of tosyl esters with *N,N*-diisopropylehtylamine and rhodamine B lactone in acetonitrile.[270,271]

Here, the synthesis of MeOPCLRhod shown in Scheme 5.3 is similar to the synthetic route of Packard and coworkers.[270,271] Figure 5.9 and Figure 5.10 show the ^{1}H and ^{13}C NMR spectra of MeOPCLRhod. The resonances correspond to literature values.[250,271]

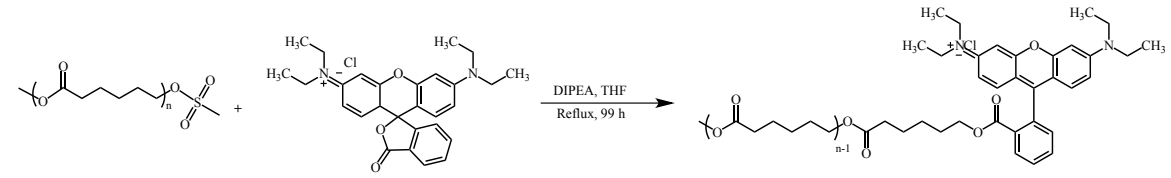

Scheme 5.3: Synthesis of MeOPCLRhod

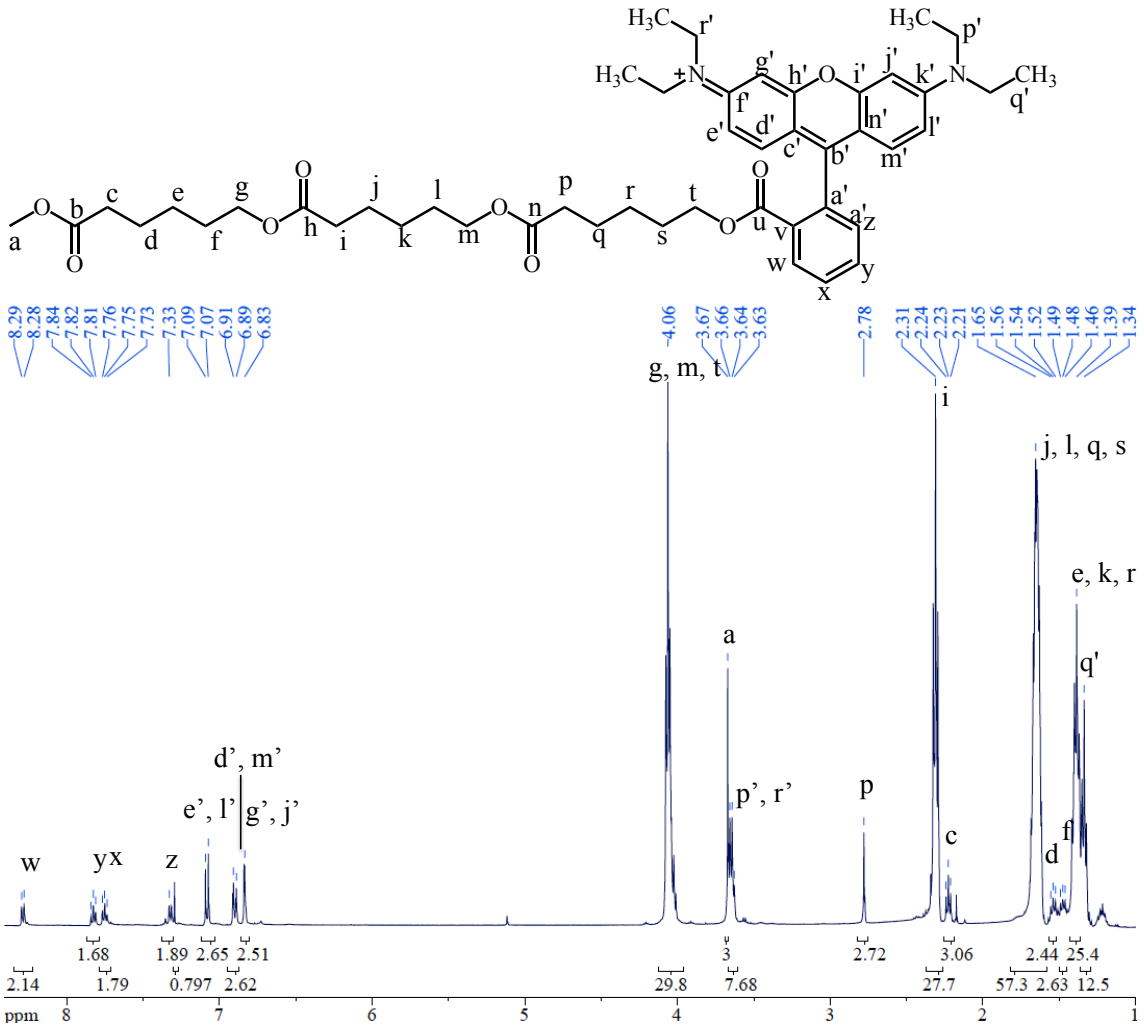

Figure 5.9: ^{1}H NMR Spectrum of MeOPCLRhod. M_n=2.99*10^3 g/mole, PDI=1.13

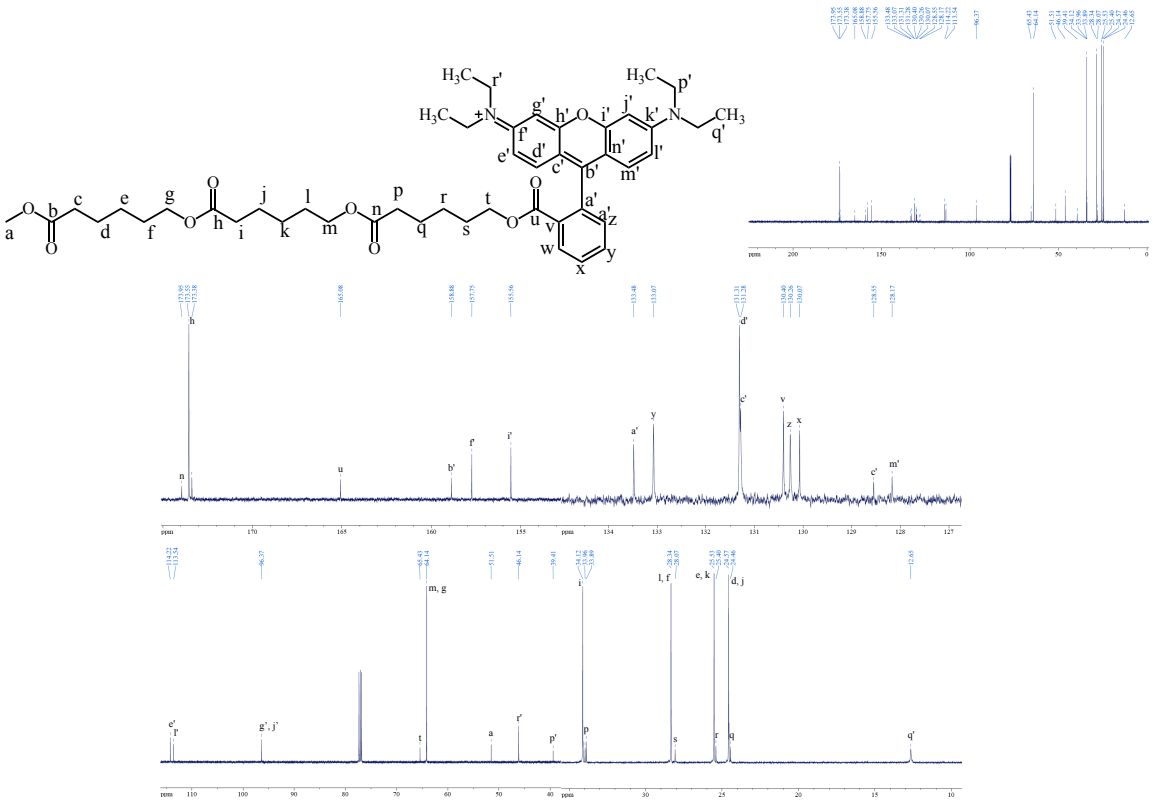

Figure 5.10: ^{13}C NMR Spectrum of MeOPCLRhod. M_n=2.99*10^3 g/mole, PDI=1.13

Figure 5.11 shows the MALDI-ToF MS of MeOPCLRhod that confirms the synthesis and purity of this polymer. The main polymer distribution corresponds to polymer that is self-ionized by the imine positive charge, but without the chloride counterion. The minor distribution corresponds to the polymer that has chloride as counterion and ionizes with potassium. No unfunctionalized polymer was detected. The GPC traces of MeOPCL, MeOPCLMs, and MeOPCLRhod in Figure 5.12 show that the molecular weight and molecular weight distribution remained essentially constant

throughout the three synthetic steps and the work-up. Also the polymer hydrodynamic radii are very similar for the polymers in each step of the synthesis.

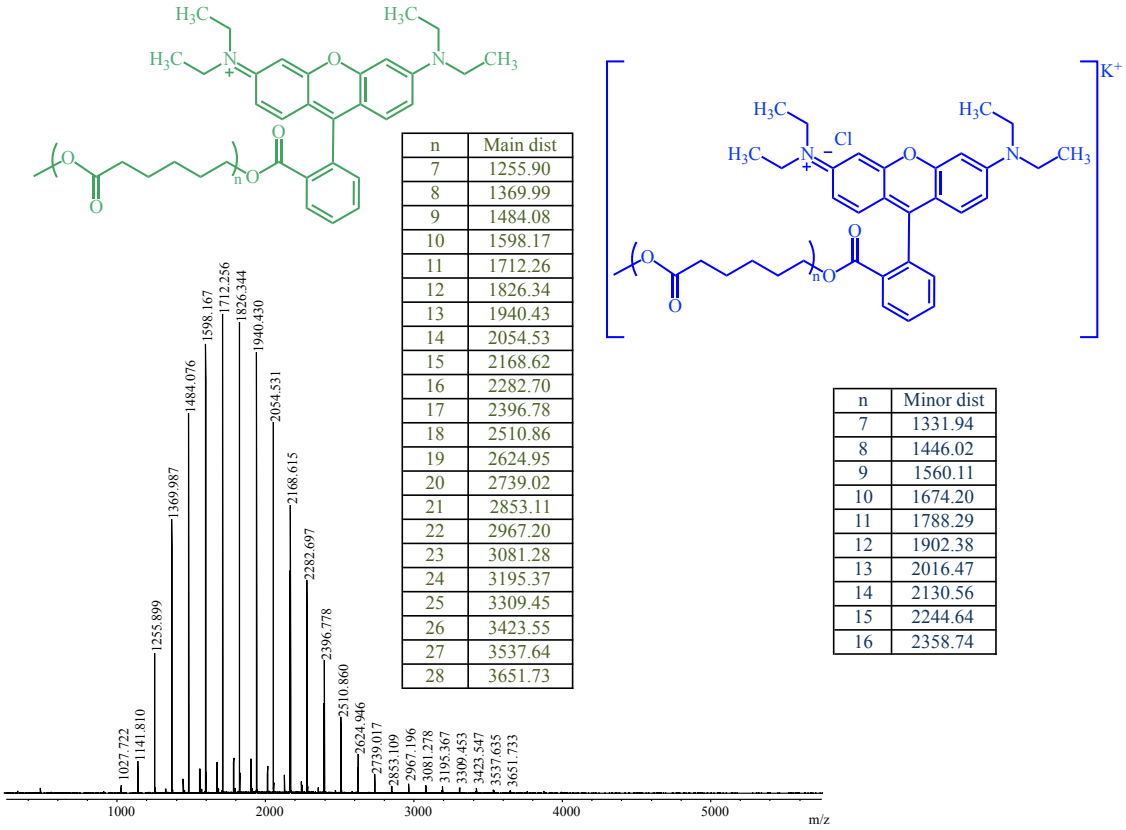

n	Main dist
7	1255.90
8	1369.99
9	1484.08
10	1598.17
11	1712.26
12	1826.34
13	1940.43
14	2054.53
15	2168.62
16	2282.70
17	2396.78
18	2510.86
19	2624.95
20	2739.02
21	2853.11
22	2967.20
23	3081.28
24	3195.37
25	3309.45
26	3423.55
27	3537.64
28	3651.73

n	Minor dist
7	1331.94
8	1446.02
9	1560.11
10	1674.20
11	1788.29
12	1902.38
13	2016.47
14	2130.56
15	2244.64
16	2358.74

Figure 5.11: MALDI-ToF MS of MeOPCLRhod. M_n=2.99*10^3 g/mole, PDI=1.13

5.3.4 Synthesis of PEG-*b*-PCL Fluorescent Diblock Copolymers

Section 5.3.3 discussed the synthesis of a model fluorescently labeled PCL polymer. This section discusses the synthesis of a fluorescently-labeled PEG-*b*-PCL diblock copolymer in three steps analogous as the ones used for MeOPCLRhod.

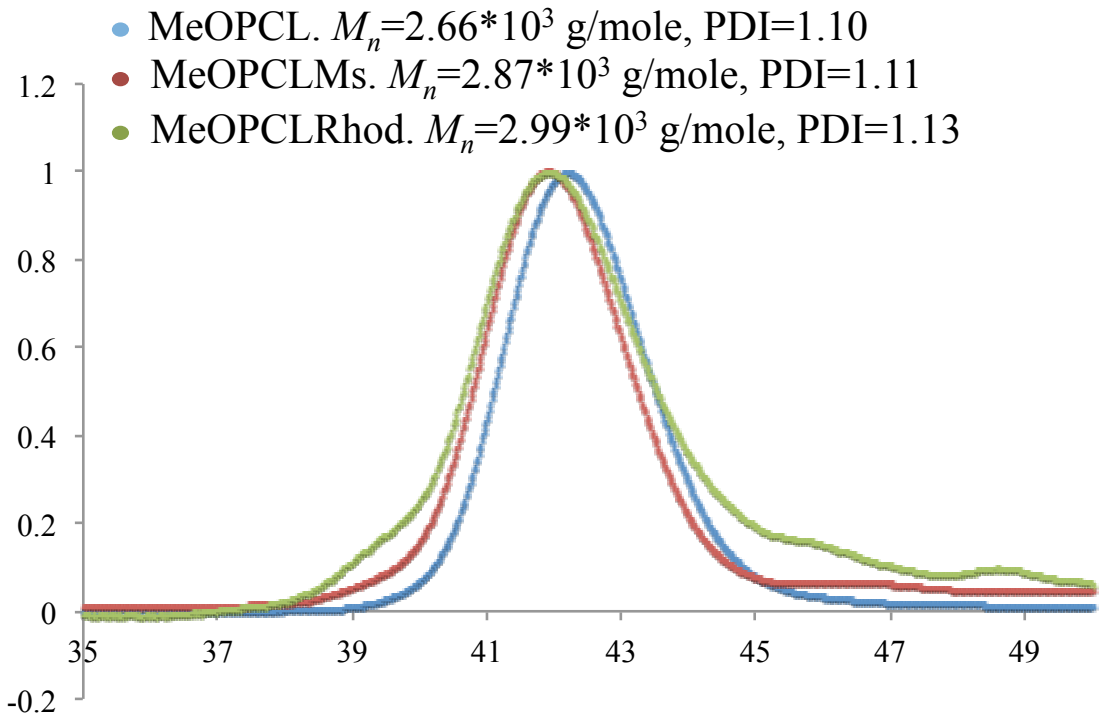

Figure 5.12: GPC Traces of MeOPCLRhod and Precursors

5.3.4.1 Synthesis of MeOPEGPCL

The synthesis of PEG-*b*-PCL diblock copolymers by ring-opening polymerization of ε-caprolactone using tin octoate as a catalyst and THF as solvent was discussed in the previous sections.[80,235,236,238,240-242,244-246] Here, MeOPEGPCL was synthesized in 100% yield as shown in Scheme 5.4. This diblock copolymer was used for the preparation of the micelles used in the protein adsorption studies by fluorescence microscopy. Figure 5.13 and Figure 5.14 show the ^{1}H and ^{13}C NMR spectra of MeOPEGPCL. The resonances correspond to the literature values.[250]

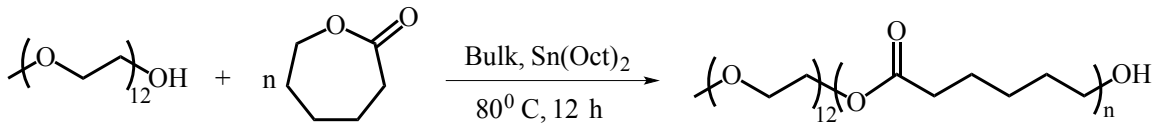

Scheme 5.4: Synthesis of MeOPEGPCL. M_n=1.99*10^3 g/mole, PDI =1.17

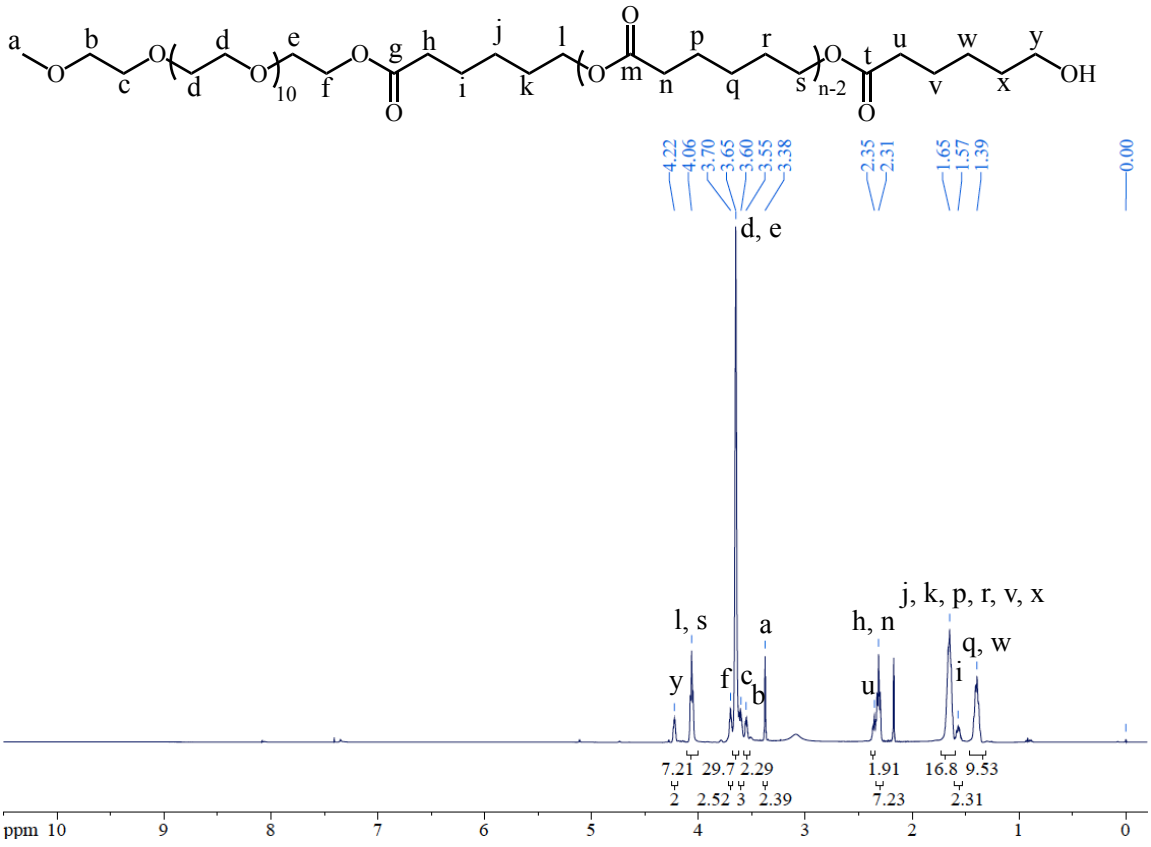

Figure 5.13: ^{1}H NMR Spectrum of MeOPEGPCL. M_n=1.99*10^3 g/mole, PDI =1.17

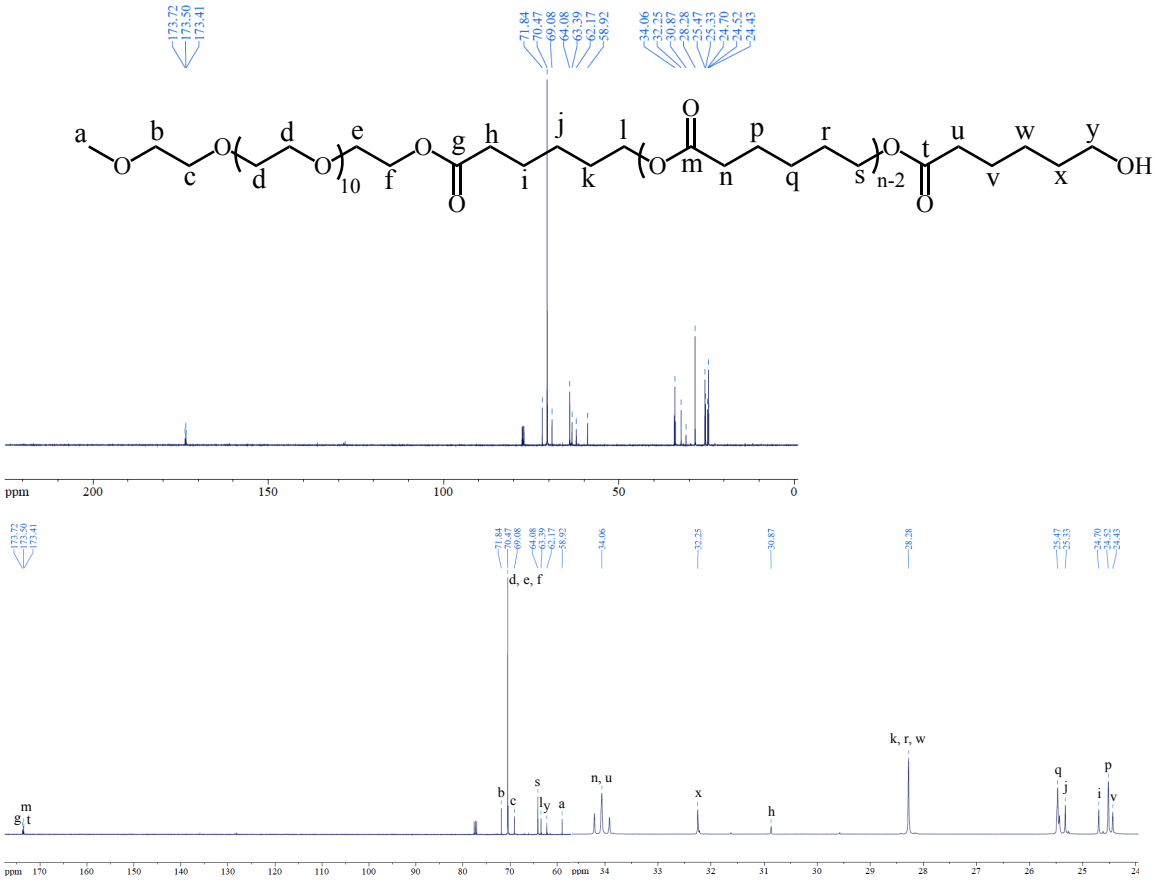

Figure 5.14: ^{13}C NMR of MeOPEGPCL. M_n=1.99*10^3 g/mole, PDI =1.17

5.3.4.2 Synthesis of MeOPEGPCLMs

Pugh and coworkers[228,229] synthesized MsPEG600Ms in 81–93% yield in the presence of triethylamine in dichloromethane with methanesulfonyl chloride. Here, MeOPEGPCLMs was synthesized in quantitative yield using the route in Scheme 5.5, similar to Pugh and coworkers, using THF as solvent instead of dichloromethane.

Figure 5.15 and Figure 5.16 show the ^{1}H and ^{13}C NMR spectra, respectively, of MeOPEGCLMs at room temperature. The resonances in these spectra correspond to the literature values.[250]

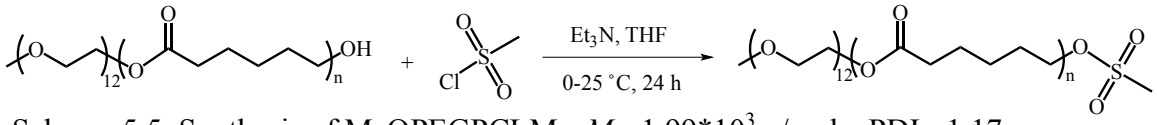

Scheme 5.5: Synthesis of MeOPEGPCLMs. M_n=1.99*10^3 g/mole, PDI =1.17

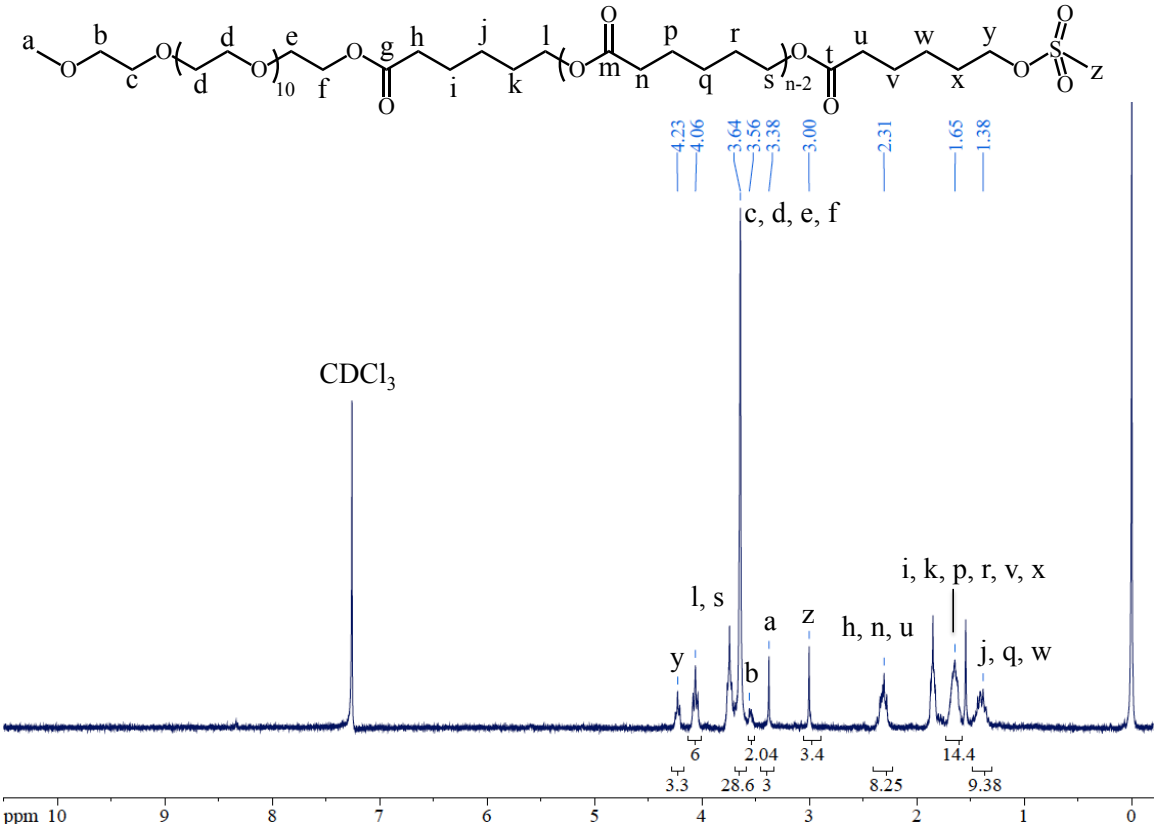

Figure 5.15: ^{1}H NMR Spectrum of MeOPEGPCLMs. M_n=1.99*10^3 g/mole, PDI =1.17

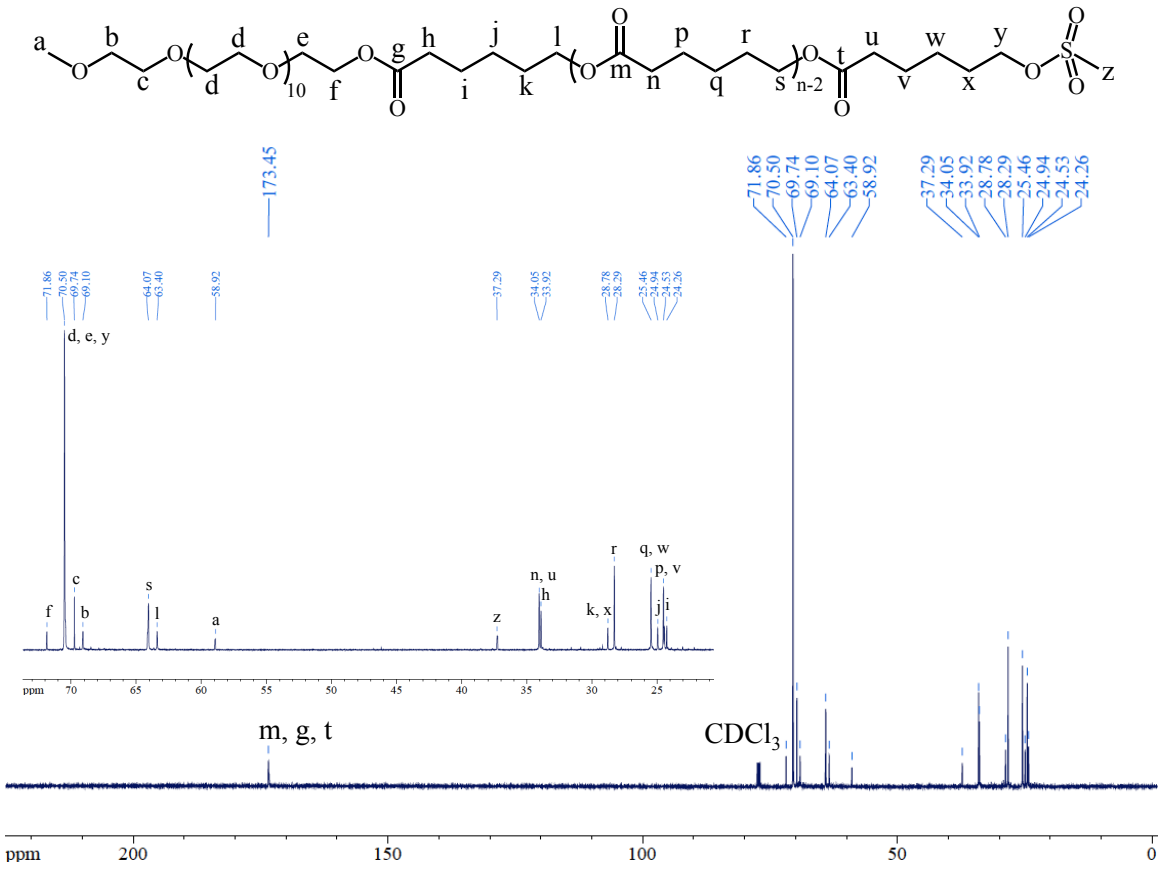

Figure 5.16: ^{13}C NMR Spectrum of MeOPEGPCLMs. M_n=1.99*10^3 g/mole, PDI =1.17

5.3.4.3 Synthesis of MeOPEGPCLRhod

The literature precedence for the synthesis of fluorescently labeled PEG-*b*-PCL diblock copolymers and the reaction a mesylated molecule with rhodamine B lactone was discussed in section 5.3.3.3.[123,269-271] Here, MeOPEGPCLRhod was synthesized in 25% yield using the route shown in Scheme 5.6.

Figure 5.17 and Figure 5.18 show the ^{1}H and ^{13}C NMR spectra, respectively, of MeOPEGPCLRhod. The resonances correspond to literature values.[250,270]

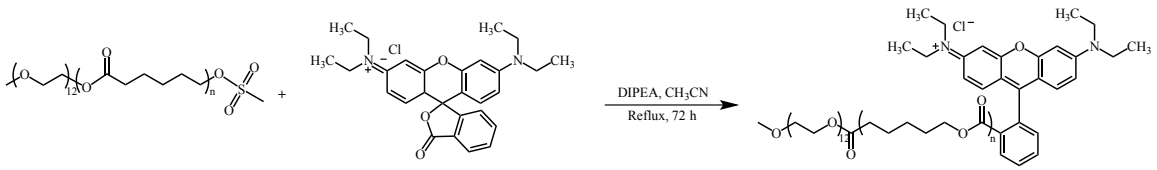

Scheme 5.6: Synthesis of MeOPEGPCLRhod. M_n=1.80*10^3 g/mole, PDI =1.17

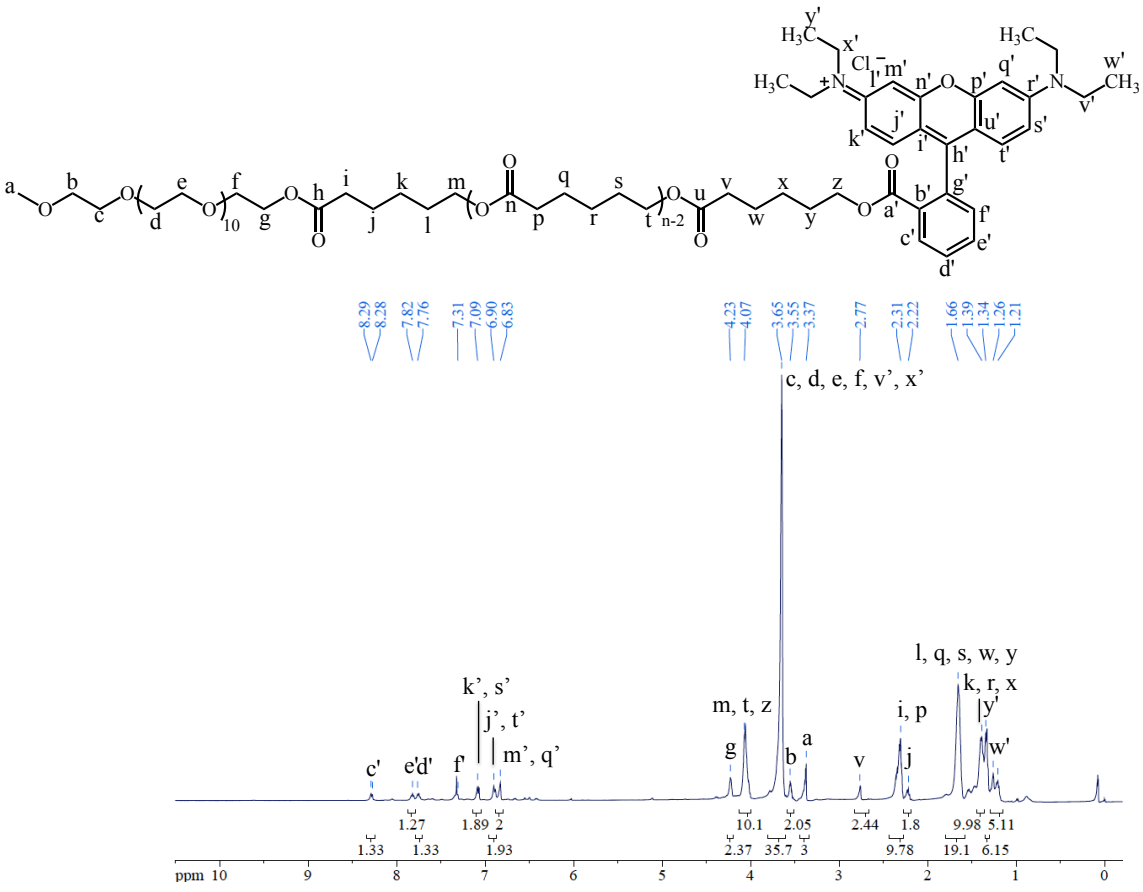

Figure 5.17: ^{1}H NMR Spectrum of MeOPEGPCLRhod. M_n=1.80*10^3 g/mole, PDI =1.17

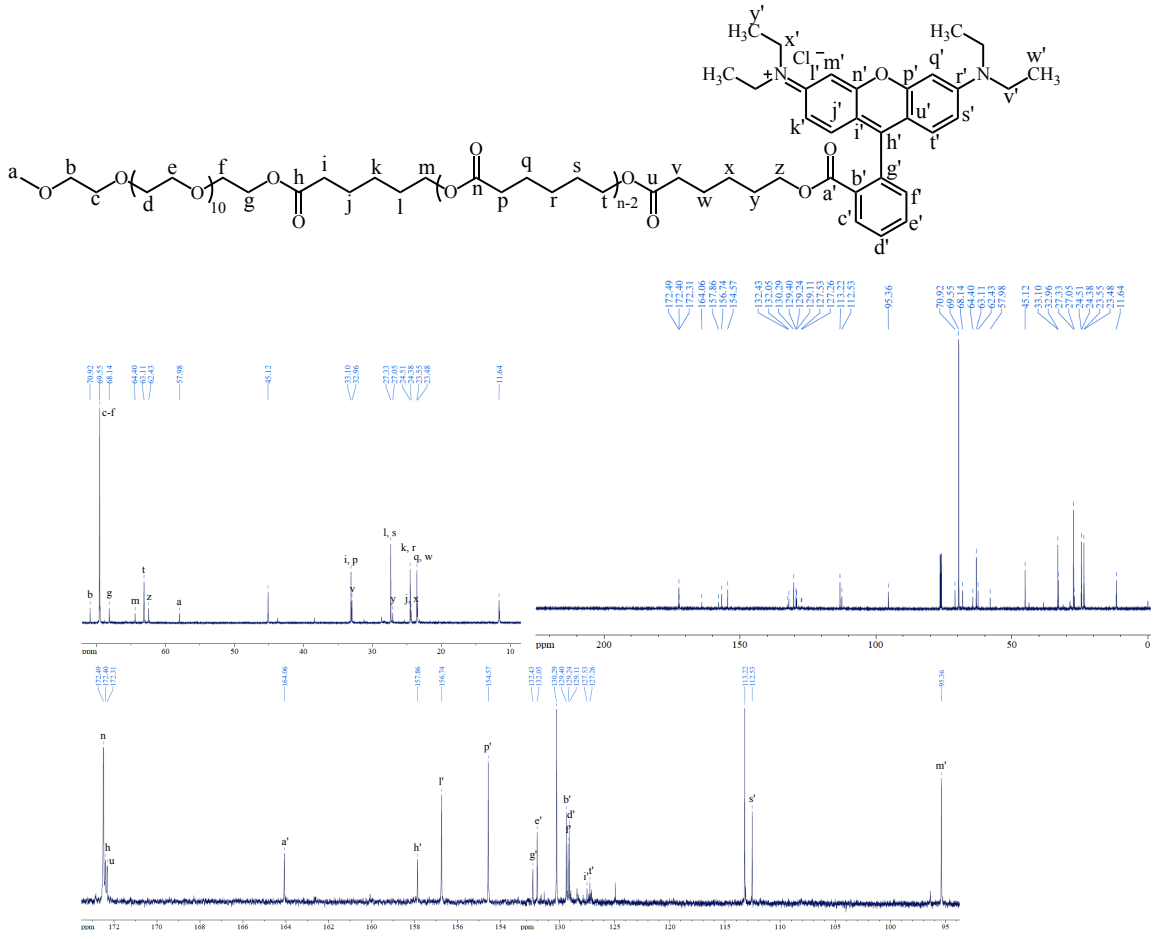

Figure 5.18: ^{13}C NMR Spectrum of MeOPEGPCLRhod. M_n=1.80*10^3 g/mole, PDI =1.17

5.3.5 Conclusion

A fluorescently-labeled PEG-b-PCL diblock copolymer was synthesized in two steps from MeOPEGPCL in 25% yield. The method presented here for the synthesis of PEG-*b*-PCLRhod is less expensive than the one used by Maysinger and coworkers.[123]

The price of tetramethylrhodamine-5-carbonyl azide ($19/μmol) is 25000 times more expensive than rhodamine lactone ($0.8/mmol).

5.4 Fluorescently Labeled Micelles

This section gives an introduction to the criteria for the preparation of fluorescently labeled micelles. Micelle preparation and characterization by DLS, FCS, and FCCS is also discussed for systems before and after incubation under biological conditions.

5.4.1 Introduction

As explained in section 5.1.1, the motivation for this work was the study of protein adsorption onto micelles that have different polymer architecture in the corona. The lower the protein adsorption onto the micelles, the longer the blood circulation time should be, leading to the advantages cited in chapter II.

5.4.2 Preparation and DLS Characterization of Fluorescently Labeled Micelles

The preparation of tagged micelles was very similar to the non-tagged micelles described in section 5.2.2. The main difference between the two methods is the use of PEG-*b*-PCLRhod. In order to determine the appropriate tagged-polymer concentrations, different experiments were performed with different ratios of tagged polymer/non-tagged polymer. For example, Figure 5.19 shows the FCCS average curve for the intial attempts

to prepare fluorescently labeled micelles using PEG-*b*-PCLRhod. The correlation curves show good quantum yield but a fluorophore concentration that is too high to give reliable results.

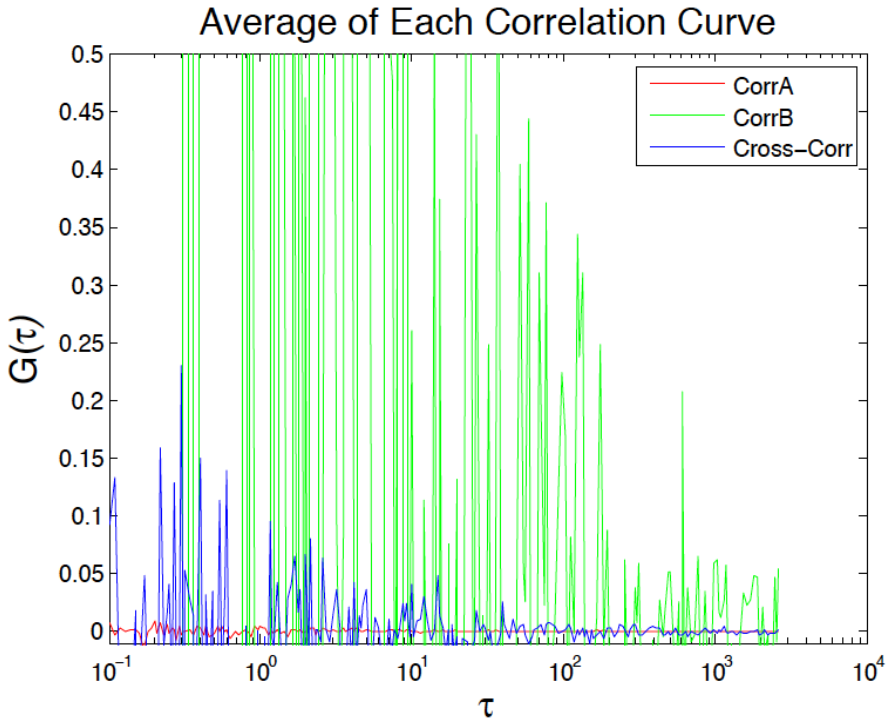

Figure 5.19: FCCS Average Curve for MeOPEG550PCL4k Micelles (30 μM) Tagged with MeOPEG550-*b*-PCL400Rhod (4.2% mol)

Table 5.4: Polymer Molecular Weight and Micelle Aggregation Number

PEG M_n (g/mole)	PCL M_n (g/mole)	Nagg	Reference
5000	6000	72	64
5000	10000	175	64
5000	18000	67	64
3420	13600	3000	41
2000	2500	125	25

A molar concentration of 0.5% gave good fluorescence results; however every micelle must have at least one fluorescently tagged polymer molecule in order to be able to accurately quantify protein adsorption onto the micelles. Table 5. shows the molecular weight and aggregation number for different PEG-*b*-PCL diblock copolymers in water.[121,217,272] Since the last entry in Table 5. has molecular weights closest to the polymers studied here, we calculated the amount of fluorescent polymer required to have one or two fluorescent polymers per micelle, assuming the micelles have an aggregation number of 125.[121]

Table 5.5 and Table 5.6 show the sizes by DLS for micelles made from MeOPEG550BnOPCL and MCBnOPCL, respectively. Three different populations are seen before filtration for micelles from L1x and C1x. As mentioned in section 5.2.3, micelles made with polymers with the lowest PCL molecular weight are the least stable, and form large aggregates (8 μm and 7 μm in size) shown in the third population in Table 5. and Table 5.6. Two size populations were seen for L3x, L5x, C3x, and C5x. The largest populations for L3x and C3x were about 3 μm, while the largest population for C5x was about 5 μm. Only one population was seen after filtering through a 0.45 μm poly(ether sulfone) filter.

Figure 5.20 shows the micelle sizes for the smallest population before and after filtering. The micelle sizes are relatively uniform and are between 101 and 280 nm. In general smaller sizes were seen after filtering; however the size differences before and after filtering were small to negligible.

Table 5.5 DLS Characterization of Fluorescent Micelles From MeOPEG550BnOPCL Before and After Filtering Through a 0.45 μm PES filter

		MeOPEG550BnOPCL400 =L1x		MeOPEG550BnOPCL1k =L3x		MeOPEG550BnOPCL2k =L5x	
		Size (nm)	Std dev (nm)	Size (nm)	Std dev (nm)	Size (nm)	Std dev (nm)
Before filtering	Pop 1	101	21	169	27	194	23
	Pop 2	694	153	3185	488	1509	192
	Pop 3	7776	1414	NA	NA	NA	NA
After filtering		136	1	162	1	172	1

Table 5.6: DLS Characterization of Fluorescent Micelles from MCBnOPCL Before and After Filtering Through a 0.45 μm PES filter

		MCBnOPCL700=C1x		MCBnOPCL2k=C3x		MCBnOPCL2.5k=C5x	
		Size (nm)	Std dev (nm)	Size (nm)	Std dev (nm)	Size (nm)	Std dev (nm)
Before filtering	Pop 1	123	24	221	26	280	153
	Pop 2	2411	511	2796	314	4392	1387
	Pop 3	7126	0	NA	NA	NA	NA
After filtering		129	24	196	1	186	64

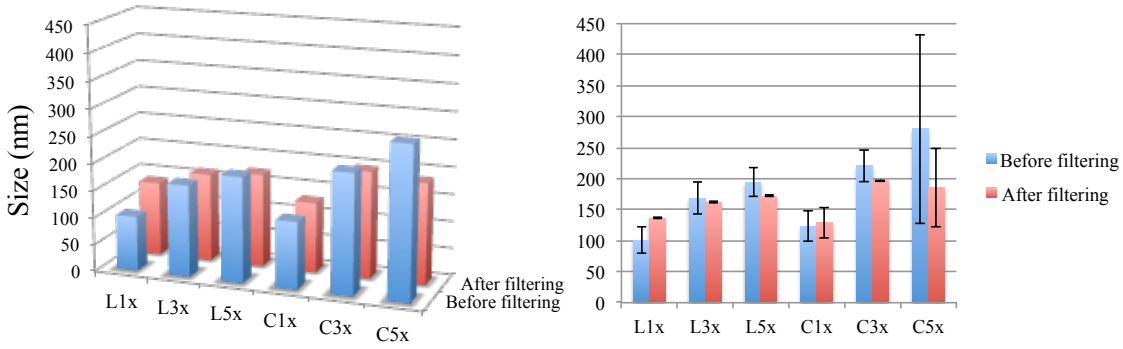

Figure 5.20: DLS Characterization of Fluorescent Micelles

.

5.5 Protein Adsorption Experiments Using DLS

This section introduces the method used to measure protein adsorption by incubating micelles with high concentrations of BSA under biological conditions. DLS

results for these experiments are discussed, highlighting the similarities and differences found for different protein concentrations, different molecular weights, and different polymer architectures.

5.5.1 Introduction

Rezwan and coworkers did not consider biologically relevant protein concentrations in their experiments of protein adsorption onto Al_2O_3 nanoparticles.[261] According to Barth and coworkers the concentration of albumin in human blood is between 35-50 mg/mL.[273] Allen and coworkers consider 45 mg/mL to be a biologically relevant concentration.[216] The highest concentration that Rezwan and coworkers worked with is 10.8 mg/mL, which is about 25% of a biologically relevant concentration. As mentioned in the previous section, we could not work at biological BSA concentrations because of signal overloading at these high concentrations. As an alternative, the following DLS experiments were performed.

5.5.2 Experimental Conditions

As discussed in the introduction to this section, different BSA solutions were prepared based on the biological concentration of 45 mg/mL.[216] Four different BSA concentrations were used in these experiments as summarized in Table 5.7. In each protein adsorption experiment, 750 μL of micelle suspension was mixed with 750 μL of either PBS only or a protein solution prepared in PBS. These mixtures were incubated at 37 °C in a shaker at 250 rpm for 16 h. After that, the sizes of the micelles were measured

at room temperature using dynamic light scattering (DLS). The DLS measurements were made with an acquisition time of 10 min by triplicate and the software estimated the diameters by intensity.

Table 5.7: BSA Concentration Used in Second Set of Experiments

mg/mL	**mM**
0	0.00
2	0.03
1	0.02
22	0.33
45	0.68

5.5.3 Incubation of BSA Solutions and Characterization by DLS

Table 5.8 and Figure 5. show the DLS characterization of incubated BSA solutions. Four size populations are seen, except at 0 mg/mL as expected. The first 7-9 nm population is monomeric BSA. Yohannes and coworkers measured the hydrodynamic diameter of native BSA at room temperature using asymmetrical flow field-flow fractionation and found a value of 7 nm.[274]

Table 5.8: Size (nm) Populations Measured by DLS in BSA Solutions After Incubation

	0 mg/mL	2 mg/mL	11 mg/mL	22 mg/mL	45 mg/mL
Pop 1	NA	9	8	8	7
Pop 2	NA	48	34	NA	40
Pop 3	NA	92	NA	NA	NA
Pop 4	NA	418	363	418	221

San Biagio and coworkers also studied the effect of intermediates in the aggregation of BSA and found that 5-6 monomer aggregates were common.[275] This is consistent with the population 2 that has a size of 34-48 nm. Honda and coworkers found a third population with a size close to 100 nm,[276] which corresponds to the third population seen in the DLS experiments. Finally, the last population has a size around 400 nm.

In order to use DLS to determine size, particles should diffuse according to Brownian motion. According to a technical report published by rheosense.com, the viscosities of BSA solutions in PBS are relatively constant in the interval between 1.2 and 50 mg/mL.[277] Puntes and coworkers used DLS and TEM to monitor protein adsorption onto metallic gold nanoparticles at a protein concentration of 100 mg/mL. They obtained consistent sizes by DLS and TEM that confirm that DLS can be used at these protein concentrations.[278] Finally, Figure 5. shows the size populations listed above for BSA solutions incubated at 37 °C for 16 h.

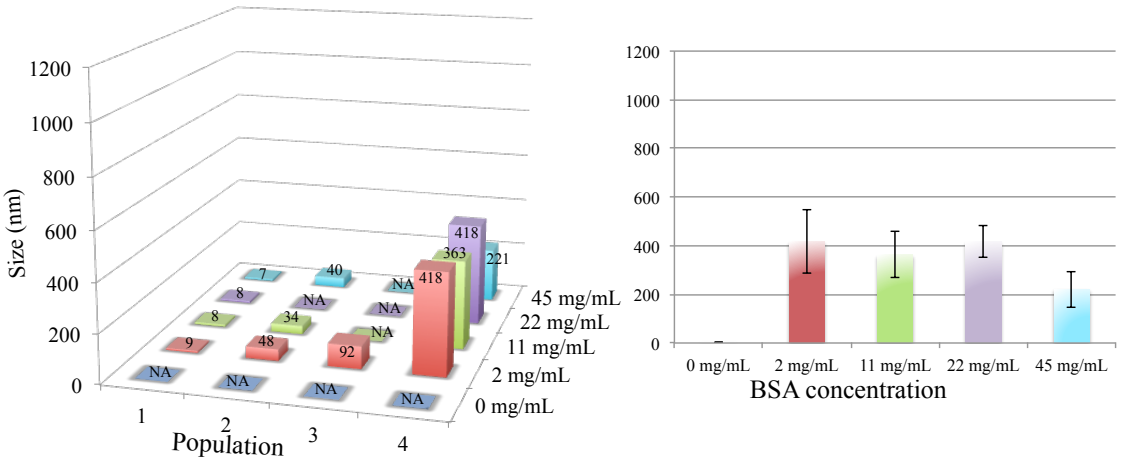

Figure 5.21: DLS Characterization of Incubated BSA Solutions

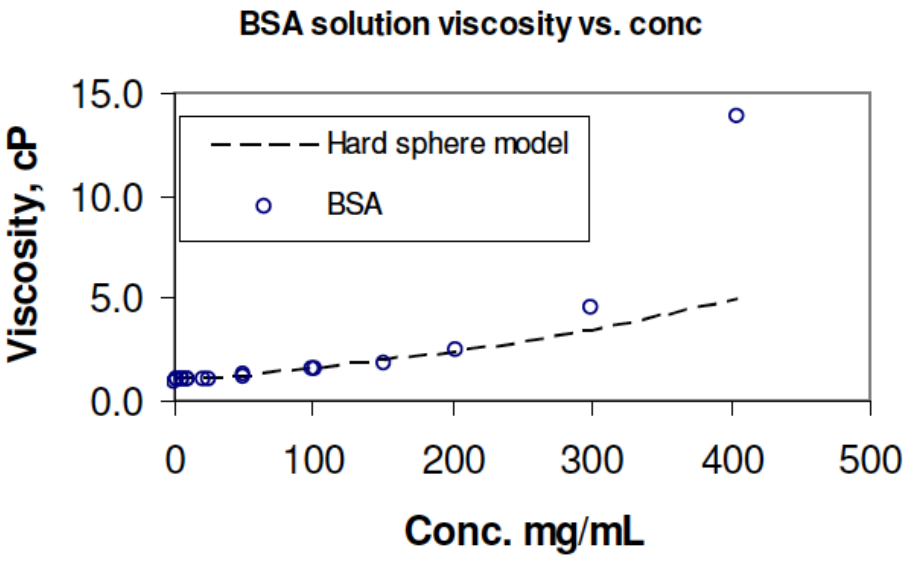

Figure 5.22: Viscosity of BSA Solutions in PBS as a Function of Concentration.[68]

5.5.4 Protein Adsorption onto Micelles from MeOPEG550BnOPCL Linear-*b*-Linear Diblock Copolymers

Table 5.9, Table 5.10, and Table 5. and Figure 5.23 show DLS characterization of L1x, L3x, and L5x, respectively, incubated with different concentrations of BSA at 37 °C for 16 h. Different BSA concentrations are shown in each column. The first three BSA size populations are seen at biological conditions, which was the highest BSA concentration (45 mg/mL), except for population 2 of L3x. Only the two smallest BSA populations are seen for 11 and 22 mg/mL for L1x and L3x, while only the smallest BSA population is seen for L1x, L3x, and L5x at 2 mg/mL and also for L5x at 11 mg/mL indicating that the presence of the micelles in the incubation system prevents BSA aggregation. A comparison between Table 5. and Table 5.9 show that the size of L1x increased upon incubation from 136 to 303 nm. As presented in Table 5. and discussed in

section 5.2.3, the PEG-*b*-PCL samples studied here have low melting temperatures and are therefore likely to disassemble and reassemble upon incubation at 37 °C. BSA binding is not seen for either 2 nor for 11 mg/mL. There is a relative size reduction for L1x from 2 to 11 mg/mL; this might be due to micelle stabilization due to the presence of the protein at 11 mg/mL. Finally, evidence of BSA binding to micelles is seen at 22 and 45 mg/mL. As explained before, the largest BSA aggregates seen at 22 mg/mL are those corresponding to the second population in Table 5. and Figure 5..

Therefore, population 4 at 22 mg/mL corresponds to a micelle-protein aggregate. This is confirmed at 45 mg/mL where the micelle-protein aggregate has essentially the same size (650 ± 166 nm vs. 709 ± 182 nm). BSA binding can be estimated as a layer 225 nm thick assuming the micelle size stays constant between 11 and 22 mg/mL. Taking into account a monomeric BSA units has a size of 7 nm, this layer coating the micelle would consist of about 28 BSA monomeric units.

Table 5.9: Size (nm) Populations Measured by DLS in L1x Micelle Suspensions After Incubation with BSA

	0 mg/mL	2 mg/mL	11 mg/mL	22 mg/mL	45 mg/mL
Pop 1	NA	8	8	8	7
Pop 2	NA	NA	31	35	29
Pop 3	NA	NA	NA	NA	92
Pop 4	303	278	222	650	709

Table 5.10: Size (nm) Populations Measured by DLS in L3x Micelle Suspensions After Incubation with BSA

	0 mg/mL	2 mg/mL	11 mg/mL	22 mg/mL	45 mg/mL
Pop 1	NA	9	8	7	8
Pop 2	NA	NA	23	26	NA
Pop 3	NA	NA	110	NA	105
Pop 4	372	261	349	284	797

Table 5.11: Size (nm) Populations Measured by DLS in L5x Micelle Suspensions After Incubation with BSA

	0 mg/mL	2 mg/mL	11 mg/mL	22 mg/mL	45 mg/mL
Pop 1	NA	9	9	8	8
Pop 2	NA	NA	NA	33	35
Pop 3	86	NA	NA	NA	80
Pop 4	353	188	254	492	585

Similar results were obtained for L3x and L5x. Upon incubation L3x increased its size from 162 ± 1 to 372± 75 nm while L5x went from 172±1 to 353± 60 nm. L3x sizes were more stable over the different BSA concentrations. Evidence of BSA binding was only seen at 45 mg/mL where the BSA layer is about 200 nm thick. This is the same BSA layer thickness seen for L1x at 22 and 45 mg/mL. Finally BSA binding binds to L5x at 22 and 45 mg/mL with a BSA layer of about 150 nm, similar to the BSA layers seen for L1x and L3x.

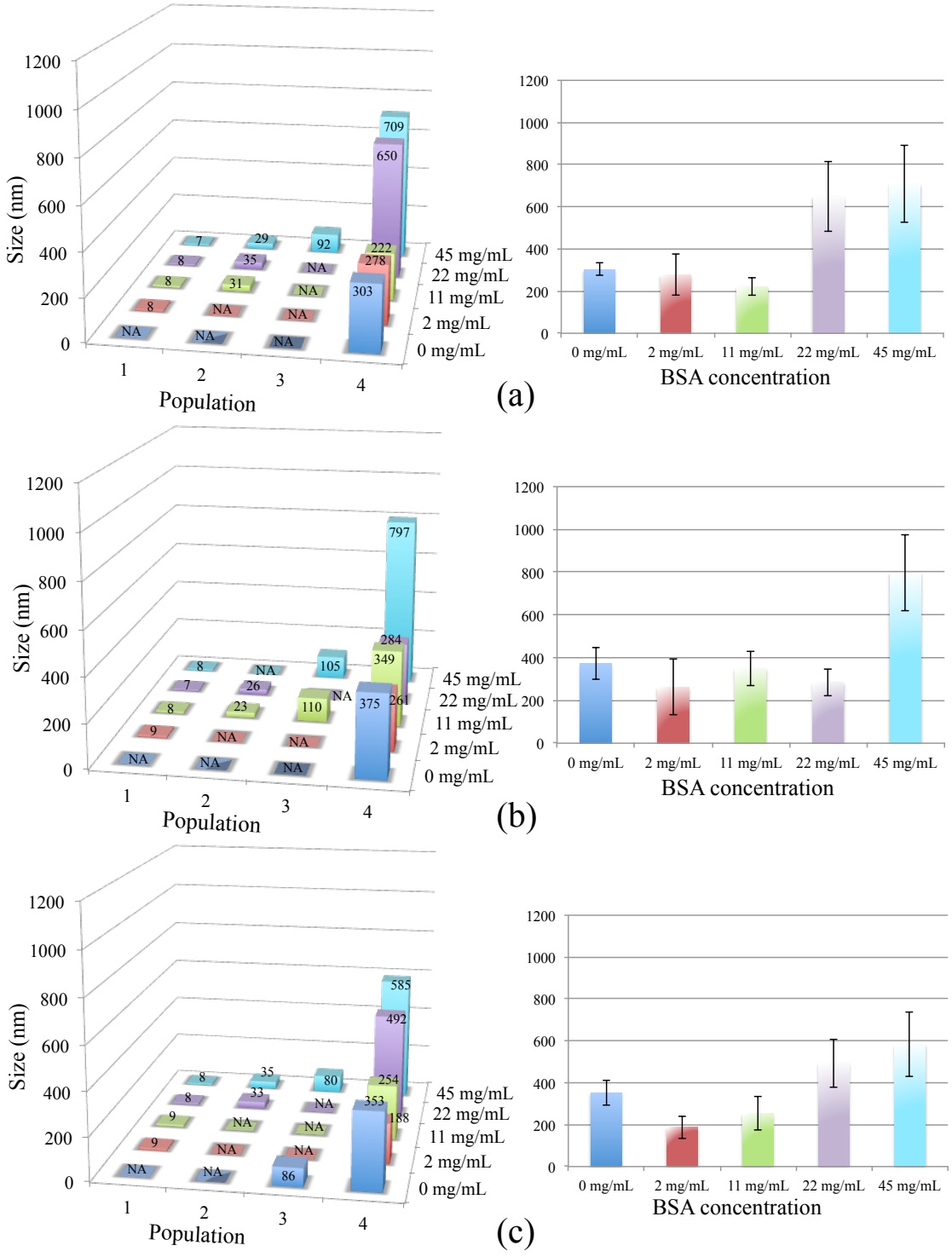

Figure 5.23: DLS Characterization of Incubated (a) L1x, (b) L3x, and (c) L5x

5.5.5. Protein Adsorption onto Micelles from MCBnOPCL Cyclic-*b*-Linear Diblock Copolymers

Table 5.12, Table 5.13, Table 5.14, and Figure 5.24 show the DLS characterization of C1x, C3x, and C5x incubated with different concentrations of BSA at 37 °C for 16 h. Comparison of Table 5. with the tables in this section, shows that C1x went from 129±24 to 498±89 nm, C3x from 196±1 nm to 516±79 and C5x from 186±64 to 702±166 nm upon incubation at 37 °C for 16 h. There is no strong evidence of BSA binding. The sizes for C3x and C5x are consistent throughout all BSA concentrations. C1x is the exception with size reduction from 498±89 to 217±69 nm from 0 mg/mL to 2 mg/mL, and a large size increase at 11 to 22 mg/mL. As mentioned before, this data inconsistency might have to do with the low PCL molecular weight causing low micelle stability.

Table 5.12: Size (nm) Populations Measured by DLS in C1x Micelle Suspensions After Incubation with BSA

	0 mg/mL	2 mg/mL	11 mg/mL	22 mg/mL	45 mg/mL
Pop 1	NA	9	8	8	8
Pop 2	NA	NA	NA	25	Seen
Pop 3	NA	42	48	91	NA
Pop 4	498	217	602	939	577

Table 5.13: Size (nm) Populations Measured by DLS in C3x Micelle Suspensions After Incubation with BSA

	0 mg/mL	2 mg/mL	11 mg/mL	22 mg/mL	45 mg/mL
Pop 1	NA	9	8	8	7
Pop 2	NA	49	39	26	31
Pop 3	NA	NA	NA	NA	NA
Pop 4	516	532	559	471	631

Table 5.14 : Size (nm) Population Measured by DLS in C5x Micelle Suspensions After Incubation with BSA

	0 mg/mL	22 mg/mL	45 mg/mL
Pop 1	NA	8	8
Pop 2	NA	NA	SEEN
Pop 3	NA	45	295
Pop 4	702	613	782

5.5.6 Conclusion

Micelles from PEG-*b*-PCL diblock copolymers with cyclic architecture in the PEG block (MCBnOPCL) did not show protein binding when incubated at 37 °C for 16 h with BSA at biological concentration (45 mg/mL). In contrast, micelles from PEG-*b*-PCL diblock copolymers with linear architecture in both the PEG and PCL blocks (MeOPEG550BnOPCL) showed BSA binding at 22 and 45 mg/mL. The thickness of the BSA layer was estimated to be around 200 nm, which corresponds to about 28 monomeric BSA units.

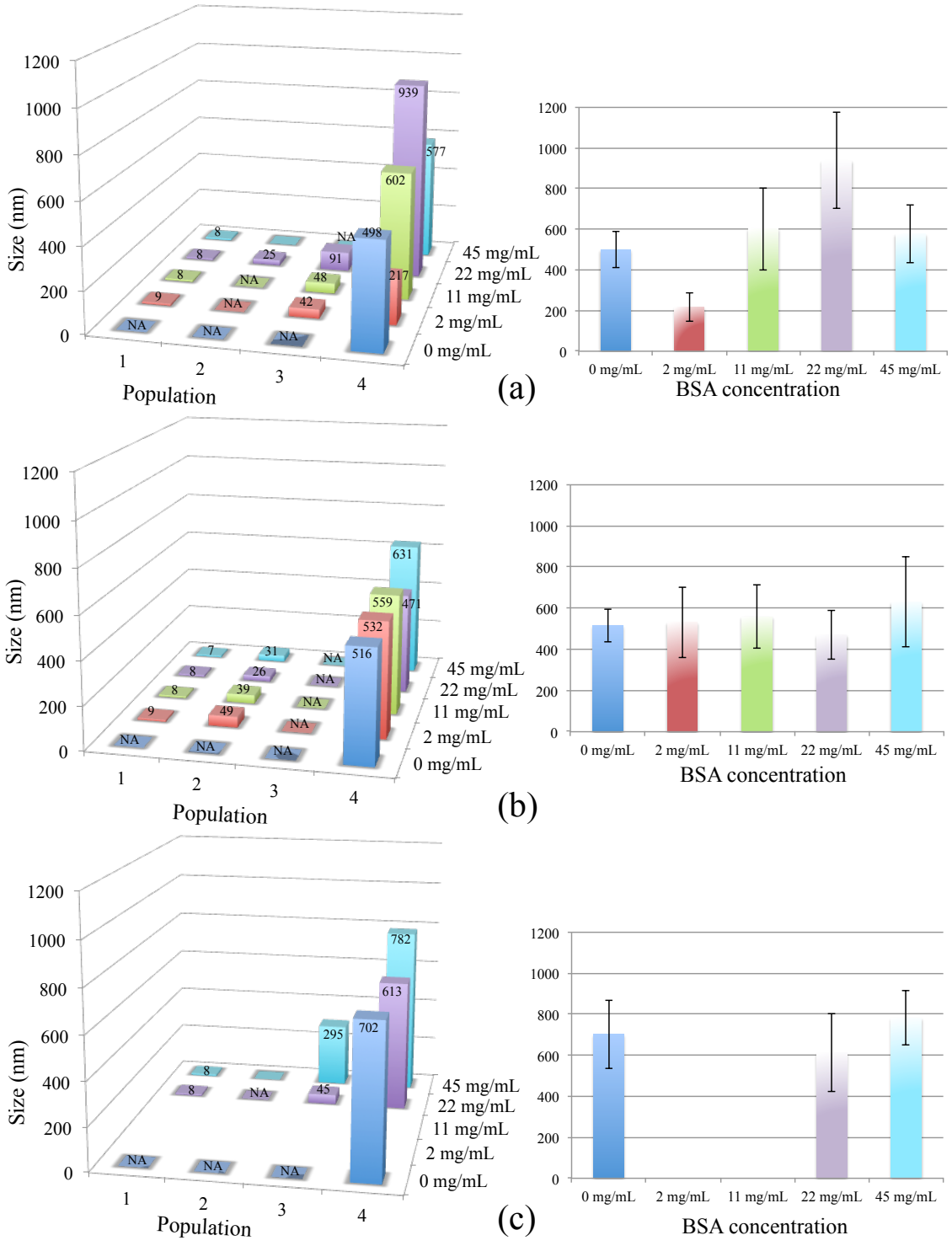

Figure 5.24: DLS Characterization of (a) C1x, (b) C3x, and (c) C5x After Incubation

These results indicate that if cyclic rather than linear PEG coatings are used in nanoparticles for drug delivery, the protein binding will be reduced, minimizing the immune response against these particles. In other words, the circulation time of nanoparticles in drug delivery should be increased by using a PEG coating that has a cyclic architecture with no end groups.

CHAPTER VI

CONCLUSIONS AND FUTURE DIRECTIONS

We successfully synthesized PEG-*b*-PCL diblock copolymers that had either a cyclic or a linear architecture in the PEG block. Three different PCL molecular weights were prepared corresponding to one, three, and five times the molecular weight of PEG. Two different PEG macroinitiators with a linear or a cyclic structure were synthesized. The linear PEG macroinitiator was synthesized in 2 steps in 55% yield and the cyclic PEG macroinitiator was synthesized in 3 steps in 20% yield. From these macroinitiators, a PCL block was grown by ring-opening polymerization of ε-caprolactone. Linear-*b*-linear diblock copolymers with PDI between 1.03 and 1.20 were synthesized in 99-100% conversion. Cyclic-*b*-linear PEG-*b*-PCL diblock copolymers with PDI between 1.12 and 1.23 were synthesized in 92-96% conversion.

Self-assembled micelles were prepared by a co-solvent evaporation method using MilliQ water or PBS. These micelles were characterized using DLS and TEM. Better defined micelles were formed from cyclic-*b*-linear than from linear-*b*-linear diblock copolymers.

In order characterize these micelles using FCS and FCCS, we attempted to entrap fluorescent dyes in the micelles but had problems of low entrapment efficiency or low quantum yield. In order to overcome these problems, we decided to synthesize a diblock copolymer with a covalently bound fluorescent molecule. The model fluorescently labeled PCL homopolymer was prepared in three steps in 11% yield in order to develop the synthetic route. A fluorescently labeled PEG-*b*-PCL diblock copolymer was synthesized in three steps in 25% yield.

Protein adsorption was studied by incubation of the micelle suspensions with different concentrations of BSA up to the biological concentration. Upon incubation at 37 °C for 16 h, micelles increased their size by 200-400%. BSA binding onto micelles from linear-*b*-linear polymers was seen at 22 and 45 mg/mL, and consisted of a 150-225 nm thick layer (19-28 BSA monomeric units).

No BSA binding was seen for micelles from cyclic-*b*-linear polymers. Therefore, BSA binding was minimized by using a cyclic PEG architecture without end groups, confirming our original hypothesis: lower protein adsorption should be measured on micelles from diblock copolymers with a cyclic PEG architecture compared to linear architectures currently used.

This project sets the basis for further progress in the study of cyclic PEG architectures in polymers used for drug delivery. For example, the molecular weight of the cyclic PEG and linear PCL blocks could be increased to prepare more stable (i.e. both in

terms of concentration and temperature) micelles making it easier to characterize them and study protein adsoption and circulation times, particularly using FCS and FCCS. Another important future direction is to measure blood circulation times in mice, which would continue the progress towards the use of these new polymers for therapeutic purposes. Finally, the synthesis of hyperbranched polymers that behave as unimolecular micelles from the inimer presented here with an oligooxyethylene glycol side chain, but also with larger molecular weight ethylene oxide oligomers, and cyclic PEG moieties of different molecular weights will enable the study of protein adsorption onto stable unimolecular micelles that could have even better properties in terms of lower protein adsorption and increased circulation times.

REFERENCES

(1) Chen, D.; Chen, H.; Bei, J.; Wang, S. Morphology and biodegradation of microspheres of polyester–polyether block copolymer based on polycaprolactone/polylactide/poly (ethylene oxide). *Polym. Int.* **2000**, *49*, 269–276.

(2) Koleske, J. Blends containing poly-caprolactone and related polymers. *Polymer Blends* **1978**, *2*, 369–389.

(3) Huang, M.-H.; Li, S.; Hutmacher, D. W.; Coudane, J.; Vert, M. Degradation characteristics of poly(ε-caprolactone)-based copolymers and blends. *J. Appl. Polym. Sci.* **2006**, *102*, 1681–1687.

(4) Ekholm, M.; Hietanen, J.; Lindqvist, C.; Rautavuori, J.; Santavirta, S.; Suuronen, R. Histological study of tissue reactions to epsilon-caprolactone-lactide copolymer in paste form. *Biomaterials* **1999**, *20*, 1257–1262.

(5) Sinha, V. R.; Bansal, K.; Kaushik, R.; Kumria, R.; Trehan, A. Poly-ϵ-caprolactone microspheres and nanospheres: an overview. *Int. J. Pharm.* **2004**, *278*, 1–23.

(6) Lengsfeld, C. S.; Manning, M. C.; Randolph, T. W. Encapsulating DNA within biodegradable polymeric microparticles. *Curr Pharm Biotechnol* **2002**, *3*, 227–235.

(7) Vicent, M. J.; Duncan, R. Polymer conjugates: nanosized medicines for treating cancer. *Trends Biotechnol.* **2006**, *24*, 39–47.

(8) Bae, Y.; Nishiyama, N.; Fukushima, S.; Koyama, H.; Yasuhiro, M.; Kataoka, K. Preparation and Biological Characterization of Polymeric Micelle Drug Carriers with Intracellular pH-Triggered Drug Release Property: Tumor Permeability, Controlled Subcellular Drug Distribution, and Enhanced in Vivo Antitumor Efficacy. *Bioconj. Chem.* **2005**, *16*, 122–130.

(9) Gref, R.; Minamitake, Y.; Peracchia, M. T.; Trubetskoy, V.; Torchilin, V.; LANGER, R. Biodegradable long-circulating polymeric nanospheres. *Science* **1994**, *263*, 1600–1603.

(10) Mosqueira, V. C.; Legrand, P.; Morgat, J. L.; Vert, M.; Mysiakine, E.; Gref, R.; Devissaguet, J. P.; Barratt, G. Biodistribution of long-circulating PEG-grafted nanocapsules in mice: effects of PEG chain length and density. *Pharm Res* **2001**, *18*, 1411–1419.

(11) Owens, D.; Peppas, N. Opsonization, biodistribution, and pharmacokinetics of polymeric nanoparticles. *Int. J. Pharm.* **2006**, *307*, 93–102.

(12) Stolnik, S.; Ilum, L.; Davis, S. S. Long circulating microparticle drug carriers. *Adv. Drug Delivery Rev.* **1995**, *16*, 195–214.

(13) Béduneau, A.; Saulnier, P.; Anton, N.; Hindré, F.; Passirani, C.; Rajerison, H.; Noiret, N.; Benoit, J.-P. Pegylated Nanocapsules Produced by an Organic Solvent-Free Method: Evaluation of their Stealth Properties. *Pharm Res* **2006**, *23*, 2190–2199.

(14) Gref, R. R.; Minamitake, Y. Y.; Peracchia, M. T. M.; Domb, A. A.; Trubetskoy, V. V.; Torchilin, V. V.; Langer, R. R. Poly(ethylene glycol)-coated nanospheres: potential carriers for intravenous drug administration. *Pharm Biotechnol* **1997**, *10*, 167–198.

(15) Gref, R.; Lück, M.; Quellec, P.; Marchand, M.; Dellacherie, E.; Harnisch, S.; Blunk, T.; Müller, R. "Stealth" corona-core nanoparticles surface modified by polyethylene glycol (PEG): influences of the corona (PEG chain length and surface density) and of the core composition on phagocytic uptake and plasma protein adsorption. *Colloids Surf B Biointerfaces* **2000**, *18*, 301–313.

(16) Torchilin, V. P.; Papisov, M. I. Why do Polyethylene Glycol-Coated Liposomes Circulate So Long?: Molecular Mechanism of Liposome Steric Protection with Polyethylene Glycol: Role of Polymer Chain Flexibility. *J. Lip. Res.* **1994**, *4*, 725–739.

(17) Juliano, R. L.; Stamp, D. The effect of particle size and charge on the clearance rates of liposomes and liposome encapsulated drugs. *Biochem. Biophys. Res. Commun.* **1975**, *63*, 651–658.

(18) Devine, D. V.; Wong, K.; Serrano, K.; Chonn, A.; Cullis, P. R. Liposome-complement interactions in rat serum: implications for liposome survival studies. *Biochimica et Biophysica Acta* **1994**, *1191*, 43–51.

(19) Moghimi, S. M.; Porter, C. J.; Muir, I. S.; Illum, L.; Davis, S. S. Non-phagocytic uptake of intravenously injected microspheres in rat spleen: influence of particle size and hydrophilic coating. *Biochem. Biophys. Res. Commun.* **1991**, *177*, 861–866.

(20) Cabral, H.; Matsumoto, Y.; Mizuno, K.; Chen, Q.; Murakami, M.; Kimura, M.; Terada, Y.; Kano, M. R.; Miyazono, K.; Uesaka, M.; Nishiyama, N.; Kataoka, K. Accumulation of sub-100 nm polymeric micelles in poorly permeable tumours depends on size. *Nature Nanotech* **2011**, *6*, 815–823.

(21) Fox, M. E.; Szoka, F. C.; Fréchet, J. M. J. Soluble Polymer Carriers for the Treatment of Cancer: The Importance of Molecular Architecture. *Acc. Chem. Res.* **2009**, *42*, 1141–1151.

(22) Langer, R. New methods of drug delivery. *Science* **1990**, *249*, 1527–1533.

(23) Amidon, G. L.; Lennernas, H.; Shah, V. P.; Crison, J. R. A Theoretical Basis for a Biopharmaceutic Drug Classification: The Correlation of in Vitro Drug Product Dissolution and in Vivo Bioavailability. *Pharm Res* **1995**, *12*, 413–420.

(24) Yu, L. X.; Amidon, G. L.; Polli, J. E.; Zhao, H.; Mehta, M. U.; Conner, D. P.; Shah, V. P.; Lesko, L. J.; Chen, M.-L.; Lee, V. H. L.; Hussain, A. S. Biopharmaceutics classification system: the scientific basis for biowaiver extensions. *Pharm Res* **2002**, *19*, 921–925.

(25) Langer, R. Where a pill won't reach. *Scientific American* **2003**.

(26) Gref, R.; Domb, A.; Quellec, P.; Blunk, T.; Müller, R. H.; Verbavatz, J. M.; Langer, R. The controlled intravenous delivery of drugs using PEG-coated sterically stabilized nanospheres. *Adv. Drug Delivery Rev.* **1995**, *16*, 215–233.

(27) Saez, A. A.; Guzmán, M. M.; Molpeceres, J. J.; Aberturas, M. R. M. Freeze-drying of polycaprolactone and poly(D,L-lactic-glycolic) nanoparticles induce minor particle size changes affecting the oral pharmacokinetics of loaded drugs. *Eu. J. Pharm. and Biopharm.* **2000**, *50*, 379–387.

(28) Tong, R.; Cheng, J. Anticancer Polymeric Nanomedicines. *Polymer Revs.* **2007**, *47*, 345–381.

(29) Minko, T.; Paranjpe, P.; Qiu, B.; Lalloo, A.; Won, R.; Stein, S.; Sinko, P. Enhancing the anticancer efficacy of camptothecin using biotinylated poly(ethyleneglycol) conjugates in sensitive and multidrug-resistant human ovarian carcinoma cells. *Cancer Chem. and Pharm.* **2002**, *50*, 143–150.

(30) Thomson, A.; Vasey, P.; Murray, L.; Cassidy, J.; Fraier, D.; Frigerio, E.; Twelves, C. Population pharmacokinetics in phase I drug development: a phase I study of PK1 in patients with solid tumours. *British journal of cancer* **1999**, *81*, 99.

(31) Greenwald, R. B.; Conover, C.; Choe, Y. Poly(ethylene glycol) conjugated drugs and prodrugs: a comprehensive review. *Crit Rev Ther Drug Carrier Syst.* **2000**, *17*, 101–161.

(32) Pendri, A.; Conover, C.; Greenwald, R. Antitumor activity of paclitaxel-2'-glycinate conjugated to poly(ethylene glycol): a water-soluble prodrug. *Anticancer Drug Des* **1998**, *13*, 387–395.

(33) Conover, C. D. C.; Greenwald, R. B. R.; Pendri, A. A.; Gilbert, C. W. C.; Shum, K. L. K. Camptothecin delivery systems: enhanced efficacy and tumor accumulation of camptothecin following its conjugation to polyethylene glycol via a glycine linker. *Cancer Chemotherapy and Pharmacology* **1998**, *42*, 407–414.

(34) Greenwald, R. B.; Pendri, A.; Conover, C.; Gilbert, C.; Yang, R.; Xia, J. Drug Delivery Systems. 2. Camptothecin 20- O-Poly(ethylene glycol) Ester Transport Forms. *J. Med. Chem.* **1996**, *39*, 1938–1940.

(35) Bhatt, R.; de Vries, P.; Tulinsky, J.; Bellamy, G.; Baker, B.; Singer, J. W.; Klein, P. Synthesis and in Vivo Antitumor Activity of Poly(l-glutamic acid) Conjugates of 20(S)-Camptothecin. *J. Med. Chem.* **2003**, *46*, 190–193.

(36) Mitsui, I. I.; Kumazawa, E. E.; Hirota, Y. Y.; Aonuma, M. M.; Sugimori, M. M.; Ohsuki, S. S.; Uoto, K. K.; Ejima, A. A.; Terasawa, H. H.; Sato, K. K. A new water-soluble camptothecin derivative, DX-8951f, exhibits potent antitumor activity against human tumors in vitro and in vivo. *Jpn J Cancer Res* **1995**, *86*, 776–782.

(37) Cheng, J.; Khin, K. T.; Davis, M. E. Antitumor Activity of β-Cyclodextrin Polymer−Camptothecin Conjugates. *Mol. Pharm.* **2004**, *1*, 183–193.

(38) Kim, S.; Shi, Y.; Kim, J. Y.; Park, K.; Cheng, J.-X. Overcoming the barriers in micellar drug delivery: loading efficiency, in vivostability, and micelle–cell interaction. *Expert Opin. Drug Deliv.* **2010**, *7*, 49–62.

(39) Moghimi, S. M.; Hunter, A. C.; Murray, J. C. Long-circulating and target-specific nanoparticles: theory to practice. *Pharmacol. Rev.* **2001**, *53*, 283–318.

(40) Borgman, M. P.; Aras, O.; Geyser-Stoops, S.; Sausville, E. A.; Ghandehari, H. Biodistribution of HPMA Copolymer-Aminohexylgeldanamycin-RGDfK Conjugates for Prostate Cancer Drug Delivery. *Mol. Pharm.* **2009**, *6*, 1836–1847.

(41) Letchford, K.; Burt, H. A review of the formation and classification of amphiphilic block copolymer nanoparticulate structures: micelles, nanospheres, nanocapsules and polymersomes. *J. Pharm. and Biopharm* **2007**, *65*, 259–269.

(42) Nishiyama, N.; Kataoka, K. Current state, achievements, and future prospects of polymeric micelles as nanocarriers for drug and gene delivery. *Pharmacol. Ther.* **2006**, *112*, 630–648.

(43) Kwon, G. S.; Kataoka, K. Block copolymer micelles as long-circulating drug vehicles. *Adv. Drug Delivery Rev.* **1995**, *16*, 295–309.

(44) Lavasanifar, A.; Samuel, J.; Kwon, G. S. Poly(ethylene oxide)-block-poly(-amino acid) micelles for drug delivery. *Adv. Drug Delivery Rev.* **2002**, *54*, 169–190.

(45) Torchilin, V. P. Block copolymer micelles as a solution for drug delivery problems. *Expert Opin. Drug Deliv.* **2005**, *15*, 63–75.

(46) Huang, H.; Remsen, E. E.; Kowalewski, T.; Wooley, K. L. Nanocages Derived from Shell Cross-Linked Micelle Templates. *J. Am. Chem. Soc.* **1999**, *121*, 3805–3806.

(47) Holowka, E. P.; Sun, V. Z.; Kamei, D. T.; Deming, T. J. Polyarginine segments in block copolypeptides drive both vesicular assembly and intracellular delivery. *Nature Mat* **2006**, *6*, 52–57.

(48) Bellomo, E. G.; Wyrsta, M. D.; Pa kstis, L.; Pochan, D. J.; Deming, T. J. Stimuli-responsive polypeptide vesicles by conformation-specific assembly. *Nature Mat* **2004**, *3*, 244–248.

(49) Holowka, E. P.; Pochan, D. J.; Deming, T. J. Charged Polypeptide Vesicles with Controllable Diameter. *J. Am. Chem. Soc.* **2005**, *127*, 12423–12428.

(50) Discher, D. E.; Ahmed, F. Polymersomes. *Annual Review of Biomedical Engineering* **2006**, *8*, 323–341.

(51) Discher, D. E.; Eisenberg, A. Polymer Vesicles. *Science* **2002**, *297*, 967.

(52) Discher, B. M. Polymersomes: Tough Vesicles Made from Diblock Copolymers. *Science* **1999**, *284*, 1143–1146.

(53) Ahmed, F.; Discher, D. E. Self-porating polymersomes of PEG–PLA and PEG–PCL: hydrolysis-triggered controlled release vesicles. *J. of Cont. Rel.* **2004**, *96*, 37–53.

(54) Meng, F.; Engbers, G. H. M.; Feijen, J. Biodegradable polymersomes as a basis for artificial cells: encapsulation, release and targeting. *J. of Cont. Rel.* **2005**, *101*, 187–198.

(55) Photos, P. J.; Bacakova, L.; Discher, B. M.; Bates, F. S.; Discher, D. E. Polymer vesicles in vivo: correlations with peg molecular weight. *J Control Rel* **2003**, *90*, 323.

(56) Newkome, G. R.; Yao, Z.; Baker, G. R.; Gupta, V. K. Micelles. Part 1. Cascade molecules: a new approach to micelles. A [27]-arborol. *J. Org. Chem.* **1985**, *50*, 2003–2004.

(57) Tomalia, A. A new class of polymers: starburst-dendritic macromolecules. *Pol Journal* **1985**, *17*, 117.

(58) Buhleier, E.; Wehner, W.; Voegtle, F. "Cascade"- and “nonskid-chain-like” syntheses of molecular cavity topologies. *Synthesis* **1978**, *2*, 155–158.

(59) Svenson, S.; Tomalia, D. Dendrimers in biomedical applications—reflections on the field. *Advanced Drug Delivery Reviews* **2005**, *57*, 2106–2129.

(60) Demanuelle, A.; Attwood, D. Dendrimer–drug interactions. *Adv. Drug Delivery Rev.* **2005**, *57*, 2147–2162.

(61) Lee, C. C.; MacKay, J. A.; Fréchet, J. M. J.; Szoka, F. C. Designing dendrimers for biological applications. *Nat Biotechnol* **2005**, *23*, 1517–1526.

(62) Lee, C. C.; Gillies, E. R.; Fox, M. E.; Guillaudeu, S. J.; Frechet, J. M. J.; Dy, E. E.; Szoka, F. C. A single dose of doxorubicin-functionalized bow-tie dendrimer cures mice bearing C-26 colon carcinomas. *Proc. Natl. Acad. Sci. U.S.A.* **2006**, *103*, 16649–16654.

(63) Qiu, L. Y.; Bae, Y. H. Polymer Architecture and Drug Delivery. *Pharm Res* **2006**, *23*, 1–30.

(64) Esfand, R.; Tomalia, D. Poly (amidoamine)(PAMAM) dendrimers: from biomimicry to drug delivery and biomedical applications. *Drug Disc. Today* 427–436.

(65) Yang, H.; Kao, W. J. Dendrimers for pharmaceutical and biomedical applications. *J Biomater Sci Polym Ed* **2006**, *17*, 3–19.

(66) D, J. W.; Kataoka, K. Bioinspired applications of functional dendrimers. *J Drug Deliv Sci Tech* **2005**, *15*, 19–30.

(67) Malik, N.; Evagorou, E. G.; Duncan, R. Dendrimer-platinate: a novel approach to cancer chemotherapy. *Anticancer Drugs* **1999**, *10*, 767–776.

(68) Maeda, H.; Wu, J.; Sawa, T.; Matsumura, Y.; Hori, K. Tumor vascular permeability and the EPR effect in macromolecular therapeutics: a review. *J Control Rel* **2000**, *65*, 271–284.

(69) Kukowska-Latallo, J. F. Nanoparticle Targeting of Anticancer Drug Improves Therapeutic Response in Animal Model of Human Epithelial Cancer. *Cancer Res* **2005**, *65*, 5317–5324.

(70) Pitt, C. G.; Gratzl, M. M.; Jeffcoat, A. R.; Zweidinger, R.; Schindler, A. Sustained drug delivery systems II: Factors affecting release rates from poly(epsilon-caprolactone) and related biodegradable polyesters. *J Pharm Sci* **1979**, *68*, 1534–1538.

(71) Husseini, G. A.; Pitt, W. G. Ultrasonic-activated micellar drug delivery for cancer treatment. *J Pharm Sci* **2009**, *98*, 795–811.

(72) Kim, S. Y.; Lee, Y. M.; Shin, H. J.; Kang, J. S. Indomethacin-loaded methoxy poly (ethylene glycol)/poly (ε-caprolactone) diblock copolymeric nanosphere: pharmacokinetic characteristics of indomethacin in the normal Sprague–Dawley rats. *Biomaterials* **2001**, *22*, 2049–2056.

(73) Shin, I. G. I.; Kim, S. Y. S.; Lee, Y. M. Y.; Cho, C. S. C.; Sung, Y. K. Y. Methoxy poly(ethylene glycol)/epsilon-caprolactone amphiphilic block copolymeric micelle containing indomethacin. I. Preparation and characterization. *J Control Release* **1998**, *51*, 1–11.

(74) La, S. B.; Okano, T.; Kataoka, K. Preparation and characterization of the micelle-forming polymeric drug indomethacin-incorporated poly(ethylene oxide)-poly(beta-benzyl L-aspartate) block copolymer micelles. *J Pharm Sci* **1996**, *85*, 85–90.

(75) Allen, C.; Han, J.; Yu, Y.; Maysinger, D.; Eisenberg, A. Polycaprolactone–b-poly (ethylene oxide) copolymer micelles as a delivery vehicle for dihydrotestosterone. *J Control Rel* **2000**, *63*, 275–286.

(76) Allen, C.; Yu, Y.; Maysinger, D.; Eisenberg, A. Polycaprolactone-b-poly (ethylene oxide) block copolymer micelles as a novel drug delivery vehicle for neurotrophic agents FK506 and L-685,818. *Bioconjugate Chem.* **1998**, *9*, 564–572.

(77) Hu, Y.; Jiang, X.; Ding, Y.; Zhang, L.; Yang, C.; Zhang, J.; Chen, J.; Yang, Y. Preparation and drug release behaviors of nimodipine-loaded poly (caprolactone)-poly (ethylene oxide)-polylactide amphiphilic copolymer nanoparticles. *Biomaterials* **2003**, *24*, 2395–2404.

(78) Cho, H.; Lai, T. C.; Kwon, G. S. Poly(ethylene glycol)-block-poly(ε-caprolactone) micelles for combination drug delivery: Evaluation of paclitaxel, cyclopamine and gossypol in intraperitoneal xenograft models of ovarian cancer. *J Control Release* **2013**, *166*, 1–9.

(79) Kataoka, K.; Matsumoto, T.; Yokoyama, M.; Okano, T.; Sakurai, Y.; Fukushima, S.; Okamoto, K.; Kwon, G. S. Doxorubicin-Loaded Poly (Ethylene Glycol)-Poly ([Beta]-Benzyl Aspartate) Copolymer Micelles: Their Pharmaceutical Characteristics and Biological Significance. *J Control Rel* **2000**, *64*, 143–153.

(80) Mikhail, A. S.; Allen, C. Poly(ethylene glycol)-*b*-poly(ε-caprolactone) Micelles Containing Chemically Conjugated and Physically Entrapped Docetaxel: Synthesis, Characterization, and the Influence of the Drug on Micelle Morphology. *Biomacromolecules* **2010**, *11*, 1273–1280.

(81) Torchilin, V. P. Structure and design of polymeric surfactant-based drug delivery systems. *J Control Rel* **2001**, *73*, 137–172.

(82) Metzler, C. M. Usefulness of theTwo-Compartment Model in Pharmacokinetics. *J Am Stat Assoc* **1971**, *66*, 49–53.

(83) Wilchinsky, A. V.; Faria, S. H.; Hutter, K. Thermodynamic modelling of polymer solutions with molecular form birefringence. *J of Non-Newtonian Fluid Mech* **2001**, *99*, 57–77.

(84) Male, D.; Brostoff, J.; Roth, D. B.; Roitt, I. *Immunology*; Seventh edition. Elsevier: Canada, 2006; pp. 87–104.

(85) Johnson, R. J. The complement system. In *Biomaterials Science: An Introduction to Materials in Medicine*; Ratner, B. D.; Hoffmann, A. S.; Schoen, F. J.; Lemons, J. E., Eds. Elsevier Academic Press: Amsterdam, 2004; pp. 318–328.

(86) Torchilin, V. P.; Trubetskoy, V. S. Which polymers can make nanoparticulate drug carriers long-circulating? *Adv. Drug Delivery Rev.* **1995**, *16*, 141–155.

(87) Wieder, K. J.; Palczuk, N. C.; van Es, T.; Davis, F. F. Some properties of polyethylene glycol:phenylalanine ammonia-lyase adducts. *J. Biol. Chem.* **1979**, *254*, 12579–12587.

(88) Harris, J. M.; Martin, N. E.; Modi, M. Pegylation: a novel process for modifying pharmacokinetics. *Clin Pharmacokinet* **2001**, *40*, 539–551.

(89) Ameller, T.; Marsaud, V.; Legrand, P.; Gref, R.; Barratt, G.; Renoir, J.-M. Polyester-poly(ethylene glycol) nanoparticles loaded with the pure antiestrogen RU 58668: physicochemical and opsonization properties. *Pharm Res* **2003**, *20*, 1063–1070.

(90) Bradley, A. J.; Devine, D. V.; Ansell, S. M.; Janzen, J.; Brooks, D. E. Inhibition of liposome-induced complement activation by incorporated poly(ethylene glycol)-lipids. *Arch. Biochem. Biophys.* **1998**, *357*, 185–194.

(91) Vega-Villa, K. R.; Takemoto, J. K.; Yáñez, J. A.; Remsberg, C. M.; Forrest, M. L.; Davies, N. M. Clinical toxicities of nanocarrier systems. *Adv. Drug Delivery Rev.* **2008**, *60*, 929–938.

(92) Nakada, Y.; Tudomi, R.; Sakurai, K.; Takahashi, Y. Evaluation of long-circulating nanoparticles using biodegradable ABA triblock copolymers containing of poly(L-lactic acid) A-blocks attached to central poly(oxyethylene) B-blocks in vivo. *Int. J. Pharm.* **1998**, *175*, 109–117.

(93) Otsuka, H. Novel approaches for the construction of functionalized PEG layer on surfaces using heterobifunctional PEG-PLA block copolymers and their micelles. *ACS Symposium Series* **2000**, *764*, 311.

(94) Sawhney, A. S.; Pathak, C. P.; Hubbell, J. A. Bioerodible hydrogels based on photopolymerized poly (ethylene glycol)-co-poly (. alpha.-hydroxy acid) diacrylate macromers. *Macromolecules* **1993**, *26*, 581–587.

(95) Malmsten, M. Studies of serum protein adsorption at phospholipid surfaces in relation to intravenous drug delivery. *Colloid Surface A* **1999**, *159*, 77–87.

(96) Shibuya-Fujiwara, N. N.; Hirayama, F. F.; Ogata, Y. Y.; Ikeda, H. H.; Ikebuchi, K. K. Phagocytosis in vitro of polyethylene glycol-modified liposome-encapsulated hemoglobin by human peripheral blood monocytes plus macrophages through scavenger receptors. *Life Sci* **2001**, *70*, 291–300.

(97) Simone, E. A.; Dziubla, T. D.; Arguiri, E.; Vardon, V.; Shuvaev, V. V.; Christofidou-Solomidou, M.; Muzykantov, V. R. Loading PEG-Catalase into Filamentous and Spherical Polymer Nanocarriers. *Pharm Res* **2008**, *26*, 250–260.

(98) Wan, L.; Zhang, X.; Pooyan, S.; Palombo, M. S.; Leibowitz, M. J.; Stein, S.; Sinko, P. J. Optimizing Size and Copy Number For PEG-fMLF (N-Formyl-methionyl-leucyl-phenylalanine) Nanocarrier Uptake by Macrophages. *Bioconjugate Chem.* **2008**, *19*, 28–38.

(99) Zalipsky, S. Chemistry of Polyethylene-Glycol Conjugates with Biologically-Active Molecules. *Adv. Drug Delivery Rev.* **1995**, *16*, 157–182.

(100) Harris, J. M.; Chess, R. B. Effect of pegylation on pharmaceuticals. *Nat Rev Drug Discov* **2003**, *2*, 214–221.

(101) Inactive Ingredient Search for Approved Drug Products **2013**, 1–4.

(102) Alconcel, S. N. S.; Baas, A. S.; Maynard, H. D. FDA-approved poly(ethylene glycol)–protein conjugate drugs. *Polym. Chem.* **2011**, *2*, 1442.

(103) Yamaoka, T.; Tabata, Y.; Ikada, Y. Distribution and tissue uptake of poly(ethylene glycol) with different molecular weights after intravenous administration to mice. *J Pharm Sci* **1994**, *83*, 601–606.

(104) Kingshott, P.; Wei, J.; Bagge-Ravn, D.; Gadegaard, N.; Gram, L. Covalent Attachment of Poly(ethylene glycol) to Surfaces, Critical for Reducing Bacterial Adhesion. *Langmuir* **2003**, *19*, 6912–6921.

(105) Holmberg, K.; Tiberg, F.; Malmsten, M.; Brink, C. Grafting with hydrophilic polymer chains to prepare protein-resistant surfaces. *Colloid Surface A* **1997**, *123*, 297–306.

(106) Jeon, S. I.; Lee, J. D.; Andrade, J. D.; De Gennes, P. G. Protein-surface interactions in the presence of polyethylene oxide. I. Simplified theory. *J Colloid and Int Sci* **1991**, *142*, 149.

(107) Jeon, S. I.; Andrade, J. D. Protein-surface interactions in the presence of poly(ethylene oxide). II. Effect of protein size. *J Colloid and Int Sci* **1991**, *142*, 159.

(108) Patel, S.; Tirrell, M.; Hadziioannou, G. A simple model for forces between surfaces bearing grafted polymers applied to data on adsorbed block copolymers. *Colloids and Surfaces* **1988**, *31*, 157–179.

(109) De Gennes, P. G. Polymers at an interface. 2. Interaction between two plates carrying adsorbed polymer layers. *Macromolecules* **1982**, *15*, 492–500.

(110) Uziely, B.; Jeffers, S.; Isacson, R.; Kutsch, K.; Wei-Tsao, D.; Yehoshua, Z.; Libson, E.; Muggia, F. M.; Gabizon, A. Liposomal doxorubicin: antitumor activity and unique toxicities during two complementary phase I studies. *J Chem Phys* **1995**, *13*, 1777–1785.

(111) Israel, V. P.; Garcia, A. A.; Roman, L.; Muderspach, L.; Burnett, A.; Jeffers, S.; Muggia, F. M. Phase II Study of Liposomal Doxorubicin in Advanced Gynecologic Cancers. *Gynecologic Oncology* **2000**, *78*, 143–147.

(112) Ranson, M. R.; Carmichael, J.; O'Byrne, K.; Stewart, S.; Smith, D.; Howell, A. Treatment of advanced breast cancer with sterically stabilized liposomal doxorubicin: results of a multicenter phase II trial. *J Chem Phys* **1997**, *15*, 3185–3191.

(113) Lyass, O.; Uziely, B.; Ben-Yosef, R.; Tzemach, D.; Heshing, N. I.; Lotem, M.; Brufman, G.; Gabizon, A. Correlation of toxicity with pharmacokinetics of pegylated liposomal doxorubicin (Doxil) in metastatic breast carcinoma. *Cancer* **2000**, *89*, 1037–1047.

(114) Kwon, G.; Suwa, S.; Yokoyama, M.; Okano, T.; Sakurai, Y.; Kataoka, K. Enhanced Tumor Accumulation and Prolonged Circulation Times of Micelle-Forming Poly(Ethylene Oxide-Aspartate) Block Copolymer-Adriamycin Conjugates. *J Control Rel* **1994**, *29*, 17–23.

(115) Ma, Z.; Haddadi, A.; Molavi, O.; Lavasanifar, A.; Lai, R.; Samuel, J. Micelles of Poly(Ethylene Oxide)-*b*-Poly(ε-caprolactone) as Vehicles for the Solubilization, Stabilization, and Controlled Delivery of Curcumin. *J. Biomed. Mater. Res.* **2008**, *86A*, 300–310.

(116) Yokoyama, M.; Kwon, G. S.; Okano, T.; Sakurai, Y.; Naito, M.; Kataoka, K. Influencing Factors on in-Vitro Micelle Stability of Adriamycin-Block Copolymer Conjugates. *J Control Del*; 1994; Vol. 28, pp. 59–65.

(117) Yokoyama, M.; Fukushima, S.; Uehara, R.; Okamoto, K.; Kataoka, K.; Sakurai, Y.; Okano, T. Characterization of physical entrapment and chemical conjugation of adriamycin in polymeric micelles and their design for in vivo delivery to a solid tumor. *J Control Release* **1998**, *50*, 79–92.

(118) Li, Y.; Kwon, G. S. Methotrexate esters of poly(ethylene oxide)-block-poly(2-hydroxyethyl-L-aspartamide). Part I: Effects of the level of methotrexate conjugation on the stability of micelles and on drug release. *Pharm Res* **2000**, *17*, 607–611.

(119) Avgoustakis, K. Pegylated poly(lactide) and poly(lactide-co-glycolide) nanoparticles: preparation, properties and possible applications in drug delivery. *Curr Drug Deliv* **2004**, *1*, 321–333.

(120) Lin, W.-J.; Chen, Y.-C.; Lin, C.-C.; Chen, C.-F.; Chen, J.-W. Characterization of Pegylated Copolymeric Micelles and in Vivo Pharmacokinetics and Biodistribution Studies. *J. Biomed. Mater. Res.* **2006**, *77B*, 188–194.

(121) Allen, C.; Maysinger, D.; Eisenberg, A. Nano-engineering block copolymer aggregates for drug delivery. *Colloids Surf B Biointerfaces* **1999**, *16*, 3–27.

(122) Shuai, X.; Ai, H.; Nasongkla, N.; Kim, S.; Gao, J. Micellar carriers based on block copolymers of poly(ε-caprolactone) and poly(ethylene glycol) for doxorubicin delivery. *Journal of Controlled Release* **2004**, *98*, 415–426.

(123) Luo, L.; Tam, J.; Maysinger, D.; Eisenberg, A. Cellular Internalization of Poly(ethylene oxide)-*b*-poly(ε-caprolactone) Diblock Copolymer Micelles. *Bioconjugate Chem.* **2002**, *13*, 1259–1265.

(124) Meier, M. A. R.; Aerts, S. N. H.; Staal, B. B. P.; Rasa, M.; Schubert, U. S. PEO-b-PCL Block Copolymers: Synthesis, Detailed Characterization, and Selected Micellar Drug Encapsulation Behavior. *Macromol Rapid Comm* **2005**, *26*, 1918–1924.

(125) Cheng, J.; Teply, B.; Sherifi, I.; Sung, J.; Luther, G.; Gu, F.; Levynissenbaum, E.; Radovicmoreno, A.; Langer, R.; Farokhzad, O. Formulation of functionalized PLGA–PEG nanoparticles for in vivo targeted drug delivery. *Biomaterials* **2007**, *28*, 869–876.

(126) Liu, L.; Li, C.; Li, X.; Yuan, Z.; An, Y.; He, B. Biodegradable polylactide/poly(ethylene glycol)/polylactide triblock copolymer micelles as anticancer drug carriers. *J. Appl. Polym. Sci.* **2001**, *80*, 1976–1982.

(127) Ge, H. H.; Hu, Y. Y.; Jiang, X. X.; Cheng, D. D.; Yuan, Y. Y.; Bi, H. H.; Yang, C. C. Preparation, characterization, and drug release behaviors of drug nimodipine-loaded poly(epsilon-caprolactone)-poly(ethylene oxide)-poly(epsilon-caprolactone) amphiphilic triblock copolymer micelles. *J Pharm Sci* **2002**, *91*, 1463–1473.

(128) Dodgson, K.; Bannister, D.; Semlyen, J. Studies of cyclic and linear poly (dimethyl siloxanes). 4. Bulk viscosities. *Polymer* **1980**, *21*, 663–667.

(129) Orrah, D. J. Studies of cyclic and linear poly(dimethylsiloxanes): 27. Bulk viscosities above the critical molar mass of entanglement. *Polymer* **1988**, *29*, 1492.

(130) Dodgson, K.; Semlyen, J. Studies of cyclic and linear poly (dimethyl siloxanes): 1. Limiting viscosity number-molecular weight relationships. *Polymer* **1977**, *18*, 1265–1268.

(131) Orrah, D.; Semlyen, J.; Ross-Murphy, S. Studies of cyclic and linear poly (dimethylsiloxanes): 28. Viscosities and densities of ring and chain poly (dimethylsiloxane) blends. *Polymer* **1988**, *29*, 1455–1458.

(132) Zimm, B. H.; Stockmayer, W. H. The dimensions of chain molecules containing branches and rings. *The Journal of Chemical Physics* **1949**, *17*, 1301.

(133) Kramers, H. The behavior of macromolecules in inhomogeneous flow. *The Journal of Chemical Physics* **1946**, *14*, 415.

(134) Casassa, E. F. Some statistical properties of flexible ring polymers. *J Polym Sci A General Papers* **1965**, *3*, 605.

(135) Higgins, J.; Dodgson, K.; Semlyen, J. Studies of cyclic and linear poly(dimethyl siloxanes): 3. Neutron scattering measurements of the dimensions of ring and chain polymers. *Polymer* **2002**, *20*, 553–558.

(136) Clarson, S.; Dodgson, K.; Semlyen, J. Studies of cyclic and linear poly (dimethylsiloxanes): 19. Glass transition temperatures and crystallization behaviour. *Polymer* **1985**, *26*, 930–934.

(137) Gan, Y.; Dong, D.; Hogen-Esch, T. E. Effects of Lithium Bromide on the Glass Transition Temperatures of Linear and Macrocyclic Poly(2-vinylpyridine) and Polystyrene. *Macromolecules* **1995**, *28*, 383–385.

(138) Edwards, C.; Stepto, R. Studies of cyclic and linear poly (dimethyl siloxanes): 5. Diffusion behaviour in dilute solution. *Polymer* **1980**.

(139) Edwards, C.; Bantle, S.; Burchard, W.; Stepto, R.; Semlyen, J. Studies of cyclic and linear poly (dimethyl siloxanes): 9. Quasi-elastic light scattering and concentration dependences of diffusion coefficients. *Polymer* **1982**, *23*, 873–876.

(140) Higgins, J.; Ma, K.; Nicholson, L.; Hayter, J.; Dodgson, K.; Semlyen, J. Studies of cyclic and linear poly (dimethyl siloxanes): 12. Observation of diffusion behaviour by quasielastic neutron scattering. *Polymer* **1983**, *24*, 793–799.

(141) Pham-Van-Cang, C.; Bokobza, L.; Monnerie, L.; Clarson, S.; Semlyen, J.; Vandendriessche, J.; De Schryver, F. Studies of cyclic and linear poly (dimethylsiloxanes): 26. An investigation of the mobility of cyclic poly (dimethylsiloxane) in the melt through the excimer emission of small probes. *Polymer* **1987**, *28*, 1561–1565.

(142) Tead, S. F.; Kramer, E. J.; Hadziioannou, G.; Antonietti, M.; Sillescu, H.; Lutz, P.; Strazielle, C. Polymer topology and diffusion: a comparison of diffusion in linear and cyclic macromolecules. *Macromolecules* **1992**, *25*, 3942–3947.

(143) Gao, C.; Yan, D. Hyperbranched polymers: from synthesis to applications. *Progress in Polymer Science* **2004**, *29*, 183–275.

(144) Kim, Y. H.; Webster, O. W. Water soluble hyperbranched polyphenylene: "a unimolecular micelle?." *J. Am. Chem. Soc.* **1990**, *112*, 4592–4593.

(145) Vyasa, K.-D. The Mahabharata. **1883**, 1–5817.

(146) Odian, G. Principles of Polymerization. **2004**, 1–839.

(147) Fujimaki, T. Processability and properties of aliphatic polyesters, "BIONOLLE', synthesized by polycondensation reaction. *Polymer Degradation and Stability* **1998**, *59*, 209–214.

(148) Bailey, W. J. Free Radical Ring-Opening Polymerization. *Polymer Journal* **1985**, *17*, 85–95.

(149) Penczek, S.; Duda, A.; Libiszowski, J. Controlled polymerization of cyclic esters. Structure of initiators and of active species related to the selectivity of initiation and propagation. In; 1998; Vol. 128, pp. 241–254.

(150) Albertsson, A. C.; Varma, I. Aliphatic polyesters: synthesis, properties and applications. *Degradable aliphatic polyesters* **2002**, 1–40.

(151) Nyce, G. W.; Glauser, T.; Connor, E. F.; Möck, A.; Waymouth, R. M.; Hedrick, J. L. In situ generation of carbenes: a general and versatile platform for organocatalytic living polymerization. *J. Am. Chem. Soc.* **2003**, *125*, 3046–3056.

(152) Dubois, P.; Ropson, N.; Jérôme, R.; Teyssie, P. Macromolecular engineering of polylactones and polylactides .19. Kinetics of ring-opening polymerization of epsilon-caprolactone initiated with functional aluminum alkoxides. *Macromolecules* **1996**, *29*, 1965–1975.

(153) Agarwal, S.; Mast, C.; Dehnicke, K.; Greiner, A. Rare earth metal initiated ring-opening polymerization of lactones. *Macromol Rapid Comm* **2000**, *21*, 195–212.

(154) Duda, A.; Florjanczyk, Z.; Hofman, A.; Slomkowski, S.; Penczek, S. Living Pseudoanionic Polymerization of e-Caprolactone. Poly (e-Caprolactone) Free of Cyclics and with Controlled End Groups. *Macromolecules* **1990**, *23*, 1640–1646.

(155) Jacquier, V.; Miola, C.; Llauro, M.; Monnet, C.; Hamaide, T. Functionalized poly(epsilon-caprolactone) and copolymers with ethylene oxide through heterogeneous anionic coordinated polymerization. NMR characterization and crystallinity. *Macromol Chem Physic* **1996**, *197*, 1311–1324.

(156) Kowalski, A.; Libiszowski, J.; Duda, A.; Penczek, S. Polymerization of l, l-Dilactide Initiated by Tin(II) Butoxide. *Macromolecules* **2000**, *33*, 1964–1971.

(157) Biela, T.; Duda, A.; Penczek, S. Control of Mn, Mw:Mn, end-groups, and kinetics in living polymerization of cyclic esters. *Macromol Symp* **2002**, *183*, 1–10.

(158) Kowalski, A.; Duda, A.; Penczek, S. Polymerization of L,L-lactide initiated by aluminum isopropoxide trimer or tetramer. *Macromolecules* **1998**, *31*, 2114–2122.

(159) Kowalski, A.; Duda, A.; Penczek, S. Kinetics and mechanism of cyclic esters polymerization initiated with tin (II) octoate, 1. Polymerization of ε-caprolactone. *Macromol Rapid Comm* **1998**, *19*, 567–572.

(160) Kowalski, A.; Duda, A.; Penczek, S. Mechanism of Cyclic Ester Polymerization Initiated with Tin(II) Octoate. 2. †Macromolecules Fitted with Tin(II) Alkoxide Species Observed Directly in MALDI−TOF Spectra. *Macromolecules* **2000**, *33*, 689–695.

(161) Kowalski, A.; Duda, A.; Penczek, S. Kinetics and Mechanism of Cyclic Esters Polymerization Initiated with Tin(II) Octoate. 3. †Polymerization of l, l-Dilactide. *Macromolecules* **2000**, *33*, 7359–7370.

(162) Majerska, K.; Duda, A.; Penczek, S. Kinetics and mechanism of cyclic esters polymerisation initiated with tin(II) octoate, 4 - Influence of proton trapping agents on the kinetics of epsilon-caprolactone and L,L-dilactide polymerisation. *Macromol Rapid Comm* **2000**, *21*, 1327–1332.

(163) Degee, P.; Dubois, P.; Jérôme, R. Bulk polymerization of lactides initiated by aluminium isopropoxide .2. Beneficial effect of Lewis bases and transfer agents. *Macromol Chem Physic* **1997**, *198*, 1973–1984.

(164) Kricheldorf, H. R.; Kreiser-Saunders, I.; Stricker, A. Polylactones 48. SnOct 2-Initiated Polymerizations of Lactide: A Mechanistic Study. *Macromolecules* **2000**, *33*, 702–709.

(165) Oshimura, M.; Takasu, A.; Nagata, K. Controlled Ring-Opening Polymerization of ϵ-Caprolactone Using Polymer-Supported Scandium Trifluoromethanesulfonate in Organic Solvent and Ionic Liquids. *Macromolecules* **2009**, *42*, 3086–3091.

(166) Amgoune, A.; Thomas, C. M.; Ilinca, S.; Roisnel, T.; Carpentier, J.-F. Highly Active, Productive, and Syndiospecific Yttrium Initiators for the Polymerization of Racemic β-Butyrolactone. *Angew. Chem. Int. Ed.* **2006**, *45*, 2782–2784.

(167) Stridsberg, K.; Gruvegard, M.; Albertsson, A. Ring-opening polymerization of degradable polyesters. In; 1998; Vol. 130, pp. 367–378.

(168) Duda, A.; Kowalski, A.; Penczek, S.; Uyama, H.; Kobayashi, S. Kinetics of the Ring-Opening Polymerization of 6-, 7-, 9-, 12-, 13-, 16-, and 17-Membered Lactones. Comparison of Chemical and Enzymatic Polymerizations. *Macromolecules* **2002**, *35*, 4266–4270.

(169) Gross, R. A.; Kumar, A.; Kalra, B. Polymer Synthesis by In Vitro Enzyme Catalysis. *Chem. Rev.* **2001**, *101*, 2097–2124.

(170) Kobayashi, S. Enzymatic polymerization: a new method of polymer synthesis. *J. Polym. Sci. A Polym. Chem.* **2000**, *37*, 3041–3056.

(171) Kobayashi, S.; Uyama, H.; Ohmae, M. Enzymatic Polymerization for Precision Polymer Synthesis. *Bulletin of the Chemical Society of Japan* **2001**, *74*, 613–635.

(172) Lodish, H.; Berk, A.; Zipursky, S. L. *Molecular Cell Biology*; Freeman: New York, 2000.

(173) Uitdehaag, J. C. M. The Cyclization Mechanism of Cyclodextrin Glycosyltransferase (CGTase) as Revealed by a gamma -Cyclodextrin-CGTase Complex at 1.8-A Resolution. *Journal of Biological Chemistry* **1999**, *274*, 34868–34876.

(174) Ikeda, I.; Yamamura, S.; Nakatsuji, Y.; Okahara, M. Synthesis of Substituted Crown Ethers From Oligoethylene Glycols. *J. Org. Chem.* **1980**, *45*, 5355–5358.

(175) Jacobson, H.; Stockmayer, W. H. Intramolecular Reaction in Polycondensations. I. The Theory of Linear Systems. *.Journal of Chemical Physics 18*, 1600–1606.

(176) Pugh, C.; Singh, A.; Samuel, R.; Bernal Ramos, K. M. Synthesis of Hyperbranched Polyacrylates by a Chloroinimer Approach. *Macromolecules* **2010**, *43*, 5222–5232.

(177) Frechet, J. M. J.; Henmi, M.; Gitsov, I.; Aoshima, S.; Leduc, M. R.; Grubbs, R. B. Self-condensing vinyl polymerization: an approach to dendritic materials. *Science* **1995**, 1080–1080.

(178) Müller, A. H. E.; Yan, D.; Wulkow, M. Molecular parameters of hyperbranched polymers made by self-condensing vinyl polymerization. 1. Molecular weight distribution. *Macromolecules* **1997**, *30*, 7015–7023.

(179) Yan, D.; Müller, A. H. E.; Matyjaszewski, K. Molecular Parameters of Hyperbranched Polymers Made by Self-Condensing Vinyl Polymerization. 2. Degree of Branching †. *Macromolecules* **1997**, *30*, 7024–7033.

(180) Szwarc, M.; Levy, M.; Milkovich, R. Polymerization initiated by electron transfer to monomer. A new method of formation of block polymers1. *J. Am. Chem. Soc.* **1956**, *78*, 2656–2657.

(181) Matyjaszewski, K.; Kubisa, P.; Penczek, S. Ion⇄ ester equilibria in the living cationic polymerization of tetrahydrofuran. *Journal of Polymer Science: Polymer Chemistry Edition* **1974**, *12*, 1333–1336.

(182) Penczek, S.; Kubisa, P.; Matyjaszewski, K. *Cationic Ring Opening Polymerization. 2. Synthetic Applications*; 1985; pp. 1–298.

(183) Szwarc, M. The Determination of Bond Dissociation Energies by Pyrolytic Methods. *Chem. Rev.* **1950**, *47*, 75–173.

(184) Bengough, W. I.; Fairservice, W. H. Effects of salts of metals on vinyl polymerization. Part 1. Polymerization of methyl methacrylate in presence of cupric chloride. *Trans. Faraday Soc.* **1965**, *61*, 1206.

(185) Fischer, H. The persistent radical effect in “living” radical polymerization. *Macromolecules* **1997**, *30*, 5666–5672.

(186) Braunecker, W. A.; Matyjaszewski, K. Controlled/living radical polymerization: Features, developments, and perspectives. *Progress in Polymer Science* **2007**, *32*, 93–146.

(187) Nicolas, J.; Guillaneuf, Y.; Lefay, C.; Bertin, D.; Gigmes, D.; Charleux, B. Progress in Polymer Science. *Progress in Polymer Science* **2013**, *38*, 63–235.

(188) Debuigne, A.; Poli, R.; Jérôme, C.; Jérôme, R.; Detrembleur, C. Overview of cobalt-mediated radical polymerization: Roots, state of the art and future prospects. *Progress in Polymer Science* **2009**, *34*, 211–239.

(189) Anastas, P.; Eghbali, N. Green Chemistry: Principles and Practice. *Chem. Soc. Rev.* **2009**, *39*, 301.

(190) Braunecker, W. A.; Tsarevsky, N. V.; Gennaro, A.; Matyjaszewski, K. Thermodynamic Components of the Atom Transfer Radical Polymerization Equilibrium: Quantifying Solvent Effects. *Macromolecules* **2009**, *42*, 6348–6360.

(191) Tsarevsky, N. V.; Braunecker, W. A.; Matyjaszewski, K. Electron transfer reactions relevant to atom transfer radical polymerization. *Journal of Organometallic Chemistry* **2007**, *692*, 3212–3222.

(192) Simakova, A.; Averick, S. E.; Konkolewicz, D.; Matyjaszewski, K. Aqueous ARGET ATRP. *Macromolecules* **2012**, *45*, 6371–6379.

(193) Konkolewicz, D.; Magenau, A. J. D.; Averick, S. E.; Simakova, A.; He, H.; Matyjaszewski, K. ICAR ATRP with ppm Cu Catalyst in Water. *Macromolecules* **2012**, *45*, 4461–4468.

(194) Lang, M.; Bei, J.; Wang, S. Synthesis and characterization of polycaprolactone poly(ethylene oxide) polylactide tri-component copolymers. *J Biomater Sci Polym Ed* **1999**, *10*, 501–512.

(195) Chasin, M.; Langer, R. *Biodegradable polymers as drug delivery systems*; Marcel Dekker: New York, 1990.

(196) Lam, C. X. F.; Savalani, M. M.; Teoh, S.-H.; Hutmacher, D. W. Dynamics of in vitro polymer degradation of polycaprolactone-based scaffolds: accelerated versus simulated physiological conditions. *Biomed. Mater.* **2008**, *3*, 034108.

(197) Bazile, D.; Prud'homme, C.; Bassoullet, M. T.; Marlard, M.; Spenlehauer, G.; Veillard, M. Stealth Me. PEG-PLA nanoparticles avoid uptake by the mononuclear phagocytes system. *J Pharm Sci* **1995**, *84*, 493–498.

(198) Batrakova, E. V.; Miller, D. W.; Li, S.; Alakhov, V. Y.; Kabanov, A. V.; Elmquist, W. F. Pluronic P85 enhances the delivery of digoxin to the brain: in vitro and in vivo studies. *J. Pharmacol. Exp. Ther.* **2001**, *296*, 551–557.

(199) Rapoport, N. Physical stimuli-responsive polymeric micelles for anti-cancer drug delivery. *Progress in Polymer Science* **2007**, *32*, 962–990.

(200) Riess, G. Micellization of block copolymers. *Progress in Polymer Science* **2003**, *28*, 1107–1170.

(201) Lavasanifar, A.; Samuel, J.; Kwon, G. S. Micelles self-assembled from poly(ethylene oxide)-block-poly(N-hexyl stearate L-aspartamide) by a solvent evaporation method: effect on the solubilization and haemolytic activity of amphotericin B. *J Control Release* **2001**, *77*, 155–160.

(202) Park, E. K.; Lee, S. B.; Lee, Y. M. Preparation and characterization of methoxy poly(ethylene glycol)/poly(ε-caprolactone) amphiphilic block copolymeric nanospheres for tumor-specific folate-mediated targeting of anticancer drugs. *Biomaterials* **2005**, *26*, 1053–1061.

(203) Kim, S. Y.; Lee, Y. M. Taxol-loaded block copolymer nanospheres composed of methoxy poly (ethylene glycol) and poly (ε-caprolactone) as novel anticancer drug carriers. *Biomaterials* **2001**, *22*, 1697–1704.

(204) Kim, S. Y.; Lee, Y. M.; Baik, D. J.; Kang, J. S. Toxic characteristics of methoxy poly (ethylene glycol)/poly (ε-caprolactone) nanospheres; in vitro and in vivo studies in the normal mice. *Biomaterials* **2003**, *24*, 55–63.

(205) Vangeyte, P.; Gautier, S.; Jérôme, R. About the methods of preparation of poly(ethylene oxide)-b-poly(ε-caprolactone) nanoparticles in water. *Colloid Surface A* **2004**, *242*, 203–211.

(206) Shi, B.; Fang, C.; You, M. X.; Zhang, Y.; Fu, S.; Pei, Y. Stealth MePEG-PCL micelles: effects of polymer composition on micelle physicochemical characteristics, in vitro drug release, in vivo pharmacokinetics in rats and biodistribution in S180 tumor bearing mice. *Colloid Polym Sci* **2004**, *283*, 954–967.

(207) Aliabadi, H.; Elhasi, S.; Mahmud, A.; Gulamhusein, R.; Mahdipoor, P.; Lavasanifar, A. Encapsulation of hydrophobic drugs in polymeric micelles through co-solvent evaporation: The effect of solvent composition on micellar properties and drug loading. *International Journal of Pharmaceutics* **2007**, *329*, 158–165.

(208) Kabanov, A. V.; Nazarova, I. R.; Astafieva, I. V.; Batrakova, E. V.; Alakhov, V. Y.; Yaroslavov, A. A.; Kabanov, V. A. Micelle formation and solubilization of fluorescent probes in poly (oxyethylene-b-oxypropylene-b-oxyethylene) solutions. *Macromolecules* **1995**, *28*, 2303–2314.

(209) Yáñez, J. A.; Forrest, M. L.; Ohgami, Y.; Kwon, G. S.; Davies, N. M. Pharmacometrics and delivery of novel nanoformulated PEG-b-poly(ε-caprolactone) micelles of rapamycin. *Cancer Chemotherapy and Pharmacology* **2007**, *61*, 133–144.

(210) MS, H. C.; PhD, G. L. I.; PhD, J. W.; MS, H.-C. S.; PhD, G. S. K. In vivo cancer imaging by poly(ethylene glycol)-b-poly(ε-caprolactone) micelles containing a near-infrared probe. *Nanomedicine: Nanotechnology, Biology and Medicine* **2012**, *8*, 228–236.

(211) Yang, X.; Deng, W.; Fu, L.; Blanco, E.; Gao, J.; Quan, D.; Shuai, X. Folate-functionalized polymeric micelles for tumor targeted delivery of a potent multidrug-resistance modulator FG020326. *J. Biomed. Mater. Res.* **2008**, *86A*, 48–60.

(212) Yang, X.; Chen, Y.; Yuan, R.; Chen, G.; Blanco, E.; Gao, J.; Shuai, X. Folate-Encoded and Fe_3O_4-Loaded Polymeric Micelles for Dual Targeting of Cancer Cells. *Polymer* **2008**, *49*, 3477–3485.

(213) Tyrrell, Z. L.; Shen, Y.; Radosz, M. Near-Critical Fluid Micellization for High and Efficient Drug Loading: Encapsulation of Paclitaxel into PEG- b-PCL Micelles. *J. Phys. Chem. C* **2011**, *115*, 11951–11956.

(214) Zhou, S.; Deng, X.; Yang, H. Biodegradable poly(ε-caprolactone)-poly(ethylene glycol) block copolymers: characterization and their use as drug carriers for a controlled delivery system. *Biomaterials* **2003**, *24*, 3563–3570.

(215) Kim, S. Y.; Shin, I. L.; Lee, Y. M.; Cho, C. S.; Sung, Y. K. Methoxy poly (ethylene glycol) and-caprolactone amphiphilic block copolymeric micelle containing indomethacin.:: II. Micelle formation and drug release behaviours. *J Control Release* **1998**, *51*, 13–22.

(216) Liu, J.; Zeng, F.; Allen, C. In vivo fate of unimers and micelles of a poly(ethylene glycol)-block-poly(caprolactone) copolymer in mice following intravenous administration. *European Journal of Pharmaceutics and Biopharmaceutics* **2007**, *65*, 309–319.

(217) Gan, Z.; Jim, T. F.; Li, M.; Yuer, Z.; Wang, S.; Wu, C. Enzymatic Biodegradation of Poly(ethylene oxide- b-ε-caprolactone) Diblock Copolymer and Its Potential Biomedical Applications. *Macromolecules* **1999**, *32*, 590–594.

(218) Lin, W.-J.; Lee-Wei, J.; Chia-Ling, W.; Chen, Y.-C.; Lin, C.-C.; Kai-Ling, C. Pegylated Polyester Polymeric Micelles as a Nano-carrier: Synthesis, Characterization, Degradation, and Biodistribution. *J Exp Clin Med* **2010**, *2*, 4–10.

(219) van Krevelen, D. W. *Properties of Polymers*; 3rd ed. Elsevier: Amsterdam, 1990.

(220) *Dynamic Light Scattering: Applications of Photon Correlation Spectroscopy*; Pecora, R., Ed. 1st ed. Plenum Press: New York, 1985.

(221) Kissa, E. *Dispersions. Characterization, Testing, and Measurement*; Schick, M. J.; Hubbard, A. T., Eds. Marcel Dekker; Vol. 84.

(222) Provencher, S. W. Inverse problems in polymer characterization: direct analysis of polydispersity with photon correlation spectroscopy. *Makromol. Chem.* **1979**, *180*, 201–209.

(223) Hicks, L. D.; Alattia, J.; Ikura, M.; Kay, C. Multiangle Laser Light Scattering and Sedimentation Equilibrium. In *Calcium Binding Protein Protocols*; Vogel, H. J., Ed. Humana Press; Vol. 173, pp. 127–131.

(224) Reimer, L. *Scanning Electron Microscopy: Physics of Image Formation and Microanalysis*; 2nd ed. Springer: Berlin, 1998.

(225) Mukerjee, P.; Mysels, K. J. Critical micelle concentrations of aqueous surfactant systems. *United States Department of Commerce. National Bureau of Standards* **1971**.

(226) Amiji, M. M. *Nanotechnology for cancer therapy*; CRC Press, 2006.

(227) *Current Protocols in Cell Biology*; Bonifacino, J. S.; Dasso, M.; Harford, J. B.; Lippincott-Schwartz, J.; Yamada, K. M., Eds. Wiley, 2013.

(228) Pugh, C.; Bae, J. Y.; Scott, J. R.; Wilkins, C. L. Amphiphilic Approach for Preparing Homopolyrotaxanes of Poly(ethylene oxide). *Macromolecules* **1997**, *30*, 8139–8152.

(229) Wollyung, K. M.; Xu, K.; Cochran, M.; Kasko, A. M.; Mattice, W. L.; Wesdemiotis, C.; Pugh, C. Synthesis and Mass Spectrometry Studies of an Amphiphilic Polyether-Based Rotaxane That Lacks an Enthalpic Driving Force for Threading. *Macromolecules* **2005**, *38*, 2574–2586.

(230) Montazeri Aliabadi, H.; Brocks, D. R.; Lavasanifar, A. Polymeric micelles for the solubilization and delivery of cyclosporine A: pharmacokinetics and biodistribution. *Biomaterials* **2005**, *26*, 7251–7259.

(231) Holzl, W.; Koppold, J.; Marquais-Bienewald, S. Benzyl alcohol derivatives. WO 03/078367 A2, 2003.

(232) Collier, C. P.; Jeppesen, J. O.; Luo, Y.; Perkins, J.; Wong, E. W.; Heath, J. R.; Stoddart, J. F. Molecular-Based Electronically Switchable Tunnel Junction Devices. *J. Am. Chem. Soc.* **2001**, *123*, 12632–12641.

(233) Boyer, S.; Härter, M.; Wickens, P. L.; Patel, M.; Kumarasinghe, E. S.; Bhargava, A. K.; Thierauch, K.-H.; Beck, H.; Greschat, S.; Ellinghaus, P. Heteroaryl Substituted Pyrazole Derivatives Useful for Treating Hyper-Proliferative Disorders and Diseases Associated with Angiogenesis. WO2008/141731 A2, 2008.

(234) Silverstein, R. M.; Webster, F. X.; Kiemle, D. L. *Spectrometric Identification of Organic Compounds*; Seventh Edition. JOHN WILEY & SONS INC, 2005.

(235) Zhu, X.; Fryd, M.; Tran, B. D.; Ilies, M. A.; Wayland, B. B. Modifying the Hydrophilic–Hydrophobic Interface of PEG-*b*-PCL To Increase Micelle Stability: Preparation of PEG-*b*-PBO-*b*-PCL Triblock Copolymers, Micelle Formation, and Hydrolysis Kinetics. *Macromolecules* **2012**, *45*, 660–665.

(236) Sun, J.; He, C.; Zhuang, X.; Jing, X.; Chen, X. The crystallization behavior of poly(ethylene glycol)-poly(ε-caprolactone) diblock copolymers with asymmetric block compositions. *J Polym Res* **2011**, *18*, 2161–2168.

(237) Cho, H.; Kwon, G. S. Polymeric Micelles for Neoadjuvant Cancer Therapy and Tumor-Primed Optical Imaging. *ACS Nano* **2011**, *5*, 8721–8729.

(238) Yan, J.; Ye, Z.; Chen, M.; Liu, Z.; Xiao, Y.; Zhang, Y.; Zhou, Y.; Tan, W.; Lang, M. Fine Tuning Micellar Core-Forming Block of Poly(ethylene glycol)- block-poly(ε-caprolactone) Amphiphilic Copolymers Based on Chemical Modification for the Solubilization and Delivery of Doxorubicin. *Biomacromolecules* **2011**, *12*, 2562–2572.

(239) Xiong, X.-B.; Lavasanifar, A. Traceable Multifunctional Micellar Nanocarriers for Cancer-Targeted Co-delivery of MDR-1 siRNA and Doxorubicin. *ACS Nano* **2011**, *5*, 5202–5213.

(240) Tian, Y.; Wu, W.-C.; Chen, C.-Y.; Strovas, T.; Li, Y.; Jin, Y.; Su, F.; Meldrum, D. R.; Jen, A. K. Y. 2,1,3-Benzothiadiazole (BTD)-moiety-containing red emitter conjugated amphiphilic poly(ethylene glycol)-block-poly(ε-caprolactone) copolymers for bioimaging. *J. Mater. Chem.* **2010**, *20*, 1728–1736.

(241) Noh, T.; Kook, Y. H.; Park, C.; Youn, H.; Kim, H.; Oh, E. T.; Choi, E. K.; Park, H. J.; Kim, C. Block copolymer micelles conjugated with anti-EGFR antibody for targeted delivery of anticancer drug. *J. Polym. Sci. A Polym. Chem.* **2008**, *46*, 7321–7331.

(242) Grafahrend, D.; Lleixà Calvet, J.; Salber, J.; Dalton, P. D.; Moeller, M.; Klee, D. Biofunctionalized poly(ethylene glycol)-block-poly(ε-caprolactone) nanofibers for tissue engineering. *J Mater Sci: Mater Med* **2007**, *19*, 1479–1484.

(243) Richter, A.; Olbrich, C.; Krause, M.; Kissel, T. Solubilization of Sagopilone, a poorly water-soluble anticancer drug, using polymeric micelles for parenteral delivery. *International Journal of Pharmaceutics* **2010**, *389*, 244–253.

(244) Lemmouchi, Y.; Perry, M. C.; Amass, A. J.; Chakraborty, K.; Schacht, E. Novel synthesis of biodegradable amphiphilic linear and star block copolymers based on poly(ε-caprolactone) and poly(ethylene glycol). *J. Polym. Sci. A Polym. Chem.* **2007**, *45*, 3975–3985.

(245) Dalton, P. D.; Lleixà Calvet, J.; Mourran, A.; Klee, D.; Möller, M. Melt Electrospinning of Poly(Ethylene Glycol)-*block*-**ε**-polycaprolactone). *Biotechnol. J.* **2006**, *1*, 998–1006.

(246) Bogdanov, B.; Vidts, A.; Van Den Buicke, A.; Verbeeck, R.; Schacht, E. Synthesis and Thermal Properties of Poly(ethylene Glycol)-Poly(ε-caprolactone) Copolymers. *Polymer* **1998**, *39*, 1631–1636.

(247) Forrest, M. L.; Yáñez, J. A.; Remsberg, C. M.; Ohgami, Y.; Kwon, G. S.; Davies, N. M. Paclitaxel Prodrugs with Sustained Release and High Solubility in Poly(ethylene glycol)-b-poly(ε-caprolactone) Micelle Nanocarriers: Pharmacokinetic Disposition, Tolerability, and Cytotoxicity. *Pharm Res* **2007**, *25*, 194–206.

(248) Jette, K. K.; Law, D.; Schmitt, E. A.; Kwon, G. S. Preparation and drug loading of poly(ethylene glycol)-block-poly(epsilon-caprolactone) micelles through the evaporation of a cosolvent azeotrope. *Pharm Res* **2004**, *21*, 1184–1191.

(249) Aliabadi, H. M.; Mahmud, A.; Sharifabadi, A. D.; Lavasanifar, A. Micelles of methoxy poly(ethylene oxide)-b-poly(ε-caprolactone) as vehicles for the solubilization and controlled delivery of cyclosporine A. *Journal of Controlled Release* **2005**, *104*, 301–311.

(250) Wu, C. S. Performance of an acrylic acid grafted polycaprolactone/starch composite: characterization and mechanical properties. *J. Appl. Polym. Sci.* **2003**, *89*, 2888–2895.

(251) Piao, L.; Dai, Z.; Deng, M.; Chen, X.; Jing, X. Synthesis and characterization of PCL/PEG/PCL triblock copolymers by using calcium catalyst. *Polymer* **2003**, *44*, 2025–2031.

(252) He, C.; Sun, J.; Deng, C.; Zhao, T.; Deng, M.; Chen, X.; Jing, X. Study of the Synthesis, Crystallization, and Morphology of Poly(ethylene glycol)−Poly(ε-caprolactone) Diblock Copolymers. *Biomacromolecules* **2004**, *5*, 2042–2047.

(253) Ilum, L.; Davis, S. S.; Müller, R. H.; Mak, E.; West, P. The organ distribution and circulation time of intravenously injected colloidal carriers sterically stabilized with a block copolymer. *Life Sci* **1987**, *40*, 367–374.

(254) Vittaz, M.; Bazile, D.; Spenlehauer, G.; Verrecchia, T.; Veillard, M.; Puisieux, F.; Labarre, D. Effect of PEO surface density on long-circulating PLA-PEO nanoparticles which are very low complement activators. *Biomaterials* **1996**, *17*, 1575–1581.

(255) Alexis, F.; Pridgen, E.; Molnar, L. K.; Farokhzad, O. C. Factors Affecting the Clearance and Biodistribution of Polymeric Nanoparticles. *Mol. Pharmaceutics* **2012**, *5*, 505–515.

(256) Dobrovolskaia, M. A.; Patri, A. K.; Zheng, J.; Clogston, J.; Ayub, N.; Aggarwal, P.; Neun, B.; Hall, J.; PhD, S. E. M. Interaction of Colloidal Gold Nanoparticles with Human Blood: Effects on Particle Size and Analysis of Plasma Protein Binding Profiles. *Nanomedicine: Nanotechnology, Biology and Medicine* **2009**, *5*, 106–117.

(257) Frank, M. M.; Fries, L. F. The role of complement in inflammation and phagocytosis. *Immunology Today* **1991**, *12*, 322–326.

(258) Illum, L.; Davis, S. S. The organ uptake of intravenously administered colloidal particles can be altered using a non-ionic surfactant (Poloxamer 338). *FEBS Lett.* **1984**, *167*, 79–82.

(259) Panagi, Z.; Beletsi, A.; Evangelatos, G.; Livaniou, E.; Ithakissios, D. S.; Avgoustakis, K. Effect of dose on the biodistribution and pharmacokinetics of PLGA and PLGA-mPEG nanoparticles. *International Journal of Pharmaceutics* **2001**, *221*, 143–152.

(260) Anderson, N. L. The Human Plasma Proteome: History, Character, and Diagnostic Prospects. *Molecular & Cellular Proteomics* **2002**, *1*, 845–867.

(261) Rezwan, K.; Meier, L. P.; Rezwan, M.; Vörös, J.; Textor, M.; Gauckler, L. J. Bovine Serum Albumin Adsorption onto Colloidal Al 2O 3Particles: A New Model Based on Zeta Potential and UV−Vis Measurements. *Langmuir* **2004**, *20*, 10055–10061.

(262) Balasubramanian, V.; Grusin, N. K.; Bucher, R. W.; Turitto, V. T.; Slack, S. M. Residence-time dependent changes in fibrinogen adsorbed to polymeric biomaterials. *J. Biomed. Mater. Res.* **1999**, *44*, 253–260.

(263) Gelamo, E. L.; Tabak, M. Spectroscopic studies on the interaction of bovine (BSA) and human (HSA) serum albumins with ionic surfactants. *Spectrochim Acta A Mol Biomol Spectrosc* **2000**, *56A*, 2255–2271.

(264) Kandagal, P. B.; Ashoka, S.; Seetharamappa, J.; Shaikh, S. M. T.; Jadegoud, Y.; Ijare, O. B. Study of the interaction of an anticancer drug with human and bovine serum albumin: Spectroscopic approach. *Journal of Pharmaceutical and Biomedical Analysis* **2006**, *41*, 393–399.

(265) Dominguez-Medina, S.; McDonough, S.; Swanglap, P.; Landes, C. F.; Link, S. In situ measurement of bovine serum albumin interaction with gold nanospheres. *Langmuir* **2012**, *28*, 9131–9139.

(266) Croy, S. R.; Kwon, G. S. Polymeric micelles for drug delivery. *Current pharmaceutical design* **2006**, *12*, 4669–4684.

(267) Brehm, E. H. M. *Fluorescence Correlation Spectroscopy*; Gottingen, 2002; pp. 1–33.

(268) Schwille, P.; Meyer-Almes, F.-J.; Rigler, R. Dual-color fluorescence cross-correlation spectroscopy for multicomponent diffusional analysis in solution. *Biophysical Journal* **1997**, *72*, 1878–1886.

(269) Dossi, M.; Ferrari, R.; Dragoni, L.; Martignoni, C.; Gaetani, P.; D'Incalci, M.; Morbidelli, M.; Moscatelli, D. Synthesis of Fluorescent PMMA-Based Nanoparticles. *Macromol. Mater. Eng.* **2012**, *298*, 771–778.

(270) Heinrich, T. K.; Gottumukkala, V.; Snay, E.; Dunning, P.; Fahey, F. H.; Treves, S. T.; Packard, A. B. Synthesis of fluorine-18 labeled rhodamine B A potential PET myocardial perfusion imaging agent. *Applied Radiation and Isotopes* **2009**, *68*, 96–100.

(271) Bartholomä, M. D.; Gottumukkala, V.; Zhang, S.; Baker, A.; Dunning, P.; Fahey, F. H.; Treves, S. T.; Packard, A. B. Effect of the Prosthetic Group on the Pharmacologic Properties of 18F-Labeled Rhodamine B, a Potential Myocardial Perfusion Agent for Positron Emission Tomography (PET). *J. Med. Chem.* **2012**, 121214162907000.

(272) Forrest, M. L.; Won, C.-Y.; Malick, A. W.; Kwon, G. S. In vitro release of the mTOR inhibitor rapamycin from poly(ethylene glycol)-b-poly(ε-caprolactone) micelles. *Journal of Controlled Release* **2006**, *110*, 370–377.

(273) Barth, J.; Kenneth R, J.; Freedman, D. Harmonisation of Reference Intervals. *Clinical Biochemistry Outcomes* **2011**, 1–3.

(274) Yohannes, G.; Wiedmer, S. K.; Elomaa, M.; Jussila, M.; Aseyev, V.; Riekkola, M.-L. Thermal Aggregation of Bovine Serum Albumin Studied by Asymmetrical Flow Field-Flow Fractionation. *Analytica Chimica Acta* **2010**, *675*, 191–198.

(275) Bulone, D.; Martorana, V.; San Biagio, P. L. Effects of intermediates on aggregation of native bovine serum albumin. *Biophys. Chem.* **2001**, *91*, 61–69.

(276) Honda, C.; Kamizono, H.; Samejima, T.; Endo, K. Studies on thermal aggregation of bovine serum albumin as a drug carrier. *Chem. Pharm. Bull.* **2000**, *48*, 464–466.

(277) *Application Note: Viscosity measurement of a model protein solution of BSA*; VROC-APP-04 (5-08); www.rheosense.com, 2008; pp. 1–3.

(278) Casals, E.; Pfaller, T.; Duschl, A.; Oostingh, G. J.; Puntes, V. Time Evolution of the Nanoparticle Protein Corona. *ACS Nano* **2010**, *4*, 3623–3632.